

SERI/STR-211-3149  
DE87001172

April 1987

# Luminescent Solar Concentrator Development

**Final Subcontract Report**  
**1 June 1982 - 31 December 1984**

**P. S. Friedman**  
**C. R. Parent**  
for  
Owens/Illinois, Inc.  
Toledo, Ohio

**Prepared under Subcontract No. XE-2-02145-01**



SE

## **Solar Energy Research Institute**

A Division of Midwest Research Institute

1617 Cole Boulevard  
Golden, Colorado 80401-3393

Operated for the  
**U.S. Department of Energy**  
under Contract No. DE-AC02-83CH10093

**SERI/STR-211-3149**  
**UC Category: 63**  
**DE87001172**

# **Luminescent Solar Concentrator Development**

**Final Subcontract Report**  
**1 June 1982 - 31 December 1984**

**P. S. Friedman**  
**C. R. Parent**  
for  
Owens/Illinois, Inc.  
Toledo, Ohio

**April 1987**

SERI Technical Monitor:  
J. Benner

**Prepared under Subcontract No. XE-2-02145-01**

## **Solar Energy Research Institute**

A Division of Midwest Research Institute

1617 Cole Boulevard  
Golden, Colorado 80401-3393

Prepared for the  
**U.S. Department of Energy**  
Contract No. DE-AC02-83CH10093

#### NOTICE

This report was prepared as an account of work sponsored by the United States Government. Neither the United States nor the United States Department of Energy, nor any of their employees, nor any of their contractors, subcontractors, or their employees, makes any warranty, expressed or implied, or assumes any legal liability or responsibility for the accuracy, completeness or usefulness of any information, apparatus, product or process disclosed, or represents that its use would not infringe privately owned rights.

Printed in the United States of America  
Available from:  
National Technical Information Service  
U.S. Department of Commerce  
5285 Port Royal Road  
Springfield, VA 22161

Price: Microfiche A01  
Printed Copy A10

Codes are used for pricing all publications. The code is determined by the number of pages in the publication. Information pertaining to the pricing codes can be found in the current issue of the following publications, which are generally available in most libraries: *Energy Research Abstracts (ERA)*; *Government Reports Announcements and Index (GRA and I)*; *Scientific and Technical Abstract Reports (STAR)*; and publication, NTIS-PR-360 available from NTIS at the above address.

## ABSTRACT

The investigation of Luminescent Solar Concentrators (LSCs) was initiated by the United States Department of Energy (DOE) at Owens-Illinois, Inc. in 1978. The experimental and theoretical results developed over the past six years have been summarized. An assessment of the LSC technology has been compiled so as to provide a concise description to guide future research in this field. It is gratifying to note that since 1978, tremendous progress has been made in the development of this device as a practical non-imaging concentrator for achieving solar concentration ratios on the order of 10X. Perhaps the two most important technical achievements, however, have been, first, the understanding that dye self-absorption of radiated energy is not as serious a problem as originally thought; and second, the demonstration that organic dyes in polymeric hosts are capable of surviving outdoors in bright sunlight for years without serious degradation. System efficiencies approaching 4% have been achieved for photovoltaic conversion and theoretical efficiencies on the order of 9% appear feasible for large area devices. Finally, the numerous accomplishments of the LSC program have been achieved at a total DOE cost of only about 0.1% of the research and development money spent on photovoltaics.

## ACKNOWLEDGEMENTS

This is the fourth and last Final Report on the Luminescent Solar Concentrator (LSC) Development Program at Owens-Illinois under the sponsorship of the United States Department of Energy. Due to a corporate reorganization at Owens-Illinois in early 1984, the LSC Group was disbanded, thereby making completion of this report a much more difficult task. In this regard, I am especially indebted to the patience and understanding of John Benner at the Solar Energy Research Institute. I would also like to formally thank my colleague and friend, Bob Parent, who is now a senior physicist at Gillette, for his numerous contributions to all aspects of the LSC Program. Finally, my thanks to the many fine and talented people whom I have had the pleasure of working with at Owens-Illinois over the past six years.

Peter S. Friedman  
Vice-President  
Research and Development  
Photonics Technology, Inc.

CONTENTS

	<b>Page</b>
Abstract.....	<i>i</i>
Acknowledgements.....	<i>ii</i>
I. Background.....	2
II. Investigation of the Optical Properties of Organic Dye/Polymer Solid Solutions.....	5
A. Introduction.....	5
B. Measurement Technique and Instrumentation.....	7
C. Structural Classification of Dyes Studied.....	18
1. 7-Aminocoumarins.....	18
2. Rhodamines.....	20
3. Oxazines.....	22
4. Styryl Dyes.....	26
5. Carbocyanines.....	26
6. Miscellaneous Dyes.....	29
D. Spectral Properties and Quantum Yield of Dyes in Liquid Solution.....	34
E. Spectral Properties and Quantum Yield of Dyes in Solution in a Thin Film Polymer Host...	43
F. Summary.....	54
III. Investigation of Dye Degradation.....	57
IV. Relative Edge Luminescence.....	67
V. Theoretical Modeling.....	68
VI. Optical Properties of Cr <sup>3+</sup> Doped Transparent Glass Ceramics.....	72
A. Beta-Quartz and Beta-Spodumene Glass Ceramics..	74
B. Spinel Glass Ceramics.....	83
C. Enstatite Type Glass-Ceramics.....	91
VII. Inorganic Glasses.....	109

	Page
VIII. Total Power Output of LSCs Compared to Photovoltaic Cells.....	117
IX. Applications of Luminescent Solar Concentrators....	122
X. Concluding Thoughts on the Future of LSC Technology.....	125
REFERENCES.....	127
APPENDIX 1. Dye Stability and Device Stability Data Tables.....	131
APPENDIX 2. Relative Edge Luminescence Values for LSC Test Plates.....	161

## TABLES

<u>TABLE</u>	<u>TITLE</u>	<u>PAGE</u>
1.	Contents of LSC Development, Final Report To Sandia, 1979 . . . . .	3
2.	Contents of LSC Development-I: Inorganic Glasses, Final Report to SERI, 1981 . . . . .	3
3.	Contents of LSC Development-II, Final Report to SERI, 1983 . . . . .	4
4.	Molecular Structure of 7-Aminocoumarins. . . . .	21
5.	Molecular Structure of Rhodamines. . . . .	23
6.	Molecular Structure of Oxazines. . . . .	24
7.	Molecular Structure of Styryl Dyes . . . . .	27
8.	Molecular Structure of Carbocyanines . . . . .	30
9.	Molecular Structure of Miscellaneous Dyes. . . . .	31
10.	Fluorescence Quantum Yields of Dyes Reported in the Literature . . . . .	35
11.	Fluorescence Quantum Yields From Least Squares Analysis . . . . .	37
12.	Experimental Fluorescence Quantum Yield Data Used in the Least Squares Analysis. . . . .	38
13.	Fluorescence Quantum Yields of Dyes in Liquid Solution. . . . .	41
14.	Fluorescence Quantum Yields of Dyes in Solid Solution in Thin Films . . . . .	44
15.	Variation of Dye Quantum Efficiency with Host. . . . .	54
16.	Protocol for LSC Degradation Studies . . . . .	58
17.	Host Polymer Systems Evaluated . . . . .	59
18.	Dye/Solvent Stability for Brilliant Yellow after 50 kWh/m <sup>2</sup> Exposure . . . . .	60
19.	Host Polymer Systems Selected for Dye Screening Tests. . . . .	61



<u>TABLES</u>	<u>TITLE</u>	<u>PAGE</u>
20.	Stability Improvement Program . . . . .	63
21.	Projected Collector Efficiencies as a Function of Plate Size for Hypothetical, Three Dye LSC . . . . .	70
22.	Efficiency Improvement Program . . . . .	71
23.	Composition in Wt.% of Cr <sup>3+</sup> Doped Spinel and Gahnite Glass-Ceramics . . . . .	84
24.	Composition in Wt.% of Cr <sup>3+</sup> Doped Enstatite Glass-Ceramics . . . . .	91
25.	Emission Quantum Yields of Cr <sup>3+</sup> Doped MAS Glasses and Enstatite Glass-Ceramics . . . . .	106
26.	Classification of Luminescent Dopants in Inorganic Glasses. . . . .	109
27.	Applications of LSC Technology . . . . .	124

## ILLUSTRATIONS

<u>FIGURE</u>	<u>TITLE</u>	<u>PAGE</u>
1.	Organization of Owens-Illinois LSC Development Program 1978-1984. . . . .	2
2.	Diagram of the Spectrofluorometer Front Surface Emission Sample Chamber. . . . .	10
3.	Diagram of the Relative Geometries of the Sample and the Excitation and Detected Emission Beams . . . .	13
4.	7-Aminocoumarin. . . . .	19
5.	Rhodamine 110. . . . .	20
6.	Oxazine 118. . . . .	22
7.	Excitation and Emission Spectra of LD 688 in a CAP 504.20 Thin Film . . . . .	50
8.	Excitation and Emission Spectra of LDS 730 in a CAP 504.20 Thin Film . . . . .	52
9.	Excitation and Emission Spectra of LDS 750 in a CAP 504.20 Thin Film . . . . .	53
10.	Absorption and Emission Spectra of LDS 820 in a CAP Thin Film. . . . .	56
11.	Stability of Day - Glo Brilliant Yellow in Cellulose Acetate Crosslinked Melamine . . . . .	64
12.	Stability of Mobay LISA Amber 59-YR in Polycarbonate. . . . .	65
13.	Radiative Transport Efficiencies Calculated as a Function of Logarithm of Transverse Absorbance . . . .	69
14.	Excitation Spectrum of Cr <sup>3+</sup> : $\beta$ -Spodumene Glass-Ceramic. . . . .	77
15.	Emission Spectrum of Cr <sup>3+</sup> : $\beta$ -Spodumene Glass-Ceramic. . . . .	78
16.	Energy Diagram of d <sup>3</sup> Configuration in Octahedral Coordination . . . . .	79
17.	R Line Emission of Cr <sup>3+</sup> : $\beta$ -Spodumene Glass-Ceramic at 0.25nm Resolution . . . . .	80

<u>FIGURE</u>	<u>TITLE</u>	<u>PAGE</u>
18.	Excitation and Emission Spectra of Cr <sup>3+</sup> : Aluminosilicate Glass (SC04) . . . . .	86
19.	Excitation and Emission Spectra of Cr <sup>3+</sup> : Gahnite Glass-Ceramic (SC04) . . . . .	87
20.	Absorption Spectra of Cr <sup>3+</sup> Doped Aluminosilicate Glass and Gahnite Glass-Ceramic. . . . .	90
21.	Excitation and Emission Spectra of the Opaque Cr <sup>3+</sup> : MAS Glass-Ceramic SC12 . . . . .	92
22.	Composition Diagram of the 10% TiO <sub>2</sub> Plane of the System MgO-Al <sub>2</sub> O <sub>3</sub> -SiO <sub>2</sub> -TiO <sub>2</sub> (Wt%) . . . . .	94
23.	Appearance of Samples SC13-SC18 Following Thermal Gradient - Isothermal Two Step Heat Treatment Schedule . . . . .	96
24.	Appearance of Samples SC20-SC22, SC24-SC26 Following Thermal Gradient - Isothermal Two Step Heat Treatment Schedule. . . . .	99
25.	Absorption Spectra of Cr <sup>3+</sup> : MAS Composition SC22 Before and After Heat Treatment. . . . .	102
26.	Excitation and Emission Spectra of Cr <sup>3+</sup> : MAS Glass SC21 . . . . .	104
27.	Excitation and Emission Spectra of Cr <sup>3+</sup> : Enstatite Glass-Ceramic SC21 . . . . .	105
28.	Excitation and Emission Spectra of Ce <sup>3+</sup> Glass. . . . .	116
29.	Variable Temperature Simulator with LSC Plate-to-Cell Coupling Scheme. . . . .	118
30.	Plate Efficiency as a Function of Temperature. . . . .	119
31.	Total Power Output of LSCs Compared to Photovoltaic Cells. . . . .	120

## I. BACKGROUND

This is the fourth and last Luminescent Solar Concentrator Development Report, covering work performed at Owens-Illinois from 1982 through 1984. The Owens-Illinois program, which commenced in 1978 was organized, as shown in Figure 1, into six major tasks: inorganic glasses, organic systems, dye-polymer stability, theoretical modeling, efficiency optimization, and cost optimization. Most of the work on the various tasks has been documented in earlier Reports<sup>1,2,3</sup>. In general, each of these reports has dealt with a specific set of topics, many of which have not been repeated in later reports. For this reason, we include here, for the sake of completeness, the Table of Contents of these previous reports.

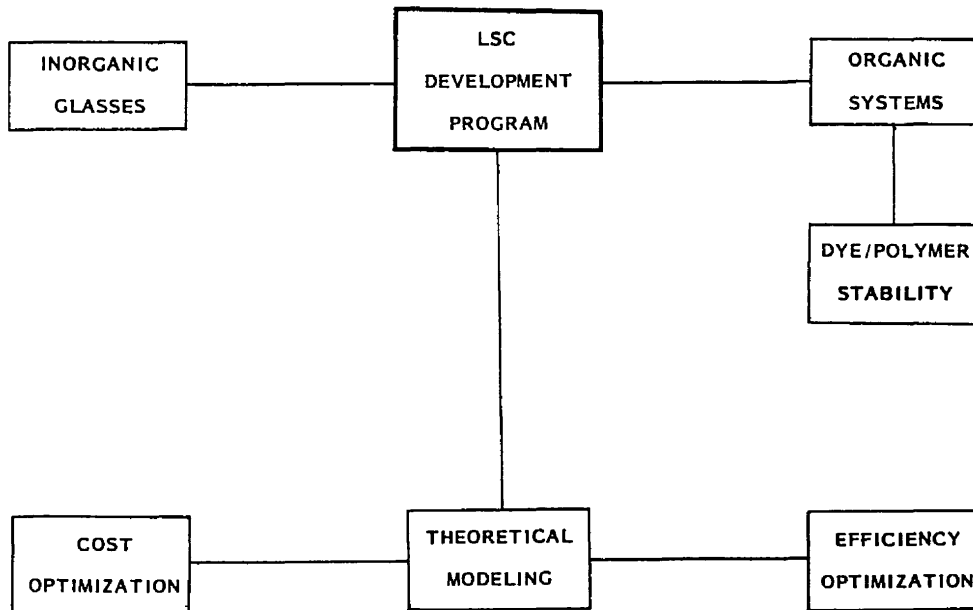


Figure 1. Organization of Owens-Illinois LSC Development Program 1978-1984

Table 1

CONTENTS OF LSC DEVELOPMENT: FINAL REPORT TO SANDIA<sup>1</sup>, 1979

## LSC EFFICIENCY PARAMETERS

New Efficiency Definitions Versus Old Figures of Merit

Collector Efficiency

Cell Efficiency

Plate Efficiency

Effective Concentration Ratio

Relative Edge Power Density

Relative Solar Power Absorption

Plate Luminescence Efficiency

## LSC DISTRIBUTION FACTORS

Edge Luminescence Distribution Factor

Edge Radiant Intensity Distribution

Cell Angular Loss Factors

Relative Coupling Coefficient

## EFFICIENCY MEASUREMENTS

## DEVICE OPERATING TEMPERATURES

## ACRYLIC ABSORPTIVITY

## INORGANIC GLASSES

Glass LSCs

Luminescent Glasses Under Investigation

Uranium Glasses

## OPTICAL COUPLING

## RELATIVE EDGE LUMINESCENCE

## DYE DEGRADATION

## PHOTOVOLTAIC CELL OPTIMIZATION

## ECONOMIC ANALYSIS

## CONCLUSIONS

APPENDIX 1. Plate Absorption Data

APPENDIX 2. Relative LSC Solar Power Transmission Spectra

APPENDIX 3. Photovoltaic Cell Angular Loss Calculations

APPENDIX 4. Photovoltaic Cell Calibration

APPENDIX 5. Measurement of Device Current-Voltage Characteristics

Table 2

CONTENTS TO LSC DEVELOPMENT I: INORGANIC GLASSES  
FINAL REPORT TO SERI<sup>2</sup>, 1981

## INORGANIC GLASS LSC EFFICIENCY ANALYSIS

## QUANTUM YIELD MEASUREMENTS

## PRELIMINARY PROPAGATION EFFICIENCY MEASUREMENTS

Intrinsic Fluorescence Line-Shape Function of  
Uranyl Ion Doped Glasses Pumped by Self-AbsorptionExperimental Measurement of the Propagation  
Efficiency in a Uranyl Ion Doped Glass

## LUMINESCENT URANYL ION DOPED GLASSES

Uranyl Doped Borosilicate Glasses

Uranyl Doped Alkali-Lime Silicate Glasses

Uranyl Doped Phosphate Glasses

## LUMINESCENT MANGANESE(2+) DOPED GLASSES

## LUMINESCENT URANYL - EUROPIUM(3+) ION CODOPED GLASSES

## LUMINESCENT MOLYBDENUM(3+) DOPED GLASSES

## VANADIUM(3+) DOPED GLASSES

## SUMMARY AND CONCLUSION

Table 3

CONTENTS OF LSC DEVELOPMENT-II, FINAL REPORT TO SERI<sup>3</sup>, 1983

THEORY OF LUMINESCENT SOLAR CONCENTRATORS

Derivation of LSC Plate Efficiency Model  
Description of LSC Plate Efficiency Computer Program  
Zeroth Order LSC Plate Efficiency Model  
Dependence of Self-Absorption on Plate Size and Optical Density

INVESTIGATION OF ORGANIC DYE DEGRADATION

Progress To Date  
Required Lightfastness  
Degradation Parameters

Dye Stability  
Fluorescence Stability  
Device Stability  
Edge Luminescence  
Integrated Exposure  
Accelerated Testing

Methodology for LSC Degradation Studies

Preliminary Results of Host Screening Program

OPTICAL PROPERTIES OF LUMINESCENT SPECIES IN SOLID HOSTS

Organic Dyes in Thin Film Polymer Hosts

Fluorescence Depolarization  
Nonradiative Energy Transfer Between Different Dye Species

Preliminary Experiments to Optimize the Coumarin 6 - Rhodamine 101 System Efficiency

Collector Efficiency of DCM

Luminescent Ions in Inorganic Glass Hosts

Mn<sup>2+</sup> and Fe<sup>3+</sup> Doped Glasses

UO<sub>3</sub> Doped Lead and Barium Silicate Glasses

Thin Film Organic Dye UO<sub>3</sub> Doped Glass Hybrid LSC Plates

PROJECTED LSC EFFICIENCY IMPROVEMENTS

Efficiency Model for a Multi-Dye Plate

Estimated Collector Efficiency of a Hypothetical Three Dye Plate that Absorbs to 800 nm

Fluorescence Quantum Yield of the Final Dye  
Radiative Transport Efficiency of the Final Dye  
Conversion Efficiency of the Photovoltaic Cell  
Relative Solar Power Absorption, Stokes Efficiency and Intersystem Energy Transfer  
Quantum Efficiency

Effect of Device Dimensions on Performance of Hypothetical, High Efficiency, Three Dye Plate

Comparison of LSCs with Photovoltaic Modules  
Dependence of Efficiency Model on Plate Dimensions  
Comparison of Calculations and Experimental Results for Plate 59D

Projected Collector Efficiency as a Function of Plate Size for Hypothetical, High Efficiency Three Dye Plate

CONCLUSIONS AND RECOMMENDATIONS

APPENDIX 1. Listing of LSCMODEL Program

APPENDIX 2. Protocol for LSC Degradation Studies

Host Screening

Dye Screening

Liquid Host Studies

Dye/Host Optimization

System Optimization

## II. INVESTIGATION OF THE OPTICAL PROPERTIES OF ORGANIC DYE/POLYMER SOLID SOLUTIONS

### II.A. Introduction

Calculations have demonstrated the feasibility of constructing a 10% device efficiency, multi-dye doped polymer LSC.<sup>3</sup> Realization of this goal, however, requires the identification of a set of dyes that simultaneously satisfy a number of optical and stability criteria:<sup>3</sup> i) The set of dyes should absorb roughly 85% or more of the solar power spectrum up to wavelengths of 800 nm. ii) Radiative or nonradiative energy transfer from one dye species to another dye species (inter-system energy transfer) should approach 90% quantum efficiency. iii) The fluorescence quantum yield of all dyes in the set should be near unity. iv) The Stoke's shift of the ultimate dye (longest wavelength emitting dye) should be large (approximately  $3000\text{ cm}^{-1}$  or greater). And v) the photodegradation lifetime of the dyes should be on the order of 10 years.

This section describes studies designed to identify dye/polymer systems that satisfy the optical property criteria i) through iv). The work was performed simultaneously with the dye degradation studies described in Section III, and the results from one series of investigations was used where appropriate to limit the scope of the other series. The optical properties of dyes with demonstrated poor stability were not comprehensively studied, and conversely the photostabilities of dyes with demonstrated poor optical properties were generally not measured.

The number of commercially available, luminescent dye/polymer systems is too large for a comprehensive survey within the scope of this contract; therefore, attention was primarily, though not exclusively, focused on red to near-IR emitting dyes. This strategy was recommended by three considerations. First, the efficiency of a multi-dye LSC depends more critically on the optical properties of the ultimate dye than on those of the shorter wavelength emitting dyes. Second, it is anticipated that it is generally more difficult to achieve high fluorescence quantum efficiency and photostability in long wavelength emitting dyes. And, finally, the optical properties of long wavelength emitting dyes are least well documented in the literature. Shorter wavelength emitting dyes with adequate optical properties have already been identified. Further optical studies in the shorter wavelength regions were done when dyes with particularly favorable stabilities were identified.

The optical properties of a particular dye/polymer system measured were the absorption spectrum, the corrected emission spectrum, and the fluorescence quantum yield. Quantum yields were determined by a relative front surface emission intensity technique.

Relative fluorescence intensities were first measured among a series of dyes in liquid solution whose absorbance maximum ranged roughly between 350 and 750 nm. This series of dye solutions included the small number of systems for which reliable absolute quantum yields have been measured and reported in the literature. An intercomparison of the liquid solution relative quantum yield measurements, therefore, provided a check of the agreement of our measurements with published values and established the quantum efficiency of a series of solutions that would serve as fluorescence quantum yield secondary standards.



The quantum efficiency of a dye of interest was then measured in a number of thin film polymer host matrices relative to a secondary fluorescence standard with similar absorption and emission spectral distributions. Generally, host polymers were chosen to include polymers in which dyes demonstrated good photostability and chosen to span a reasonable variation in matrix polarity.

## II.B. Measurement Technique and Instrumentation

The absorbance spectra of dyes were recorded with a Cary 17D UV-visible-near IR absorption spectrophotometer. Generally analog recordings were obtained. However, the spectrophotometer has been interfaced to a PDP-11-03 minicomputer, and digitized spectra of promising dye systems were obtained and stored on floppy disk for LSC computer simulation and relative solar absorption calculations.

Emission spectra and fluorescence quantum yields were determined with an SLM 8000 spectrofluorometer modified with an in-house constructed front-surface emission sample holder. Liquid samples were measured in 1 mm path length quartz cuvettes, and thin film samples were measured with the thin film facing the excitation optics. The excitation source was a 450W Xe arc lamp and emission was detected with an EMI 9658RA extended red response S-20 cooled photomultiplier tube. Emission intensity errors due to fluctuations or drift in excitation power were minimized by recording the ratio of the emission signal to the output of a quantum counter which monitored the intensity of the reflected component of the excitation beam passing through a quartz beam splitter. The excitation and emission monochromators were scanned with a microprocessor based controller, and digital electronics were

used for data acquisition, reduction, and storage. Corrected emission spectra (in units proportional to photons per second per unit wavelength interval) were obtained by multiplying technical emission spectra by an emission spectra correction function. The correction function itself was stored in non-volatile memory in the data acquisition microprocessor and was generated by SLM personnel by calibrating the responsivity of the emission monochromator/PMT with an NBS traceable standard quartz halogen lamp.

In order to minimize fluorescence self-absorption, weakly absorbing samples and a front surface emission configuration were used for all emission spectra and quantum yield measurements. All relative quantum efficiencies reported here were obtained from samples with a peak absorbance of less than 0.2. It is estimated that errors from fluorescence self-absorption effects in the integrated front surface emission intensity of 0.2 peak absorbance samples are less than 5%.

The use of weakly absorbing samples also minimized errors in the recorded absorption spectra of the samples. The monochromator in the Cary 17D is between the light source and the sample chamber; therefore, the detector responds to both the transmitted component of the sample beam and fluorescent radiation. In strongly absorbing samples, fluorescence emitted into the solid angle that can strike the detector can approach the intensity of the transmitted beam. However, for absorbances less than 0.2, no absorbance errors associated with fluorescence were observed (monitored by moving the sample from the left side to the right side of the sample chamber and looking for changes in absorbance - the sample chamber width is roughly the same as the distance from the chamber to the detector).

Modifications to the SLM 8000 spectrofluorometer sample chamber to obtain front surface emission are illustrated in Figure 2. Emission is observed normal to the front surface of the sample and collected by a 3" focal length f/6 lens. The excitation monochromator exit slit is imaged on the front surface of the sample with another 3" focal length f/6 lens. The angle of incidence of the axis of the excitation beam was 20°.

The fluorescence quantum yield of samples were determined relative to the quantum yield of a fluorescence standard from the expression<sup>4</sup>:

$$\eta_{f,x} = \eta_{f,s} \cdot \frac{n_x^2}{n_s^2} \cdot \frac{I_s(\lambda_{ex})}{I_x(\lambda_{ex})} \cdot \frac{B_s(\lambda_{ex})}{B_x(\lambda_{ex})} \cdot \frac{E_x}{E_s} \quad (1)$$

where the subscripts x and s refer to the unknown sample and the fluorescence standard, respectively. The index of refraction of the sample media at the average wavelength of luminescence is n, and  $I(\lambda_{ex})$  is the relative intensity of the excitation beam at the excitation wavelength,  $\lambda_{ex}$ . Each of the pair of relative quantum yield measurements (unknown and standard) were obtained at the same excitation wavelength. E is the relative emission intensity integrated over the emission band in arbitrary units proportional to photons per second. Since the recorded corrected emission signal was internally ratioed to the output of the quantum counter monitoring excitation beam intensity, the quotient  $E/I(\lambda_{ex})$  on the right hand side of Equation (1) is simply proportional to the area under the corrected emission spectrum. The integration of earlier corrected emission spectra was done mechanically with a planimeter. However, the spectrofluorometer has now been interfaced to an Apple II+ micro-computer, and later integrations were performed numerically.

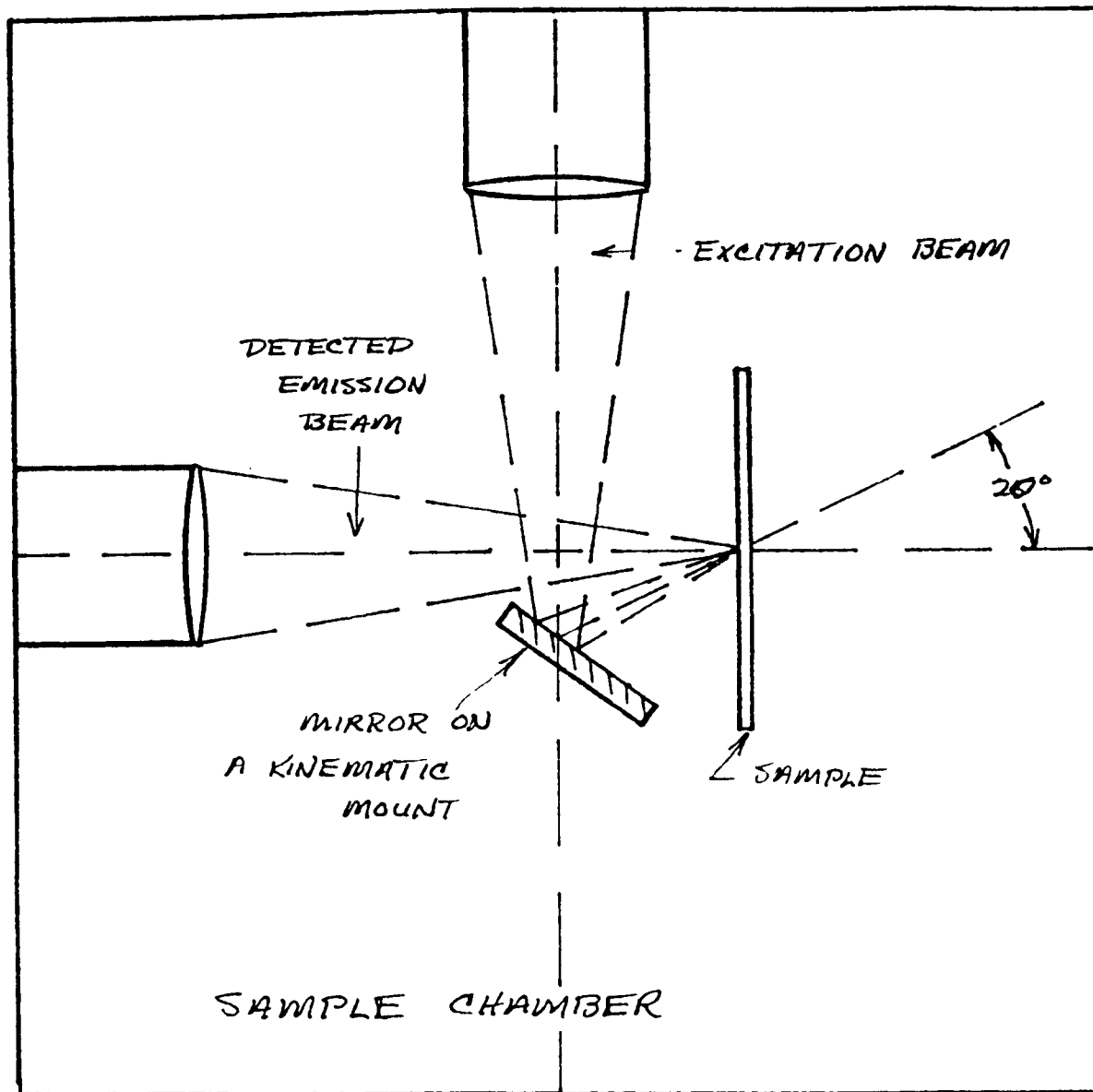


Figure 2. Diagram of the Spectrofluorometer  
Front Surface Emission Sample Chamber

The remaining term on the right hand side of Equation (1) is  $B(\lambda_{\text{ex}})$ , the fraction of excitation power absorbed by the sample, which was determined from:

$$B(\lambda_{\text{ex}}) = 1 - 10^{-\frac{A(\lambda_{\text{ex}})}{\cos \theta_r}} \quad (2)$$

where  $A(\lambda_{\text{ex}})$  is the sample absorbance at the excitation wavelength measured normal to the front surface and  $\theta_r$  is the angle of refraction of the axis of the excitation beam within the sample.

Precautions were taken to minimize two potential sources of error associated with the measurement of  $B(\lambda_{\text{ex}})$ . The thickness of thin films varied typically on the order of 10% over the face of a plate; therefore, care was taken to measure  $A(\lambda_{\text{ex}})$  and  $E$  at the same location on a plate. Furthermore, it was often necessary to choose an excitation wavelength at values where the variation of  $A(\lambda)$  with  $\lambda$  was large. To avoid errors that may have arisen because of a relative miscalibration of the wavelength scales of the Cary 17D monochromator and the SLM 8000 excitation monochromator, the first was calibrated with respect to the second by measuring the absorption and excitation spectra of a  $\text{Eu}^{3+}$  doped soda-lime silicate glass.  $\text{Eu}^{3+}$  has a number of sharp absorption lines (line width at half maximum of approximately 2 nm) between 350 and 600 nm that are also readily observed in the excitation spectrum.

A third, less obvious source of error in the measurement of the quantum yield of samples relative to that of a fluorescence standard, particularly when the absorbance at

$\lambda_{ex}$  or the thickness of unknown and standard differ significantly, is the dependence of measured emission intensity on the relative geometry of the sample and the emission and excitation optics. This potential problem will be discussed with the aid of Figure 3. If  $W_{ex}$  is the width of the excitation beam at the sample (equal to the excitation monochromator slit width times the magnification of the excitation optics), then the volume of the sample excited to luminescence is represented by the vertically ruled area in Figure 3. The excitation beam (and the detected emission beam) is not actually collimated at the sample as illustrated in Figure 3; however, in order to simplify the discussion without greatly sacrificing accuracy, collimation will be assumed.

If each photon emitted from the excitation volume at an angle  $\theta_{em}$  were collected by the emission optics, the emission intensity would be proportional to the relative excitation power absorbed, given by Equation (2). However, the emission optics only collects photons emitted from a volume whose width is  $W_{em}$ , the width of the emission monochromator entrance slit imaged on the sample. Therefore, the sample volume whose emission can be detected (collection volume) is represented by the horizontally ruled area in Figure 3.

It is clear by inspecting Figure 3 that unless the thickness and absorbance at  $\lambda_{ex}$  of the unknown sample and reference standard are the same, the quantum yield of the unknown relative to the standard will not generally be given by Equations 1 and 2. In only two cases do additional complex geometrical factors disappear, and one can be confident that relative quantum yields are given by Equations (1) and (2).

Case a) occurs when the luminescent volume is completely included within the collection volume. In terms of excitation and emission monochromator bandwidths,  $\Delta\lambda_{ex}$  and  $\Delta\lambda_{em}$ , it can be shown that this requires that:

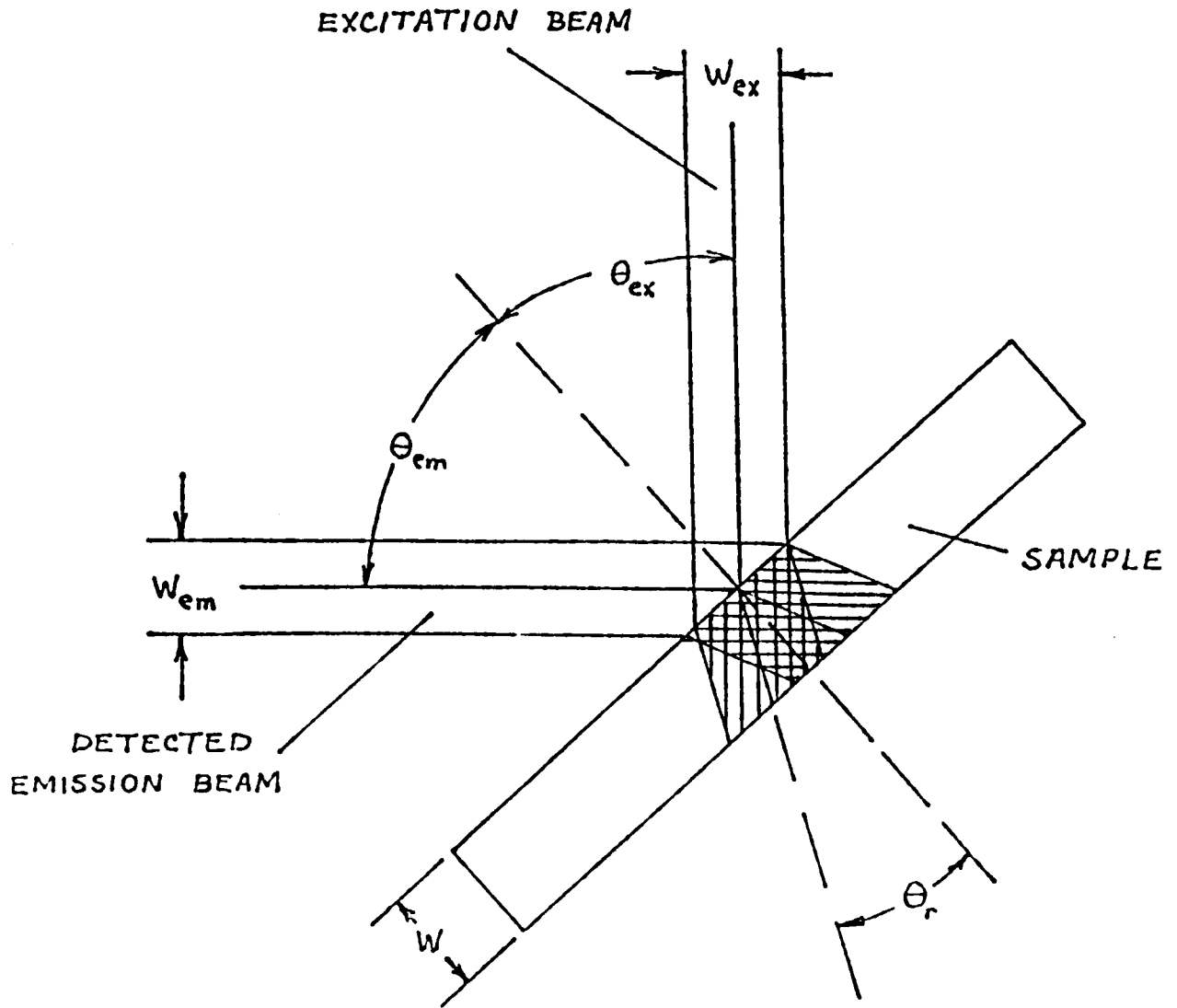


Figure 3.

Diagram of the Relative Geometries of the Sample and the Excitation and Detected Emission Beams

$$\Delta \lambda_{em} > \Delta \lambda_{ex} \frac{\cos \theta_{em}}{\cos \theta_{ex}} + \frac{WK}{Mn} \cos \theta_{em} (\sin \theta_{ex} + \sin \theta_{em}) \quad (3)$$

where K is the reciprocal linear dispersion of the monochromators (2 nm/mm), M is the magnification of the excitation and emission optics (both 1.5), and n is the index of refraction of the sample. Other symbols are defined in Figure 3.

Case b) occurs when the collection volume is completely included within the luminescent volume. The requirements are then:

$$\Delta \lambda_{ex} > \Delta \lambda_{em} \frac{\cos \theta_{ex}}{\cos \theta_{em}} + \frac{WK}{Mn} \cos \theta_{ex} (\sin \theta_{ex} + \sin \theta_{em}) \quad (4)$$

The requirements imposed by Equations (3) or (4) are uncomfortably restrictive for realistically thick samples when  $\theta_{ex}$  and  $\theta_{em}$  are large. Therefore, the front surface emission sample holder was constructed with  $\theta = 20^\circ$  and  $\theta_{em} = 0^\circ$ . Equations (3) and (4) (assuming  $n = 1.5$ ) then reduce to:

$$\text{Case a): } \Delta \lambda_{em} > 1.06 \Delta \lambda_{ex} + 0.30w \quad (5)$$

$$\text{Case b): } \Delta \lambda_{ex} > 0.94 \Delta \lambda_{em} + 0.29w \quad (5)$$

when  $\Delta \lambda$  is measured in nm and W is measured in mm. The quantum yield measurements described below in Sections II.D. and II.E. were all obtained with an emission monochromator bandpass at least twice the excitation monochromator bandpass (all satisfy the Case a) criterion).



A final concern in the measurement of relative quantum efficiencies, particularly for dyes in a thin film host, is the influence of fluorescence anisotropy. Earlier measurements of the fluorescence polarization anisotropy of coumarine-6 in a CAB thin film showed that depolarization is near complete (anisotropy parameter  $r \approx 0$ ) in heavily doped films (coumarin-6 concentration  $\approx 10^{-2}$  mol/L) and incomplete ( $r \approx 0.3$ ) in more lightly doped films (concentration  $\approx 10^{-3}$  mol/L).<sup>3</sup> The depolarization mechanism in heavily doped films was assigned to rapid nonradiative energy transfer. The polarization anisotropy of dyes in low viscosity solvents is near zero because of rapid rotational depolarization. The thin film samples used for quantum yield measurements were lightly doped to minimize fluorescence self-absorption; therefore, it was anticipated that fluorescence intensity and polarization would be anisotropic.

Fluorescence anisotropy effects were determined by the formalism of Cehelnik, Mielenz, and Velapoldi.<sup>5</sup> One defines the three parameters F, G, and D as follows: F is the ratio of vertically to horizontally polarized excitation photon flux density at the peak excitation wavelength; G is the ratio of sensitivities of the emission monochromator/detection system to vertically divided by horizontally polarized components at the peak emission wavelength; and D is a quantity related to the anisotropy parameter by:

$$D = \frac{1 + 2r}{1 - r} \quad (7)$$

These three parameters may be evaluated from experimental measurements via the set of coupled equations:

$$\frac{R_V^V(\alpha)}{R_H^V(\alpha)} = DG \quad (8a)$$

$$\frac{R_H^V(\alpha)}{R_V^H(\alpha)} = F/G \quad (8b)$$

$$\frac{R_H^H(\alpha)}{R_V^V(\alpha)} = \{ \cos^2 \alpha + (1/D) \sin^2 \alpha \} / FG \quad (8c)$$

where  $R_j^i(\alpha)$  is the spectrofluorometer response with polarizers in the excitation and emission beam paths,  $i$  and  $j$  denoting the orientation of excitation and emission polarizers, respectively (V = vertical, H = horizontal), and  $\alpha$  is the internal angle between excitation and detected emission beams.

Cehelnik et al. have shown that the ratio of fluorescence intensity measured at  $\alpha$ ,  $I(\alpha)$ , to the intensity averaged over all angles,  $I_0$ , both measured without polarizers in excitation or emission beam paths is given by

$$\frac{I(\alpha)}{I_0} = \frac{FG(1 + 2r) + G(1 - r) + F(1 - r) + \{ (1 - r) + 3r \cos^2 \alpha \}}{(1 + F)(1 + G)} \quad (9)$$

Emission spectra reported here were all recorded without a polarizer in the excitation path and with a vertical component transmitting Glan-Thompson polarizer in the emission beam path.

Under these instrumental conditions, it can easily be shown that

$$\frac{I_{0,u}}{I_{0,s}} = \frac{I_{V,u}(\alpha)}{I_{V,s}(\alpha)} \times \frac{(F+1) + r_s(2F-1)}{(F+1) + r_u(2F-1)} \quad (10)$$

where  $I_V(\alpha)$  is the intensity at  $\alpha$  of the vertically polarized fluorescence component, and the subscripts u and s refer to the unknown sample and the fluorescence standard, respectively.

Clearly, the left-hand side (LHS) of equation (10) is the ratio of fluorescence intensities required for substitution into equation (1). The first term of the right-hand side (RHS) is the ratio of fluorescence intensities measured, and the second term of the RHS represents a fluorescence anisotropy correction factor. If the anisotropy parameter of the dye and the fluorescence standard are identical, the correction factor is unity. Values of the correction factor maximally different from unity occur when the fluorescent standard is a low viscosity solution ( $r_s = 0$ ) and the unknown dye is a lightly doped thin film sample ( $r_u = 0.2 - 0.3$ ). The value of F over a range of emission wave-lengths from the green to the red spectral regions in the SLM 8000 spectrofluorometer is roughly 0.3. Therefore, one may anticipate fluorescence anisotropy correction factors for thin film samples measured relative to liquid solution fluorescence standards of 1.06 - 1.10.

It was, of course, possible to measure the anisotropy parameter of each thin film sample studied in order to make the fluorescence anisotropy correction to the measured quantum yield. However, because the magnitude of the correction is less than the 15% uncertainty in the measured quantum yield

that arises from other factors, the fluorescence anisotropy correction factor was ignored.

## II.C. Structural Classification of Dyes Studied

Central to chemistry is the belief that physical and chemical properties can be understood and ultimately predicted on the basis of molecular structure. Unfortunately, the present state of understanding of the optical and energy transfer properties of organic dyes does not allow one to make more than general qualitative statements about the relationship between dye structure and those optical properties that are crucial to the development of a high efficiency LSC.

The principal purpose of this section is to catalog the molecular structure of the large number of dyes that have been investigated for this report, and to classify the dyes according to molecular structure. Where previous studies reported in the literature have illuminated structure-property relationships that are pertinent to the present investigation, these will be reviewed.

The majority of the dyes studied here are commercially available laser dyes. A lesser number of luminescent dyes that have been commercially developed principally for display or decorative applications have also been studied. Because they are examples of a large number of structural types, they have been grouped below under miscellaneous dyes. Also included in this group are a number of proprietary dyes for which structural information has not been released.

### II.C. 1. 7-Aminocoumarins

Derivatives of 7-aminocoumarin are the most important

group of laser dyes emitting in the blue and green regions of the spectrum. A number of derivatives have been reported with quantum efficiencies exceeding 0.70 and with photochemical stability "unmatched...by other dyes which lase at this wavelength."<sup>6</sup>

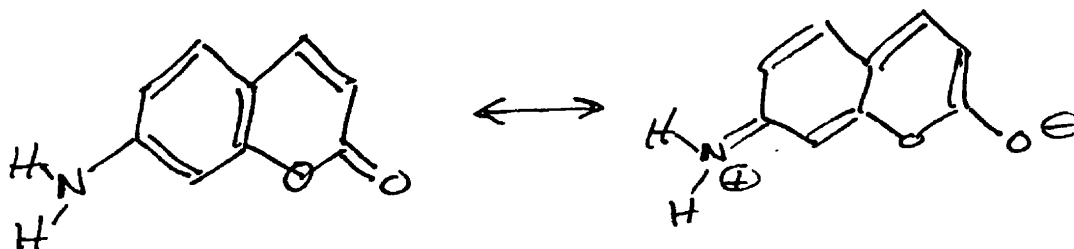


Figure 4 - 7-Aminocoumarin

The ground electronic state is characterized principally by the right mesomeric form illustrated in Figure 4, and the excited state by the more polar left mesomeric form. The large difference in ground and excited state dipole moments causes a large Stokes' shift which increases in more polar solvents. The wavelength of the absorption maxima also increases in more polar solvents.<sup>7</sup> Stabilization of the more polar excited state by alkylating the amino group or substituting ring positions, particularly with heteroatoms or trifluoromethyl groups, causes a shift in absorption and emission toward the red.<sup>8</sup>

The amino group has been shown to play an important role in the rate of nonradiative relaxation. Di-N-alkyl substituted coumarins have reduced quantum yields in liquid solvents. It has been suggested that the electron releasing character of alkyl groups reduces the double bond nature of the N-benzene ring bond in the excited state, and the resultant greater torsional mobility of the amino group enhance nonradiative transfer. This is consistent with observation that coumarins with amino groups rigidized within saturated ring systems show high fluorescence quantum efficiencies.<sup>8,9</sup>

The structure of the 7-aminocoumarins investigated for this report are presented in Table 4.

## II.C. 2. Rhodamines

The rhodamines are a class of xanthenes with amino end groups and a carboxyphenyl group in the 9-position. Rhodamine-110 may be considered the prototype of the series.

The rhodamines are the most important group of red emitting laser dyes.

The transition moment of the main absorption band is parallel to the long axis of the molecule. Since there is no static dipole moment in either the ground or excited state along this axis, the Stokes' shift is small (typically on the order of 20 nm), and there is little variation in the wavelength of absorption or fluorescence maxima with solvent polarity. Electron releasing substituents, particularly on the amino groups, shift the absorption and emission maxima to the red.<sup>7</sup>

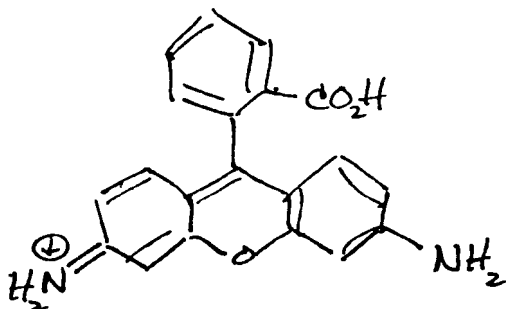
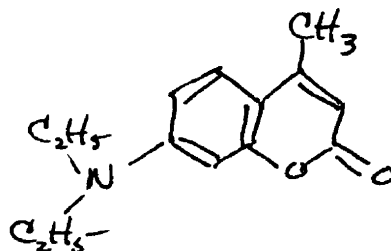


Figure 5 - Rhodamine-110

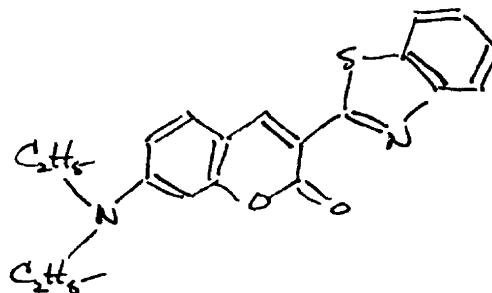
Table 4  
Molecular Structure of 7-Aminocoumarins

Eastman Name	Exciton Name	Structure
--------------	--------------	-----------

Coumarin-1 Coumarin-460

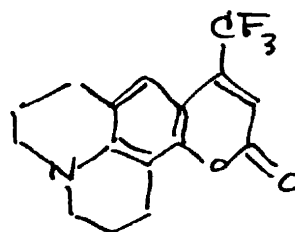


Coumarin-6 Coumarin-540



Coumarin-153

Coumarin-540A



Substituents on the amino group affect the nonradiative transition rate in a manner, and apparently by a mechanism, that is similar to that operating in 7-aminocoumarins. Rhodamines with two alkyl substituents on each nitrogen have fluorescence quantum efficiencies that vary strongly with solvent and temperature. Rhodamines with amino groups rigidized within rings have temperature insensitive, near unity quantum efficiencies.<sup>7,10</sup>

The structure of rhodamines studied here can be found in Table 3.

### II C. 3. Oxazines

The oxazines are a class of dyes formally related to the rhodamines by the replacement of the central carbon atom with a nitrogen. Oxazine 118 may be taken as the prototype of the series. The central N-atom acts as a sink for  $\pi$ -electron density and causes a shift in the absorption and emission maxima relative to the rhodamines by roughly 100 nm toward the red. The lower excited state energy favors nonradiative relaxation, and the oxazines generally as a class have lower fluorescence quantum yields than do the rhodamines. Drexhage, however, claims that oxazine dyes are photochemically much more stable than rhodamines.<sup>6</sup>

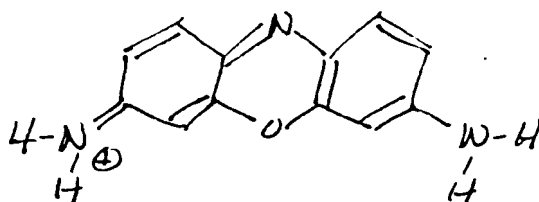
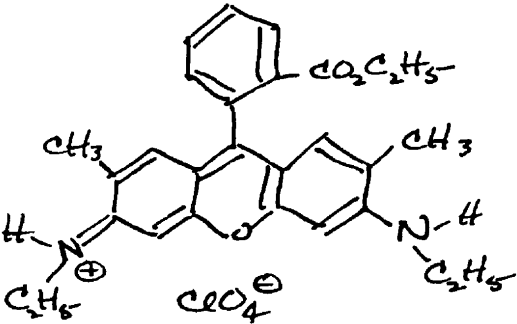
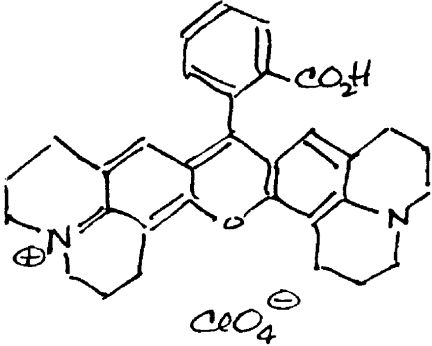
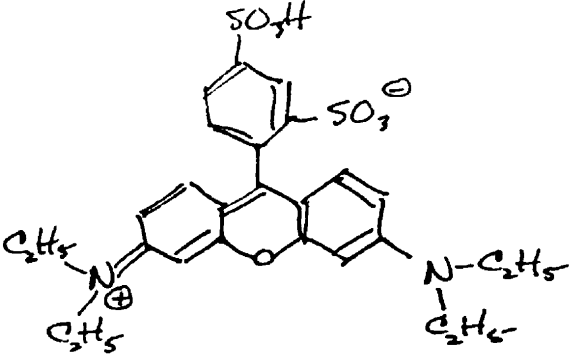


Figure 6 - Oxazine 118



Table 5

Molecular Structure of Rhodamines

Eastman Name	Exciton Name	Structure
Rhodamine-6G	Rhodamine-590	 <p>The structure shows a central xanthene ring system. At the 6-position, there is a diethylamino group (N(CH<sub>2</sub>CH<sub>3</sub>)<sub>2</sub>) with a positive charge. At the 3-position, there is another diethylamino group (N(CH<sub>2</sub>CH<sub>3</sub>)<sub>2</sub>) with a positive charge. At the 4-position, there is a methyl group (CH<sub>3</sub>). At the 5-position, there is another methyl group (CH<sub>3</sub>). At the 10-position, there is a phenyl ring substituted with an ethyl ester group (CO<sub>2</sub>C<sub>2</sub>H<sub>5</sub>). At the 9-position, there is a carboxylate group (CO<sub>4</sub><sup>⊖</sup>).</p>
Rhodamine-101	Rhodamine-640	 <p>The structure shows a central xanthene ring system. At the 6-position, there is a diethylamino group (N(CH<sub>2</sub>CH<sub>3</sub>)<sub>2</sub>) with a positive charge. At the 3-position, there is another diethylamino group (N(CH<sub>2</sub>CH<sub>3</sub>)<sub>2</sub>) with a positive charge. At the 4-position, there is a methyl group (CH<sub>3</sub>). At the 5-position, there is another methyl group (CH<sub>3</sub>). At the 10-position, there is a phenyl ring substituted with a carboxylic acid group (CO<sub>2</sub>H). At the 9-position, there is a carboxylate group (CO<sub>4</sub><sup>⊖</sup>).</p>
Sulforhodamine-B	Kiton Red 620	 <p>The structure shows a central xanthene ring system. At the 6-position, there is a diethylamino group (N(CH<sub>2</sub>CH<sub>3</sub>)<sub>2</sub>) with a positive charge. At the 3-position, there is another diethylamino group (N(CH<sub>2</sub>CH<sub>3</sub>)<sub>2</sub>) with a positive charge. At the 4-position, there is a methyl group (CH<sub>3</sub>). At the 5-position, there is another methyl group (CH<sub>3</sub>). At the 10-position, there is a phenyl ring substituted with a sulfonic acid group (SO<sub>3</sub>H) and a sulfonate group (SO<sub>3</sub><sup>⊖</sup>). At the 9-position, there is a carboxylate group (CO<sub>4</sub><sup>⊖</sup>).</p>

The transition moment is again parallel to the long axis of the molecules, and there is no static dipole moment along this axis in either the ground or excited state. Therefore, the Stokes' shift is small (typically about 30 nm).

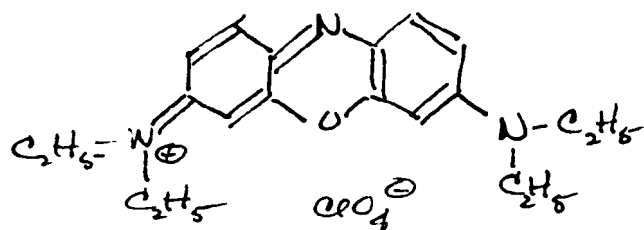
Internal rotation of the terminal amino groups affect quantum yields in a way that is again very similar to the effect observed in 7-aminocoumarins and rhodamines. If one or both amino groups is fully alkylated, the quantum yields are low in low viscosity solvents (ethanol) and somewhat higher, but still low, in high viscosity solvents (ethylene glycol). If, however, each amino group carries at least one H, a multi-phonon process involving N-H vibrations seems to be the principal nonradiative relaxation mechanism. Oxazines of this structural type have quantum efficiencies in methanol or ethanol in the range 0.5-0.7. In deuterated alcohol solution, H-D exchange results in quantum efficiencies increased to the range 0.8-0.9.<sup>11</sup>

The molecular structure of oxazines that have been investigated here are presented in Table 6.

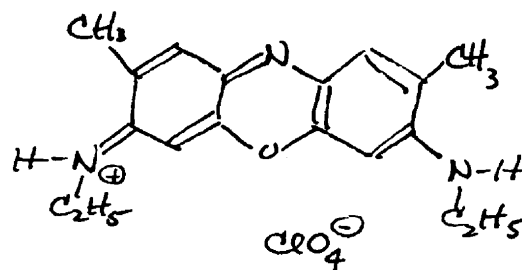
Table 6  
Molecular Structure of Oxazines

Eastman Name	Exciton Name	Structure
-----------------	-----------------	-----------

Oxazine 1	Oxazine 725	
-----------	-------------	--

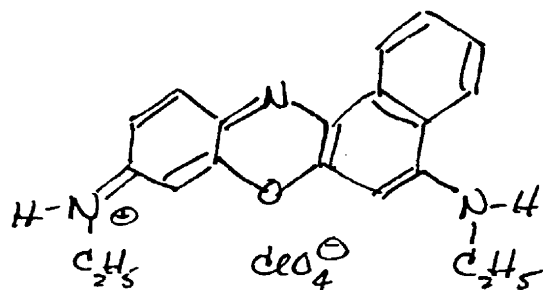


Oxazine 4



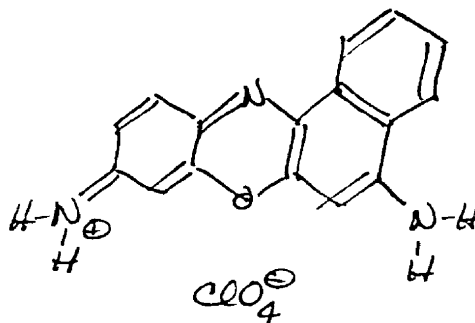
Oxazine 170

Oxazine 720

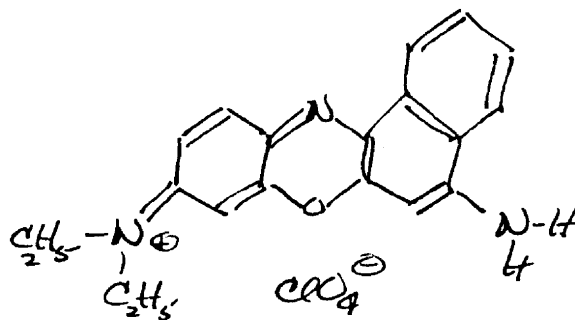


Cresyl  
Violet

Cresyl  
Violet 670



Nile Blue Nile Blue  
690



Oxazine 750 Proprietary Structure

#### II. C. 4. Styryl Dyes

The group of arylidene laser dyes loosely classified under this heading are all formally derivatives of p-dimethylaminostyrene. The structure of the dyes investigated here are given in Table 7.

DCM was the first member of the group commercially available. It is characterized by broad absorption and emission bands (emission is in the red region of the spectrum) separated by a large Stokes' shift (160 nm in DMSO). A quantum efficiency of 0.71 in DMSO has been reported.<sup>12</sup> The Stokes' shift is considerably diminished when DCM is cast in PMMA.<sup>13</sup>

The spectral properties of other members of the group are broadly similar, with absorption and emission shifted farther to the red. Quantum yields of roughly 0.7 in ethylene glycol have been reported for LDS 730, LDS 750, and LDS 820.<sup>14</sup>

The most distinctive structural feature of the styryl dyes is the dissimilarity of the two aromatic ring systems that are linked by the polymethine chain. This suggests that the dipole moment in the ground and excited states are considerably different, and may account for the large Stokes' shift observed in polar liquid solution and the reduced Stokes' shift observed in a rigid medium.<sup>15</sup>

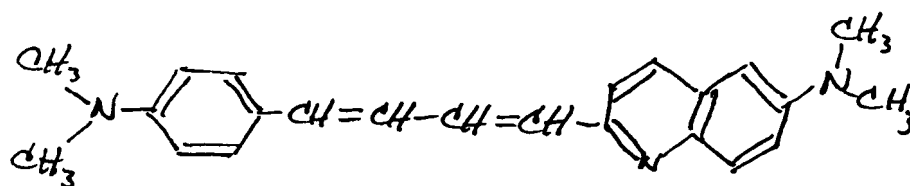
#### II.C. 5. Carbocyanines

Members of this group are among the few dyes known that are relatively stable and fluoresce well in the near-infrared region of the spectrum. Structurally, the majority of the dyes are composed of two identical heteronuclear aromatic rings

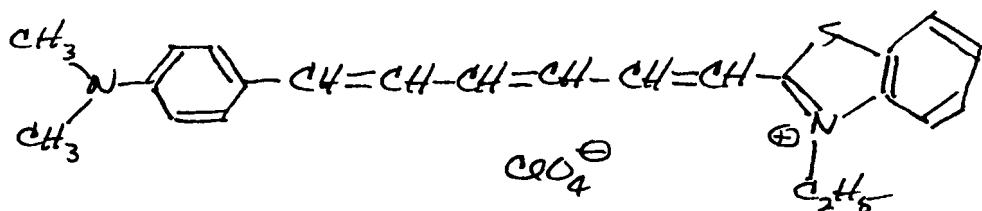
Table 7  
Molecular Structure of Styryl Dyes

Exciton Name	Name	Alternate	Structure
DCM			
LD688			
LDS730 Styryl-6			
LDS750 Styryl-7			

LDS751 Styryl-8



LDS820 Styryl-9



LDS798 Styryl-11

Structure unknown

symmetrically linked by a polymethine chain with an odd number of C-atoms. If A represents an aromatic nucleus, the group may be represented by  $A=CH(-CH=CH)_n-A$ . The earliest synthesized members of the group were derivatives of quinoline; therefore, dyes in which A is a quinoline nucleus and  $n = 1$ , are called in common nomenclature carbocyanines. The dicarbocyanines, tricarbocyanines, etc. are higher vinylene homologs with  $n = 2, 3, \dots$  etc. Numerous carbocyanine dyes have since been prepared with bases other than quinoline. If A represents benzothiazole, benzoxazole, or indole, the dyes are named, respectively, thiocarbocyanines, oxacarbocyanines, and indocarbocyanines.<sup>16</sup>

Of the large number of red to near-IR emitting carbocyanine dyes commercially available, to date we have only investigated four. Their structures may be found in Table 8.

The carbocyanines make an interesting comparison with the styryl dyes. Both groups are members of the larger class of polymethine dyes. However, the carbocyanines, unlike the styryl dyes, are symmetric along their long axis and (like the rhodamines and oxazines) have small Stokes' shifts.

## II.C. 6. Miscellaneous Dyes

The molecular structure (where known) of those dyes that have been studied and which do not fall conveniently into one of the previous classes are presented in Table 9. Also presented (where known) are the Color Index name and the Color Index number of each dye. The dyes are listed in order of increasing wavelength of maximum emission.

It should be noted that BASF Thermoplast Fluorescent

Table 8

## Molecular Structure of Carbocyanines

Name

Structure

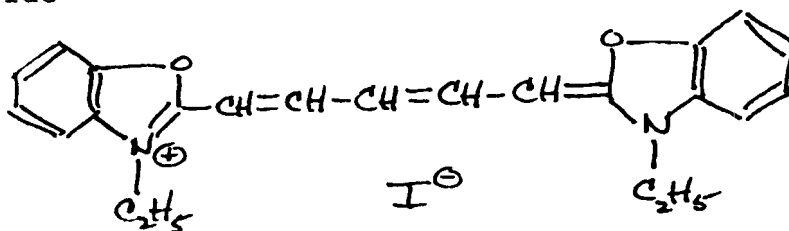
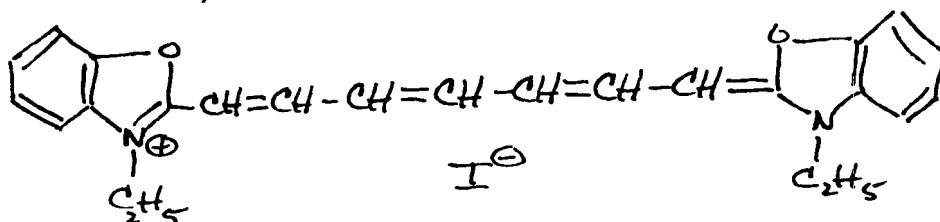
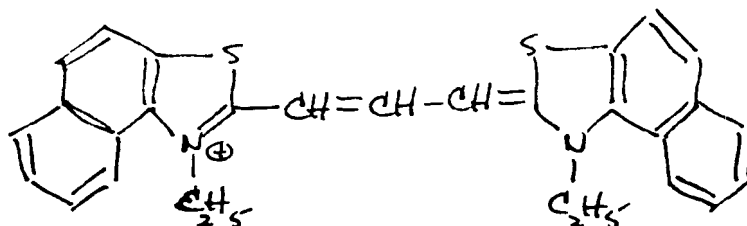
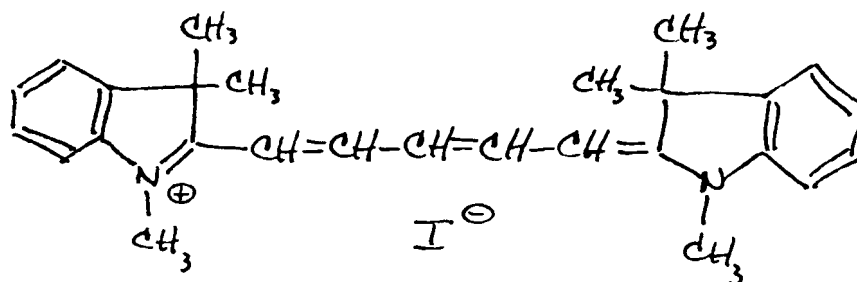
DODC (3,3'-diethyloxadicyanin  
iodide)DOTC (3,3'-diethyloxatri-  
cyanin iodide)3,3'-Diethyl-4,5,4',5'-dibenz-  
thiacarbocyanin iodideHIDC (1,1',3,3,3',3'-Hexamethyl-  
indodicarbocyanin iodide)

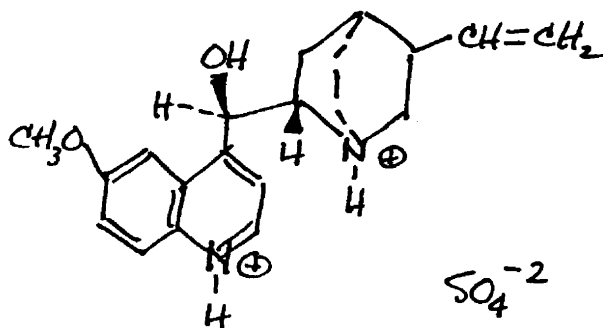


Table 9

Molecular Structure of Miscellaneous Dyes

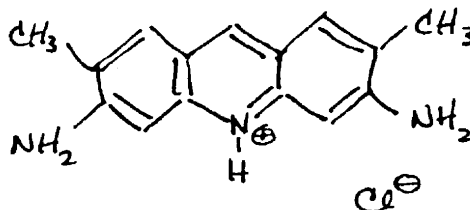
Name (C.I. Name - C.I. Number)	Structure
-----------------------------------	-----------

Quinine Sulfate



Mobay Macrolex  
Fluorescent Yellow 10GN  
(Solvent Yellow 160)

A coumarin of unknown structure

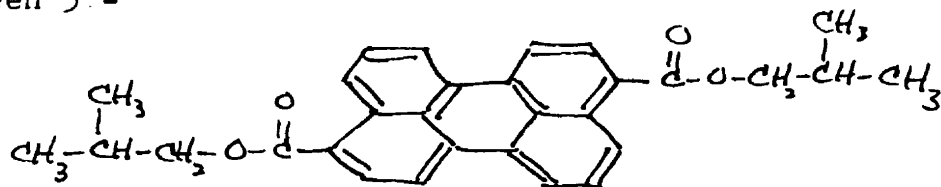


Acridine Yellow

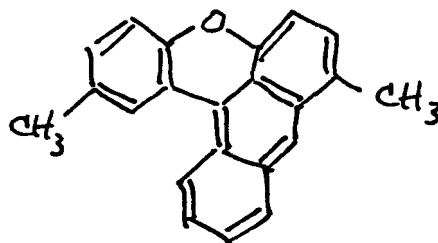
Hoechst Hostasol Yellow  
8G (Solvent Yellow 126)

A xanthene of unknown structure

BASF Fluorol Green Gold  
084 (Solvent Green 5.-  
C.I. No. 59075)



BASF Fluorol Yellow 088  
(Solvent Green 4 - C.I.  
No. 45550)



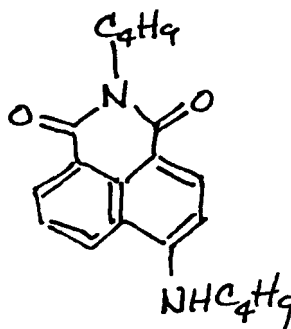
Hoechst Hostasol Yellow  
3G (Solvent Yellow 98)

A xanthene of unknown structure

Day-Glo Brilliant Yellow

Unknown structure

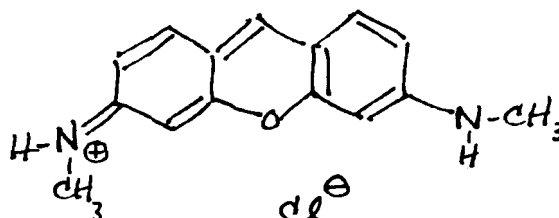
Exciton Fluorol 555



Day-Glo Brilliant Orange

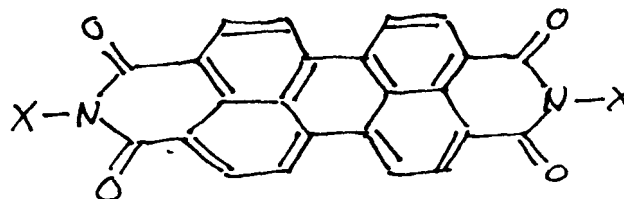
Unknown structure

Acridine Red



BASF Thermoplast Fluorescent Orange 274 (Solvent Orange 90)

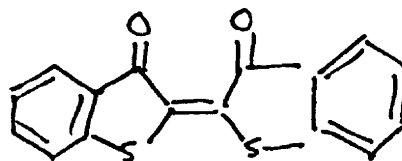
Absorption and emission spectra suggests that the dye is a derivative of 3,4,9,10-perylenebis (dicarboximide)



Hoechst Hostasol Red GG  
(Solvent Orange 63)

A thioxanthene of unknown  
structure

Hoechst Hostasol Red 5B or  
Mobay Macrolex Fluorescent  
Red 5B (Vat Red 41 - C.I.  
No. 73300)



Orange 274 is apparently a commercially available member of a series of experimental perylene dyes that have been recently reported and which have near unity quantum efficiency and high photostability.

#### II. D. Spectral Properties and Quantum Yield of Dyes in Liquid Solution

Quantum yields of dyes in liquid solution were measured in order to check the accuracy of our measurement technique and to provide a set of secondary fluorescence standards with emission maxima extending from the blue to the far red.

Relative quantum yields (the ratio of the quantum efficiency of a sample dye to that of a standard dye) were determined by the relative fluorescence intensity method described in Section II.B. Emission intensities were measured from solutions in 1 mm thick quartz cuvettes at concentrations such that the peak dye absorbance/mm was 0.2. Typically, this required dye concentrations of  $5 \times 10^{-6}$  -  $3 \times 10^{-5}$  mol/L. A pair of solutions involved in any individual relative quantum yield measurement could be selected whenever the two absorption spectra sufficiently overlapped to allow excitation of both solutions at the same wavelength. A single 1 mm thick uranyl glass sample was also involved in the measurements.

The first series of measurements were designed primarily to assess the accuracy of our experimental technique. The quantum yield of a number of dyes in liquid solution that absorb and fluoresce in spectral regions of interest to our program have been reported in the literature. Literature values determined by techniques that should yield an accuracy of  $\pm 10\%$  or less are summarized in Table 10. Relative quantum yields involving all of the dyes in Table 10 were then measured

Table 10

## Fluorescence Quantum Yields of Dyes Reported in the Literature

Dye	Solvent	Technique <sup>a)</sup>	$\lambda_{em}$	$\eta_f$	Ref. <sup>b)</sup>
Quinine Sulfate	EtOH	1	450	0.546	1
Coumarin 1	EtOH	2	460	0.64	2
Acridine Yellow	EtOH	2	517	0.47	2
Fluorol 555	MeOH	3	553	0.68	3
Rhodamine 6G	EtOH	5	558	0.95	8
Rhodamine 6G	EtOH	4	569	0.94	4
Rhodamine 6G	EtOH	2	575	0.88	2
Rhodamine 101	EtOH	5	588	0.96	8
Cresyl Violet	EtOH	2	623	0.505	2
Cresyl Violet	EtOH	3	648	0.56	5
Cresyl Violet	MeOH	2,3,5	638	0.545	6
Cresyl Violet	MeOH	3	654	0.57	5
DCM	DMSO	5	644	0.71	7
Oxazine 4	EtOH	3	651	0.62	5
Oxazine 170	EtOH	3	675	0.60	5
Oxazine 1	EtOH	3	693	0.11	5
Nile Blue	EtOH	3	702	0.27	5

- a)
- 1 - Spectroradiometry
  - 2 - Photomicrocalorimetry
  - 3 - Thermal Lens
  - 4 - Thermal Expansion
  - 5 - Relative Fluorescence Intensity

- b)
1. R. A. Velapoldi and K. D. Mielenz, "A Fluorescence Standard Reference Material: Quinine Sulfate Dihydrate," NBS Special Publication 260-64, U.S. Government Printing Office, Washington, 1980.
  2. John Olmsted III, J. Phys. Chem. 83, 2581 (1979).
  3. Michael L. Lesiecki and J. Michael Drake, Appl. Optics 21, 557 (1982).
  4. A. V. Butenin, B. Ya. Kogan, and N. V. Gundobin, Opt. Spectrosc. (U.S.S.R) 47, 568 (1980).
  5. Rudiger Sens and Karl H. Drexhage, J. Lumin. 24/25, 709 (1981).
  6. Douglas Magde, James H. Brannon, Teresa L. Cremers, and John Olmsted III, J. Phys. Chem. 83, 696 (1979).
  7. P. R. Hammond, Opt. Commun. 29, 331 (1979).
  8. R. F. Kubin and A. N. Fletcher, J. Lumin. 27, 455 (1982).

here, and the reliability of both our values and the literature values were assessed by the consistency of the two sets.

It was observed that our measurements were in poor agreement with the quantum yields in the literature for Fluorol 555 (MeOH), DCM (DMSO), and Nile Blue (EtOH). The quantum yield of Nile Blue in ethanol (0.27) was determined by Sens and Drexhage by the thermal blooming method<sup>11</sup>. The technique is essentially a calorimetric method and liable to large percentage errors when applied to low luminescence efficiency dyes<sup>17</sup>. Therefore, it is felt that the quantum yield of Nile Blue reported by Sens and Drexhage may have an uncertainty on the order of  $\pm 50\%$ . For the same reason the reported quantum yield of oxazine 1 (0.11) was considered unreliable, although agreement with our measurements was very good. The quantum yield of purified DCM, in DMSO (0.71) was determined by Hammond by the relative fluorescence intensity method<sup>12</sup>. Hammond claimed that DCM from a commercial source showed an inferior dye laser performance due to the presence of an impurity. Our measurements were performed on DCM as received from the vendor (Exciton), and impurities in our samples may account for the lower quantum efficiencies reported here. The quantum efficiency of Fluorol 555 in methanol (0.68) was measured by Lesiecki and Drake by the thermal blooming method<sup>18</sup>. We both used samples as received (Exciton) and the source of the poor agreement between our two sets of measurements is unknown.

Quantitative agreement between our measurements and the literature values was evaluated by performing a linear least squares analysis which yielded quantum efficiencies,  $\eta_f^{ls}$ , minimizing the residuals in both our relative measurements,  $(\eta_f^x / \eta_f^s)^{exp}$ , and the absolute measurements from the literature,  $\eta_f^{lit}$ . The literature values for Fluorol 555, DCM, Nile Blue, oxazine 1, and Olmsted's value for rhodamine 6G<sup>19</sup> were not utilized. The latter because of its relatively poor agreement with other literature values<sup>5,20</sup>. The fluorescence

quantum yields from the least squares analysis are presented in Table 11, and the experimental measurements used in the analysis together with their residuals are presented in Table 12.

Table 11  
Fluorescence Quantum Yields from Least Squares Analysis

Dye Name (Solvent)	Abrev <sup>a)</sup>	$\lambda_{em}^{max}$	$n_f$ <sup>b)</sup>		
			I	II	III
Coumarin 1 (EtOH)	C-1	449	0.681	0.606	
Quinine Sulfate (Perchloric Acid)	QS	453	0.622	0.551	
Acridine Yellow (EtOH)	AY	496	0.509	0.484	
Coumarin 6 (EtOH)	C-6	505	0.796	0.740	
Brilliant Yellow (EtOH)	BY	523	0.684	0.622	
Coumarin 153 (EtOH)	C-153	532	0.521	0.446	
Fluorol 555 (EtOH)	F-555	534	0.555	0.504	
Fluorol 555 (MeOH)	F-555(M)	542	0.447	0.431	
Rhodamine 6G (EtOH)	R-6G	555	0.937		0.969
Acridine Red (EtOH)	AR	568	0.680		0.703
Sulforhodamine B (EtOH)	SR-B	576	0.653		0.665
Rhodamine 101 (EtOH)	R-101	591	0.936		0.952
DODC Iodide (EtOH)	DODC	606	0.414		0.421
DCM (EtOH)	DCM	622	0.429	0.363	0.443
DCM (DMSO)	DCM(D)	650	0.534	0.432	0.585
Oxazine 4 (EtOH)	OX-4	636	0.567		0.579
Cresyl Violet (EtOH)	CV	626	0.537		0.555
Cresyl Violet (MeOH)	CV(M)	626	0.516		0.524
Oxazine 170 (EtOH)	OX-170	645	0.585		0.595
LD 688 (EtOH)	LD688	663	0.190		0.197
Nile Blue (EtOH)	NB	666	0.126		0.130
Oxazine 1 (EtOH)	OX-1	668	0.119		0.123
LD 700 (EtOH)	LD700	679	0.320		0.331
Oxazine 750 (EtOH)	OX-750	684	0.196		0.203
0.11 Mol% UO <sub>2</sub> Doped Borosilicate Glass	UG	536	0.611	0.556	

a) Abbreviation of dye name used in Table 12.

b) I, II, and III are results of fit to data of all dyes, of blue-yellow emitting dyes, and of red emitting dyes, respectively.

Table 12

Experimental Fluorescent Quantum Yield Data  
Used in the Least Squares Analysis

Data from the Literature						
Dye	$\lambda_{em}^{max}$	Ref <sup>a)</sup>	$\eta_f^{lit}$	Residuals <sup>b)</sup>		
				I	II	III
C-1	449		0.64	-0.041	0.034	
QS	453		0.544	-0.082	-0.011	
AY	496		0.47	-0.039	-0.014	
R-6G	555		0.95	0.013		-0.019
R-6G	555		0.94	0.003		-0.029
R-101	591		0.98	0.044		0.028
R-101	591		0.96	0.024		0.008
CV	626		0.505	-0.032		-0.050
CV	626		0.56	0.024		0.005
CV(M)	626		0.55	0.034		0.026
OX-4	636		0.62	0.053		0.041
OX-170	645		0.60	0.015		0.005
Data Measured Here						
Sample Dye	Ref. Dye	$\lambda_{ex}$	$(\eta_f^x / \eta_f^s)^{exp}$	Residuals <sup>b)</sup>		
				I	II	III
C-1	QS	360	1.103	0.005	0.001	
C-1	QS	360	1.114	0.012	0.007	
C-1	QS	360	1.111	0.010	0.006	
C-1	QS	360	1.146	0.031	0.025	
C-1	QS	360	1.053	-0.026	-0.026	
C-1	QS	360	1.040	-0.035	-0.033	
DCM(D)	QS	360	0.824	-0.022	0.022	
DCM(D)	QS	360	0.824	-0.022	0.022	
C-153	QS	375	0.737	-0.063	-0.040	
C-153	C-1	380	0.738	-0.019	0.001	
C-153	C-1	390	0.762	-0.002	0.016	
C-153	C-1	390	0.740	-0.017	0.003	
C-153	C-1	390	0.733	-0.022	-0.002	
C-153	UG	410	0.823	-0.018	0.012	
BY	UG	410	1.119	0.000	0.000	
F-555	UG	410	0.895	-0.007	-0.007	
F-555	UG	420	0.919	0.007	0.007	



Table 12 Continued

Sample Dye	Ref. Dye	$\lambda_{ex}$	$(\eta_f^x / \eta_f^s)^{exp}$	Residuals <sup>b)</sup>		
				I	II	III
F-555(M)	UG	420	0.755	0.014	-0.011	
C-6	UG	410	1.330	0.017	-0.001	
DCM	UG	420	0.653	-0.029	-0.000	
C-6	AY	445	1.530	-0.017	0.001	
F-555(M)	AY	445	0.851	-0.014	-0.018	
DCM(D)	C-153	440	0.984	-0.021	0.007	
DCM(D)	C-153	440	0.981	-0.023	0.005	
DCM(D)	C-153	440	0.916	-0.057	-0.024	
DCM(D)	C-153	450	0.930	-0.050	-0.032	
DCM(D)	DCM	470	1.188	-0.025	-0.000	
DCM	R-6G	500	0.457	-0.001		0.000
DCM(D)	R-6G	500	0.610	0.037		0.006
DCM(D)	R-6G	500	0.579	0.008		-0.024
DCM(D)	R-6G	500	0.591	0.019		-0.012
DCM(D)	R-6G	510	0.598	0.026		-0.006
DCM(D)	R-6G	520	0.617	0.044		0.013
AR	R-6G	500	0.726	0.000		0.000
LD688	R-6G	500	0.203	0.000		0.000
R-6G	R-101	510	1.033	0.030		0.015
R-6G	R-101	510	1.039	0.036		0.020
SR-B	R-101	520	0.698	0.000		0.000
DCM(D)	CV	540	1.079	0.045		0.014
DCM(D)	CV	540	1.072	0.041		0.011
DODC	CV(M)	540	0.803	0.000		0.000
CV(M)	CV	570	0.898	-0.034		-0.026
NB	CV	580	0.235	0.000		0.000
OX-170	CV	580	1.063	-0.015		-0.005
OX-1	CV	580	0.222	0.000		0.000
OX-750	CV	580	0.366	0.000		0.000
OX-4	CV	580	1.013	-0.024		-0.017
OX-4	CV	580	1.002	-0.030		-0.023
LD700	CV	590	0.596	0.000		0.000

a) Residual =  $\eta_f^{ex} - \eta_f^{ls}$

b) Residual =  $(\eta_f^x / \eta_f^s)^{ex} \cdot (\eta_f^s)^{ls} - (\eta_f^x)^{ls}$

A concurrent fit of the data from all the dyes studied was obtained and the results are presented under the column labeled I in Tables 11 and 12. Although agreement with  $\eta_f^{lit}$  is generally within the  $\pm 10\%$  uncertainty limits anticipated in our measurements, it was observed that  $\eta_f^{ls}$  for the blue - yellow emitting dyes was consistently greater than  $\eta_f^{lit}$ , and consistently less for the red emitting dyes (see entries in first 12 rows of Table 12). The systematic error suggested by this observation is thought to be due to an error of 10-15% in the emission spectra correction function in the red region relative to that in the green region. The quantum efficiency of dyes emitting in the two regions were linked by measurements of the quantum yield of DCM (which emits in the red and has appreciable absorption out to the UV) relative to a set of green emitting dyes and a set of red emitting dyes. The accuracy of the first set of relative measurements are, therefore, very sensitive to the accuracy of the emission correction function.

The systematic errors were largely eliminated by separately fitting the data from the blue - yellow emitting dyes (results under the columns labeled II in Tables 11 and 12) and from the red emitting dyes (results under the columns labeled III in Tables 11 and 12). Agreement was very satisfactory. The root mean square (rms) percentage deviation between the three literature values for the blue - yellow emitting dyes utilized in the calculation and the corresponding least squares values was 3.7%. The rms percentage deviation of the nine literature values for the red emitting dyes was 4.6%. Although the literature values for Fluorol 555, DCM, and Nile blue were not included in the analyses because of the poor fits obtained, it is to be emphasized that successful fits were obtained for all dyes whose quantum yields have been reported and found in agreement from more than one laboratory (quinine sulfate, rhodamine 6G, rhodamine 101, and cresyl violet). It is felt, therefore, that the quantum yields reported here are accurate roughly to  $\pm 10\%$ . However, larger deviations from

intrinsic quantum efficiencies are possible where unknown impurity quenching or rapid temperature quenching effects are encountered.

The quantum efficiency of a further number of dyes in liquid solution were measured in order to extend the list of potential secondary fluorescence standards. All were measured relative to a dye in Table 11 using quantum yield values from the least squares analyses (columns labeled II and III in Table 11). Results are presented in Table 13, and for completeness the least squares quantum yields in Table 11 have also been included in Table 13.

Table 13  
Fluorescence Quantum Yields of Dyes in Liquid Solution

Sample Dye (Solvent)	$\lambda_{em}^{max}$	Ref. Dye <sup>a)</sup>	$\lambda_{ex}$	$(\eta_f^x/\eta_f^s)^{exp}$	$\eta_f$
Coumarin 1 (EtOH)	449				0.606
Quinine Sulfate (Perchloric Acid)	453				0.551
Macrolex Yellow 10GN (EtOH)	494	C-6	410	0.749	0.554
Acridine Yellow (EtOH)	496				0.484
Hostasol Yellow 8G (EtOH)	497	C-6	410	1.065	0.788
Coumarin 6 (EtOH)	505				0.740
Fluorol Green Gold 084 (EtOH)	510	C-6	410	0.993	0.735
Fluorol Yellow 088 (EtOH)	521	C-6	410	0.424	0.314
Brilliant Yellow (EtOH)	523	UG	410	1.119	0.622
Hostasol Yellow 3G (EtOH)	523	C-6	410	0.971	0.719
Coumarin 153 (EtOH)	532				0.446
Fluorol 555 (EtOH)	534				0.504
Thermoplast Fluorescent Orange 274 (Xylene)	540	R-6G	490	1.066	1.033
Fluorol 555 (MeOH)	542				0.431
Brilliant Orange (DMSO)	543	R-6G	490	0.900	0.872
Rhodamine 6G (EtOH)	555				0.969
Acridine Red (EtOH)	568	R-6G	500	0.726	0.703
Hostasol Red GG (Xylene)	569	R-6G	500	0.953	0.923
Sulforhodamine B (EtOH)	576	R-101	520	0.698	0.665

Table 13 Continued

Sample Dye (Solvent)	$\lambda_{em}^{max}$	Ref Dye <sup>a)</sup>	$\lambda_{ex}$	$(\eta_f^x / \eta_f^s)^{exp}$	$\eta_f$
Rhodamine 101 (EtOH)	591				0.952
Hostasol Red 5B (Xylene)	600	R-6G	500	0.377	0.365
Macrolex Fluorescent Red 5B (Xylene)	601	R-6G	500	0.383	0.371
DODC (EtOH)	606	CV(M)	540	0.803	0.421
Brilliant Yellow (DMSO)	527	BY(EtOH)	440	0.946	0.588
DODC (EtOH)	606	CV	570	0.726	0.403
3,3'-Diethyl-4,5,4',5'- dibenzthiacarbocyanine (EtOH)	619	CV	570	0.175	0.097
DCM (EtOH)	622				0.443
Cresyl Violet (EtOH)	626				0.555
Cresyl Violet (MeOH)	626				0.524
Oxazine 4 (EtOH)	636				0.579
Oxazine 170 (EtOH)	645				0.595
DCM (DMSO)	650				0.585
LD 688 (EtOH)	663	R-6G	500	0.202	0.197
Nile Blue (EtOH)	666				0.130
Oxazine 1 (EtOH)	668				0.123
LD 700 (EtOH)	679	CV	590	0.596	0.331
Oxazine 750 (EtOH)	684	CV	580	0.366	0.203
LDS 750 (EtOH)	718	CV	575	0.154	0.085
LDS 751 (EtOH)	732	CV	575	0.112	0.062
HIDC (DMSO)		CV	578	0.709	0.393

a) The quantum yield of dyes without an entry in this column were taken from Table 11.

## II. E. Spectral Properties and Quantum Yield of Dyes in Solution in a Thin Film Polymer Host

The fluorescence quantum efficiency and peak emission wavelength of dyes in solid solution in a thin film are presented in Table 14. The quantum yields were measured by the relative emission intensity technique described in Section IIB. In most instances the fluorescence standard used in an individual relative fluorescence intensity measurement was a liquid solution (usually ethanol) of the same dye present in the thin film. The principal exception being the measurement of the deep red emitting styryl dyes where cresyl violet was used as a fluorescence standard because of the low fluorescence efficiency of the styryl dyes in ethanol solution. The estimated uncertainty in the quantum yield of fluorescent thin films is 15%.

Among dyes emitting in the green spectral region, here rather arbitrarily expanded to include peak emission wavelengths between 450 and 550 nm, only modest attention was given to the coumarins because tests had indicated relatively poor photostability. Fluorescence of the most stable of the coumarins, coumarin 6, was studied in PMMA and CAP polymers. The quantum efficiency was roughly 0.75, almost identical to that of the ethanol solution. This was contrary to expectations that freezing the torsional motion of the di-N-ethylamino group in solid solution would increase the quantum efficiency.

Greatest attention in the green region was given to dyes commercially developed for fluorescent display applications. Within this group Hoechst Hostasol Yellow 8G in a CAP polymer showed a quantum yield of essentially unity, while Mobay Macrolex Fluorescent Yellow 10GN in CAP, Fluorol 555 in both CAP and PMMA, and BASF Fluorol Green Gold 084 in PMMA had quantum efficiencies above 0.75. Unfortunately, Day-Glo

Table 14  
Fluorescence Quantum Yields of Dyes in Solid  
Solution in Thin Film

Sample Dye (Ref Dye - Solvent)	Polymer Matrix	$\lambda_{ex}$	$\lambda_{em}$	$\eta_f$
Macrolex F Yellow 10GN (Macrolex F Yellow 10GN - EtOH)	Elvacite 2010	440	489	0.71
Macrolex F Yellow 10GN (Macrolex F Yellow 10GN - EtOH)	CAP 504.20	440	494	0.87
Coumarin 6 (Coumarin 6 - $2 \times 10^{-5}$ M EtOH)	Elvacite 2010	410	493	0.77
Coumarin 6 (Coumarin 6 - $2 \times 10^{-5}$ M EtOH)	CAP 504.20	410	502	0.75
Hostasol Yellow 8G (Hostasol Yellow 8G - EtOH)	CAP 504.20	440	493	0.99
Hostasol Yellow 8G (Hostasol Yellow 8G - EtOH)	Elvacite 2010	440	496	0.65
Acridine Yellow (Acridine Yellow - $2.7 \times 10^{-5}$ M EtOH)	CAP 504.20	440	496	0.53
Acridine Yellow (Acridine Yellow - $2.7 \times 10^{-5}$ M EtOH)	Elvacite 2010	440	498	0.17
Fluorol 555 (Fluorol 555 - $3.2 \times 10^{-5}$ M EtOH)	Elvacite 2010	430	500	0.85
Fluorol 555 (Fluorol 555 - $3.2 \times 10^{-5}$ M EtOH)	CAP 504.20	430	513	0.79
Hostasol Yellow 3G (Hostasol Yellow 3G - EtOH)	Elvacite 2010	460	508	0.60
Hostasol Yellow 3G (Hostasol Yellow 3G - EtOH)	CAP 504.20	460	512	0.31
Fluorol Green Gold 084 (Fluorol Green Gold 084 - EtOH)	Elvacite 2010	435	508	0.78
Fluorol Green Gold 084 (Fluorol Green Gold 084 - EtOH)	CAP 504.20	435	510	0.74
Brilliant Yellow (Brilliant Yellow - 1.2mg/100ml DMSO)	Elvacite 2010	440	510	0.58

Table 14 (Continued)

Brilliant Yellow (Brilliant Yellow - DMSO)	CAP 482-0-20	440	514	0.45
Brilliant Yellow (Brilliant Yellow - DMSO)	CAB 553.40	440	516	0.32
Brilliant Yellow (Brilliant Yellow - 1.2mg/100ml DMSO)	CAP 504.20	440	522	0.28
Fluorol Yellow 088 (Fluorol Yellow 088 - EtOH)	Elvacite 2010	450	517	0.54
Fluorol Yellow 088 (Fluorol Yellow 088 - EtOH)	CAP 504.20	450	521	0.45
Brilliant Orange (Brilliant Orange - 0.70mg/50ml DMSO)	Elvacite 2010	490	567	0.59
Brilliant Orange (Brilliant Orange - 0.70mg/50ml DMSO)	CAP 504.20	490	571	0.78
Sulforhodamine-B (Sulforhodamine-B - $2.0 \times 10^{-5}$ M EtOH)	Elvacite 2010	520	576	0.76
Sulforhodamine-B (Sulforhodamine-B - $2.0 \times 10^{-5}$ M EtOH)	CAP 504.20	520	582	0.88
Hostasol Red GG (Hostasol Red GG - EtOH)	Elvacite 2010	500	577	0.65
Hostasol Red GG (Hostasol Red GG - Xylene)	CAP 504.20	500	593	0.68
Acridine Red (Acridine Red - $4 \times 10^{-5}$ M EtOH)	CAP 504.20	490	579	1.12
Acridine Red (Acridine Red - $4 \times 10^{-5}$ M EtOH)	Elvacite 2010	490	580	1.07
Hostasol Red 5B (Hostasol Red 5B - Xylene)	Elvacite 2010	535	586	0.37
Hostasol Red 5B (Hostasol Red 5B - Xylene)	CAP 504.20	535	597	0.23
Rhodamine 101 (Rhodamine 101 - $1.6 \times 10^{-5}$ M EtOH)	CAP 504.20	530	598	1.07
Rhodamine 101 (Rhodamine 101 - $1.6 \times 10^{-5}$ M EtOH)	Elvacite 2010	530	600	1.01

Table 14 (Continued)

LD 688 (LD 688 - CAP 504.20)	CAB 553.40	490	600	0.66
LD 688 (LD 688 - $1 \times 10^{-5}$ M EtOH)	Elvacite 2010	490	607	0.89
LD 688 (LD 688 - CAP 504.20)	CAP 504.20 & Cymel 303	490	607	0.67
LD 688 (Rhodamine 101 - $2.0 \times 10^{-5}$ M EtOH)	CAP 504.20	530	609	0.65
LD 688 (LD 688 - $1 \times 10^{-5}$ M EtOH)	CAP 504.20	490	611	0.89
Oxazine 4 (Oxazine 4 - $1.8 \times 10^{-5}$ M EtOH)	Elvacite 2010	575	633	0.38
Oxazine 4 (Oxazine 4 - $1.8 \times 10^{-5}$ M EtOH)	CAP 504.20	575	636	0.53
Oxazine 170 (Oxazine 170 - $2.1 \times 10^{-5}$ M EtOH)	Elvacite 2010	590	644	0.49
Oxazine 170 (Oxazine 170 - $2.1 \times 10^{-5}$ M EtOH)	CAP 504.20	590	652	0.56
Nile Blue (Nile Blue - $2.4 \times 10^{-5}$ M EtOH)	Elvacite 2010	600	662	0.24
Nile Blue (Nile Blue - $2.4 \times 10^{-5}$ M EtOH)	CAP 504.20	600	668	0.22
Oxazine 1 (Oxazine 1 - $1.4 \times 10^{-5}$ M EtOH)	Elvacite 2010	610	663	0.48
Oxazine 1 (Oxazine 1 - $1.6 \times 10^{-5}$ M EtOH)	CAP 482-0-20	610	670	0.29
Oxazine 1 (Oxazine 1 - $1.6 \times 10^{-5}$ M EtOH)	CAP 504.20	610	673	0.26
Oxazine 1 (Oxazine 1 - $1.6 \times 10^{-5}$ M EtOH)	CAB 553.40	610	673	0.25
Oxazine 750 (Oxazine 750 - $1.9 \times 10^{-5}$ M EtOH)	Elvacite 2010	620	682	0.27
Oxazine 750 (Oxazine 750 - $1.9 \times 10^{-5}$ M EtOH)	CAP 504.20	620	688	0.26



Table 14 (Continued)

LDS 730 (Cresyl Violet - $2.8 \times 10^{-5}$ M EtOH)	CAP 504.20 & Cymel 303	540	695	0.51
LDS 730 (DOTC - $7.9 \times 10^{-6}$ M EtOH)	CAP 504.20 & Cymel 303	540	695	0.51
LDS 730 (LDS 730 - CAP 504.20)	CAP 504.20 & Cymel 303	570	695	0.51
LDS 730 (LDS 730 - CAP 504.20)	CAB 553.40	570	696	0.46
LDS 730 (Cresyl Violet - $2.4 \times 10^{-5}$ M EtOH)	CAP 504.20	570	698	0.46
LDS 751 (Cresyl Violet - $2.4 \times 10^{-5}$ M EtOH)	CAP 504.20	570	696	0.30
LDS 750 (LDS 750 - CAP 504.20)	CAP 504.20 & Cymel 303	560	698	0.34
LDS 750 (LDS 750 - CAP 504.20)	CAB 553.40	560	699	0.46
LDS 750 (Cresyl Violet - $2.4 \times 10^{-5}$ M EtOH)	CAP 504.20	570	700	0.49
LDS 798 (LDS 798 - CAP 504.2)	CAB 553.40	570	722	0.43
LDS 798 (LDS 798 - CAP 504.20)	CAP 504.20 & Cymel 303	570	726	0.41
LDS 798 (Cresyl Violet - $2.4 \times 10^{-5}$ M EtOH)	CAP 504.20	570	736	0.42
LDS 820 (Cresyl Violet - $2.4 \times 10^{-5}$ M EtOH)	CAP 504.2	570	770	0.23

Brilliant Yellow, which has demonstrated superior photostability, is a rather indifferent emitter. The maximum quantum yield was 0.58 in PMMA, and efficiencies are less than 0.5 in CAP or CAB.

Again somewhat arbitrarily, the red spectral region is defined as spanning wavelengths between 550 and 620 nm. The rhodamines, the most important laser dyes emitting in this region, were not studied extensively because of the poor stability of most members of the group. Sulforhodamine-B, the most stable member, was studied in PMMA and CAP and showed quantum efficiencies of 0.76 and 0.88, respectively. In ethanol the quantum yield of sulforhodamine-B is 0.67, the improvement in fluorescence efficiency in solid solution apparently due to the restriction of the di-N-ethylamino torsion. For rhodamine 101, in which the amino end groups are rigidized within ring systems, the quantum efficiency is essentially unity in ethanol and PMMA or CAP.

A related red-emitting molecule, acridine red, shows a particularly large improvement in quantum yield when in solid solution. Acridine red is a pyronin with N-methylamino end groups (the pyronins differ from the rhodamines only by the absence of the 9-carboxyphenyl group). The 0.70 quantum yield of acridine red in ethanol becomes essentially unity in PMMA or CAP solid solution, suggesting that internal rotation of the terminal amino groups is also the principal nonradiative relaxation path in this molecule.

Among the red emitting dyes studied that were commercially developed for fluorescent display applications only Day-Glo Brilliant Orange in CAP with a quantum efficiency of 0.78 has an efficiency above 0.75. One of the more interesting display dyes, Thermoplast Fluorescent Orange 274, could not be introduced into a thin film because of limited solubility.

A final dye of some interest in the red emitting group is the styryl dye, LD 688. Like the other styryl dyes, LD 688 is characterized by broad absorption and emission bands and a large Stokes' shift. It has been reported that the wavelength of peak emission of the styryl dye DCM is considerably shifted toward the blue when cast in PMMA.<sup>13</sup> This effect is particularly noted in LD 688 with the peak emission wavelength in ethanol of 663 nm moving to 600-611 nm in a variety of polymers. The quantum efficiency of LD 688 in a number of thin film hosts is apparently near 0.65. Two yields of approximately 0.9 were measured, but are suspect because they both were obtained relative to a weakly emitting ( $\eta_f = 0.20$ ) LD 688 ethanol solution. The excitation and emission spectra of LD 688 in a CAP thin film is illustrated in Figure 7.

The spectral region that has received the most attention is the far red region, the region with wavelengths longer than 620 nm. This is the most critical region because dyes emitting here have relatively low lying first excited states and, therefore, it is anticipated that greatest difficulty will be found in identifying dyes with adequate fluorescence efficiency and stability.

The principal dye groups which emit in the far red region are the oxazines, carbocyanines, and styryl dyes. The carbocyanine dyes, were found to be unstable in thin film hosts, frequently bleaching during preparation of the plates. Therefore, no quantum yield measurements of carbocyanines were performed. There are no far red dyes that have been developed for display applications because the greater portion of the far red region lies beyond the long wavelength sensitivity limit of the human eye. Commercial activity in this region has been almost exclusively devoted to dye laser applications.

The quantum efficiency of the oxazines that have demonstrated the best stability have been reasonably thoroughly

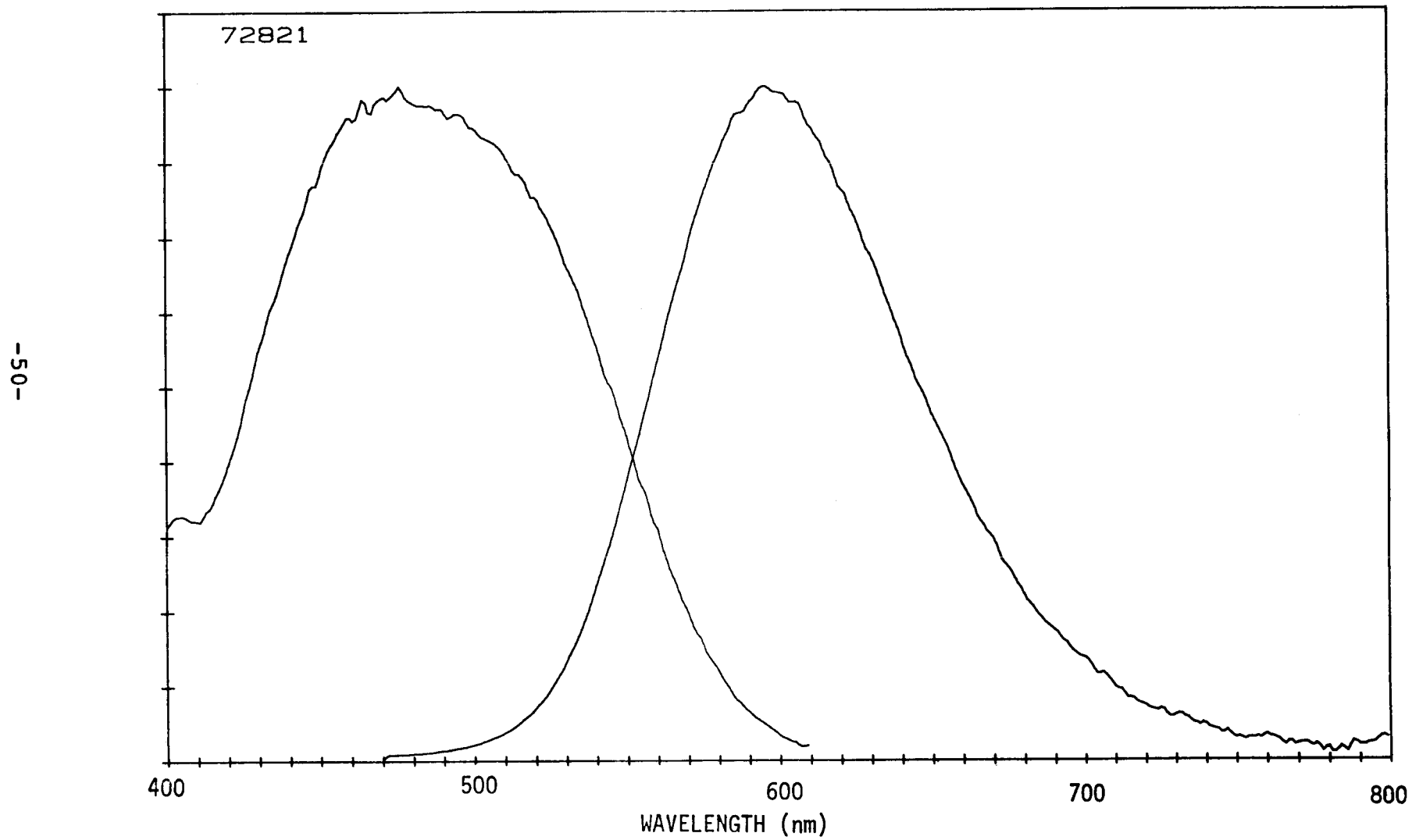


Figure 7. Excitation and Emission Spectra of LD 688 in a CAP 504.20 Thin Film

studied. Those oxazines in which one or both terminal amino groups are fully alkylated, oxazine 1 and nile blue, show large increases in quantum efficiency when in solid solution in a thin film. Overall fluorescence efficiency, however, remains disappointing. The most striking case is oxazine 1, whose quantum yield increases from 0.12 in ethanol to 0.48 in PMMA. Those oxazines in which both terminal amino groups are partially alkylated, oxazine 4 and oxazine 170, show quantum yields in thin films that are essentially the same or somewhat reduced from the ethanol solution values. The largest efficiencies measured in this group are 0.56 and 0.53 from oxazine 170 and oxazine 4, respectively, both in CAP.

The most interesting molecules emitting in the far red region are the styryl dyes. A member of the group, LD 688, has been discussed above. The group is interesting because of broad absorption bands, a large Stokes' shift, and particularly because the peak emission of the longer wavelength emitting members occur well to the red of any of the oxazines. The quantum efficiency of the styryl dyes in ethanol is low. Large efficiency improvements in solid solution in thin films were observed; however, quantum yields substantially above 0.5 were not achieved. Quantum yields between 0.51 and 0.45 were measured in LDS 730 and LDS 750 in a variety of polymers. The excitation and emission spectra of LDS 730 and LDS 750 in a CAP thin film are given in Figures 8 and 9. Generally, as expected, it was observed that fluorescence efficiencies dropped as the peak emission wavelength moved further toward the red.

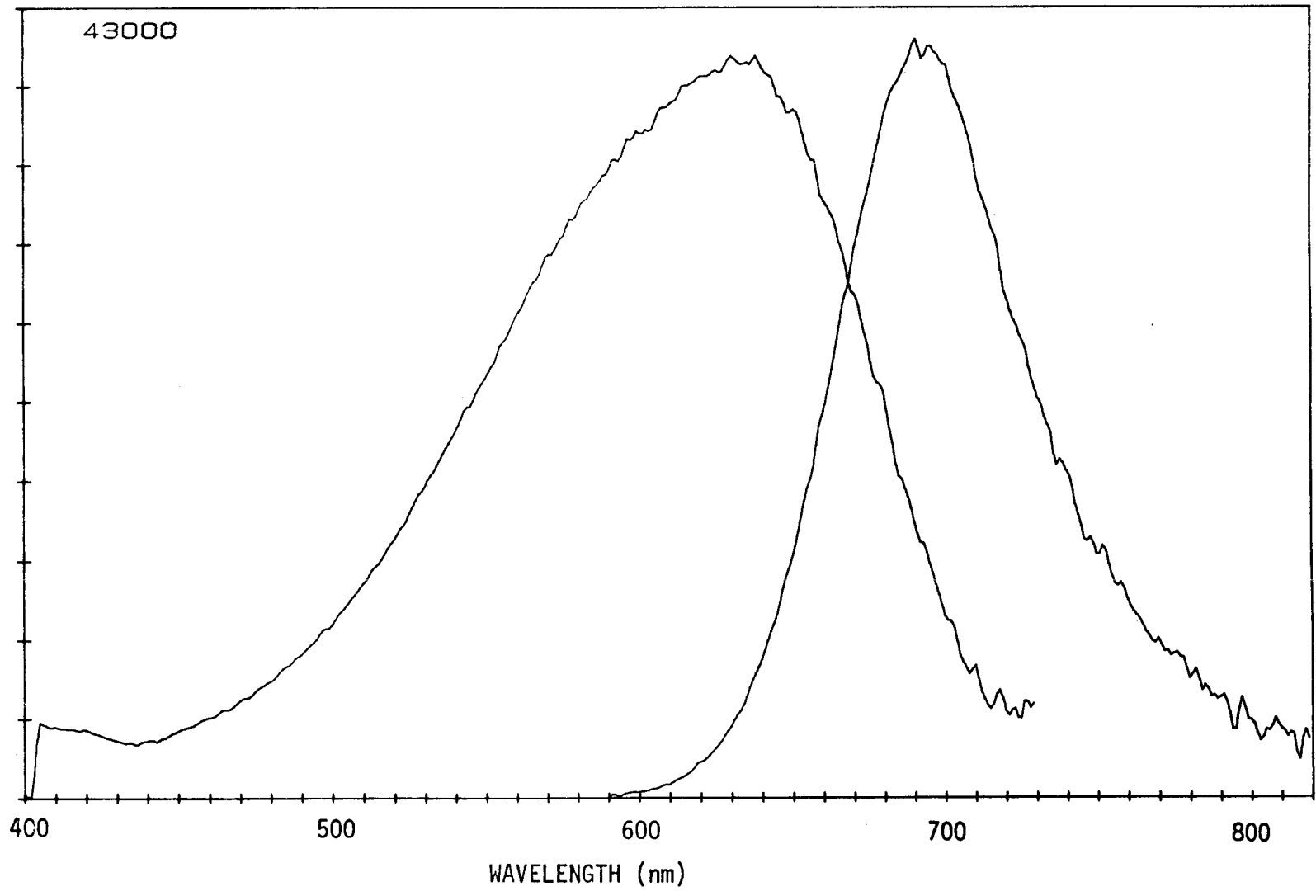


Figure 8. Excitation and Emission Spectra of LDS 730 in a Cap 504.20 Thin Film

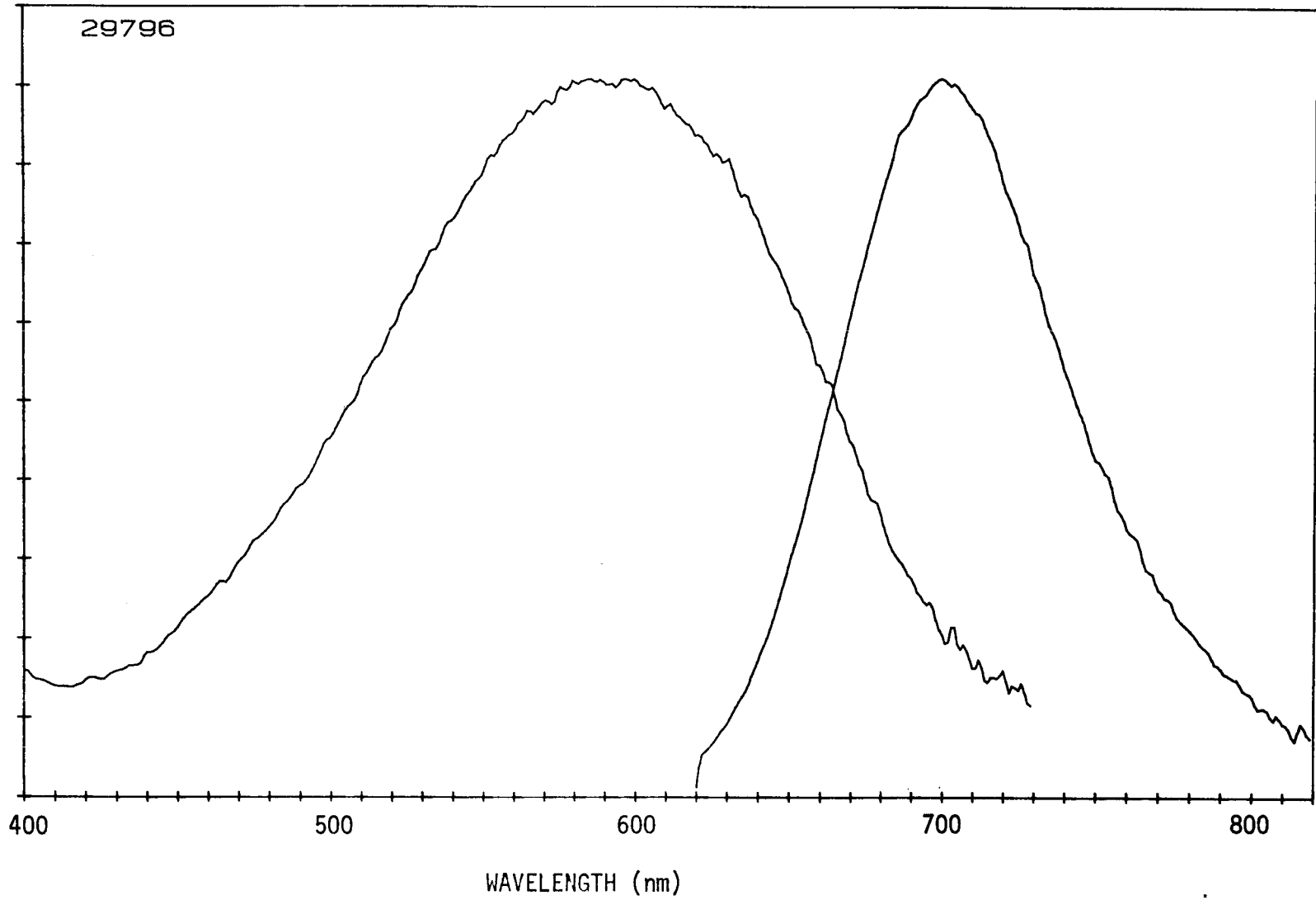


Figure 9. Excitation and Emission Spectra of LDS 750 in a CAP 504.20 Thin Film

## II. F. Summary

The quantum efficiency and absorption and emission spectral distribution of roughly 200 luminescent organic dye/polymer matrix combinations have been measured. Frequently, particularly for red-near IR emitting dyes, quantum efficiencies are larger in solid solution than in liquid solution, presumably because a more rigid matrix disfavors nonradiative relaxation. However, this is not always the case as can be seen in Table 15 for the dyes Hostasol Yellow-3G and Oxazine-4. In various solid matrices the quantum efficiency has been observed to vary by as much as a factor of two, as is the case for Hostasol Yellow-3G in Table 15.

Table 15

Variation of Dye Quantum Efficiency with Host

Dye	Quantum Efficiency		
	(EtOH)	(PMMA)	(CAP)
Hostasol Yellow - 3G*	.81	.68	.35
Oxazine - 4**	.51	.33	.46
LD-688**	.19	.84	.84
Fluorol-555**	.56	.95	.87

\*Hoechst

\*\*Exciton

NOTE: EtOH = ethyl alcohol  
PMMA = polymethyl methacrylate  
CAP = cellulose acetate propionate

A sizable number of green-red emitting dye/polymers have



been identified with quantum efficiencies greater than 0.9. The choice among these for use in an optimized LSC will depend largely on Stokes shift and stability criteria. Considerable work remains to be done in the far red-near IR spectral region. Dyes emitting in this region have been identified with excellent Stokes shifts (see Figure 10); however, dye/polymer combinations with quantum efficiencies in excess of 0.5 have not yet been identified.

One final note, the Edge Emission Spectrofluorometer previously used for measuring edge emission lineshape from a single emitter<sup>3</sup> has been used to measure the integrated plate edge emission spectrum in various two dye plates. It is observed that for a "typical" high efficiency two dye plate, such as 59D<sup>3</sup>, approximately 99% of the emission from the first dye will be reabsorbed by the second dye before reaching the plate edge. This experimentally measured value was determined by integrating and subsequently comparing the edge emission spectrum recorded over the entire spectral range encompassing both dyes. It is believed that the 1% emission by the first dye that is apparently not absorbed by the second dye, probably represents emission from the first dye in the immediate vicinity of the plate edge.

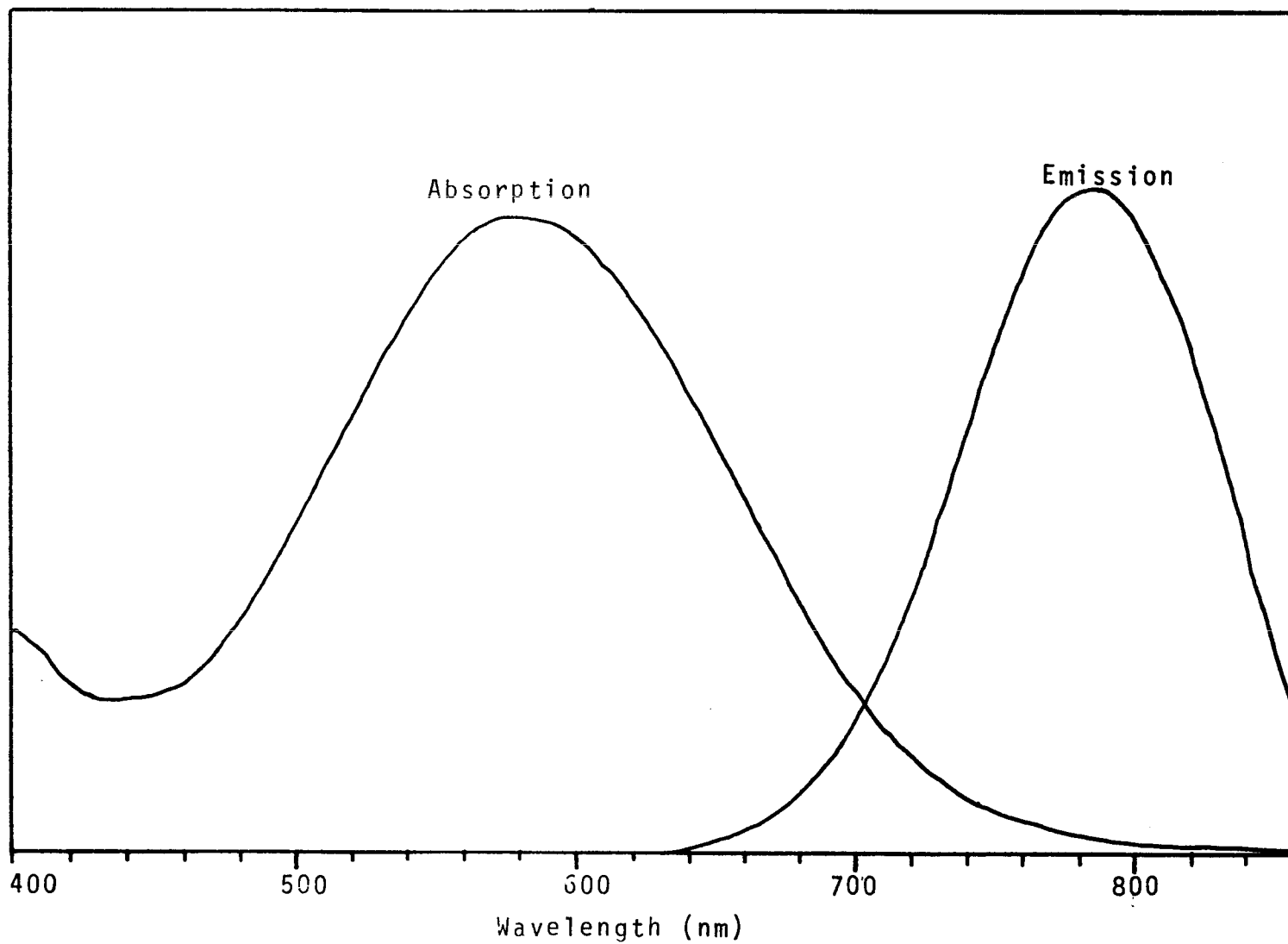


Figure 10. Absorption and Emission Spectra of LDS 820 in a Cap Thin Film

### III. INVESTIGATION OF DYE DEGRADATION

Tremendous progress has been made over the course of this investigation in a number of key areas affecting organic dye degradation. The methodology for the LSC degradation studies has been revised with the program organized into five phases (Table 16). The first phase, which is the host polymer screening, has been completed with 17 different host systems identified from 61 host systems tested (Table 17) that show for at least one (1) dye, no visual sign of degradation after 50 kWh/m<sup>2</sup> (i.e., approximately 14 days) of outdoor exposure. These results and those described below for the solvent studies confirm preliminary data reported previously that dye photostability is very strongly dependent on host composition.

The second phase of the degradation study is the solvent screening program. This phase has also been completed, and of 19 different solvents studied, eight of the most stable have been selected for use as preferred dye/polymer solvents. These solvents, as can be seen in Table 18 for Brilliant Yellow, show dye stabilities greater than 0.9 after 50 kWh/m<sup>2</sup> of outdoor exposure when used as a host for a number of different dyes.

In the third phase of the stability program, quantitative screening of 46 different commercially available dyes in up to eleven (11) different hosts (Table 19) has been completed. Measurement of both the dye and device stabilities (Appendix I) has been carried out to 1000 kWh/m<sup>2</sup> (i.e., almost 300 days). Dramatic progress is now evident from this first group of measurements. The dye stabilities of our best dyes are now on the order of years; in 1978 our best stability was approximately one day.

The above reported stabilities (with the exception of the

Table 16

---

Protocol for LSC Degradation Studies

---

1. Host Polymer Screening

Qualitative screening of each host (with up to six dyes) in both an air and nitrogen atmosphere for 50 kWh/m<sup>2</sup> of outdoor exposure.

2. Liquid Host Studies

Quantitative screening of each solvent (with up to six dyes) in both an air and nitrogen atmosphere for at least 50 kWh/m<sup>2</sup> of exposure.

3. Dye Screening

Quantitative screening of each dye (in at least two hosts) in both an air and nitrogen atmosphere. The quantum efficiency, dye stability and device stability of each dye/host combination is to be measured.

4. Dye/Host Optimization

Detailed quantitative analysis of the effect on stability of dye and host purification, UV-screening, and the addition of triplet quencher.

5. System Optimization

Accelerated testing to evaluate dye-dye interaction, spectral sensitivity, variation of O.D., temperature, humidity, plasticizers, and barrier coatings.

Table 17

Host Polymer Systems Evaluated

12	-	Acrylic Isocyanates*
8	-	Acrylics
8	-	Cellulose Esters*
5	-	Aliphatic Epoxies
4	-	Melamine Acrylates*
4	-	Polyester Isocyanates
3	-	Melamine Silicates*
2	-	Cellulose Melamines*
2	-	Cellulose Silicates*
2	-	Urethanes
1	-	Acrylic Silicate
1	-	Acrylonitrile
1	-	Polycarbonate Isocyanate
1	-	Polystyrene
1	-	Polyvinyl Alcohol
1	-	Vinyl Acetate Acrylate

---

\*17 of 56 Host Systems Tested Show No Visual Sign of Degradation After 50 kWh/m<sup>2</sup> of Outdoor Exposure.

+Dyes Used Include: Brilliant Yellow, Coumarine-6, Coumarin-30, Nile Blue, Oxazine-1, Rhodamine-6G, Rhodamine-101, Sulforhodamine-B, Sulforhodamine-101.

Table 18

Dye/Solvent Stability for Brilliant Yellow\*  
After 50 kWh/m<sup>2</sup> Exposure

Solvent	Dye Stability (A <sub>t</sub> )
Anhydrous Alcohol	.98
Benzyl Alcohol	.58
n-Butyl Acetate**	.97
Carbon Tetrachloride	.25
Chloroform**	.99
Cyclohexanone	.12
1,2-Dichloroethane	.60
Dimethyl Acetamide	.07
Dimethyl Formamide	.86
Dimethyl Sulfoxide**	.94
Ethoxyethanol	.85
2-Methoxyethanol**	1.00
Methyl Isobutyl Ketone**	.96
2-Propanol**	.98
Propylene Carbonate**	.99
Toluene	.85
1,2,4-Trichlorobenzene	.87
2-Xylene	.13
Water**	NS

\* Day-Glo Color Corp.

\*\* Selected for use as Dye/Polymer Solvent.

NS = Not Soluble

NOTE: All Values are for Samples in Air Atmosphere.

Table 19

Host Polymer Systems Selected for Dye Screening Tests

<u>Host Code</u>	<u>Host Polymer System</u> <sup>3</sup>
AC-H	Acrylate (Elvacite 2010, which is PMMA)
AC-I	Acrylate (Elvacite 2041)
AI-E	Acrylic Crosslinked Isocyanate (Polytex 975/ Desmodur KL5-2444)
AI-I	Acrylic Crosslinked Isocyanate (Acryloid AT-400/Desmodur Z-4370)
CE-A	Cellulose Ester (Cellulose Acetate Butyrate 553-0.4)
CE-B	Cellulose Ester (Cellulose Acetate Propionate 482-20)
CE-D	Cellulose Ester (Cellulose Acetate Propionate 504-0.2)
CE-E	Cellulose Ester (Cellulose Acetate Butyrate 381-0.1)
CM-A	Cellulose Crosslinked Melamine (Cellulose Acetate Propionate 504-0.2/Cymel 303)
CS-A	Cellulose Crosslinked Silicate (Cellulose Acetate Propionate 504-0.2/Hydrolyzed Ethyl Silicate)
MA-C	Melamine Crosslinked Acrylate (Cymel 303/ Polytex 910)

Mobay LISA dyes) have been achieved without purification of either the dye or host polymer beyond the level supplied by the vendor. In addition, no life-time enhancing compounds, such as "triplet quenchers," have been added to the dye/host system, nor has use been made of protective gaseous barrier films. In fact, little of what could be done to improve stability (see Table 20) has been done. We have only made a preliminary attempt to optimize the dye/host/ solvent chemistry. However, the results to date leave ample room for optimism that the required lifetimes for a practical device can and perhaps have already been achieved.

Our experimental results for both the dye stability ( $A_t$ ) and device stability ( $S_t$ ) appear in Appendix I. The eleven different hosts used in these tests are listed in Table 19. The dye stability and device stability have previously been defined<sup>3</sup> as follows:

$$A_t = \frac{A_f}{A_i} = \frac{\text{plate absorbance after exposure}}{\text{plate absorbance before exposure}}$$

$$S_t = \frac{L_t}{L_o} = \frac{\text{corrected edge luminescence after exposure}}{\text{corrected edge luminescence before exposure}}$$

As can be seen from the data in Figure 11 for Day - Glo Brilliant Yellow, the dye stability which is a measure of dye bleaching, generally tends to decrease with time. For the most stable systems, however, such as Mobay (Baeyer) LISA Amber 59YR (Figure 12), the dye stability sometimes appears to remain nearly constant with time. In contrast, the device stability, which measures the device edge power output, initially often



Table 20

Stability Improvement Program

- A. Host Screening
- B. Dye Screening
- C. Solvent Screening
- D. Dye/Host/Solvent Optimization
- E. Host Copolymer Optimization
- F. Materials Ultrapurification
- G. Addition of Triplet Quencher to Host Matrix
- H. UV Protection/Fluorescent Glass Substrates
- I. Optimization of Dye Salt Co-Ionic Species and Matrix pH
- J. Use of Barrier Film to Reduce Gaseous Exchange of Oxygen, H<sub>2</sub>O, and Pollution
- K. Initiate Degradation Mechanistic Studies
- L. Dye Synthesis/Molecular Engineering
- M. Reduction of Excited State Lifetime of High Energy Dyes by Nonradiative Transfer into Low Energy Acceptor

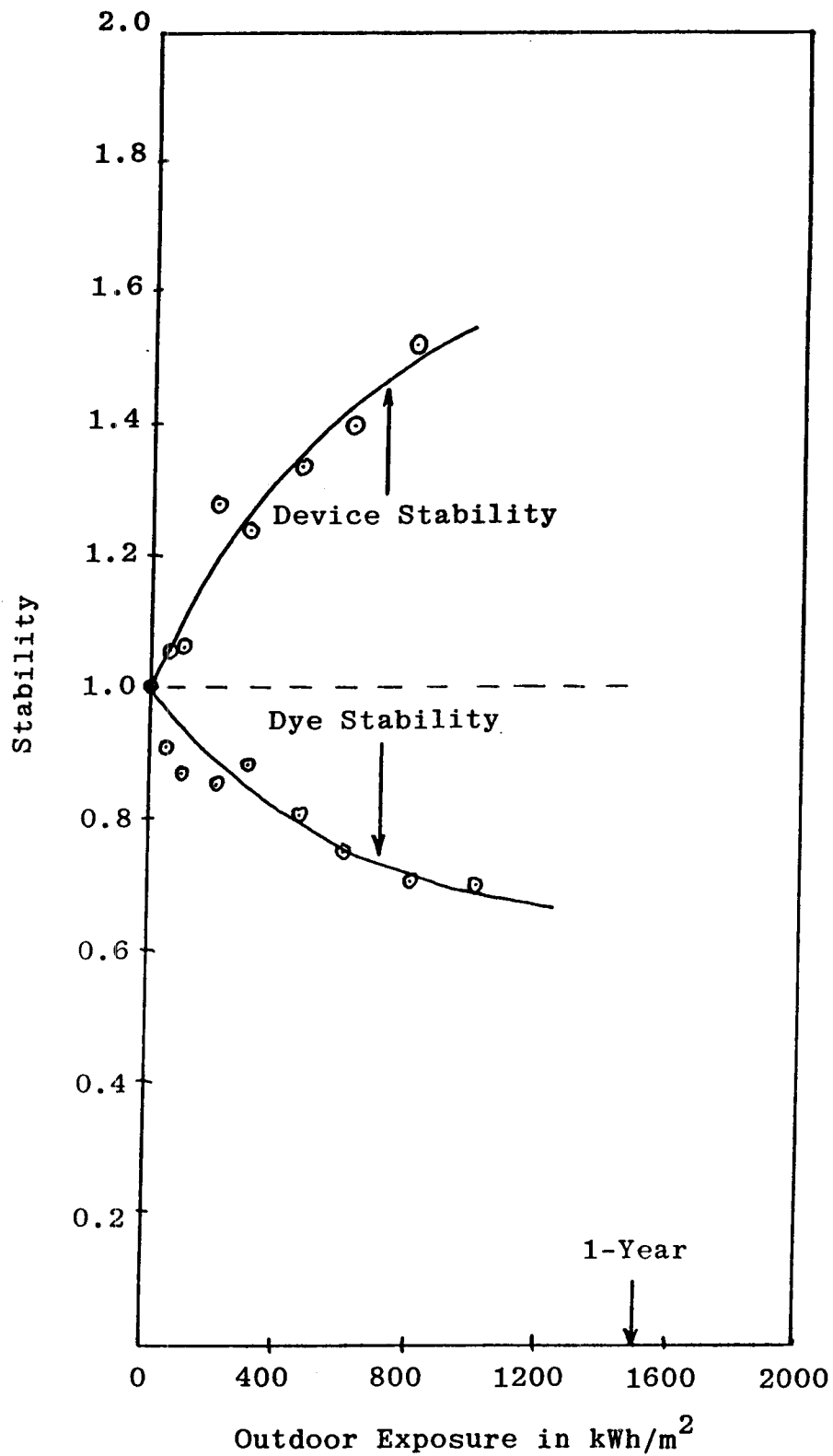


Figure 11. Stability of Day-Glo Brilliant Yellow in Cellulose Acetate Crosslinked Melamine

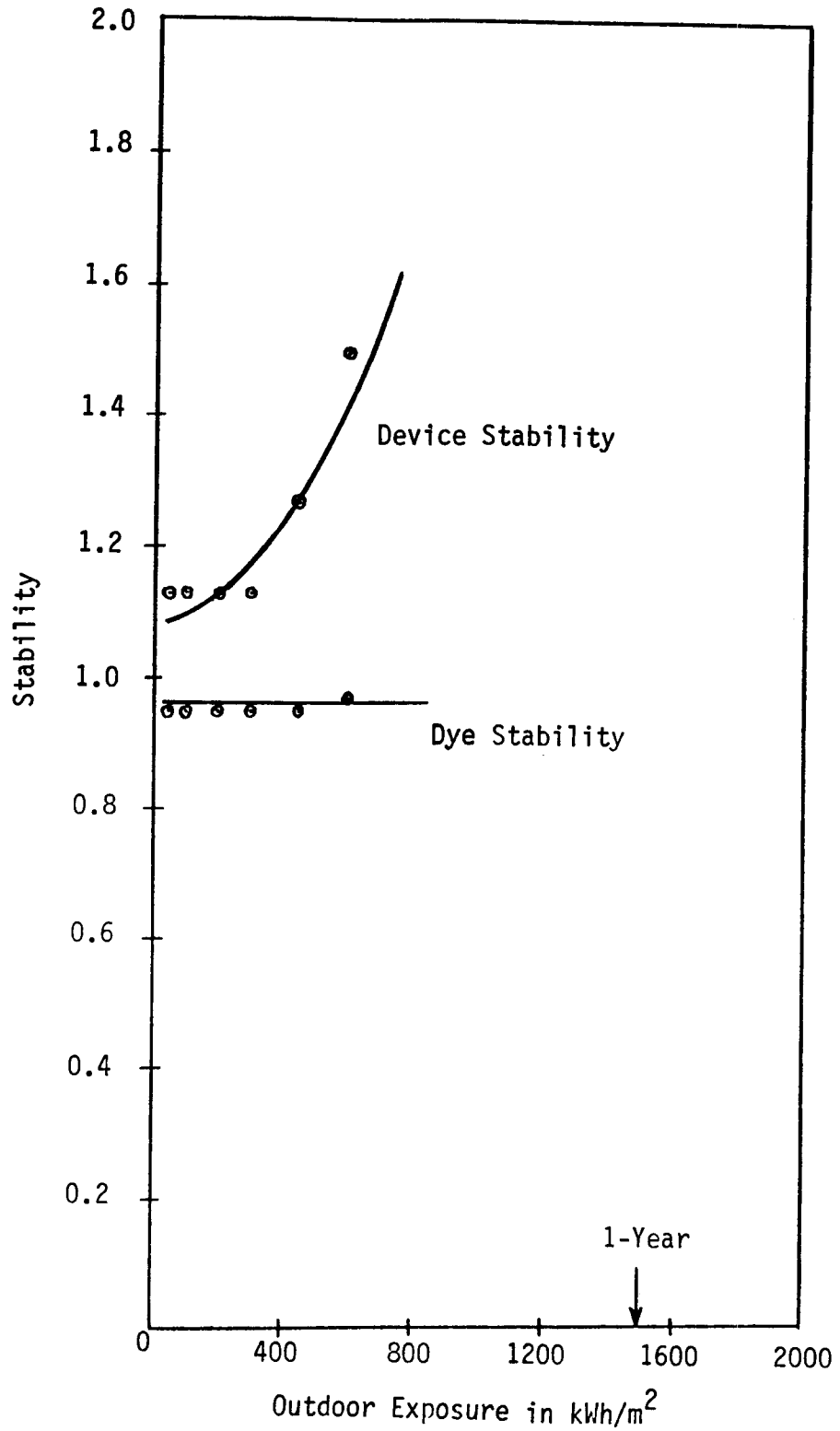


Figure 12. Stability of Mobay LISA Amber 59-YR in Polycarbonate

tends to improve with time, especially for high optical density plates (Figures 11 and 12). The reason for this is that for plates with high optical density, a given amount of bleaching has less effect on the solar absorption of the plate than for plates with low optical density. For example, if a plate with an optical density of 3.0 is 33% bleached, the peak solar absorption is reduced from 99.9% to 99%. However, for the same dye bleached 33% in a plate with an initial optical density of 0.5, the peak solar absorption will be reduced from 68% to 54%. Thus, in the first case of a high optical density plate, 33% bleaching results in reducing the peak solar power absorbed by less than 1%, while in the second case for a low optical density plate, the same 33% bleaching results in reducing the peak solar power absorbed by 20%. Moderate bleaching, therefore, has very little effect on the amount of solar power absorbed for high optical density plates. However, high optical density plates have a higher degree of self-absorption of emitted radiation.<sup>3</sup> Therefore, solar bleaching of the plate will significantly reduce the amount of self-absorption of emitted luminescence. The net effect is that for high optical density plates, moderate amounts of bleaching (i.e., moderate reduction of dye stability) has little effect on the amount of solar power absorbed, but has a larger effect on reducing the degree of self-absorption of emitted radiation, thus in many cases the amount of luminescent power actually reaching the plate edge increases.

#### IV. RELATIVE EDGE LUMINESCENCE

The Relative Edge Luminescence ( $L_r$ ) is defined as the LSC short-circuit current output in milliamps per centimeter of LSC plate edge, from an air-coupled photovoltaic cell located at the center of the plate edge, under uniform simulated AM-1.5 global insolation, assuming an incident power density from 300-2500nm of  $100 \text{ mW/cm}^2$ . The actual apparatus and procedure used for measuring the edge luminescence ( $L$ ) has been previously described<sup>3</sup> and will not be repeated here.

$$L_r = \frac{L_o}{l_c} = \frac{100 (L_i - L_{bi})}{I_{ss}^i l_c}$$

where:  $L_o$  = corrected edge luminescence before exposure  
 $L_i$  = edge luminescence before exposure  
 $L_{bi}$  = initial detector background signal  
 $l_c$  = length in centimeters of the edge coupled photovoltaic cell  
 $I_{ss}^i$  = initial power density in  $\text{mW/cm}^2$  incident upon the LSC plate from the solar simulator

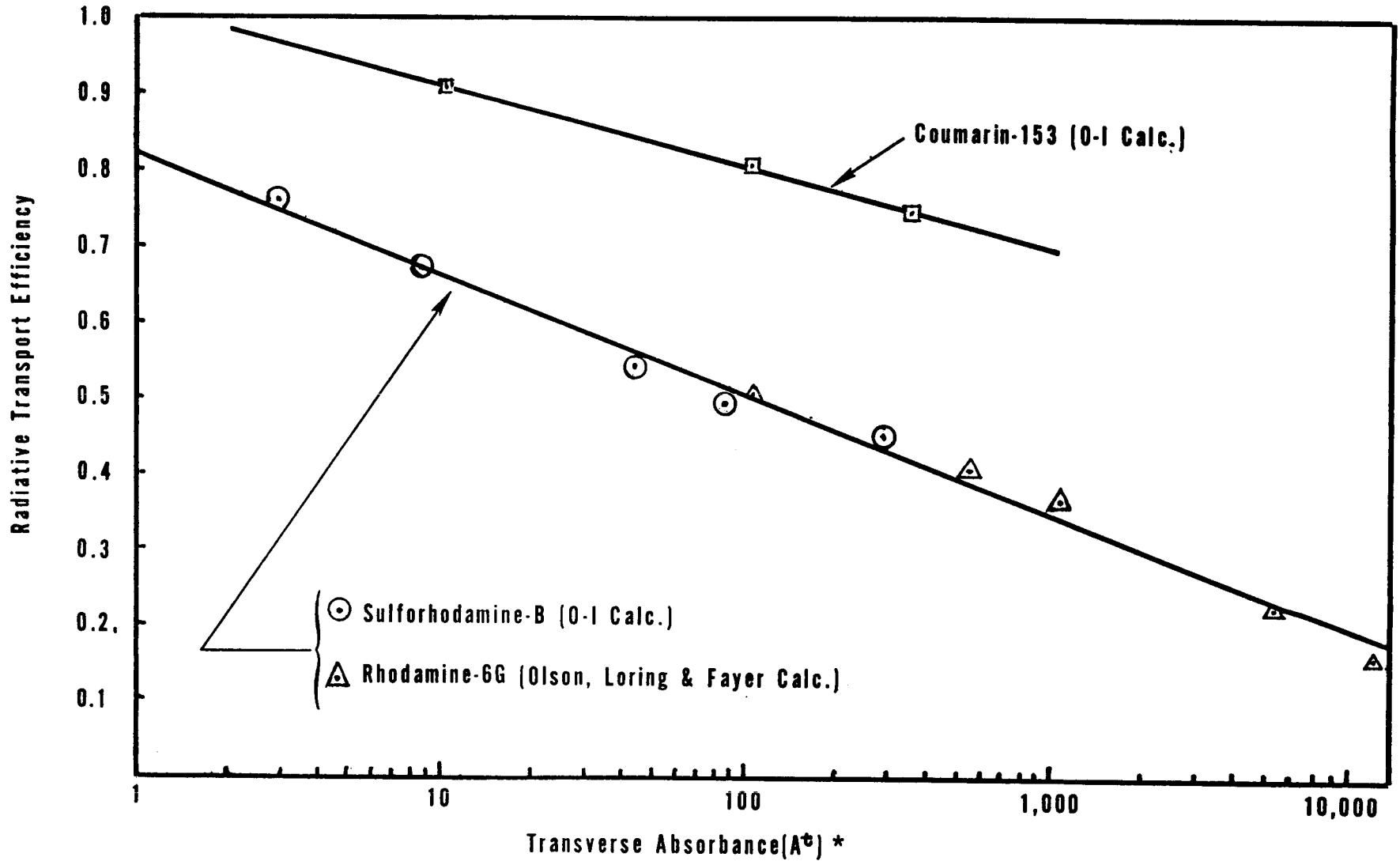
The relative edge luminescence values for all of the LSC plates tested are listed in the extensive set of tables constituting Appendix II. In addition, edge luminescence measurements as a function of outdoor exposure have been made on all of the LSC plates listed in Appendix I for the calculation of device stability.

## V. THEORETICAL MODELING

It has long been recognized that one of the major factors limiting the efficiency of an LSC is the loss due to self-absorption. Self-absorption losses (of luminescence) from the final emitting dye depend in a complex fashion on the substrate refractive index, plate dimensions, dye concentration, luminescence quantum yield, absorption spectrum, and emission spectral distribution. The influence of these factors on LSC device efficiency was computed with a finite dimensional element LSC computer modeling program.<sup>3</sup> The program can model up to five successive self-absorption events and utilizes digitized absorbance and front surface emission spectra. Calculations have shown that the radiative transport efficiency (1 - self-absorption loss) falls approximately linearly with the logarithm of plate width or peak optical density, and that the negative slope increases with decreasing Stokes shift (see Figure 13). The radiative transport efficiency of a 1 m square, 3 mm thick coumarin-153 plate ( $3000 \text{ cm}^{-1}$  Stokes shift) with a peak optical density of roughly 1 (transverse absorbance<sup>3</sup> is 333), is 0.75 (see Figure 13). A similar sulforhodamine-B plate ( $900 \text{ cm}^{-1}$  Stokes shift) has a radiative transport efficiency of 0.45 (see Figure 13).

Self-absorption losses have been experimentally determined by measuring the dependence of plate efficiency on plate size. Experimental and computed results are consistent, and indicate that a 3.5 mm thick plate doped with a coumarin type of dye at a concentration such that the peak optical density is 3, suffers only a 10% loss in collector efficiency when the surface area is increased from  $200 \text{ cm}^2$  to  $2000 \text{ cm}^2$  (Table 21).<sup>3</sup>

We have used the theoretical modeling results to guide the experimental program for developing a higher efficiency LSC. Our most recent calculations<sup>3</sup> indicate that collector efficien-



\*Transverse Absorbance =  $\frac{\text{Peak Optical Density} \times \text{Plate Width}}{\text{Plate Thickness}}$

Figure 13. Radiative Transport Efficiencies Calculated as a Function of Logarithm of Transverse Absorbance

Table 21

Projected Collector Efficiencies\* As a Function  
of Plate Size For Hypothetical, Three Dye LSC<sup>3</sup>

Size Sensitive Parameters	Plate Size (cm <sup>2</sup> )		
	10	200	2000
Transverse Abs.	27	120	380
Edge Emission Peak (nm)	785	800	801
Matrix Eff.	.99	.97	.90
Rad. Transport Eff.	.87	.80	.75
Plate Eff.	.29	.26	.23
Eff. Conc. Ratio	1.2	4.8	13.5
Si Cell Eff.	.32	.33	.34
Collector Eff.	9.4%	8.7%	7.8%

\*Projection based on ratioed improvement of plate 63D which had a measured collector efficiency of 3.2% and a transverse absorbance of 120 (area of 200 cm<sup>2</sup>). Note that the annualized collector efficiencies will be considerably higher than the peak efficiencies calculated here (see Section VIII).



cies of approximately 9% are realistic for a 3-dye LSC (Table 21). This calculation assumes that the third dye absorbs 85% of the solar photons between 650 and 800 nm, has a quantum efficiency of 0.9, a Stokes shift of approximately  $2500 \text{ cm}^{-1}$ , and a peak edge emission wavelength of about 800 nm. The experimental efficiency improvement program is outlined in Table 22. It is noted that since the total daily output energy-to-peak power ratio of an LSC is at least 20% greater than that of a crystalline silicon photovoltaic array (see Section VIII), a 9% LSC collector efficiency would be equivalent to an 11% efficient crystalline silicon photovoltaic array. We thus expect annualized collector efficiencies in excess of 10% to be reasonable for a single plate LSC coupled to a silicon photovoltaic cell. In addition, higher efficiencies for more sophisticated LSC configurations would be anticipated.

Table 22

Efficiency Improvement Program

- A. Expand Solar Absorption Region
- B. Optimize Host for Maximum Dye Quantum Efficiency
- C. Optimize Dye-Dye Energy Transfer
- D. Optimize Multilayer Film Structure
- E. Minimize Self-Absorption
- F. Cell Optimization
- G. Optimize Thin Film and Substrate for Maximum Internal Reflectivity and Minimum Bulk Attenuation Loss

## VI. OPTICAL PROPERTIES OF CR(III) DOPED TRANSPARENT GLASS-CERAMICS

The work to be described in this section was performed over the period October 16, 1980 to March 5, 1982, under internal Owens-Illinois, Corporate Glass and Ceramic Technology funding. Because the work is relevant to the Luminescent Solar Concentrator program, it has been decided to release the information in this report.

A study of  $\text{Cr}^{3+}$  doped transparent glass-ceramics was undertaken to address the poor efficiency of inorganic glasses in converting solar energy into luminescence. Six-fold coordinated  $\text{Cr}^{3+}$  ions, because of two broad spin-allowed absorption bands in the visible spectral region, are efficient absorbers of solar radiation. The ion is also known to luminesce with high efficiency in a large number of crystalline systems. However, the luminescence quantum efficiency of  $\text{Cr}^{3+}$  doped glasses are generally poor.<sup>21</sup> Cost, of course, precludes the use of  $\text{Cr}^{3+}$  doped single crystals in an LSC. Therefore, the idea was developed that high optical efficiency and low cost forming technology may be combined by doping an otherwise transparent glass-ceramic with  $\text{Cr}^{3+}$ .

The same considerations have led Lempicki and co-workers to a similar investigation. At the October 25, 1980 SERI Luminescent Solar Concentrator review meeting, Andrews and Lempicki reported that fluorescence from  $\text{Cr}^{3+}$  in a boron-alumino phosphate glass was shifted to longer wavelength and that the fluorescence lifetime was lengthened after crystallizing the glass through heat treatment.<sup>22</sup> At the March 26, 1982 SERI Luminescent Solar Concentrator review meeting, Lempicki and co-workers presented spectral and lifetime measurements of  $\text{Cr}^{3+}$  doped  $\beta$ -quartz, gahnite, and mullite

glass-ceramics.<sup>23</sup> The first two of these systems had also been studied here and our results are in substantial agreement.

Glass-ceramics are multi-phase materials produced by the controlled crystallization of certain glass compositions.<sup>24</sup> Typically, a nucleant is added to the glass batch composition and a homogeneous (usually) glass is first prepared by a normal glass melting and annealing process. The glass-ceramic transformation is achieved by subjecting the glass to a carefully controlled heat-treatment schedule which results in the nucleation and growth of crystal phases within the glass.

The first step in the heat-treatment schedule is usually to hold the glass for a controlled time at a temperature (somewhat above the annealing temperature of the glass) at which a large volume number of crystalline nuclei form within the amorphous glass. The nucleated glass is then heated to and held at a higher temperature for a controlled time during which crystal growth occurs. The nucleation and growth crystal phases are generally different, and depending on initial glass composition and heat-treatment schedule more than one crystal phase may form during the growth period. In some systems, heating to and holding the material at a third temperature causes a transformation of the major crystalline phase formed during the first growth period into a different crystal phase. The crystallization process can be taken almost to completion in many cases, but more usually a significant proportion of residual glass phase remains.

Glass-ceramics are usually opaque; however, a number of fine-grained transparent materials have been described in the literature. Beall and Duke in 1969 described the conditions required for visible transparency: either the crystallites of all species in the glass-ceramic must be much smaller than the wavelength of visible light or the birefringence of the crystals and the difference in the refractive index between

crystals and glass must be very small.<sup>25</sup> Also described were examples of transparent glass-ceramics in which the major crystalline phase was a solid solution of  $\beta$ -quartz, spinel, or mullite. A number of transparent perovskite glass-ceramics have also been reported: barium titanate, sodium niobate and various mixed niobates.<sup>26,27</sup>

In the following subsections details of investigations of four  $\text{Cr}^{3+}$  doped transparent glass-ceramic systems are presented. Each of the systems studied here had at least one property that was inconsistent with the requirements of an LSC material. The  $\beta$ -quartz glass-ceramics were essentially non-luminescent, presumably because the  $\text{Cr}^{3+}$  ions remained in the residual glass phase. The  $\beta$ -spodumene glass-ceramics emitted strongly in a resonant zero-phonon  ${}^2\text{E}$  line, and, hence, luminescence was strongly self-absorbed by other  $\text{Cr}^{3+}$  ions in the crystal phase. The gahnite glass-ceramics also emitted strongly from the  ${}^2\text{E}$  state; however, most of the emission occurred in phonon sidebands. Although self-absorption due to  $\text{Cr}^{3+}$  ions in crystal sites was not severe, absorption due to  $\text{Cr}^{3+}$  ions in the residual glass phase was strong. The enstatite glass-ceramics showed low field emission from the  ${}^4\text{T}_2$  state. Emission was deeper toward the red, and, therefore, absorption of luminescence due to  $\text{Cr}^{3+}$  ions in crystal or glass phases was weaker. However, measured quantum efficiencies were low, approximately 0.1, apparently because of low volume fraction crystallinity.

#### VI. A. Beta-Quartz and Beta-Spodumene Glass-Ceramics

The first  $\text{Cr}^{3+}$  doped transparent glass-ceramics investigated here were in the lithium aluminum silicate system. Glasses with a major base glass composition lying within the range 50-75 wt.%  $\text{SiO}_2$ , 16-35 wt.%  $\text{Al}_2\text{O}_3$ , and 3-5.5 wt.%  $\text{Li}_2\text{O}$  and with 2-10 wt.% of the heterogeneous nucleants  $\text{TiO}_2$  and/or  $\text{ZrO}_2$  can be thermally devitrified to produce transparent glass-

ceramics. A heat treatment schedule of: 1300-1350°F (2-5 hrs.), 1450-1600°F (1-2 hrs.) produces a material whose major crystalline phase is a solid solution of  $\beta$ -quartz- $\beta$ -eucryptite. A third heat treatment step of 1800-1850°F (1 hr.) produces a reconstructive transformation of the major crystalline phase to a solid solution of  $\beta$ -spodumene.

Transparent glass-ceramics of the  $\beta$ -quartz and  $\beta$ -spodumene-type doped with various transition metal ions were studied by Babcock, Busdiecker, and Hagedorn at Owens-Illinois, and a patent filed in 1965.<sup>28</sup> It was reported that up to 0.2 wt.%  $\text{Cr}_2\text{O}_3$  produces a green glass which may be thermally devitrified to a pink transparent  $\beta$ -spodumene glass-ceramic.

Spectral emission and lifetime studies were made of three 0.025 wt.%  $\text{Cr}_2\text{O}_3$  samples made by Babcock, et al. in their earlier investigation. The three samples were of identical batch composition -- the first was an as-melted lithium aluminum silicate (LAS) glass, the second a transparent  $\beta$ -quartz glass-ceramic, and the third a transparent  $\beta$ -spodumene glass-ceramic. Composition and heat-treatment schedules were similar to those of examples 13 and 14 described in the patent of Babcock, et al.<sup>28</sup>

The  $\text{Cr}^{3+}$  : LAS glass sample had two broad absorption bands with maxima at 450 and 650 nm. In the  $\text{Cr}^{3+}$  :  $\beta$ -quartz glass-ceramic, the longer wavelength absorption band maxima was at 675 nm and the position of the shorter wavelength band was obscured by scattering or absorption in the near UV. Neither sample showed detectable emission. Recently, Kisilev, et al. have reported the excitation and emission spectra of a  $\text{Cr}^{3+}$  doped  $\beta$ -quartz glass-ceramic.<sup>29</sup> Excitation and emission spectra are similar to those from  $\text{Cr}^{3+}$  doped glasses. Therefore, there was no evidence to conclude that the observed emission originated in the  $\beta$ -quartz phase.

The spectral characteristics of the  $\beta$ -spodumene glass-ceramic were considerably different from those of the LAS glass or the  $\beta$ -quartz glass-ceramic. The absorption bands were shifted to shorter wavelength (420 and 560 nm) and intense emission, principally in a narrow line at 694.4 nm, was observed (see Figures 14 and 15).

The spectral features of the three samples can be interpreted with the aid of the simplified Tanabe-Sugano diagram for  $d^3$  ions in octahedral coordination given in Figure 16. The energy levels that participate in the major absorption and emission bands of  $Cr^{3+}$  are plotted as a function of crystal field strength,  $Dq$ . Both  $E$  and  $Dq$  are given in units of  $B$ , a parameter that is expected to vary little for a particular ion.

The crystal field strength in  $Cr^{3+}$  :  $\beta$ -spodumene glass-ceramic is high (very similar to ruby) and the lowest energy excited state is the  ${}^2E$  state. Absorption is principally via spin-allowed transitions into the  ${}^4T_1$  and  ${}^4T_2$  states, and excitation very rapidly relaxes to the metastable  ${}^2E$  state from which emission is observed. Because the high field electron configurations of the  ${}^4A_2$  ground state and the  ${}^2E$  state are the same ( $t_2^3$ ), the equilibrium position of the ions in both states is expected to be essentially the same, and Franck-Condon arguments suggest that emission will principally be in a narrow zero-phonon line. The zero-phonon line, historically labeled the R line, is split into two poorly resolved components in Figure 15 by spin-orbit coupling and trigonal distortion crystal field terms.<sup>30</sup> The R line emission splitting is better resolved in Figure 17 obtained with a Spec Fluorolog spectrofluorometer at 0.25 nm resolution. Evidence for trigonal distortion is also present in the asymmetry of the 420 nm excitation band in Figure 14. When symmetry is lowered by trigonal distortion, the  ${}^4T_1$  state is split into  ${}^4A_2$  and  ${}^4E$  states. The broad, low intensity, structured emission also seen in Figure 15 is principally phonon side band emission from

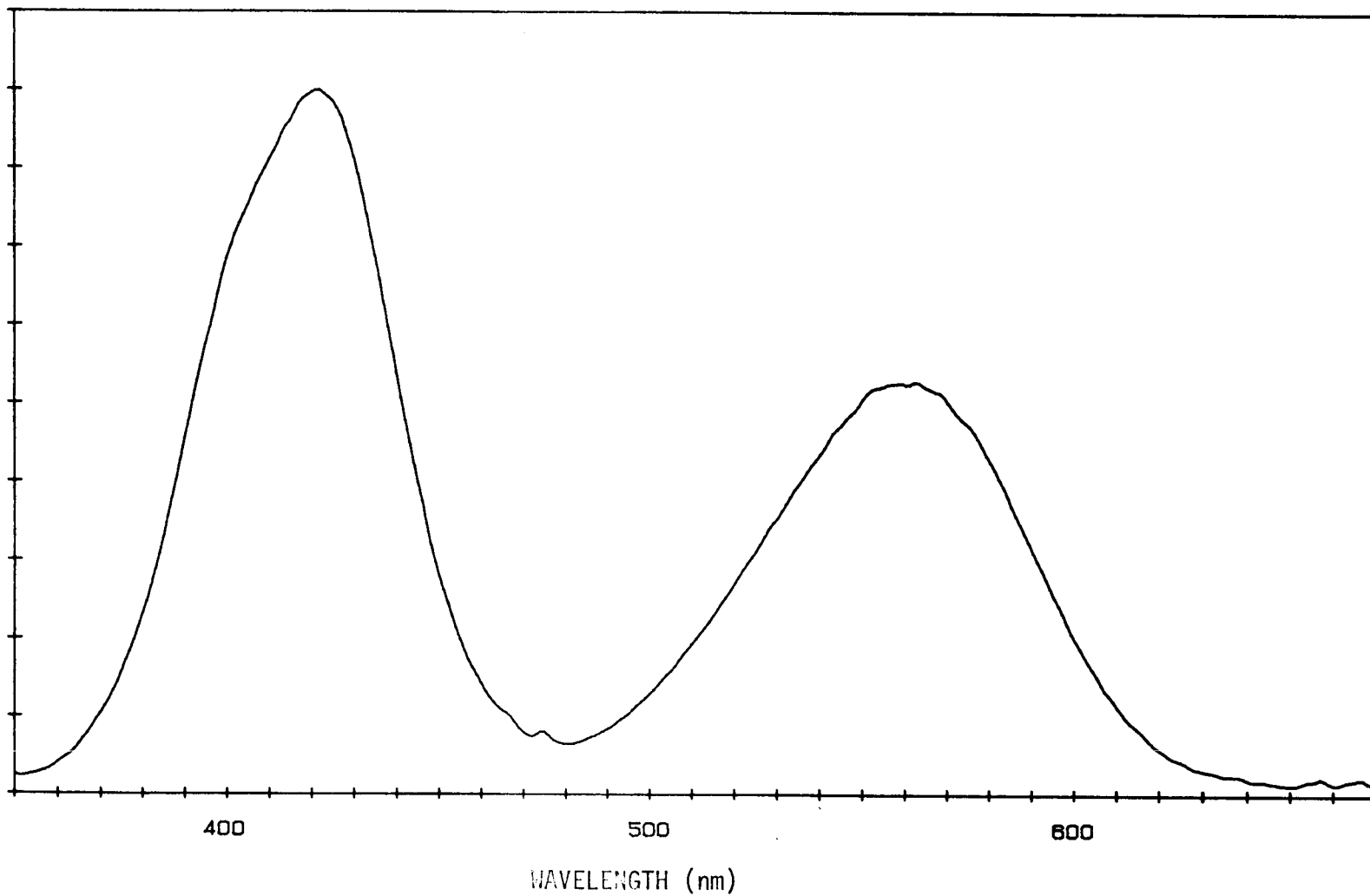


Figure 14. Excitation Spectrum of Cr<sup>3+</sup> :  $\beta$ -Spodumene Glass-Ceramic

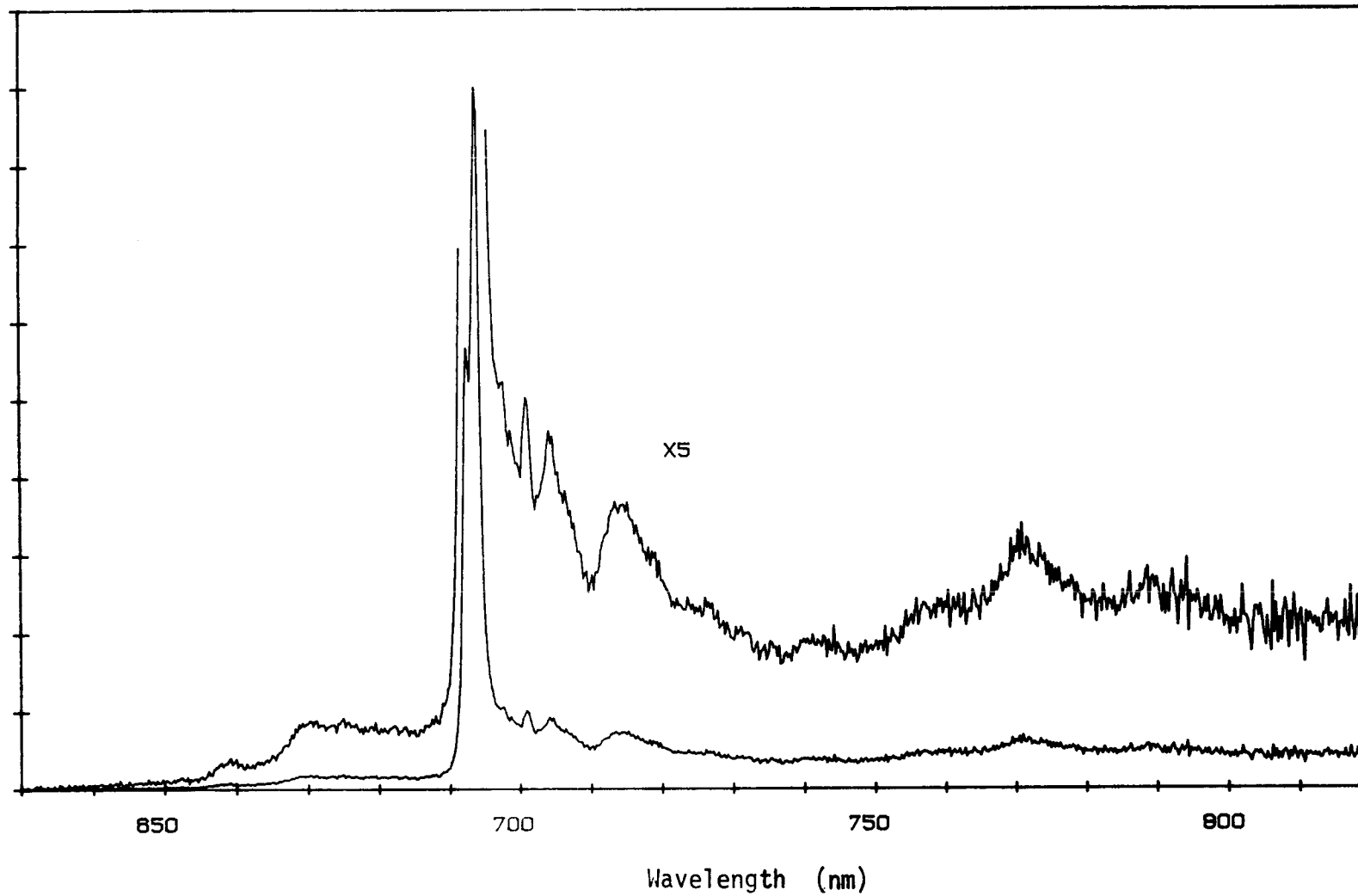


Figure 15. Emission Spectrum of Cr<sup>3+</sup>: β-spodumene Glass-Ceramic



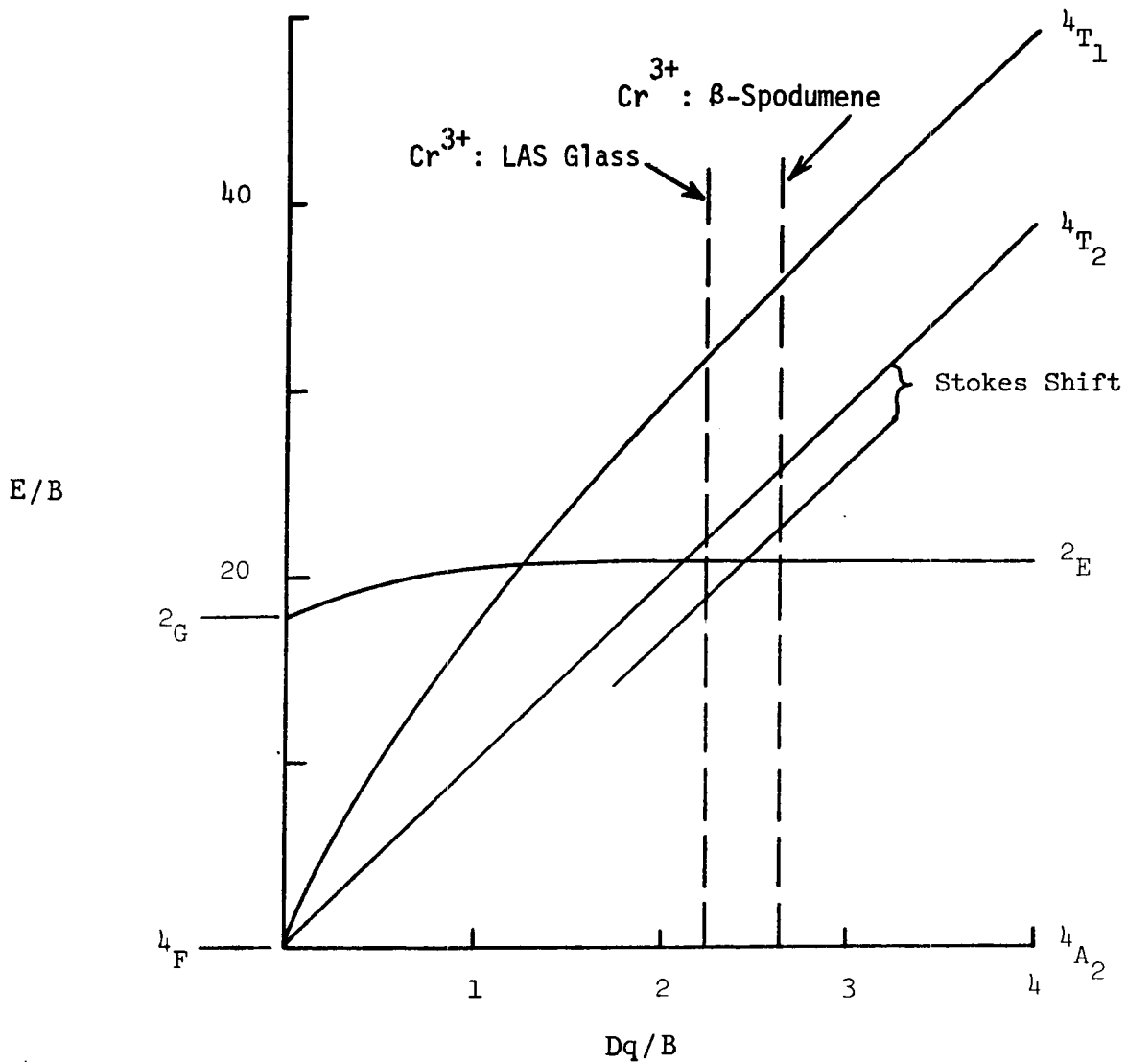


Figure 16. Energy Diagram of  $d^3$  Configuration in Octahedral Coordination

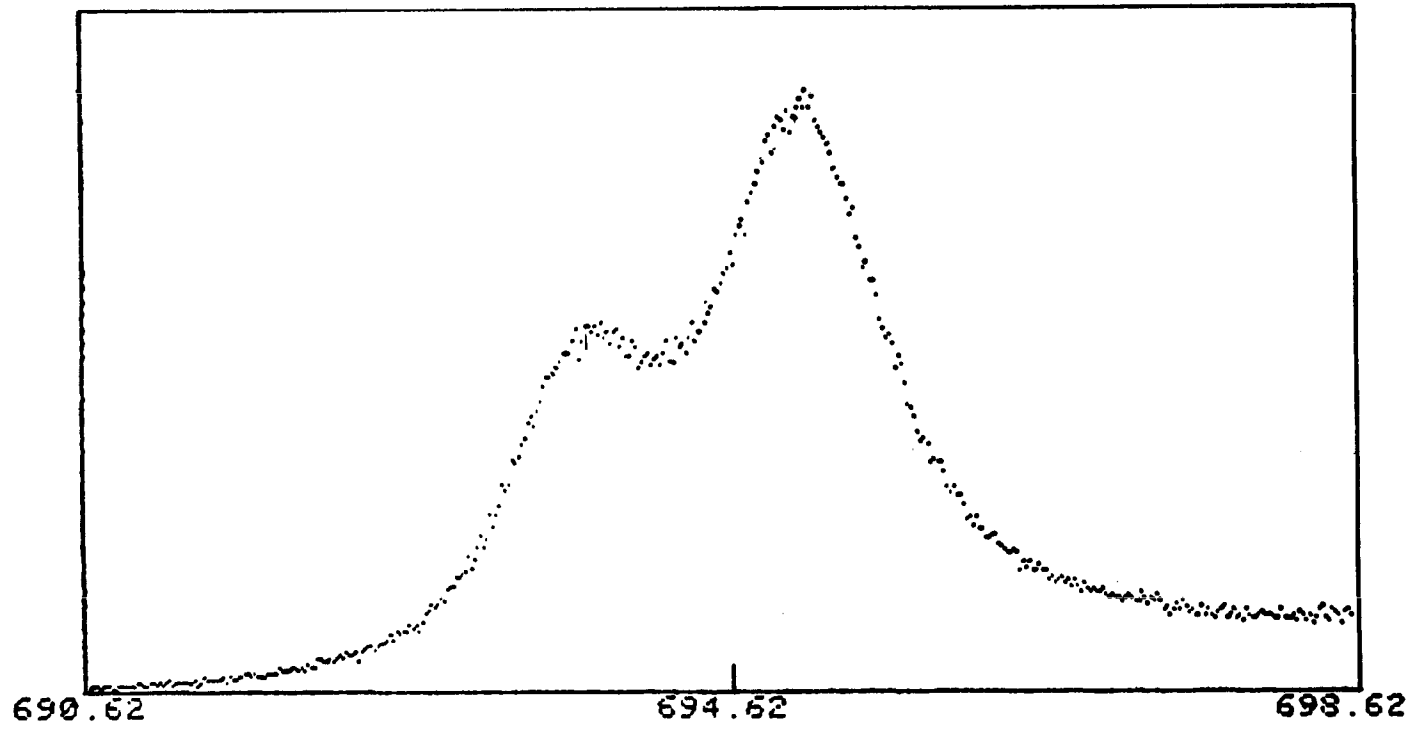


Figure 17. R Line Emission of Cr<sup>3+</sup>:  $\beta$ -Spodumene  
Glass-Ceramic at 0.25nm Resolution

those  $\text{Cr}^{3+}$  sites from which the R line emission arises. However, the narrower features lying within 15 nm to the red of the R line may be zero-phonon emission from  $\text{Cr}^{3+}$  ion pairs (N lines).

Lifetime measurements were also made of the  $\text{Cr}^{3+}$  :  $\beta$ -spodumene sample. Excitation was with a 5  $\mu\text{s}$  duration Xe flash lamp passing through a 459.5 nm interference filter. The sample emission passed by a Schott RG610 glass filter (passes wavelengths longer than 610 nm) was detected by an S-20 response photomultiplier tube and displayed as a function of time on an oscilloscope. The observed emission decay was non-exponential with a first 1/e folding time of 920  $\mu\text{s}$  and a second 1/e folding time of 1.2 ms. The long observed lifetime is consistent with emission from the  ${}^2\text{E}$  state.

The absorption spectrum of the  $\text{Cr}^{3+}$  : LAS glass is similar to that observed in a wide variety of  $\text{Cr}^{3+}$  : glasses<sup>21</sup> and a number of low crystal field crystalline materials. The mean crystal field strength is lower because of the relatively more open structure characteristic of glasses and results in the observed shift to longer wavelength of the  ${}^4\text{T}_1$  and  ${}^4\text{T}_2$  absorption bands.

Crystallographic studies provide some clarification of the optical properties of  $\text{Cr}^{3+}$  in  $\beta$ -spodumene and  $\beta$ -quartz glass-ceramics. Crystalline  $\text{Cr}_2\text{O}_3$  has a structure in which the oxygen positions approximate hexagonal close packing, and  $\text{Cr}^{3+}$  occupies two-thirds of the octahedral interstices with Cr-O distances of 2.02 and 1.97 Å. Corundum,  $\alpha\text{-Al}_2\text{O}_3$ , is isomorphous with Al-O distances of 1.97 and 1.86 Å<sup>31</sup>; therefore,  $\text{Cr}^{3+}$  may be easily introduced substitutionally for Al into crystal structures that contain octahedrally coordinated Al (i.e., ruby,  $\text{Cr}^{3+}$  :  $\alpha\text{-Al}_2\text{O}_3$ ). Crystalline alumino-silicates; however, consist typically of a

three-dimensional framework of  $\text{SiO}_4$  and  $\text{AlO}_4$  tetrahedra. It is presumed, therefore, that  $\text{Cr}^{3+}$  can only enter these structures interstitially, occupying approximately octahedral cavities.

The crystalline phase of the  $\beta$ -quartz glass-ceramic is a solid solution of  $\beta$ -quartz ( $\text{SiO}_2$ ) and a crystal variously called in the literature  $\beta$ -eucryptite or  $\gamma$ -spodumene ( $\text{LiAlSi}_2\text{O}_6$ ) whose framework is isotopic with  $\beta$ -quartz. Li determined the crystal structure of  $\beta$ -quartz solid solution and identified a large cavity which was found to have a six-fold coordination with oxygen.<sup>32</sup> The average distance from the center of the cavity to the six nearby oxygens was 2.40 Å with a range from 2.28 to 2.66 Å. These distances are much larger than the typical Cr-O bond length, and it is likely that there is insufficient crystal field stabilization energy for  $\text{Cr}^{3+}$  to occupy the site. It is, therefore, presumed that  $\text{Cr}^{3+}$  in the  $\beta$ -quartz glass-ceramic remains principally in the residual glassy phase.

The  $\beta$ -spodumene glass-ceramics have a major crystal phase which is a solid solution of  $\beta$ -spodumene (an isomorph of  $\text{LiAlSi}_2\text{O}_6$ ) and keatite (an isomorph of  $\text{SiO}_2$ ). The structure of  $\beta$ -spodumene consists of a three-dimensional framework of  $(\text{Si,Al})\text{O}_4$  tetrahedra. Distorted octahedral cavities have been identified by Li and Peacor in  $\beta$ -spodumene, but the distance from the center of the cavity to the six nearby oxygens, 1.84, 2.54, and 2.65 Å,<sup>33</sup> while smaller than those observed in  $\beta$ -quartz solid solution, again seem large to accommodate  $\text{Cr}^{3+}$ . Nevertheless, Hummel, Auh and Johnson<sup>34</sup> have demonstrated that  $\text{Cr}^{3+}$  is soluble in  $\beta$ -spodumene and tentatively suggested that the chromium enters the octahedral sites identified by Li and Peacor.<sup>33</sup> Our emission data demonstrates conclusively that  $\text{Cr}^{3+}$  occupies high field octahedral crystalline sites; however, whether the sites are those identified by Li and Peacor in  $\beta$ -spodumene or other as-yet-unidentified sites cannot be established.

In the Luminescent Solar Concentrator context,  $\text{Cr}^{3+}$  :  $\beta$ -spodumene glass-ceramics fail to satisfy the minimum optical properties criteria. Emission intensity appears strong (quantum yields were not measured); however, a large fraction of the emission intensity is in the resonant R lines. Therefore, self-absorption by other  $\text{Cr}^{3+}$  ions in the crystalline phase is expected to be unacceptably large.

## VI. B. Spinel Glass-Ceramics

The composition and heat-treatment schedules for preparing transparent spinel-type glass-ceramics have been described by Beall and Duke.<sup>25</sup> Beall also reported in a patent disclosure that transparent spinel glass-ceramics can be doped with  $\text{Cr}_2\text{O}_3$  to produce red transparent materials that exhibit photoluminescence similar to ruby.<sup>35</sup> The absorption and emission spectra of  $\text{Cr}^{3+}$  doped single crystal spinels have been described by Wood, *et al.*<sup>36</sup> and by Mikenda and Preisinger.<sup>37</sup>

The spinels constitute a group of double oxides with the general formula  $\text{AB}_2\text{O}_4$ . In the normal spinel structure characteristic of natural crystals, cation A occupies a tetrahedral site and cation B occupies a trigonally distorted octahedral site. Synthetic samples are, however, partially inverse where the inverted structure is  $\text{B}^{(\text{tet})}\text{A}^{(\text{oct})}\text{B}^{(\text{oct})}\text{O}_4$ . The two members of the spinel group of concern here are spinel itself,  $\text{MgAl}_2\text{O}_4$ , and gahnite,  $\text{ZnAl}_2\text{O}_4$ . Mg-spinel forms a solid solution series with alumina whose end members are  $\text{MgO} \cdot \text{Al}_2\text{O}_3$  and roughly  $\text{MgO} \cdot 3.5\text{Al}_2\text{O}_3$ .<sup>38</sup> It can be safely presumed that gahnite forms a similar solid solution series. The Al-O interatomic distance in Mg-spinel is 1.91 Å,<sup>39</sup> and, therefore,  $\text{Cr}^{3+}$  easily enters the structure substitutionally for Al.

A number of transparent spinel glass-ceramics containing various levels of  $\text{Cr}^{3+}$  were prepared using base glass batch

compositions 5 and 6 of Beall and Duke.<sup>25</sup> Low levels of  $\text{As}_2\text{O}_3$  were also added to stabilize the Cr(III) oxidation state. The composition of the glasses prepared here are presented in Table 23.

Table 23 - Composition in Wt.% of  $\text{Cr}^{3+}$   
Doped Spinel and Gahnite Glass-Ceramics

I.D.	$\text{Cs}_2\text{O}$	MgO	ZnO	$\text{Al}_2\text{O}_3$	$\text{SiO}_2$	$\text{ZrO}_2$	$\text{Cr}_2\text{O}_3$	$\text{As}_2\text{O}_3$
SC01	--	4.62	5.54	17.55	64.65	7.39	0.05	0.20
SC02	--	4.62	5.54	17.54	64.62	7.38	0.10	0.20
SC03	--	4.61	5.53	17.52	64.55	7.38	0.20	0.20
SC04	--	4.60	5.52	17.49	64.42	7.36	0.40	0.20
SC05	--	4.58	5.50	17.42	64.16	7.33	0.80	0.20
SC06	--	4.55	5.46	17.27	63.64	7.27	1.60	0.20
SC07	--	4.63	5.56	17.59	64.81	7.41	--	--
SC08	3.63	--	11.79	15.41	63.47	5.44	0.05	0.20
SC09	3.63	--	11.78	15.41	63.44	5.44	0.10	0.20
SC10	3.62	--	11.77	15.39	63.38	5.43	0.20	0.20
SC11	3.64	--	11.82	15.45	63.63	5.45	--	--

$\text{Cr}_2\text{O}_3$  itself is a nucleant, and a number of compositions with higher levels of  $\text{Cr}_2\text{O}_3$ ; SC05, SC06 and SC10; partially devitrified when the melts were cooled. Transparent glass-ceramics were made of the remaining compositions by subjecting samples to the following two-step heat-treatment schedule: samples SC01-SC07: 800°C (4 hrs.), 950°C (4 hrs.); samples SC08-SC10: 800°C (4 hrs.), 1000°C (4 hrs.)

Glass-ceramics SC08-SC11, because of the absence of MgO, clearly can only devitrify to gahnite. Beall and Duke identified the crystal phase present in composition SC07, and presumably also in the compositions derived from SC07 by the addition of  $\text{Cr}_2\text{O}_3$ , as a spinel solid solution. The close similarity of the lattice parameters of Mg-spinel ( $a = 8.080 \text{ \AA}$ ) and gahnite ( $a = 8.088 \text{ \AA}$ ) suggest the possibility of the presence of a  $(\text{Zn,Mg})\text{Al}_2\text{O}_4$  solid solution.<sup>40</sup> However, Stryjak

and McMillan have also studied composition SC07 thermally devitrified by the heat-treatment schedule of Beall and Duke, and from x-ray diffraction results concluded that the major crystalline phase was gahnite.<sup>41</sup> (To be precise, Stryjak and McMillan reported that 9.1 wt.%  $ZrO_2$  is required in SC07 for the precipitation of gahnite; at lower  $ZrO_2$  levels a  $\beta$ -quartz solid solution phase forms. However, our emission data clearly shows that compositions SC01-SC06 formed a crystalline phase within the spinel group.)

The excitation and emission spectra of composition SC04 before devitrification and after devitrification is presented in Figures 18 and 19. Emission from the gahnite glass-ceramic is very similar to reported room temperature emission from  $Cr^{3+}$  doped gahnite single crystals.<sup>36</sup> Unresolved R line emission occurs at 683 nm and the additional observed structure has been assigned to N line emission (due to  $Cr^{3+}$ - $Cr^{3+}$  pairs and inverse spinel disordered sites) and phonon side bands. Thermally populated  $^4T_2$  emission probably contributes to the underlying broad unstructured emission.

Quantum yield measurements were made using a 0.11 mol%  $UO_3$  doped potassium borosilicate glass secondary fluorescence standard. Glass-ceramics of composition SC02 (0.10 wt.%  $Cr_2O_3$ ), SC03 (0.20 wt.%  $Cr_2O_3$ ) and SC04 (0.40 wt.%  $Cr_2O_3$ ) had measured quantum yields of 0.62, 0.35 and 0.28, respectively. Emission lifetimes of the three gahnite glass-ceramics were also measured using the apparatus described in the previous section with the exception that excitation pulses were filtered with a Schott BP44 glass filter (passes wavelengths shorter than 440 nm) and emission was observed through a Schott RG630 glass filter (passes wavelengths longer than 630 nm). The decay curve of SC02 showed a very weak fast component with a  $1/e$  lifetime of 60  $\mu s$ , and an intense non-exponential slow component with an apparent first order  $1/e$  lifetime of 5 ms at

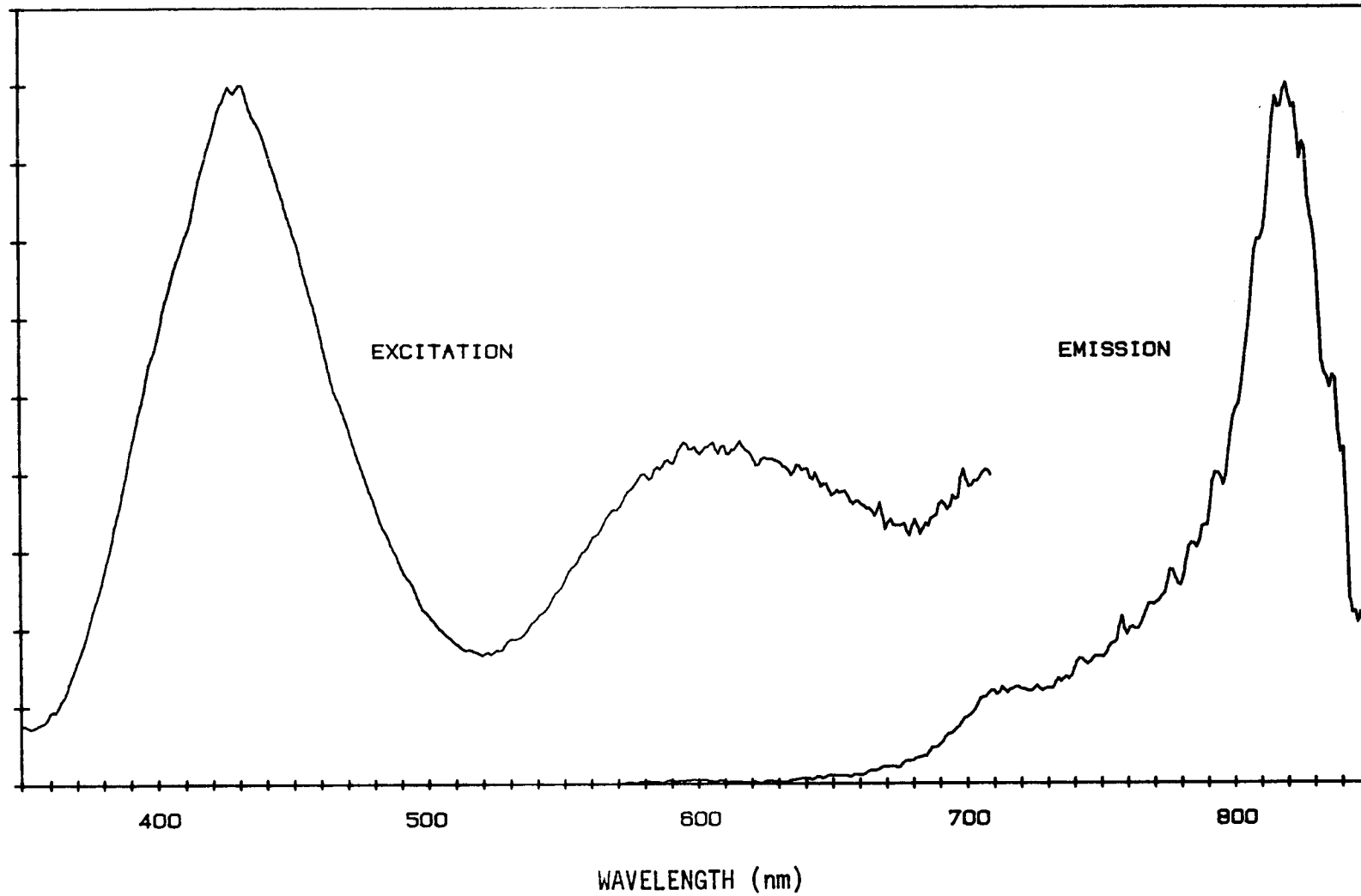


Figure 18. Excitation and Emission Spectra of  $\text{Cr}^{3+}$ : Aluminosilicate Glass (SC04)



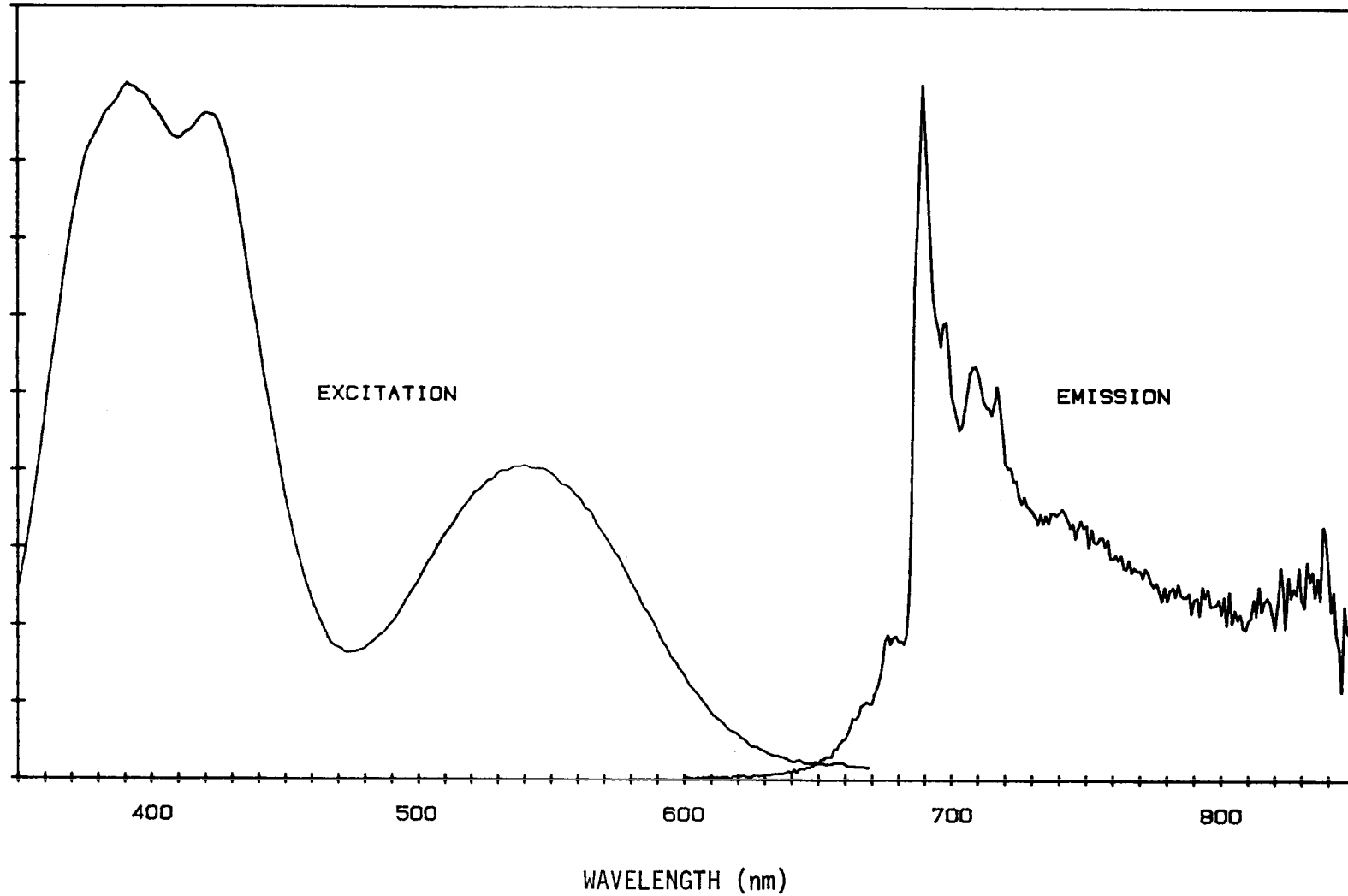


Figure 19. Excitation and Emission Spectra of  $\text{Cr}^{3+}$ : Gahnite Glass-Ceramic (SC04)

$t = 5$  ms and 19 ms roughly between  $t = 15$  and  $t = 50$  ms. At  $t = 3.5$  ms glass-ceramics SC02 (0.10 wt.%  $\text{Cr}_2\text{O}_3$ ), SC03 (0.20 wt.%  $\text{Cr}_2\text{O}_3$ ) and SC04 (0.40 wt.%  $\text{Cr}_2\text{O}_3$ ) showed apparent first-order  $1/e$  lifetimes of 4.4, 3.2, and 2.7 ms, consistent with the concentration quenching observed in the quantum yield measurements.

On the basis of the emission spectral distribution and lifetime data, the gahnite glass-ceramics appear to be better candidates for an LSC material than the  $\beta$ -spodumene glass-ceramics. The smaller distribution of emission intensity among zero phonon lines and the longer  ${}^2\text{E}$  lifetime (which indicates a smaller  ${}^2\text{E}$  absorption cross-section) suggests that resonant self-absorption is less probable in the gahnite glass-ceramics. Concentration quenching is, however, clearly a problem in the gahnite materials. The peak absorbance of the  ${}^4\text{T}_2$  band in a 3 mm thick sample of the 0.40 wt.%  $\text{Cr}_2\text{O}_3$  glass-ceramic (SC04) is 0.55 and the quantum yield has been reduced by concentration quenching to 0.28. Therefore, the product of relative solar absorbance and quantum yield at the optimum  $\text{Cr}_2\text{O}_3$  concentration will be poor.

Unfortunately, a more serious difficulty associated with absorption by  $\text{Cr}^{3+}$  ions in the residual glass phase of luminescence from  $\text{Cr}^{3+}$  ions in the gahnite phase is also present. The absorbance spectra of 3 mm thick samples of a glass and a heat-treated gahnite glass-ceramic of composition SC04 are presented in Figure 20. It is observed that the glass has an intense absorption tail that extends from 650 nm out past 1  $\mu\text{m}$ . The glass-ceramic has weaker absorbance over the same region; however, the absorbance is sufficiently strong ( $0.27 \text{ cm}^{-1}$  at 700 nm) to cause large absorption losses, particularly if the absorbing species is essentially non-luminescent.

It is suggested that the source of the far-red absorption

tail in the gahnite glass-ceramic is absorption by  $\text{Cr}^{3+}$  ions in the residual glassy phase. This is indicated by the observations that the absorption tail was not seen in the excitation spectra of the gahnite glass-ceramic (Figure 19) nor in the absorption spectra of the undoped glass-ceramic (SC07). It is to be expected that a fraction of  $\text{Cr}^{3+}$  ions will remain in the glassy phase following heat treatment. Stryjak and McMillan have shown that gahnite glass-ceramics with a base glass composition (without  $\text{Cr}_2\text{O}_3$ ) very similar to SC01-SC07 and devitrified with a heat-treatment schedule identical to that used here have a residual glassy phase volume fraction of 70-80%.<sup>41</sup> Despite the low gahnite volume fraction, the absorption spectra indicate that the larger fraction of  $\text{Cr}^{3+}$  ions do segregate in the gahnite phase (because of the large crystal field stabilization energy of  $d^3$  ions and the higher crystal field strength in the gahnite phase). Sufficient  $\text{Cr}^{3+}$ , however, remains in the glassy phase to account for the far red absorption tail.

This problem is probably general for all  $\text{Cr}^{3+}$  doped high crystal field glass-ceramics. All reported  $\text{Cr}^{3+}$  doped silicate and phosphate glasses have appreciable  $^4\text{T}_2$  absorption in the range 650-800 nm. The absorbance over this range in the gahnite glass-ceramics would have to be reduced by 2 orders of magnitude to achieve a reasonable plate efficiency in a 100 cm square LSC. This, of course, requires a reduction by a similar magnitude in the product of the volume fraction of residual glassy phase times the concentration of  $\text{Cr}^{3+}$  in the phase. It is difficult to envision achieving this goal.

Since the completion of our work described in this section, a more thorough report of the work of Andrews and Lempicki on  $\text{Cr}^{3+}$  doped gahnite glass-ceramics has appeared.<sup>42</sup>

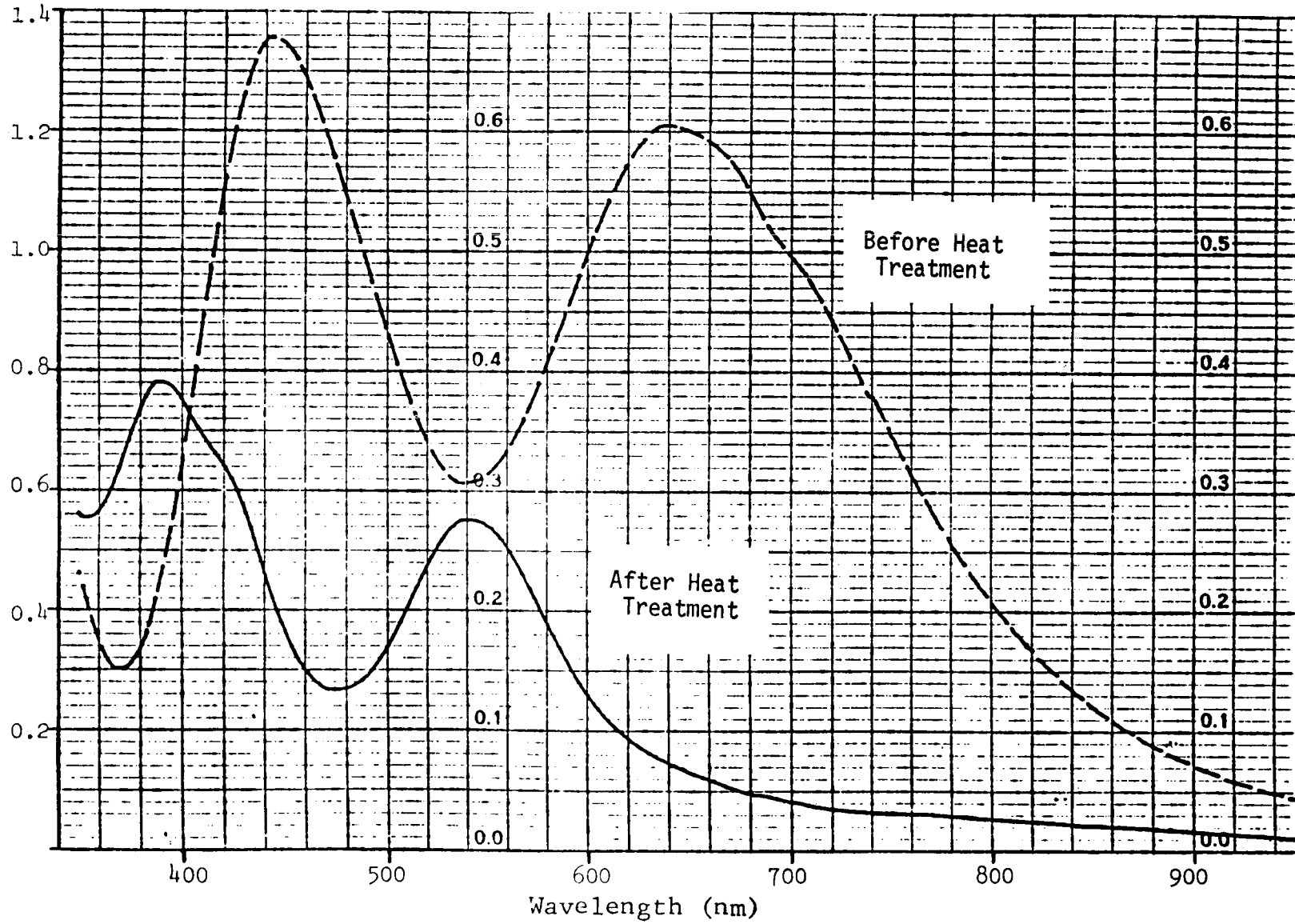


Figure 20. Absorption Spectra of  $\text{Cr}^{3+}$  Doped Aluminosilicate Glass and Gahnite Glass-Ceramic (3mm thick samples)

## VI. C. Enstatite Type Glass-Ceramics

An investigation of  $\text{Cr}^{3+}$  doped transparent enstatite type glass-ceramics developed from an initially empirical search for a low field crystal phase in the  $\text{MgO} \cdot \text{Al}_2\text{O}_3 \cdot \text{SiO}_2$  system. A glass of composition SC12 (see Table 24) was melted which completely devitrified upon cooling to a grey opaque ceramic. Front surface emission and excitation spectra were obtained which showed strong luminescence from  $\text{Cr}^{3+}$  in at least two different crystalline phases (Figure 21). Chromium (III) : spinel luminescence was clearly assigned from the excitation and emission spectra. A low crystal field phase was also observed that had a broad  $\text{Cr}^{3+}$  emission band (excitation at 440 nm) with a maximum at approximately 830 nm. The  $^4\text{T}_1$  and  $^4\text{T}_2$  states were observed in the excitation spectrum (monitoring emission at 790 nm) at 430 and approximately 620 nm, respectively. Powder x-ray diffraction spectra were also obtained from SC12 which confirmed the presence of spinel,  $\text{MgAl}_2\text{O}_4$ , and suggested that the second major crystalline phase was enstatite,  $\text{MgSiO}_3$ .

Table 24 - Composition in Wt.% of  $\text{Cr}^{3+}$  Doped Enstatite Glass-Ceramics

I.D.	MgO	$\text{Al}_2\text{O}_3$	$\text{SiO}_2$	$\text{TiO}_2$	$\text{As}_2\text{O}_3$	$\text{Cr}_2\text{O}_3$
SC12	29.97	25.09	44.67	--	--	0.26
SC13	14.71	22.34	52.65	10.00	0.20	0.10
SC14	22.06	15.95	51.69	10.00	0.20	0.10
SC15	17.95	22.70	49.05	10.00	0.20	0.10
SC16	25.66	16.23	47.81	10.00	0.20	0.10
SC17	21.29	23.08	45.33	10.00	0.20	0.10
SC18	29.38	16.52	43.80	10.00	0.20	0.10
SC19	24.74	23.47	41.49	10.00	0.20	0.10
SC20	22.08	15.95	51.71	10.00	0.20	0.05
SC21	22.06	15.95	51.59	10.00	0.20	0.10
SC22	22.04	15.93	51.53	10.00	0.20	0.20
SC23	21.99	15.89	51.51	10.00	0.20	0.40
SC24	22.55	16.30	52.84	8.00	0.20	0.10
SC25	23.05	16.56	53.99	6.00	0.20	0.10
SC26	23.54	17.01	55.14	4.00	0.20	0.10

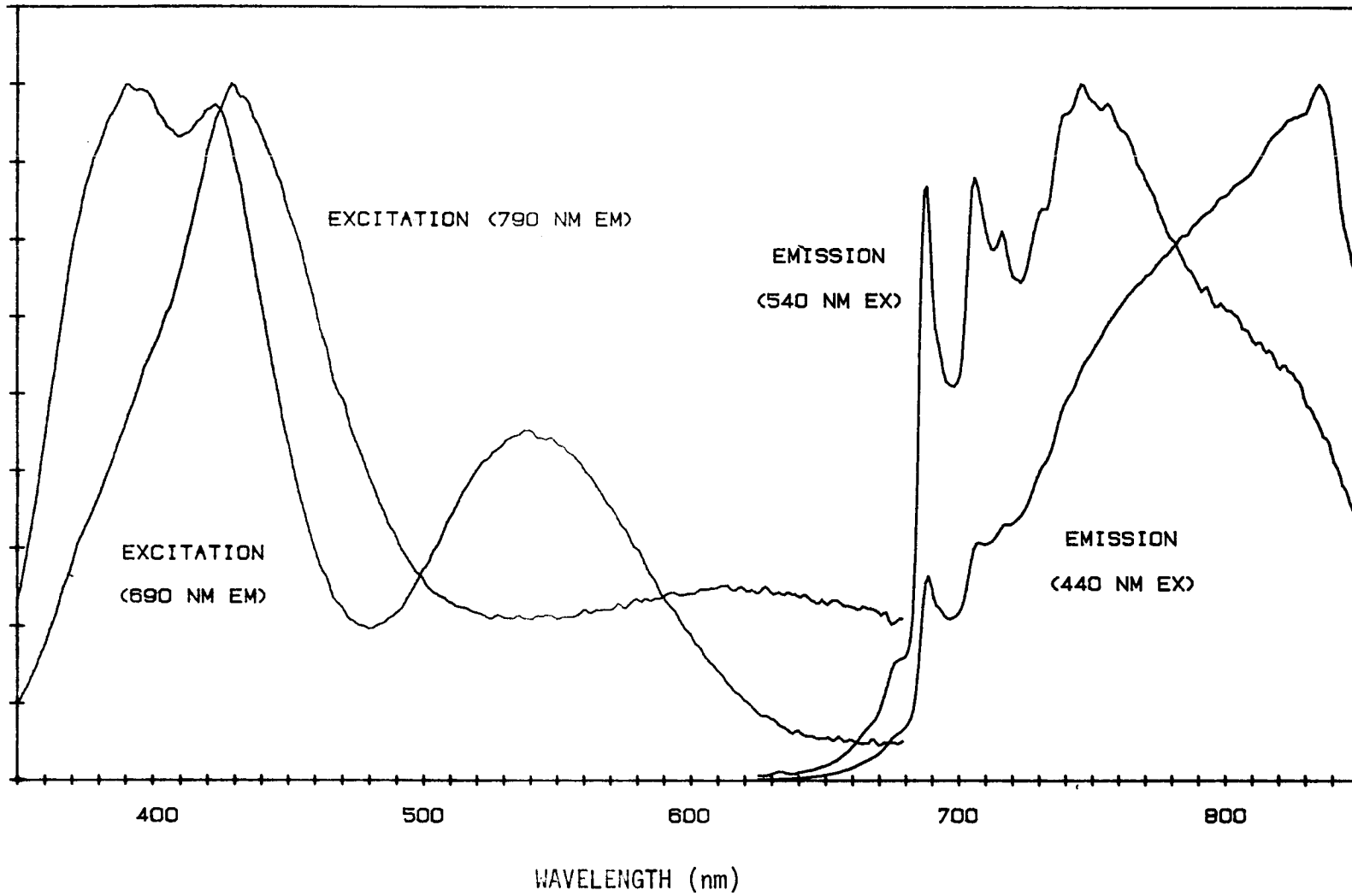


Figure 21. Excitation and Emission Spectra of the Opaque Cr<sup>3+</sup>: MAS Glass-Ceramic SC12

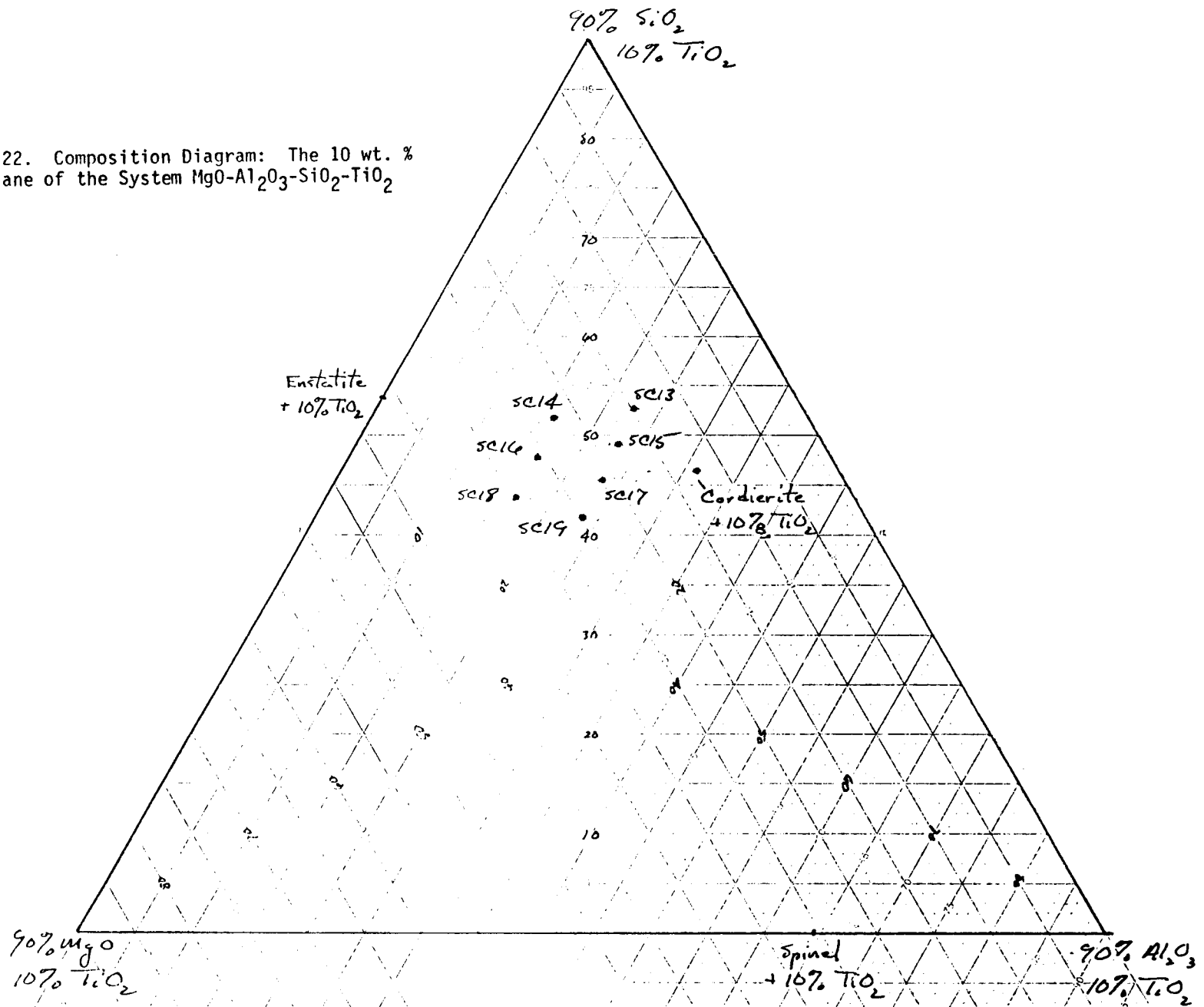
Crystallographic structural data is not inconsistent with an assignment of the observed low crystal field  ${}^4T_2$  emission to  $Cr^{3+}$  : enstatite. The structure of enstatite consists of chains of linked  $SiO_4$  tetrahedra with the Mg atoms occupying two sites, one of which is approximately octahedrally coordinated with Mg-O distances between 2.036 and 2.166 Å.<sup>44</sup> Substitution of Cr for Mg (and Al for Si to maintain charge balance) could yield a low crystal field octahedral  $Cr^{3+}$  site.

A program to develop a transparent  $Cr^{3+}$  doped enstatite glass-ceramic was initiated for two reasons. First, the low crystal field emission observed from SC12 and tentatively assigned to  $Cr^{3+}$  : enstatite has optical properties that may be well suited to an LSC device. Emission (presumably fluorescence from the  ${}^4T_2$  state) is to the red of the  ${}^2E$  emission observed in other  $Cr^{3+}$  doped crystalline systems studied here, and, therefore, residual glass phase  $Cr^{3+}$  absorption should be less problematic. Second, there is reason to expect that transparent enstatite glass-ceramics can be readily formed. Leger and Bray,<sup>45</sup> Plumat,<sup>46</sup> and Guzew, et al.<sup>47</sup> have reported the formation of fine grained enstatite glass-ceramics in the  $MgO-CaO-Al_2O_3-SiO_2 (+ TiO_2)$  system.

In order to define the composition and heat-treatment schedule required for the formation of transparent  $Cr^{3+}$  doped enstatite glass-ceramics, the following thermal gradient-isothermal heat-treatment tests were performed. Batches of composition SC13-SC19 (see Table 24) were melted and approximately 1 cm diameter cane was drawn directly from the melts. Each melt contained 10 wt.%  $TiO_2$  for nucleation and 0.1 wt.%  $Cr_2O_3$ . The location of the experimental melts is shown in the composition diagram, Figure 22.

Lengths of cane were then placed in a calibrated thermal gradient furnace for a length of time,  $t_{grad}$ . The minimum and maximum temperatures in the thermal gradient furnace were 900°F

Figure 22. Composition Diagram: The 10 wt. %  $TiO_2$  Plane of the System  $MgO-Al_2O_3-SiO_2-TiO_2$





and 1550°F. When removed from the gradient furnace, a length of cane that had been held at higher temperatures had typically devitrified to a very light green opaque ceramic. The temperature corresponding to the boundary between opaque ceramic and transparent glass is  $T_1$ , the minimum temperature for sensibly rapid crystal growth.

In order to successfully form a transparent microcrystalline glass-ceramic it is required that the rate of nuclei formation is rapid over some temperature range below the minimum temperature of rapid crystal growth. The temperature range of rapid nuclei formation was determined by placing cane samples from the thermal gradient furnace into an isothermal furnace held at a temperature  $T_{iso}$  somewhat above  $T_1$  for a time  $t_{iso}$ . At temperature  $T_{iso}$  crystal growth is rapid and a volume of glass that had not been extensively nucleated during the thermal gradient heat-treatment will be converted to a coarse grained opaque ceramic. A volume of glass, however, that had been extensively nucleated during the thermal gradient step will be converted to a fine grained transparent glass-ceramic. Therefore, if a transparent to translucent region remains after the isothermal heat-treatment step between boundaries corresponding to the lower temperature  $T_2$  and approximately  $T_1$ , it indicates that over this temperature range nucleation is rapid and crystal growth is slow.

The appearance of samples SC13-SC18 after subjection to thermal gradient-isothermal two-step heat-treatment tests are shown in Figure 23. Cane drawn from SC19 showed stone (macroscopic crystalline regions) formation upon cooling and was not further tested. In all tested samples bulk crystallization occurred after 4 hr. at temperatures above 1375-1500°F (observed  $T_1$  temperatures are indicated by red arrows in Figure 23). An isothermal time-temperature schedule of 4 hr. at 1600°F was, therefore, used for all samples. The low-silica, low alumina compositions SC18 and SC16 showed very

Figure 23. - Appearance of Samples SC13-SC18 Following Thermal Gradient-Isothermal Two Step Heat Treatment Schedule ( $t_{iso} = 4$  hr.,  $T_{iso} = 1600^{\circ}\text{F}$ )

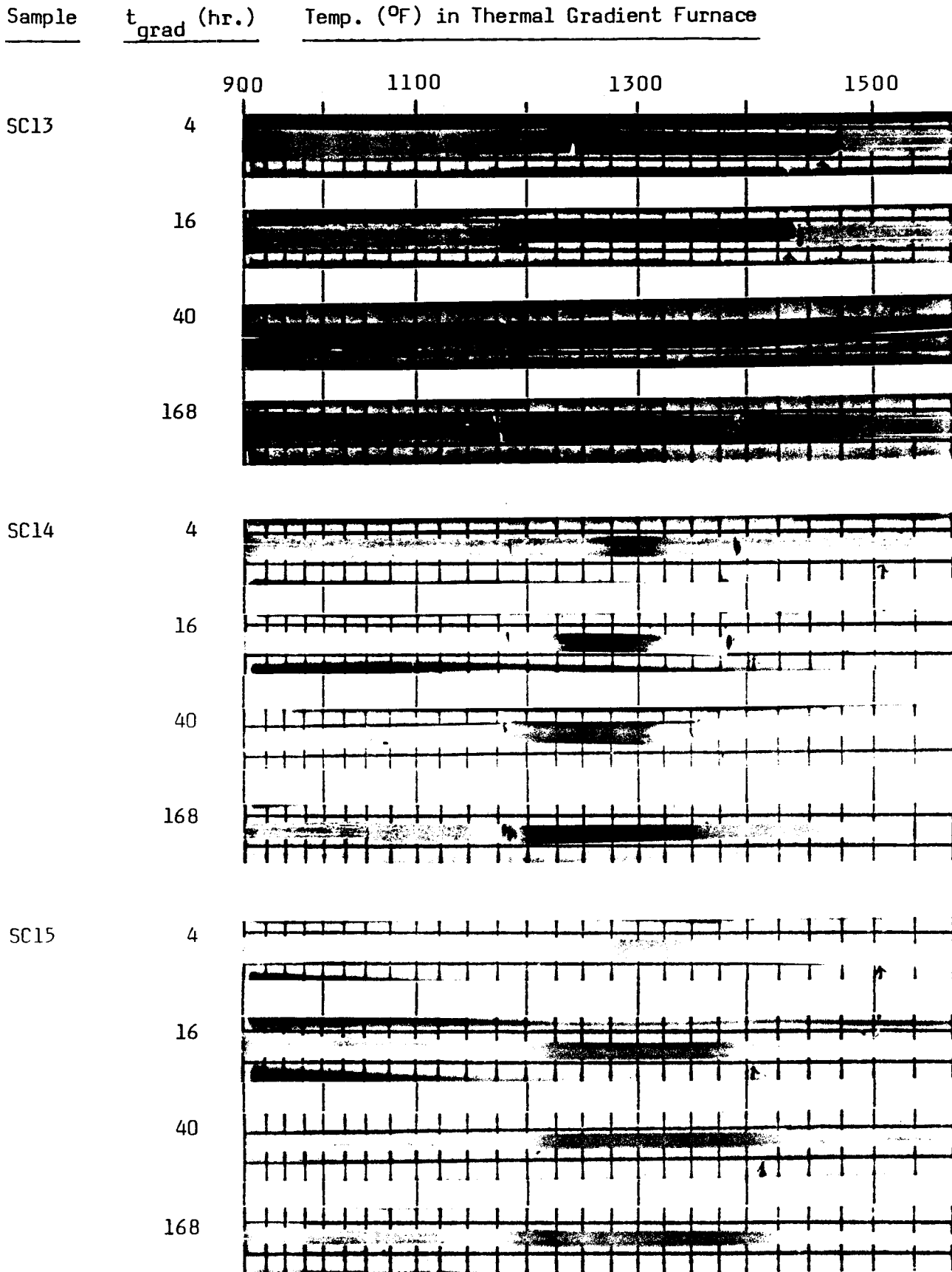
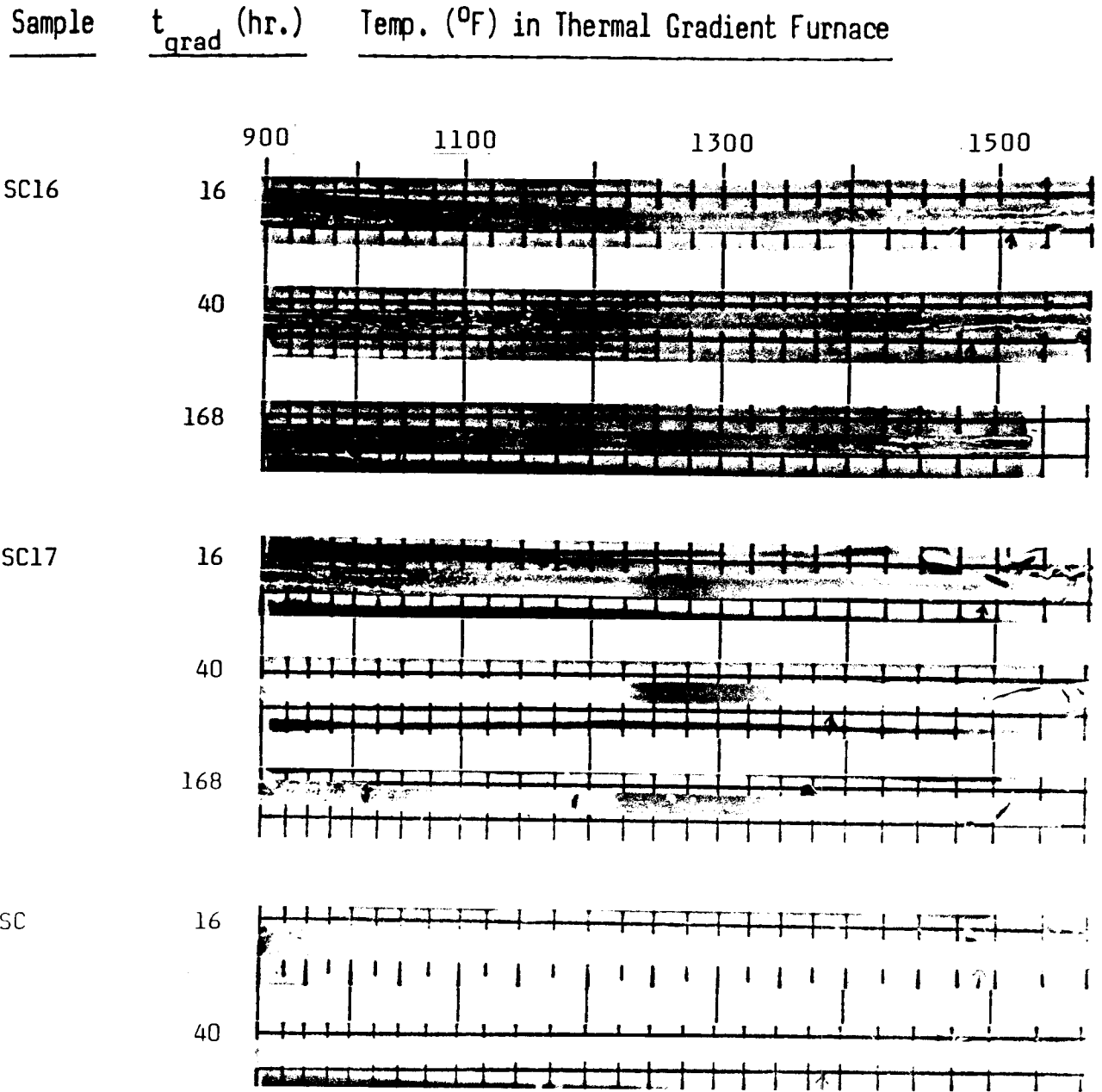


Figure 23. (Continued)



little nucleation at temperatures below  $T_1$ . The most transparent glass-ceramic region occurred in the high silica composition SC14. Transparency was improved by long thermal gradient (nucleation) times, and following a nucleation time of 40-168 hr.,  $T_2$  in SC14 was approximately 1200°F.

The effects of varying  $Cr_2O_3$  and  $TiO_2$  concentrations on the nucleation and crystallization behavior of the enstatite system were also investigated. Compositions SC20-SC26 (Table 24) were melted and cane was drawn from the melt as previously described. The relative concentrations of  $MgO$ ,  $Al_2O_3$ , and  $SiO_2$  were identical to SC14. In the series SC20-SC23,  $Cr_2O_3$  levels were increased from 0.05 to 0.4 wt.%, and in the series SC21, SC24-SC26,  $TiO_2$  levels were decreased from 10 to 4 wt.%.

Thermal gradient-isothermal two-step heat-treatment tests were performed and the appearance of samples following heat treatment can be found in Figure 24. SC23 devitrified upon cooling from the melt and was not heat-treated.

The appearance of SC20 (0.05 wt.%  $Cr_2O_3$ ), SC21 (0.1 wt.%  $Cr_2O_3$ ), and SC22 (0.2 wt.%  $Cr_2O_3$ ) shows that increasing  $Cr_2O_3$  levels has a relatively minor accelerating effect on nucleation rate ( $T_2$  decreases slightly with increasing  $Cr_2O_3$  wt.%).

The effect of  $TiO_2$  level on crystallization behavior is more dramatic. SC20 (10 wt.%  $TiO_2$ ) has a well-developed transparent glass-ceramic region. SC24 (8 wt.%  $TiO_2$ ) shows bulk crystallization to an opaque ceramic when the first step of the heat treatment schedule is 16 hr. (64 hr.) at temperatures between 1200-1325°F (1150-1375°F). Surface crystallization, perhaps involving a different crystal phase, also occurs when the sample is held above 1525°F (1475°F) for 16 hr. (54 hr). SC25 (6 wt.%  $TiO_2$ ) and SC26 (4 wt.%  $TiO_2$ ) show only surface crystallization at temperatures above 1500°F. These experimental results suggest the following conclusions.

Figure 24, Appearance of Samples SC20-SC22, SC24-SC26 Following Thermal Gradient-Isothermal Two Step Heat Treatment Schedule ( $t_{iso} = 4 \text{ hr.}, T_{iso} = 1600^{\circ}\text{F}$ )

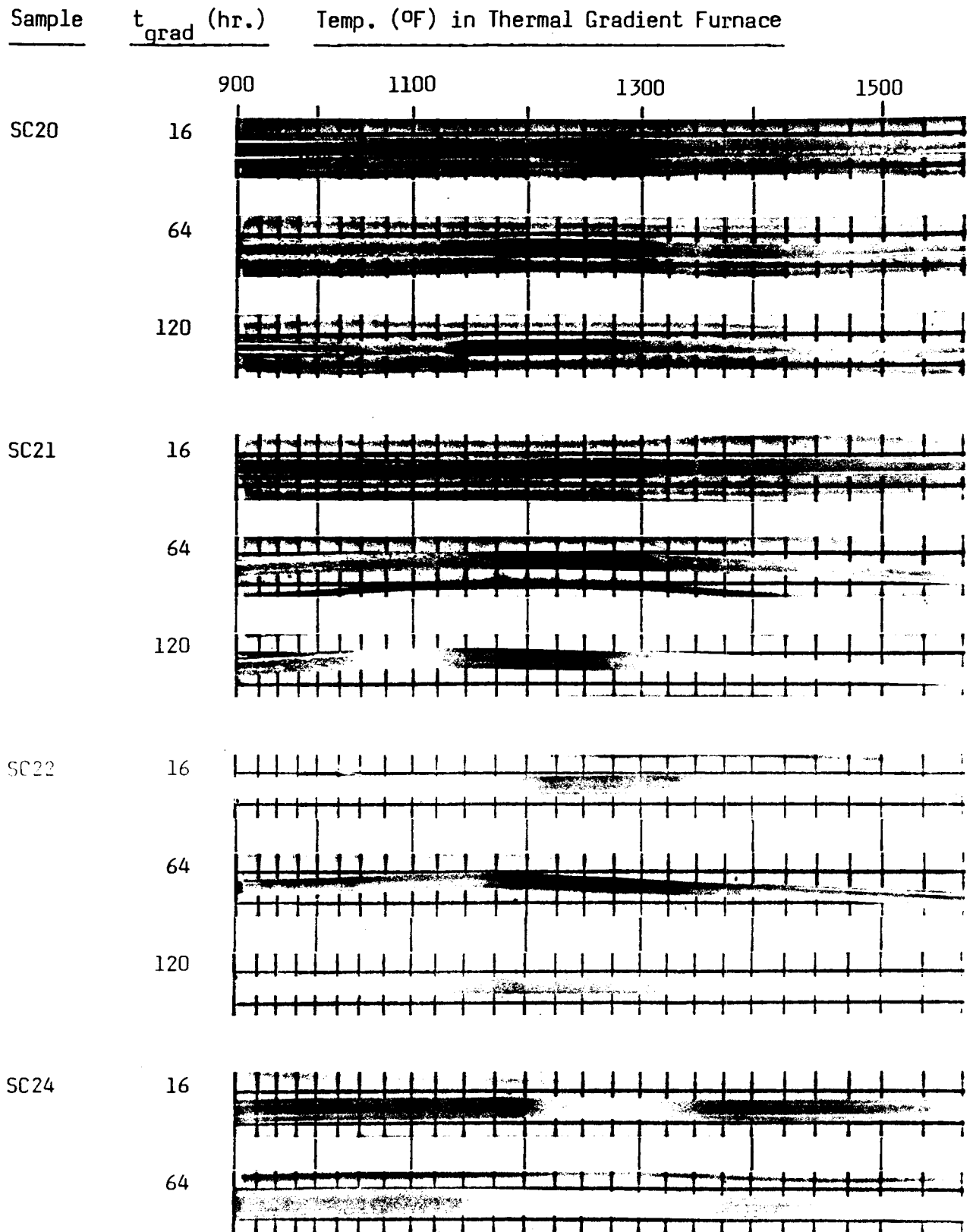
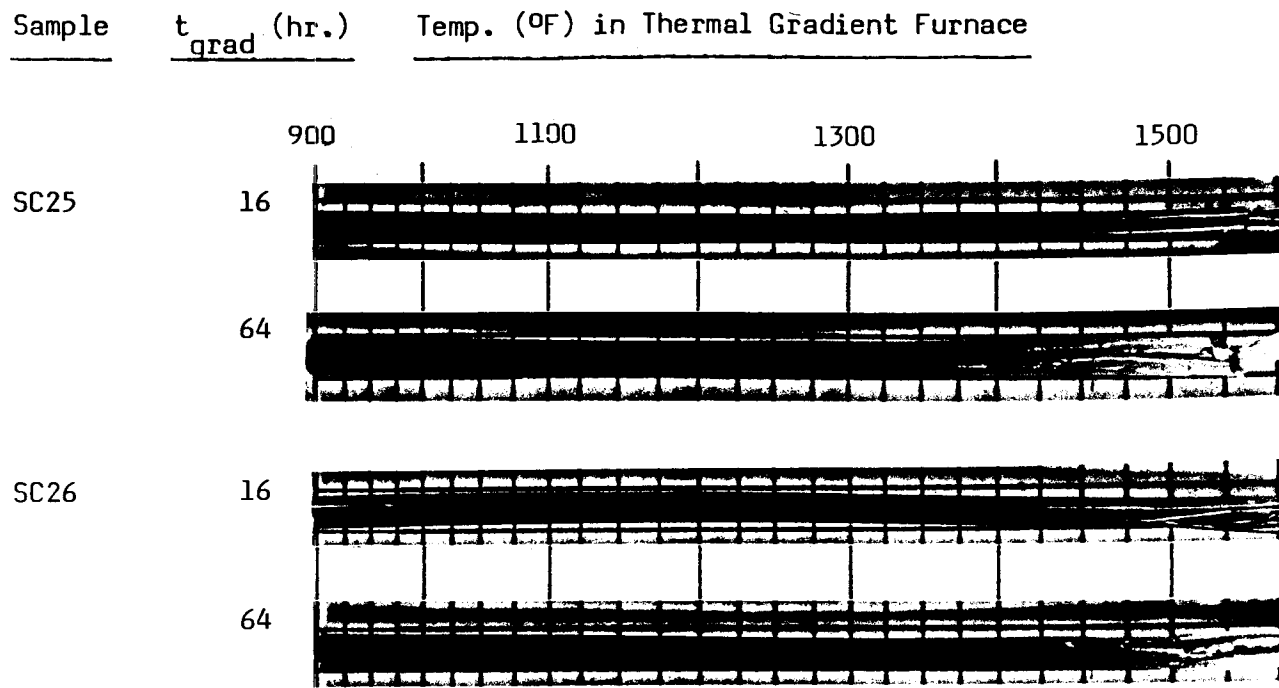


Figure 24. (Continued)



i.) Bulk crystal growth does not occur in the enstatite system without heterogeneous nucleation. ii.)  $\text{TiO}_2$  is ineffective as a heterogeneous nucleant at concentrations below 8-10 wt.%. iii.) At the 8 wt.%  $\text{TiO}_2$  level the rate of nuclei formation is too low for the formation of a fine grained transparent glass-ceramic and rapid enough for the formation of a coarse grained opaque ceramic only over the temperature range roughly 1200-1350°F. iv.) At the 10 wt.%  $\text{TiO}_2$  level rapid nucleation and slow crystal growth can be achieved over the temperature range roughly 1200-1400°F and rapid crystal growth can be achieved above roughly 1500°F.

Larger samples of  $\text{Cr}^{3+}$  doped transparent enstatite glass-ceramics were then prepared for an investigation of their optical properties. Batch compositions and heat-treatment schedules that appeared to optimize transparency were used. Compositions SC20 (0.05 wt.%  $\text{Cr}_2\text{O}_3$ ), SC21 (0.1 wt.%  $\text{Cr}_2\text{O}_3$ ), and SC22 (0.2 wt.%  $\text{Cr}_2\text{O}_3$ ) were melted, annealed, and cast. Samples 3 mm in thickness were cut and polished for optical investigation of the magnesium alumino-silicate (MAS) glass. A number of the samples were then converted to transparent enstatite glass-ceramics by the following two-step heat-treatment schedule: 1350°F (64 hr.), 1600°F (4 hr.). Glass-ceramic SC20 was slightly translucent; however, SC21 and SC22 appeared transparent to the eye. Glass-ceramic SC21 was investigated by x-ray diffraction. All significant diffraction peaks above the broad scatter due to the vitreous phase were assigned to enstatite.

Absorption spectra of the most heavily doped samples (SC22) are presented in Figure 25.  $^4\text{T}_1$  absorption appears as a shoulder at roughly 420 nm on an intense near-UV absorption edge in the MAS glass sample and is totally obscured (presumably by Rayleigh scattering) in the enstatite glass-ceramic. The position of the  $^4\text{T}_2$  absorption maxima in the MAS glass and the enstatite glass-ceramic (SC22, 0.2 wt.%

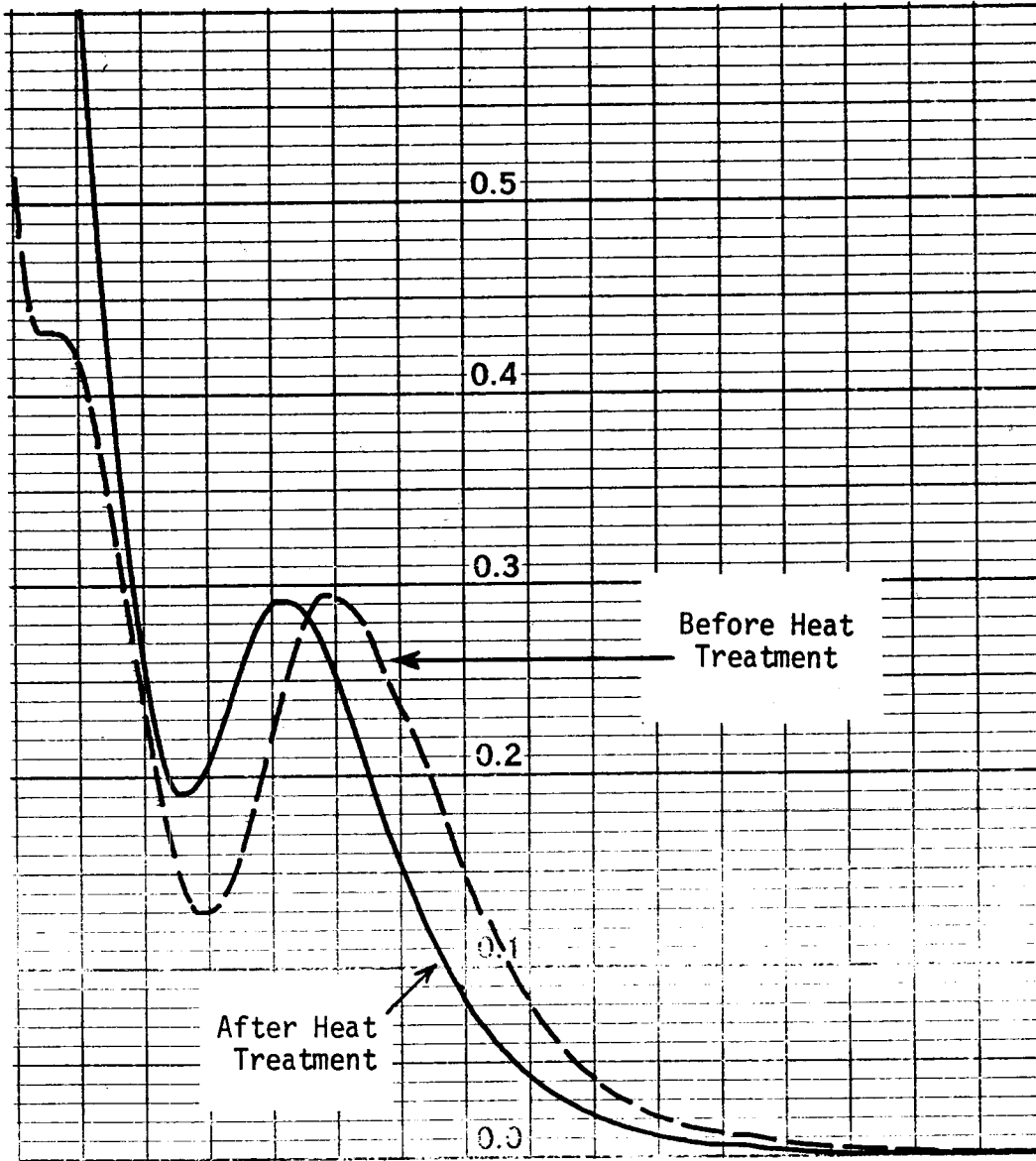


Figure 25. Absorption Spectra of Cr<sup>3+</sup>: MAS Composition SC22 Before and After Heat Treatment (3mm thick samples)



$\text{Cr}_2\text{O}_3$ ) are 645 nm and 615 nm, respectively. This relatively small shift in peak position indicates that the mean crystal field of  $\text{Cr}^{3+}$  sites in the glass-ceramic is only modestly greater than that in the glass.

Representative excitation and emission spectra of the MAS glass and enstatite glass-ceramic can be found in Figures 26 and 27. The glass (SC21) shows broad emission with a peak at roughly 825 nm. Emission in the enstatite glass-ceramic (SC21) is more intense and shifted somewhat to longer wavelength. Tentatively, one can resolve the glass-ceramic emission into three bands. A shoulder occurs at 700 nm which may be  ${}^2\text{E}$  emission from  $\text{Cr}^{3+}$  sites in a small amount of a spinel phase. The emission maximum occurs at roughly 835 nm. This appears to be the peak of a  ${}^4\text{T}_2$  emission band that has a bandwidth approximately one-third that of the glass emission band. Lying beneath the narrower  ${}^4\text{T}_2$  emission band appears to be a broader band with a position and width similar to the glass emission band. An assignment of the narrower band to  ${}^4\text{T}_2$  emission from  $\text{Cr}^{3+}$  sites in enstatite and of the broader band to  ${}^4\text{T}_2$  emission from sites in the residual glass phase is consistent with these observations.

Both glass and glass-ceramic samples showed evidence in the excitation spectra for the presence of a distribution of  $\text{Cr}^{3+}$  sites. The  ${}^4\text{T}_1$  and  ${}^4\text{T}_2$  excitation maxima occurred at shorter wavelength when emission was monitored at the short wavelength edge of the emission band (see Figures 26 and 27). A distribution of sites characterized by a continuous variation of crystal field parameters about some average set is anticipated in the vitreous phase. In the glass-ceramic there is additionally a discontinuous distribution of sites in the crystalline phase(s).

The emission quantum yield of glass and enstatite glass-ceramic samples of composition SC20-SC22 were measured with an

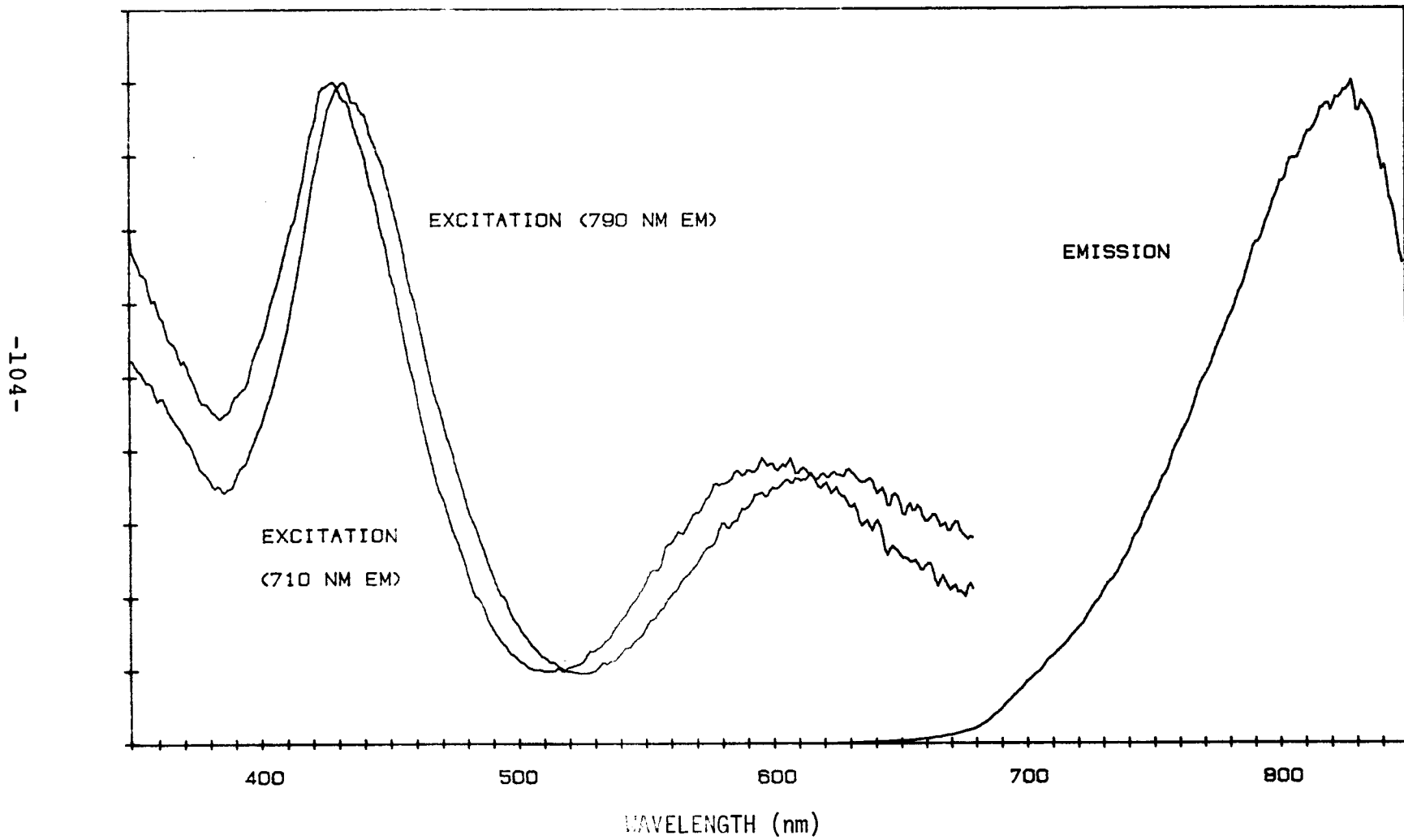


Figure 26. Excitation and Emission Spectra of Cr<sup>3+</sup>: MAS Glass SC21

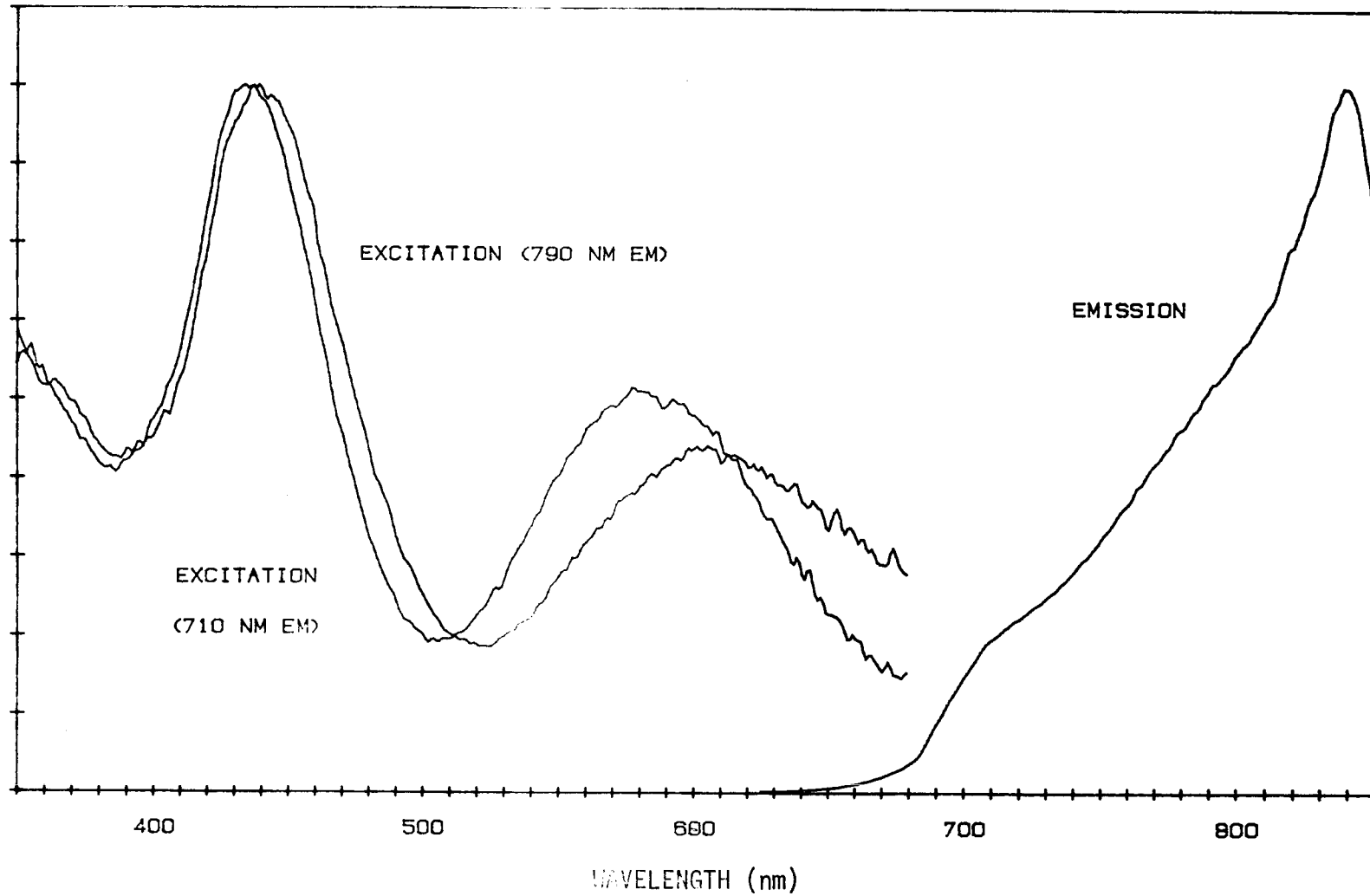


Figure 27. Excitation and Emission Spectra of  $\text{Cr}^{3+}$ : Enstatite Glass-Ceramic SC21

SLM-8000 spectrofluorometer relative to a 0.11 mol%  $UO_3$  doped potassium borosilicate glass secondary fluorescence standard. The  $Cr^{3+}$  doped samples were excited at 600 nm and the fluorescence standard was excited at 420 nm. A quantum counter of 8 g/L rhodamine-B in ethylene glycol was used to correct for the relative excitation intensities at 420 and 600 nm. The measured values are presented in Table 25. Because of the poor sensitivity of the system past 800 nm and the large dissimilarity in the excitation and emission wavelengths between standard and samples, the absolute quantum yields have uncertainties on the order of 50%. Uncertainties in the relative quantum yields, however, are probably on the order of 20%.

The quantum efficiency of the  $Cr^{3+}$  doped transparent enstatite glass-ceramics in Table 25 are all less than 0.1. Although heat-treatment in each case increased the quantum yield of the glass by roughly a factor of four, the resulting glass-ceramic quantum efficiencies need to be improved by another order of magnitude to be realistically considered for use in an LSC device.

Table 25 - Emission Quantum Yields of  $Cr^{3+}$  Doped MAS Glasses and Enstatite Glass-Ceramics

Composition ID	wt.% $Cr_2O_3$	$\eta_f$ (glass)	$\eta_f$ (g-c)
SC20	0.05	0.029	0.075
SC21	0.10	0.024	0.091
SC22	0.20	0.016	0.079

The source of the low measured glass-ceramic quantum yields has not been unambiguously determined. If one assumes that the increased quantum efficiencies of the heat-treated samples are due to the formation of  $Cr^{3+}$  : enstatite, then the

observation that the  $\text{Cr}^{3+}$  : enstatite glass-ceramics have quantum efficiencies on the order of 0.1 indicates that the percent enstatite crystallinity of the glass-ceramics is low, or that the quantum efficiency of the  $\text{Cr}^{3+}$  : enstatite phase itself is low or both. It appears, based on the following evidence, that the first alternative is the more likely. A comparison was made of the front surface emission intensity of the fully crystallized opaque ceramic SC12 and the transparent enstatite glass-ceramic SC22. Both were excited at 600 nm and the emission spectral distribution of both were similar, with the exception that SC12 showed a minor amount of  $^2\text{E}$  emission that had previously been assigned to  $\text{Cr}^{3+}$  : spinel. The ratio of emitted power of SC12 to SC22 was 10.9, and the percent absorption (at 600 nm) of SC22 is 76%. If one assumes that the percent absorption of the opaque ceramic is 100%, a lower bound to the quantum efficiency of SC12 of 0.65 can be calculated. Provided that the majority of the emission observed in both samples arises from  $\text{Cr}^{3+}$  : enstatite, this indicates that the quantum efficiency of the  $\text{Cr}^{3+}$  : enstatite phase is high, and that the low quantum efficiency of the transparent glass-ceramic is due to low percent crystallinity (the majority of absorbing  $\text{Cr}^{3+}$  ions occupying sites in the vitreous phase that are weakly luminescent).

Alternatively, the data does not allow one to rule out the possibility that the bulk of observed emission in the transparent glass-ceramics originates from  $\text{Cr}^{3+}$  ions in the vitreous phase. The quantum efficiency improvement observed after heat treatment may be associated with structural relaxation and a compositional change (due to the precipitation of  $\text{MgSiO}_3$ ) of the vitreous phase that occurs during the heat treatment schedule.

In either event, the possibility of substantially improving the luminescence efficiency of the  $\text{Cr}^{3+}$  doped transparent enstatite glass-ceramic system appears remote. The

composition and heat-treatment schedule range required to form a transparent glass-ceramic are narrow; therefore, there is little opportunity to substantially improve percent crystallinity without degrading transparency. If emission does arise from  $\text{Cr}^{3+}$  ions in the residual glass phase, the observed poor quantum yield of  $\text{Cr}^{3+}$  doped glasses <sup>21</sup> also suggests that the possibility of improving luminescence efficiency is poor.

## VII. INORGANIC GLASSES

Attention was first drawn to luminescent inorganic glasses because of their excellent long-term stability and generally superior separation of luminescence and absorption bands (hence, low luminescence self-absorption). The properties of a number of luminescent inorganic glass systems have been discussed in previous reports<sup>2,3</sup>. The purpose of this section is to place the earlier specific investigations into a broader context, while reviewing their suitability as an LSC plate material.

Glasses with properties potentially suitable for use in an LSC can be classified into one of the five groups listed in Table 26. The classification is generally on the basis of the nature of the optical transitions involved in emission; however, for convenience multiphase glass-ceramics are listed separately.

Table 26

Classification of Luminescent Dopants  
in Inorganic Glasses

- 
- (1) Molecular Phosphors  
i.e.:  $\text{UO}_2^{2+}$
  - (2) Rare Earth Ions with Intraconfigurational f-f Transitions  
i.e.: Trivalent rare earth ions -  $\text{Nd}^{3+}$ ,  $\text{Eu}^{3+}$ , etc.
  - (3) Rare Earth and Transition Metal Ions with Interconfigurational Transitions  
i.e.:  $f^{n-1}d \rightarrow f^n$ :  $\text{Ce}^{3+}$ ,  $\text{Eu}^{2+}$   
 $d^{10} \rightarrow d^9p$ :  $\text{Ag}^+$ ,  $\text{Cu}^+$   
 $s^2 \rightarrow sp$ :  $\text{Sn}^{2+}$ ,  $\text{Sb}^{3+}$ ,  $\text{Pb}^{2+}$ ,  $\text{Bi}^{3+}$

(4) Transition Metal Ions with Intraconfigurational d-d Transitions

i.e.:  $d^3$ :  $Cr^{3+}$ ,  $Mo^{3+}$

$d^5$ :  $Mn^{2+}$ ,  $Fe^{3+}$

$d^2$ :  $V^{3+}$

(5) Transparent Glass-Ceramics

---

Inorganic glasses doped with molecular phosphors are exemplified essentially only by the uranyl ion doped glasses. Small amounts of a variety of luminescent organic molecules can also be introduced into low melting phosphate and borate glass; however, the poor chemical stability of these glasses would seem to preclude their practical significance. Energies of the uranyl glasses are determined largely by the structure of the  $UO_2^{2+}$  molecular ion, and, therefore, changing base glass composition has only a modest influence on the position of absorption and emission bands. Quantum yields, however, are glass-composition dependent. Uranyl glasses have been studied by our group and others. Quantum efficiencies of 0.6 - 0.7 have been measured in dilute  $UO_3$  doped borosilicate glasses. However, the occurrence of concentration quenching and the fact that absorption is only in the UV - blue spectral region results in weak relative solar absorption.

The absorption and emission bands of glasses doped with trivalent rare earth ions are associated with intraconfigurational f-f transitions. Because the transitions are intraconfigurational, absorption is Laporte forbidden and weak. And because f electrons are well shielded, crystal field perturbations are weak and absorption and emission lines are narrow and occur at almost the same frequency regardless of the structure of the host. The weak crystal field perturbations also cause very small Stokes shift values; however, the terminal level



in many emission lines is a lower excited state, and, therefore, in these cases self-absorption is very weak. Trivalent rare earth ion doped glasses can emit with high quantum efficiency and have been thoroughly studied largely because of their technical importance as laser gain media. The  $\text{Eu}^{3+}$  ion has been studied here as an acceptor of  $\text{UO}_2^{2+}$  excitation with the aim of shifting emission farther to the red. However, further studies of trivalent rare earth ion doped glasses have not been attempted because the rare earth oxides are costly and achieving large relative solar absorption would require large dopant levels of a number of rare earth oxides. It is felt that such a glass, were it successfully developed with adequate optical properties, would be uneconomical for a primary luminescence solar concentrator.

A number of luminescent rare earth and transition metal ions can be introduced into a glass host in which the UV - visible absorption and emission bands are associated with interconfigurational transitions. The transitions are orbitally allowed, and, hence absorption is very strong. The mean radius of the excited state electron configuration is generally significantly larger than that of the ground state. Therefore, crystal field perturbations and Stokes shifts are generally large. The large crystal field perturbations also result in broad absorption and emission linewidths and a large sensitivity of the frequency of absorption and emission bands to the structure of the host matrix. Factors that influence the magnitude of luminescence quantum efficiencies are poorly understood; however, values of 0.6 - 0.7 have been measured in a number of  $\text{Eu}^{2+}$  and  $\text{Cu}^+$  systems. A major difficulty apparently shared by all luminescent glasses of this classification is evident in the observation that the literature does not describe a single glass in which visible absorption occurs to wavelengths longer than the blue spectral region. All described glasses have absorption maxima in the UV - near UV region. While our understanding of the energy levels involved in absorption is certainly not precise enough to preclude the possibility of shifting absorption significantly

toward the red by appropriate glass compositional changes, achieving such a goal seems very unlikely and has not been attempted here.

Transition metal ions with unfilled d orbitals have absorption bands that are associated with intraconfigurational d-d transitions. The energy levels and observed luminescent properties of the ions in a glass matrix is generally well described by crystal field theory. The causes of luminescence quenching are poorly understood, but as a general rule it is expected that those ions with electron configurations that have low-lying energy levels will be non-emitting because of rapid nonradiative transitions. On this basis, ions with  $d^1$ ,  $d^4$ ,  $d^6$ , and  $d^9$  electron configurations can be removed from consideration. Ions with  $d^3$  and  $d^5$  electron configurations have lowest excited states that lie in the green - far red spectral region, and luminescence has been described in the literature from glasses doped with such ions. The remaining electron configurations,  $d^2$ ,  $d^7$ , and  $d^8$ , are intermediate in nature. The lowest excited states lie in the near IR; therefore, luminescence efficiency would probably be low, and in most instances emission would be to longer wavelength than the bandgap of Si photovoltaic cells. Emission from this class of ions in crystalline systems has been described in the literature, but there are no reports of emission from glass systems.

Glasses doped with the  $d^3$  ions  $Cr^{3+}$  and  $Mo^{3+}$  have been briefly investigated here. Oscillator strengths are weak because the absorption transitions are Laporte forbidden. Nevertheless, good relative solar absorption values can be achieved with  $Cr^{3+}$  doped glasses because the ion has two broad spin-allowed absorption bands in the visible region and can be introduced at high concentrations into glass systems. The  $Mo^{3+}$  ion is weakly soluble in glasses, and  $Mo^{3+}$  doped glasses absorb solar radiation very weakly. The quantum efficiency of luminescent  $Cr^{3+}$  doped glasses measured here and elsewhere are unfortunately too low for

application in an LSC. Attempts have been made to improve system quantum efficiency by using  $\text{Cr}^{3+}$  as a donor in a  $\text{Cr}^{3+}$  - trivalent rare earth ion donor - acceptor system. Results to date have been modest.

Luminescent glasses doped with the  $d^5$  ions  $\text{Mn}^{2+}$  and  $\text{Fe}^{3+}$  have also been studied here. Near unity quantum efficiency can be achieved in weakly doped  $\text{Mn}^{2+}$  glasses; however, oscillator strengths are very weak because the absorption transitions are all both Laporte and spin forbidden. Even at very high dopant levels, relative solar absorption values are very low. Among the group of ions with electron configurations that may yield possible near IR luminescent transitions, a brief study was done of the  $d^7$  ion  $\text{V}^{3+}$ . On the basis of the observed absorption spectra of  $\text{V}^{3+}$  doped glasses and the Tanabe-Sugano diagram of the  $d^7$  electron configuration, one can predict a possible luminescent transition at about 1 micron. A number of  $\text{V}^{3+}$  doped boro-alumino-phosphate glasses were prepared; however, no luminescence was observed.

Members of the final classification considered here are luminescent transparent glass-ceramics. The luminescent dopant could be any ion considered previously, but clearly advantages are to be gained in going to a glass-ceramic matrix only when a crystalline phase markedly improves a particular optical property that is pertinent to the efficiency of an LSC. The greatest potential improvements are expected to be found in the luminescent efficiencies of unfilled d-shell ions.  $\text{Cr}^{3+}$  doped transparent glass-ceramics were, therefore, investigated because the ion absorbs the solar spectrum well and is known to emit with high efficiency in a number of crystalline systems. This approach, however, has not to date yielded a successful LSC material. Three luminescent  $\text{Cr}^{3+}$  doped transparent glass-ceramic systems were prepared by precipitating crystalline phases from glasses of suitable composition by heat-treatment. Two of the systems showed high luminescence quantum efficiency. All,

however, showed strong luminescence absorption by essentially non-emitting  $\text{Cr}^{3+}$  ions in the residual glass phase. This may be an intractable problem for  $d^3$  ions in a glass-ceramic. Transparent glass-ceramics are generally characterized by low volume percent crystallinity and inorganic glasses are good solvents for the smaller transition metal ions; therefore, a sizable atom fraction of dopant ions will remain in the glass phase. On the basis of the Tanabe-Sugano diagram for  $d^3$  ions and the lower crystal field strength of sites in glass relative to sites in crystal phases that can be precipitated from glass, one would generally expect poor separation of the crystalline emission band and the lowest glass absorption band.

In summary, we have experimentally investigated the following inorganic species in a variety of inorganic hosts:  $\text{Ce}^{3+}$ ,  $\text{CdS}$ ,  $\text{Cr}^{3+}$ ,  $\text{Eu}^{3+}$ ,  $\text{Fe}^{3+}$ ,  $\text{Mo}^{3+}$ ,  $\text{Mn}^{2+}$ ,  $\text{Nd}^{2+}$ ,  $\text{UO}_2^{2+}$ ,  $\text{UO}_2^{2+}\text{-Eu}^{3+}$ , and  $\text{V}^{3+}$ . The survey of luminescent glasses and glass-ceramics suitable for an LSC has thus been completed. Our studies, however, have failed to identify systems not characterized by high cost, weak solar absorption, or poor luminescence quantum yield. Attempts to improve absorption in the visible region are generally limited by the low oscillator strength of the intraconfigurational transitions responsible for absorption and are further frustrated by the appearance of luminescence quenching at phosphor concentrations necessary for sufficiently large peak optical densities.

In order to establish an upper bound on the performance of the various systems investigated, a first order plate efficiency model has been utilized to estimate plate efficiencies.<sup>3</sup> No system, however, has been identified with a collector efficiency greater than 1%, and even for co-doped inorganic systems we do not expect collector efficiencies to reach 2%. It is thus felt that an LSC composed primarily of inorganic phosphors is not practical.

Although luminescent glasses have been precluded from use as the principal active material for an LSC, it is concluded that glasses can be effectively used as the substrate for an organic dye thin film LSC.<sup>3</sup> A number of rare earth or transition metal ion-doped glasses with intraconfiguration transitions (i.e., Ce<sup>3+</sup>: aluminosilicate glass, see Figure 28) absorb strongly in the near UV-blue and emit in the visible. They can provide solar ultraviolet protection with additional visible radiative pumping to a thin film organic dye. The major driver for such a configuration, however, is the greater near-IR transparency of inorganic glasses relative to organic polymers.

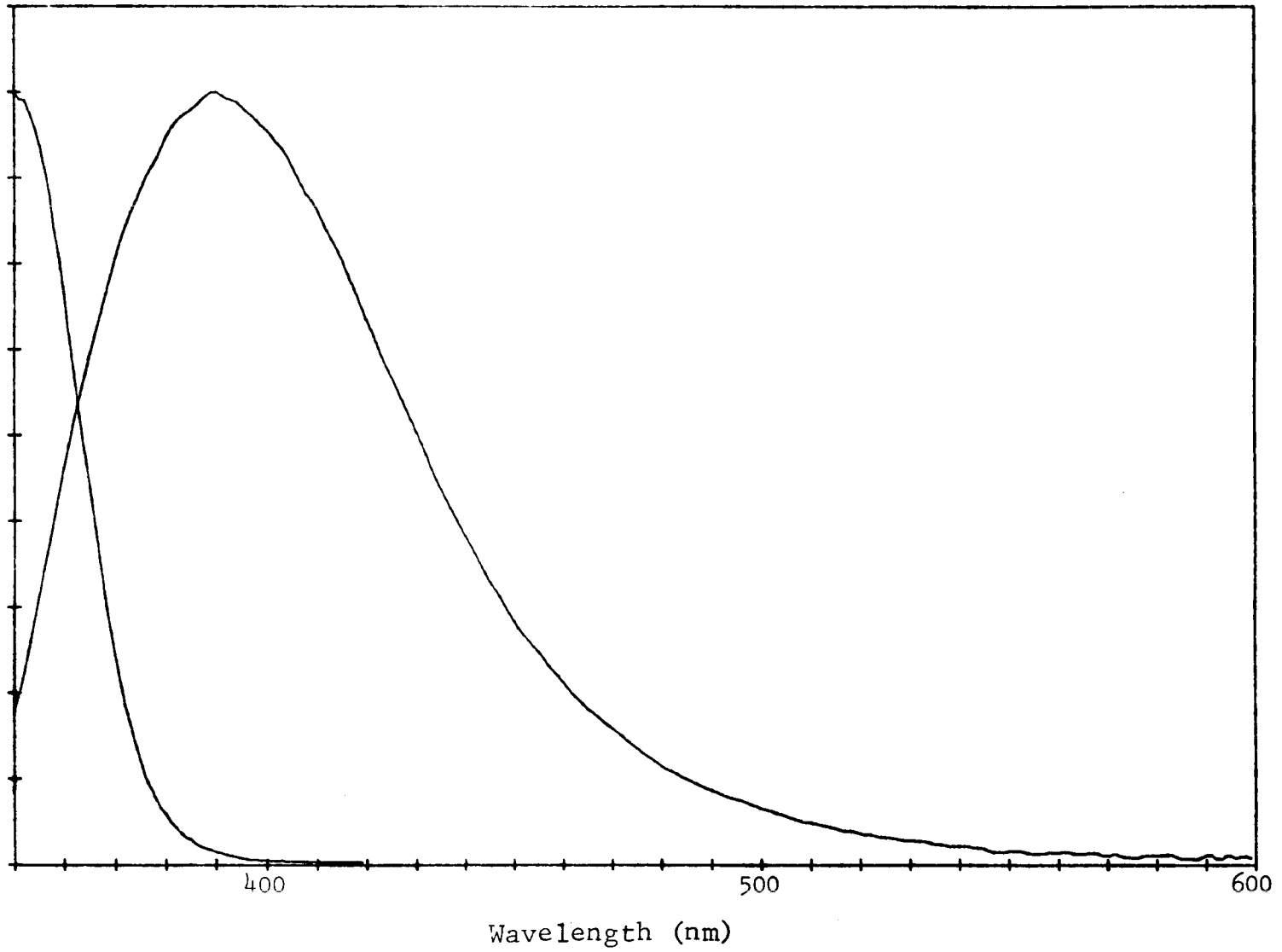


Figure 28. Excitation and Emission Spectra of Ce<sup>3+</sup> Glass

### VIII. TOTAL POWER OUTPUT OF LSCs COMPARED TO PHOTOVOLTAIC CELLS

The LSC plate efficiency has been measured as a function of plate temperature for a standard 200 cm<sup>2</sup> two dye plate. A variable temperature simulator was designed and constructed to allow close control of plate temperature while maintaining a constant cell temperature of 20°C (see Figure 29). The relative plate efficiency was calculated from the I-V curve of a water-cooled, air-coupled photovoltaic cell. This experiment showed that over the temperature range of 30°C to 80°C, the relative plate efficiency decreased linearly by approximately 5% (see Figure 30). Thus, the effect of elevated temperature on LSC plate efficiency appears to be considerably smaller than the efficiency loss expected from a silicon photovoltaic cell (i.e., approximately 2.0 mV/°C) heated over the same temperature range.

In order to compare the relative efficiency and the economics of an LSC to a flat plate photovoltaic cell array, the total output energy-to-peak power ratio was measured for an LSC collector, a high efficiency Sandia photovoltaic cell, and an Eppley Precision Spectral Pyranometer. All measurements were made on a cloudless AM-1 day and the data integrated from noon till sunset. The three devices were coplanar and tilted at 20 degrees in order to be perpendicular to the incident rays at solar noon. It can be seen from Figure 31, that the total output energy-to-peak power ratio of the LSC exceeded that of the photovoltaic cell and pyranometer by 21% and 19%, respectively. It should be noted that for fixed position solar collectors, the annualized relative flux of incident radiation at large angles to the collector normal will be greater than in this experiment, as will the average amount of scattered radiation. When these two factors are taken into account, we would expect an even greater difference in the annualized

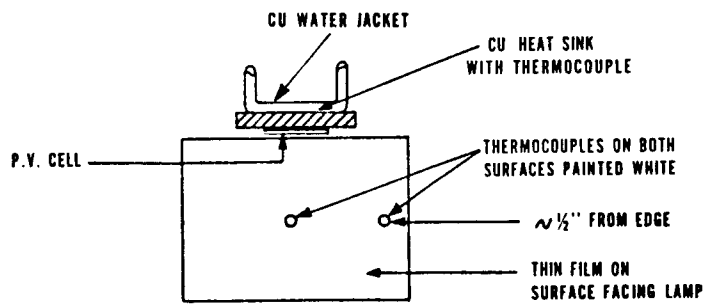
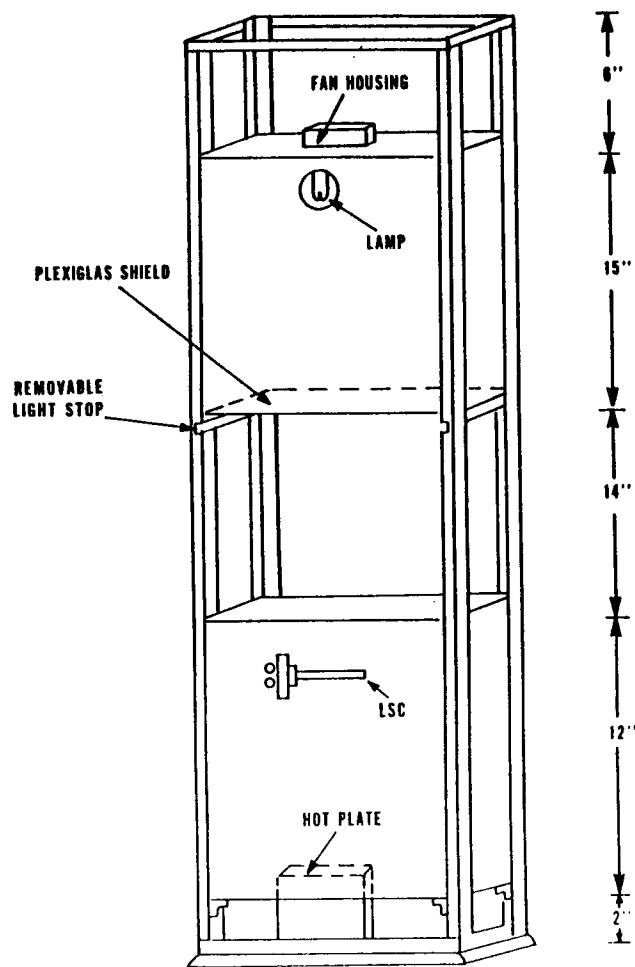


Figure 29.

Variable Temperature Simulator with LSC  
Plate-to-Cell Coupling Scheme



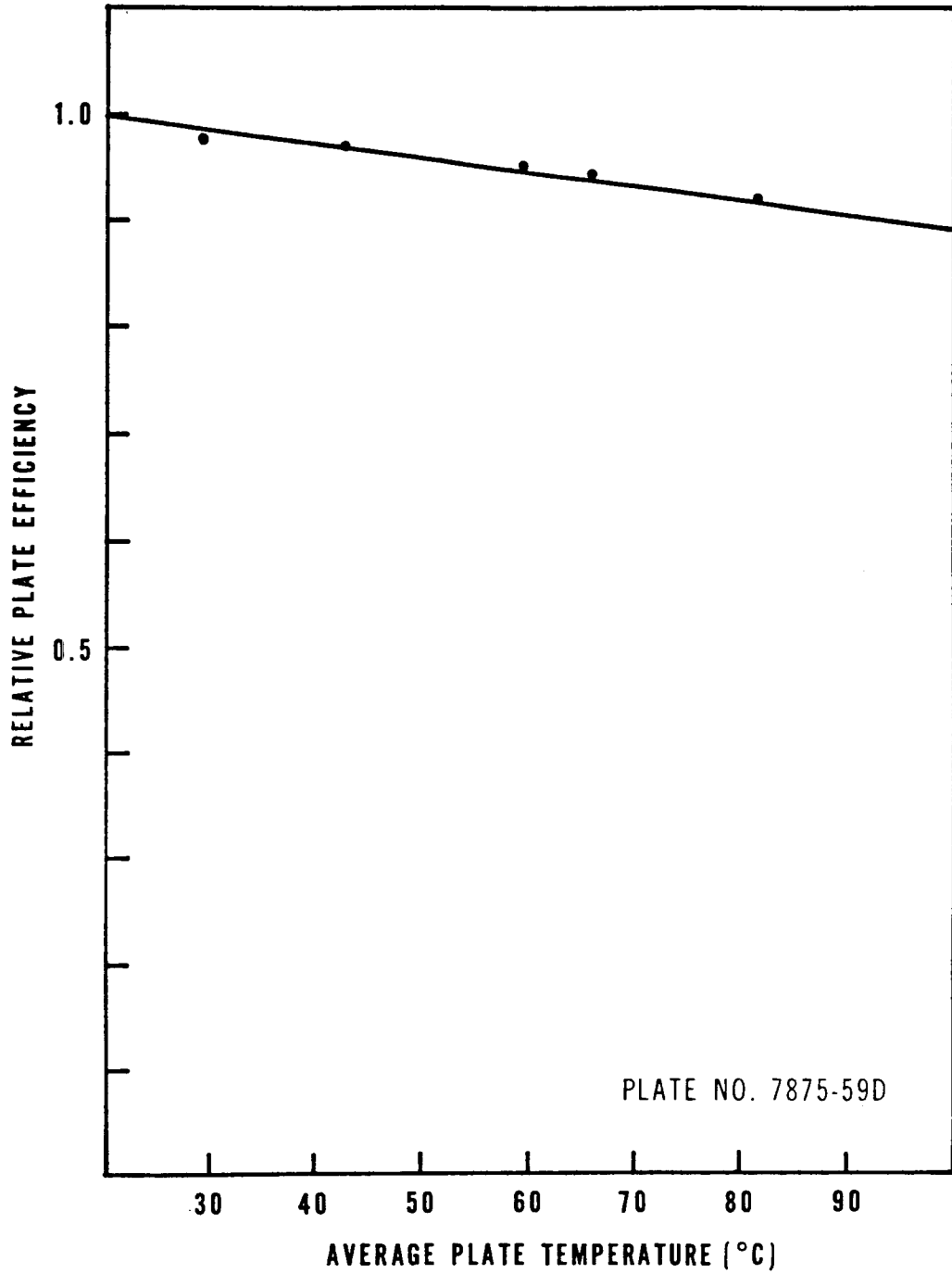
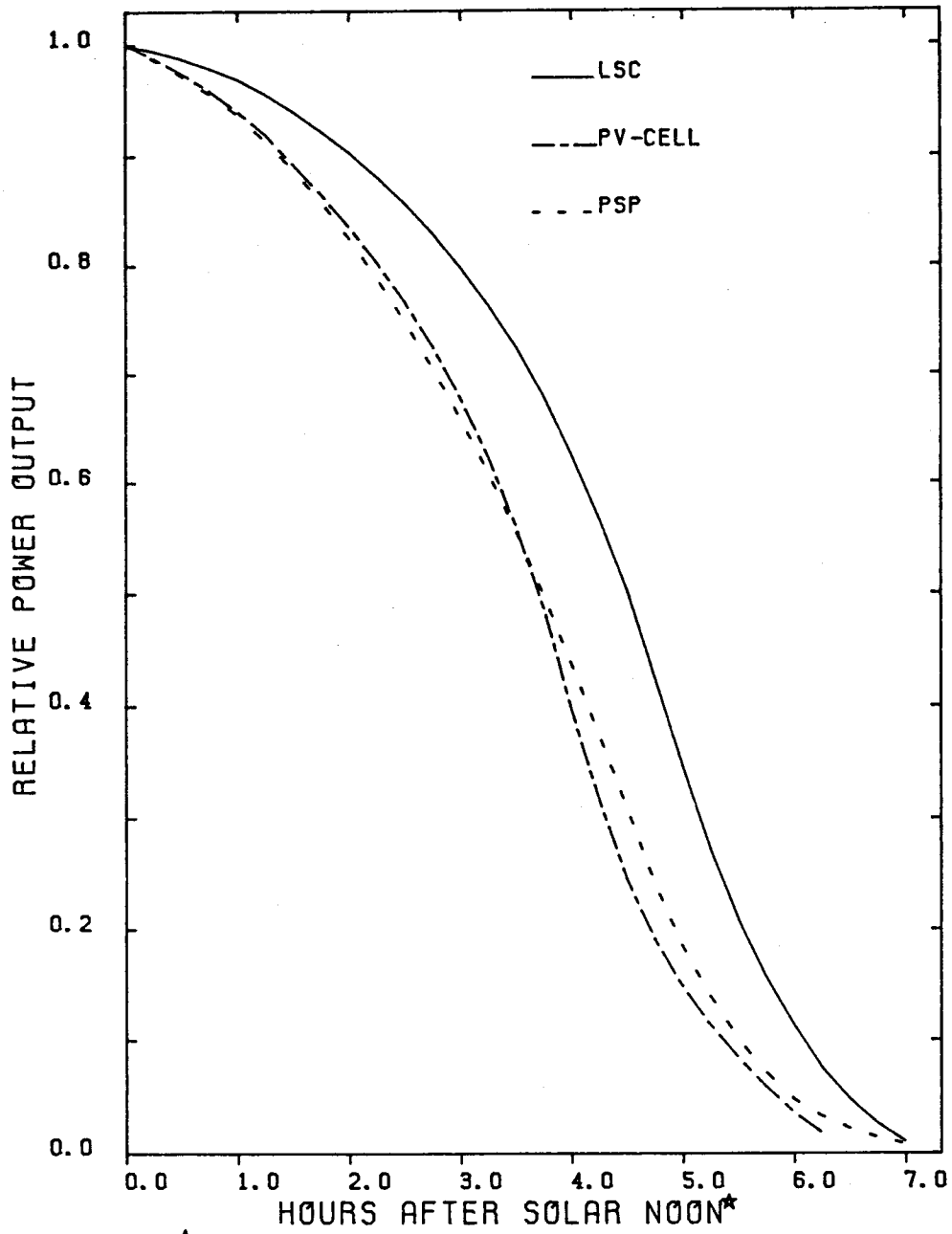


Figure 30. Plate Efficiency as a Function of Temperature



\* JUNE 10, 1980, SOLAR NOON 1:34 D.S.T., TOLEDO, OHIO

Figure 31. Total Power Output of LSCs Compared to Photovoltaic Cells

comparative efficiencies of LSCs compared to photovoltaic cells. This experiment thus needs to be averaged over the course of a full year, but the preliminary results indicate that an LSC device will produce at least 20% more electrical energy per day than a photovoltaic device of the same peak watt rating. It is, therefore, appropriate to revise both the efficiency and cost analysis for this device to take this factor into consideration.

## IX. APPLICATIONS OF LUMINESCENT SOLAR CONCENTRATORS

The United States Department of Energy LSC Program, has focused its total effort almost exclusively on the use of LSCs for photovoltaic concentration. The reasons for this emphasis were originally well founded, as electricity is generally considered the most convenient and expensive form of energy. On the basis of conversion efficiencies, the comparison is often made that one watt of electrical energy is economically equivalent to three watts of thermal energy. However, the luminescent solar concentrator is such a unique and versatile device that it has a number of other applications, some of which may prove to be of greater importance than its use for photovoltaic conversion. A partial listing of these applications is given below (also, see Section X).

The major emphasis in the use of LSCs, as stated above, has been directed towards primary photovoltaic concentrators. However, the use of luminescent cover plates for solar cells, so as to spectrally shift incident sunlight from shorter to longer wavelengths, where some cells are more sensitive, is an important area that should be more fully investigated. The possibility of increasing the efficiency for AlGaAs/GaAs cells by as much as 20% and for CdS/CuInSe<sub>2</sub> by 10% has already been demonstrated.

A third application that has received scant attention, but which holds the promise for perhaps the largest efficiency gains, is the use of LSCs for indoor building illumination<sup>49,50</sup>. An overall efficiency of 9% has been calculated for a complete LSC collection system that can deliver white light to the deep interior of a modern high rise building.<sup>49</sup> In addition, such an LSC system would be capable of providing approximately 90% of the buildings lighting requirement over an

eight (8) hour day. By way of comparison, a 10% efficient photovoltaic array can provide interior building fluorescent lighting at an overall efficiency of only 1-2%. Thus, the LSC system appears to be on the order of five (5) times more efficient than photovoltaic cells for the end use of indoor lighting. It is noted in this regard, that one of the short-falls of the DOE solar electric program, is that very little emphasis has been placed on the end use of solar generated electrical energy. If, as in the above example, solar electricity is used for electrical lighting, the system efficiency goes from 10% down to 1-2%, and one must therefore question the rational of solar generated electricity for this purpose.

Another interesting application for LSCs is in exploiting their wavelength shifting ability to increase the efficiency of hydrogen producing photosynthetic bacteria. These bacteria cannot, in general, effectively utilize the "green" spectral region of sunlight. For this application, the LSC would again be used like a photovoltaic cell coverplate. Numerous other applications for LSCs exist (see Table 27), including: luminescent enhanced display devices and signs, secondary photovoltaic concentrators, thermal concentrators, total internal reflecting face pumped lasers, photovoltaic/thermal hybrid systems, and numerous types of electro-optical detectors.

Table 27

Applications of LSC Technology

1. Primary PV concentrators (SERI, Owens-Illinois, ARCO, Exxon, Fraunhofer Institute)
2. PV Luminescent Cover Glass  
  
AlGaAs/GaAs (Owens-Illinois and Varian)  
CdS/CuInSe<sub>2</sub> (Owens-Illinois, Boeing and Drexel University)
3. Interior Building Illumination (DHR, Lawrence Berkeley Labs, T. I. R. Systems)
4. Display Devices (Photonics Technology, Siemens AG)
5. Secondary PV Concentrators-Spectral Splitting  
  
AlGaAs/Si (Owens-Illinois and Varian)
6. Thermal Concentrators (Fraunhofer Institute)
7. Total Internal Reflecting Face Pumped Lasers
8. H<sub>2</sub> Photosynthetic Bacteria/Water Purification-Spectral Splitting (SERI)
9. Photovoltaic/Thermal Hybrid Concentrators (Owens-Illinois)
10. Enhanced Electro-Optical Detectors (Photonics Technology)

## X. CONCLUDING THOUGHTS ON THE FUTURE OF LSC TECHNOLOGY

This report is the last in a series of four Final Reports over a period of seven (7) years. We have attempted here to summarize the major developments described in our previous work, as well as including those topics not previously covered. In addition, we have included the data base for all of our stability and edge luminescence measurements, and finally have presented a very brief survey of some of the non-photovoltaic applications for LSC technology.

The major reason for the reduction in research activity for LSC devices has been the low inherent efficiency of LSC photovoltaic concentrators. System efficiencies on the order of 10% are feasible, but at present still illusive. Amorphous semiconductors in comparison have achieved efficiencies in excess of 10% for small area devices. Large area amorphous arrays, however, have achieved only about half of this value, which is not all that much greater than large area LSCs.

The total expenditure by the United States Department of Energy for all LSC research in this country, since the conception of this device some ten years ago, is on the order of only 0.1% of the money spent on photovoltaic devices; yet, the technology involved in the development of luminescent solar concentrators (namely the organic synthesis of whole new classes of organic dyes) is certainly at least as complex as that required for photovoltaic cells. However, the implications of improved luminescent materials are quite possibly of even greater consequence.

In Section IX we listed only some of the applications

of LSC devices. The significance of new, high efficiency, stable chromophores is much more far reaching - including new types of lasers, color phosphors, optical memory materials, organic semi-conductors, etc. to name but a few. It is our hope that the LSC technology developed at Owens-Illinois under the DOE sponsorship will prove useful in guiding future research in this field.



## REFERENCES

1. P. S. Friedman, Luminescent Solar Concentrator Development, Final Report, Sandia Contract No. 13-2311, SAND79-7059, (January 31, 1979 - June 30, 1979).
2. P. S. Friedman and C. R. Parent, Luminescent Solar Concentrator Development - I, Final Report, SERI Subcontract XS-9-8216-1 (July 1, 1979 - September 30, 1980).
3. P. S. Friedman and C. R. Parent, Luminescent Solar Concentrator Development - II, Final Report, SERI Subcontract XW-0-9357 (September 1, 1980 - May 31, 1982).
4. J. N. Demas and G. A. Crosby, J. Phys. Chem., 75, 991 (1971).
5. E. D. Cehelnik, K. D. Mielenz, and R. A. Velapoldi, J. Res. Nat. Bur. Stand. (U.S.A.), 79A, 1 (1971).
6. K. H. Drexhage, Topics in Applied Physics, Volume 1, Dye Lasers, F. P. Schafer, ed., Springer-Verlag, Berlin, 1977, pp. 144-193.
7. K. H. Drexhage, J. Research Nat. Bur. Std., 80A, 421 (1976).
8. G. A. Reynolds and K. H. Drexhage, Optics Communications, 13, 222 (1975).
9. G. Jones, W. R. Jackson, and A. M. Halpern, Chem. Phys. Letters, 72, 391 (1980).
10. R. F. Kubin and A. N. Fletcher, J. Lumin., 27, 455 (1982).
11. R. Sens and K. H. Drexhage, J. Lumin., 24/25, 709 (1981).
12. P. R. Hammond, Opt. Commun., 29, 331 (1979).
13. J. S. Batchelder, A. H. Zewail, and T. Cole, Appl. Opt., 20, 3733 (1981).

14. K. Kato, IEEE J. Quat. Elect., QE-16, 1017 (1980).
15. R. E. Sah and G. Baur, Appl. Phys., 23, 369 (1980).
16. K. Venkataraman, The Chemistry of Synthetic Dyes, Vol. II, Ch. XXXVIII, Academic Press, New York (1952).
17. J. H. Brannon and D. Magde, J. Phys. Chem., 82, 705 (1978).
18. M. L. Lesiecki and J. M. Drake, Appl. Optics, 21, 557 (1982).
19. J. Olmsted, III, J. Phys. Chem., 83, 2581 (1979).
20. A. V. Butenin, B. Ya Kogan, and N. V. Gundobin, Opt. Spectrosc. (U.S.S.R.), 47, 568 (1980).
21. L. J. Andrews, A. Lempicki, and B. C. McCollum, J. Chem. Phys., 74, 5526 (1981).
22. L. J. Andrews and A. Lempicki, LSC Review Meeting, SERI (October 1980).
23. A. Lempicki, L. J. Andrews, B. C. McCollum, and S. M. Stone, LSC Review Meeting, SERI (March 1982).
24. P. W. McMillan, Glass Ceramics, 2nd Edition, Academic Press, London, 1979.
25. G. H. Beall and D. A. Duke, J. Mat. Sci., 4, 340 (1969).
26. M. M. Layton and A. Herczog, Glass Technol., 10, 50 (1969).
27. T. Kobubo and M. Tashiro, Bull. Inst. Chem. Res. Kyoto-Univ., 54, 301 (1976).
28. C. L. Babcock, R. A. Busdiecker, and E. C. Hagedorn, U. S. Patent No. 3,788,865, January 29, 1974, (filed June 15, 1965).

29. A. Kisilev, R. Reisfeld, E. Greenberg, A. Bush, and M. Ish-Shalom, Chem. Phys. Letters, 105, 405 (1984).
30. R. M. MacFarlane, J. Chem. Phys., 39, 3118 (1963).
31. R. E. Newham and Y. M. deHaan, Zeitschr. Kristallographie, 117, 235 (1962).
32. Chi-Tang Li, Zeitschr. Kristallographie, 127, 327 (1968).
33. Chi-Tang Li and D. R. Peacor, Zeitschr. Kristallographie, 126, 46 (1968).
34. F. A. Hummel, K. Auh, and G. H. Johnson, Mat. Res. Bull., 5, 301 (1970).
35. G. H. Beall, U. S. Patent No. 3,681,102, August 1, 1972 (filed March 27, 1970).
36. D. L. Wood, G. F. Imbush, R. M. MacFarlane, P. Kusliuk, and D. M. Larkin, J. Chem. Phys., 48, 5255 (1968).
37. W. Mikenda and A. Preisinger, J. Lumin., 26, 53 (1981); 26, 67 (1981); W. Mikenda, J. Lumin., 26, 85 (1981).
38. J. S. Reed, J. Am. Ceram. Soc., 54, 202 (1971).
39. "Structure Reports for 1968 - Metals and Inorganic Compounds," W. B. Pearson, gen. ed., V. Duckworth and C. B. Shounaker, sect. eds., Vol. 33A, p. 273.
40. R. W. G. Wyckoff, Crystal Structures, 2nd Edition, Vol. 3, Interscience, New York, 1968, pp. 75-81.
41. A. J. Stryjak and P. W. McMillan, J. Mat. Sci., 13, 1275 (1978)

42. L. J. Andrews, B. C. McCollum, S. Stone, D. E. Guenther, G. J. Murphy, and A. Lempicki, "Development of Materials for a Luminescent Solar Collector", Final Report, U. S. Department of Energy, Contract No. DE-AC02-78ER-04996 (September 1, 1979 - December 31, 1982).
43. R. Reisfeld, A. Kisilev, E. Greenberg, A. Buch, and M. Ish-Shalom, Chem. Phys. Letters, 104, 153 (1984).
44. R. W. G. Wyckoff, Crystal Structures, 2nd Edition, Vol. 4, Interscience, New York, 1968, pp. 301-4.
45. L. Leger and J. Bray, Glass Technol., 7, 134 (1966).
46. E. Plumet, Silicates Ind., 38, 97 (1972).
47. I. Gutzow, E. Zloteva, S. Alyalsov, and T. Kavatscheva, J. Mat. Sci., 12, 1190 (1977).
48. P. S. Friedman, Opt. Eng., 20, 887 (1981).
49. J. G. Bornstein and P. S. Friedman, Luminescent Solar Concentrator Building Lighting, Final Report, Pacific Northwest Laboratory Contract No. B-A3926-A-Z (1984).
50. J. G. Bornstein and P. S. Friedman, U.S. Patent No. 4,539,625, September 3, 1985 (filed July 31, 1984), Lighting System Combining Daylight Concentrators and An Artificial Source.

## APPENDIX I

### DYE STABILITY AND DEVICE STABILITY DATA TABLES

Appendix I is arranged such that the dye stability ( $A_t$ ) and device stability ( $S_t$ ) measured in a 100% nitrogen atmosphere appear in parentheses, while all other data is for an ambient air atmosphere. Interpretation of the host code is given in Table 19 (see Section III). The numbers in the tables of Appendix I immediately following the host code give the optical density of each plate, and the interger in parenthesis following the optical density denotes the number of thin film coats of dye responsible for the measured optical density. In most cases, no number follows the optical density and this means that the number of coats is one (1). It is noted that the average thickness per coat is 15-20 microns.

All of the dye and device stabilities recorded as a function of "measured" exposure in  $\text{kWh/m}^2$ , were obtained by outdoor exposure under ambient Toledo year-round sunlight conditions. Four glazed LSC Rooftop Test Boxes were constructed<sup>3</sup>, each capable of holding approximately 100 samples. A similar box was also constructed to enclose an Eppley Model 8-48 Black and White Pyranometer so as to monitor LSC sample exposure in kilowatt- hours. In order to both record and store the total daily insolation, a LI-COR Model LI-1776 solar monitor was employed. This instrument can store the daily integrated values from the pyranometer over a 24-hour period and has a memory capacity of over 100 days. In order to convert  $\text{kWh/m}^2$  to the number of equivalent exposure days, we suggest that an average day corresponds approximately to 4.5  $\text{kWh/m}^2$  incident upon a south facing glazed collector surface which is tilted at the angle of local latitude. If we take

into account cover glass reflectivity, soiling, early morning condensation, enclosure sidewall shadowing, etc., then approximately a 20-25% radiation loss can be expected, and the actual daily exposure incident upon an LSC plate will be about 3.5 kWh/m<sup>2</sup>. It is, therefore, proposed to define for the purpose of our degradation studies that an LSC plate exposure of 3.5 kWh/m<sup>2</sup> is equivalent to an average day of exposure in a suitable enclosure. It is noted that the actual daily insolation in Toledo at our test site, as measured over the course of several years, is approximately 20% less than the above proposed value.

It is noted that for a full description of the dye degradation investigation, as well as interpretation of the stability data results, refer to Section III of this report.

DYE SCREENING TESTS FOR DYE STABILITY ( $A_t$ )  
AND DEVICE STABILITY ( $S_T$ )

Dye	Stability After Given Exposure ( $\text{kWh/m}^2$ )			
	Host Code/O.D.	50	100	200
<b>Brilliant Yellow (<math>A_t</math>)</b>				
CE-A/2.8	.81( .94)	.79( .88)	.63( .81)	.57( .73)
CE-A/0.6	.94( .89)	.91( .77)	.87( .73)	.88( .68)
CE-B/3.0	.76( .89)	.55( .79)	.34( .70)	.18( .65)
CE-B/0.4	.84( .84)	.75( .75)	.65( .70)	.60( .61)
CE-D/3.1	.74(1.04)	.68(1.04)	.58( .98)	.42( .81)
CE-D/0.5	.81( .81)	.69( .68)	.56( .62)	.52( .55)
CM-A/2.3	.91( .82)	.86( .71)	.80( .65)	.84( .56)
CM-A/0.4	.91( .73)	.87( .62)	.85( .57)	.88( .50)
CS-A/2.1	.78( .85)	.63( .72)	.43( .64)	.31( .60)
CS-A/0.7	.84( .74)	.74( .62)	.61( .55)	.55( .50)
AC-H/1.5	.71( .98)	.55( .94)	.46( .88)	.41( .83)
AC-H/0.5	.73( .88)	.60( .80)	.53( .73)	.48( .61)
MA-C/1.7	.73( .78)	.61( .65)	.55( .58)	.47( .50)
MA-C/0.5	.67( .71)	.56( .56)	.50( .45)	.45( .36)
AI-E/1.8	.40( .89)	.35( .84)	.32( .81)	.21( .71)
AI-E/0.5	.54( .82)	.48( .71)	.46( .65)	.34( .50)
AI-I/2.1	.69( .93)	.61( .90)	.55( .87)	.41( .77)
AI-I/0.4	.77( .87)	.72( .82)	.66( .78)	.53( .62)
AC-I/1.1	.21( .89)	.10( .78)	.05( .70)	( .46)
<b>Brilliant Yellow (<math>S_t</math>)</b>				
CE-A/2.8	1.15(1.18)	1.08(1.13)	1.24(1.37)	1.29(1.29)
CE-A/0.6	.98( .94)	.89( .83)	.94( .95)	.91( .87)
CE-B/3.0	.89( .98)	.81( .89)	1.00(1.07)	1.08( .97)
CE-B/0.4	.93( .93)	.82( .81)	.83( .82)	.74( .71)
CE-D/3.1	1.16(1.16)	1.00(1.03)	1.32(1.42)	1.36(1.36)
CE-D/0.5	.99(1.01)	.83( .86)	.90( .95)	.83( .87)
CM-A/2.3	1.06(1.04)	1.07( .96)	1.28(1.21)	1.24(1.07)
CM-A/0.4	.93( .84)	.88( .73)	.95( .76)	.83( .66)
CS-A/2.1	1.08(1.26)	1.03(1.12)	1.38(1.48)	1.25(1.42)
CS-A/0.7	1.09(1.15)	1.01(1.00)	1.21(1.13)	1.03( .92)
AC-H/1.5	1.09(1.07)	1.10( .95)	1.30(1.10)	1.24(1.00)
AC-H/0.5	.98( .95)	.87( .86)	.91( .94)	.79( .79)
MA-C/1.7	1.16(1.01)	1.18( .88)	1.28(1.03)	1.22( .85)
MA-C/0.5	.85( .75)	.73( .61)	.75( .62)	.69( .46)
AI-E/1.8	1.21(1.05)	1.20(1.30)	1.03(1.13)	.82( .99)
AI-E/0.5	.59( .69)	.58( .65)	.49( .54)	.37( .45)
AI-I/2.1	1.29(1.06)	1.39(1.29)	1.34(1.11)	1.24(1.25)
AI-I/0.4	.88( .90)	.87( .90)	.76( .75)	.69( .71)
AC-I/.10	1.80(1.16)	1.65( .92)	1.35( .72)	

## DYE

Stability After Given Exposure (kWh/m<sup>2</sup>)

Host Code/ O. D.	450	600	800	1000
Brilliant Yellow (A <sub>t</sub> )				
CE-A/2.8	.42( .60)	.22( .46)	.10( .33)	(.28)
CE-A/0.6	.81( .56)	.72( .44)	.62( .33)	.57 (.32)
CE-B/3.0	.09( .56)	.04( .32)	(.19)	
CE-B/0.4	.47( .48)	.28( .36)	.15( .26)	
CE-D/3.1	.33( .73)	.21( .62)	.12( .51)	(.45)
CE-D/0.5	.43( .48)	.31( .35)	.22( .28)	(.26)
CM-A/2.3	.76( .44)	.66( .32)	.58( .24)	.54 (.22)
CM-A/0.4	.81( .38)	.75( .31)	.70( .23)	.70 (.24)
CS-A/2.1	.17( .46)	.08( .32)	(.22)	(.19)
CS-A/0.7	.42( .37)	.28( .28)	.21( .20)	.19 (.19)
AC-H/1.5	.31( .74)	.19( .58)	.13( .46)	(.43)
AC-H/0.5	.38( .50)	.27( .37)	.20( .29)	.20 (.27)
MA-C/1.7	.36( .36)	.24( .19)	.18( .11)	
MA-C/0.5	.35( .23)	.25( .11)	.18( ----)	
AI-E/1.8	.07( .58)	(.50)	(.40)	(.39)
AI-E/0.5	.10( .38)	(.30)	(.22)	(.22)
AI-I/2.1	.22( .68)	(.62)	(.55)	(.55)
AI-I/0.4	.32( .48)	.25( .46)	.27( .34)	.26 (.34)
AC-I/1.1				

Brilliant Yellow (S<sub>t</sub>)

CE-A/2.8	1.20(1.30)	1.16(1.20)	.28( .97)
CE-A/0.6	.86( .74)	.77( .67)	.57( .79)
CE-B/3.0	.97(1.00)	.74( .99)	(.91)
CE-B/0.4	.63( .64)	.45( .50)	.28( .41)
CE-D/3.1	1.35(1.36)	1.22(1.11)	1.15(1.18)
CE-D/0.5	.71( .76)	.60( .64)	.50( .54)
CM-A/2.3	1.34(1.20)	1.40(1.20)	1.55(1.21)
CM-A/0.4	.80( .57)	.78( .46)	.77( .40)
CS-A/2.1	1.28(1.47)	1.04(1.35)	.91(1.34)
CS-A/0.7	.96( .85)	.80( .70)	.68( .61)
AC-H/1.5	1.22(1.07)	1.06(1.02)	1.00(1.17)
AC-H/0.5	.68( .72)	.55( .61)	.45( .53)
MA-C/1.7	1.20( .88)	1.09( .69)	.99( .60)
MA-C/0.5	.55( .36)	.44( .24)	.37( )
AI-E/1.8	.38( .82)	(.75)	
AI-E/0.5	.19( .33)	(.24)	
AI-I/2.1	1.21(1.11)	(1.01)	
AI-I/0.4	.54( )	.44( .46)	



Dye		Stability After Given Exposure (kWh/m <sup>2</sup> )			
Host Code/O.D.		50	100	200	300
<b>Coumarin-6</b> (A <sub>t</sub> )					
CE-A/3.4		.26( .83)	.05( .49)	.02( .33)	.01( .20)
CE-B/2.0		.16( .45)	.05( .28)	.02( .23)	.02( .16)
CE-B/0.5		.32( .59)	.10( .40)	.04( .34)	.03( .25)
CE-D/2.6		.06( .52)	.01( .31)	( .22)	( .14)
CE-D/0.5		.39( .72)	.13( .56)	.02( .49)	.03( .41)
CM-A/2.4		.42( .38)	.19( .17)	.09( .11)	.04( .06)
CM-A/0.5		.63( .58)	.36( .37)	.23( .29)	.11( .21)
CS-A/1.9		.04( .24)	.01( .11)	( .08)	( .05)
CS-A/0.8		.24( .63)	.05( .40)	( .30)	( .22)
AC-H/1.7		.11( .23)	.04( .07)		
AC-H/0.5		.15( .38)	.07( .12)		
MA-C/1.5		.14( .27)	.02( .06)		
MA-C/0.5		.23( .31)	.06( .09)		
AI-E/2.4		.43( .65)	.29( .59)	.19( .51)	.06( .28)
AI-E/0.5		.40( .55)	.28( .45)	.19( .36)	.06( .18)
AI-I/1.8		.30( .64)	.16( .59)	.09( .52)	.03( .30)
AI-I/0.5		.29( .59)	.17( .53)	.11( .44)	.04( .28)
AC-I/.93		.13( .32)	.02( .28)	.01( .18)	
CE-E/1.1		.02( .12)			
<b>Coumarin-6</b> (S <sub>t</sub> )					
CE-A/3.4		.67( .70)	.31( .63)	.16( .69)	.11( .60)
CE-A/0.5		.62( .80)	.30( .68)	.16( .66)	.11( .56)
CE-B/2.0		.60( .81)	.29( .68)	.21( .66)	.14( .56)
CE-B/0.5		.52( .73)	.25( .54)	.17( .52)	.11( .40)
CE-D/2.6		.42( .86)	.16( .75)	( .74)	( .64)
CE-D/0.5		.60( .77)	.31( .69)	.17( .67)	.11( .56)
CM-A/2.4		.82( .63)	.65( .47)	.46( .43)	.25( .31)
CM-A/0.5		.76( .72)	.50( .49)	.37( .45)	.19( .32)
CS-A/1.9		.32( .75)	.14( .51)	( .44)	( .33)
CS-A/0.8		.52( .80)	.18( .61)	( .56)	( .45)
AC-H/1.7		.52( .58)	.22( .29)		
AC-H/0.5		.43( .56)	.20( .25)		
MA-C/1.5		.38( .50)	.11( .19)		
MA-C/0.5		.36( .44)	.14( .18)		
AI-E/2.4		.71( .68)	.66( .66)	.51( .59)	.27( .51)
AI-E/0.5		.53( .60)	.40( .53)	.29( .36)	.16( .28)
AI-I/1.8		.61( .72)	.49( .69)	.31( .90)	.17( .52)
AI-I/0.5		.44( .64)	.32( .60)	.22( .84)	.15( .35)
AC-I/0.9		.25( .53)	.14( .53)	.10( .38)	
CE-E/1.1		.19( .47)			

Dye	Stability After Given Exposure (kWh/m <sup>2</sup> )			
	Host Code/O.D.	50	100	200
Nile Blue (A <sub>t</sub> )				
CE-A/2.0	.21( .77)	.10( .59)	.05( .48)	.03( .39)
CE-A/0.6	.57( .80)	.38( .60)	.23( .62)	.16( .56)
CE-B/3.2	.38( .91)	.20( .79)	.10( .69)	.07( .60)
CE-B/0.5	.41( .76)	.26( .62)	.15( .58)	.12( .54)
CE-D/2.9	.40( .83)	.20( .73)	.08( .65)	.04( .58)
CE-D/0.7	.26( .54)	.14( .40)	.06( .35)	.03( .28)
CM-A/1.7	.46( .71)	.23( .51)	.12( .40)	.06( .30)
CM-A/0.3	.51( .39)	.26( .17)	.15( .09)	.10( .05)
CS-A/2.1	.21( .81)	.08( .66)	( .54)	( .53)
CS-A/0.6	.37( .81)	.19( .65)	( .57)	( .51)
AC-H/2.1	.55( .51)	.36( .78)	.24( .72)	.17( .65)
AC-H/0.6	.56( .45)	.38( .75)	.24( .70)	.23( .65)
MA-C/1.4	.05( .04)			
MA-C/0.4	.01( .02)			
Nile Blue (S <sub>t</sub> )				
CE-A/2.0	4.68(1.49)	4.54(1.60)	4.13(2.85)	3.08(3.05)
CE-A/0.6	.88( .89)	.73( .83)	.68( .91)	.54( .88)
CE-B/3.2	2.03( .91)	2.40( .84)	2.66(1.15)	2.08(1.20)
CE-B/0.5	1.04(1.01)	.85( .90)	.80(1.08)	.62( .97)
CE-D/2.9	2.13(1.18)	2.17(1.33)	1.96(1.88)	1.47(1.85)
CE-D/0.7	.62( .79)	.49( .72)	.41( .76)	.31( .70)
CM-A/1.7	2.12(1.23)	2.12(1.40)	2.22(1.97)	1.48(1.90)
CM-A/0.3	.65( .52)	.39( .30)	.35( .29)	.22( .21)
CS-A/2.1	4.35(1.43)	3.89(1.38)	3.36(2.63)	2.50(2.71)
CS-A/0.6	.95(1.02)	.69( .88)	.59(1.07)	.42( .96)
AC-H/2.1	1.98( .84)	2.55( .72)	3.36(1.06)	3.19(1.36)
AC-H/0.6	1.14( .85)	.98( .79)	.95( .96)	.84( .90)
MA-C/1.7	1.22(1.66)			
MA-C/0.4	.20( .24)			



Dye	Stability After Given Exposure (kWh/m <sup>2</sup> )			
Host Code/O.D.	50	100	200	300
Oxazine-725 (A <sub>t</sub> )				
CE-A/3.2	.75( .73)	.58( .56)	.46( .50)	.34( .40)
CE-A/0.5	.55( .58)	.36( .39)	.26( .32)	.18( .26)
CE-B/2.1	.69( .73)	.54( .65)	.47( .53)	.33( .53)
CE-B/0.5	.67( .71)	.54( .61)	.42( .48)	.34( .51)
CE-D/3.1	.72( .82)	.55( .70)	.41( .64)	.28( .57)
CE-D/0.4	.58( .69)	.41( .53)	.30( .45)	.17( .37)
CM-A/1.9	.50( .31)	.25( .13)	.13( .08)	.06( .04)
CM-A/0.5	.43( .32)	.20( .12)	.11( .06)	.07( .03)
CS-A/2.2	.64( .78)	.41( .63)	.27( .56)	.19( .50)
CS-A/0.7	.71( .79)	.54( .66)	.41( .60)	.30( .54)
AC-H/2.9	.45( .25)	.20( .12)	.11( .09)	.05( .07)
AC-H/0.4	.50( .40)	.27( .21)	.14( .15)	.10( .11)
MA-C/1.8	.08( .04)			
MA-C/0.3	.06( .05)			
AI-E/1.7	.56( .56)	.44( .48)	.36( .42)	.24( .32)
AI-E/0.6	.55( .57)	.44( .50)	.36( .43)	.24( .32)
AI-I/2.0	.45( .50)	.32( .43)	.24( .37)	.14( .24)
AI-I/0.4	.22( .24)	.13( .19)	.11( .17)	.34( )
CE-E/1.3	.44( .47)			
Oxazine-725 (S <sub>t</sub> )				
CE-A/3.2	1.03( .69)	.97( .69)	1.45( .87)	1.19( .77)
CE-A/.05	.79( .78)	.62( .63)	.60( .50)	.49( .57)
CE-B/2.1	1.11( .80)	1.19( .77)	1.58( .98)	1.45( .73)
CE-B/0.5	.89( .80)	.83( .72)	.85( .83)	.75( .69)
CE-D/3.1	1.26( .80)	1.33( .81)	1.79(1.04)	1.78( .98)
CE-D/0.4	.80( .82)	.68( .70)	.66( .75)	.55( .64)
CM-A/1.9	1.03( .62)	.94( .46)	.89( .49)	.54( .35)
CM-A/0.5	.70( .57)	.46( .31)	.43( .30)	.25( .20)
CS-A/2.2	1.45( .87)	1.72( .76)	2.40(1.21)	2.06( .94)
CS-A/0.7	.93( .89)	.79( .80)	.86( .86)	.72( .75)
AC-H/2.9	.82( .45)	.63( .34)	.68( .38)	.44( .31)
AC-H/0.4	.66( .58)	.46( .38)	.40( .38)	.30( .29)
MA-C/1.8	.58( .36)			
MA-C/0.3	.18( .26)			
AI-E/1.7	.61( .41)	.59( .46)	.59( .18)	.46( .11)
AI-E/0.6	.57( .53)	.54( .53)	.50( .54)	.37( .38)
AI-I/2.0	.69( .52)	.79( .57)	.75( .96)	.59( .47)
AI-I/0.4	.41( .37)	.37( .36)	.32( .87)	.28( )
CE-E/1.3	.99( .78)			

DYE	Stability After Given Exposure (kWh/m <sup>2</sup> )			
Host Code/ O. D.	450	600	800	1000
Oxazine-725 (A <sub>t</sub> )				
CE-A/3.2	.22( .29)	.11( .16)		
CE-A/0.5	.09( .16)			
CE-B/2.1	.23( .45)	.13( .32)	( .21)	
CE-B/0.5	.25( .43)	.17( .30)	( .22)	
CE-D/3.1	.18( .48)	( .36)	( .25)	
CE-D/0.4	.11( .28)	( .17)		
CM-A/1.9	.01( .01)			
CM-A/0.5	.00( .00)			
CS-A/2.2	.10( .38)	( .27)	( .18)	
CS-A/0.7	.19( .42)	( .32)	( .22)	
AC-H/2.9	.02( .04)			
AC-H/0.4	.01( .04)			
AI-E/1.7	.04( .11)			
AI-E/0.6	.03( .05)			
AI-I/2.0	.04( .11)			
AI-I/0.4	.03( .04)			
Oxazine-725 (S <sub>t</sub> )				
CE-A/3.2	1.05( .72)	.93( .73)		
CE-A/0.5	.37( .45)			
CE-B/2.1	1.45( .96)	1.25( .99)	(1.02)	
CE-B/0.5	.68( .71)	.61( .62)	( .56)	
CE-D/3.1	1.68( .97)	(1.13)	(1.21)	
CE-D/0.4	.46( .56)	( .48)		
CM-A/1.9	.28( .26)			
CM-A/0.5	.21( .18)			
CS-A/2.2	1.94(1.15)	(1.25)	(1.39)	
CS-A/0.7	.61( .74)	( .44)	( .52)	
AC-H/2.9	.34( .26)			
AC-H/0.4	.25( .24)			
AI-E/1.7	.27( .10)			
AI-E/0.6	.21( .20)			
AI-I/2.0	.44( .37)			
AI-I/0.4	.26( .22)			

Dye	Stability After Given Exposure (kWh/m <sup>2</sup> )			
	Host Code/O.D.	50	100	200
Rhodamine-101 (A <sub>t</sub> )				
CE-A/3.0	.02( .41)	( .21)	( .10)	( .07)
CE-A/0.4	.06( .36)	( .19)		
CE-B/1.3	.03( .29)	( .14)	( .09)	( .07)
CE-B/0.5	.04( .30)	( .17)	( .12)	( .11)
CE-D/2.7	.01( .35)			
CE-D/0.4	.00( .28)			
CM-A/1.4	.08( .20)	( .08)		
CM-A/0.4	.07( .09)	( .04)		
CS-A/1.7	.01( .27)	( .13)	( .08)	( .05)
CS-A/0.6	.03( .36)	( .18)	( .12)	( .09)
AC-H/1.8	.07( .32)	( .14)	( .09)	( .07)
AC-H/0.5	.17( .40)	( .20)	( .14)	( .11)
MA-C/1.8	.01( .02)			
MA-C/0.5	.01( .02)			
AI-E/1.6	.28( .72)	.22( .62)	.16( .54)	.08( .35)
AI-E/0.4	.52( .64)	.38( .53)	.29( .42)	.15( .23)
AI-I/1.7	.37( .69)	.25( .61)	.18( .54)	.10( .35)
AI-I/0.5	.36( .46)	.24( .38)	.19( .31)	.08( .16)
AC-I/.80	.06( .28)	.03( .10)		
Rhodamine-101 (S <sub>t</sub> )				
CE-A/3.0	.19( .66)	( .50)( .38)	( .28)	
CE-A/0.4	.25( .49)	( .84)		
CE-B/1.3	.19( .50)	( .32)( .28)	( .21)	
CE-B/0.4	.16( .43)	( .28)( .24)	( .20)	
CE-D/2.7	.14( .61)			
CE-D/0.4	.09( .38)			
CM-A/1.4	.37( .26)	( .21)		
CM-A/0.4	.15( .18)	( .11)		
CS-A/1.7	.15( .50)	( .34)( .28)	( .21)	
CS-A/0.6	.12( .51)	( .30)( .26)	( .19)	
AC-H/1.8	.26( .24)	( .12)( .12)	( .09)	
AC-H/0.5	.33( .36)	( .21)( .19)	( .04)	
MA-C/1.8	.06( .06)			
MA-C/0.5	.12( .09)			
AI-E/1.7	.58( .53)	.52 ( .52)	.44( .47)	.32( .28)
AI-E/0.5	.48( .43)	.39 ( .39)	.30( .32)	.20( .24)
AC-I/.80	.26( .31)	.16 ( .15)		

Dye	Stability After Given Exposure (kWh/m <sup>2</sup> )			
	Host Code/O.D.	50	100	200
Sulforhodamine-B (A <sub>t</sub> )				
CE-A/2.9	.88(.91)	.78(.81)	.67(.73)	.52(.62)
CE-A/0.5	.92(.84)	.31(.71)	.80(.61)	.77(.44)
CE-B/3.6	.61(.80)	.46(.60)	.28(.50)	.22(.39)
CE-B/0.4	.76(.66)	.63(.46)	.52(.35)	.43(.27)
CE-D/3.4	.72(.93)	.53(.83)	.34(.73)	.21(.65)
CE-D/0.6	.85(.80)	.74(.64)	.62(.52)	.54(.39)
CM-A/1.7	.92(.64)	.83(.36)	.73(.29)	.67(.19)
CM-A/0.4	.92(.73)	.84(.56)	.76(.45)	.71(.34)
CS-A/2.2	.83(.82)	.51(.69)	.59(.32)	.51(.23)
CS-A/0.6	.85(.81)	.72(.66)	.57(.52)	.42(.45)
AC-H/1.7	.28(.49)	.19(.36)	.14(.20)	.12(.13)
AC-H/0.5	.73(.15)	.57(.07)	.44(.06)	.39(.05)
MA-C/2.3	.03(.20)	.01(.15)		
MA-C/0.4	.35(.13)	.09(.08)		
AI-E/2.3	.49(.69)	.42(.61)	.37(.54)	.26(.39)
AI-E/0.5	.81(.27)	.74(.21)	.67(.16)	.52(.13)
AI-I/1.7	.26(.76)	.23(.67)	.22(.59)	.18(.45)
AI-I/0.6	.78(.41)	.72(.31)	.67(.23)	.54(.14)
AC-I/.98	.47(.41)	.38(.23)	.28(.15)	
CE-A/1.2	.82(.48)			
CM-A/.99	.84(.33)			
AI-E/.75	.32(.44)			

Sulforhodamine-B (S <sub>t</sub> )				
CE-A/2.9	.96(.78)	.85(.68)	.96(.76)	.92(.66)
CE-A/0.5	.90(.79)	.83(.69)	.86(.68)	.79(.57)
CE-B/3.6	1.53(.73)	1.60(.79)	2.03(1.06)	1.88(1.05)
CE-B/0.4	.83(.72)	.75(.58)	.72(.55)	.62(.40)
CE-D/3.4	.97(.70)	.95(.66)	1.06(.80)	1.01(.78)
CE-D/0.6	.88(.75)	.79(.66)	.79(.62)	.65(.49)
CM-A/1.7	.95(.50)	.78(.38)	.88(.44)	.78(.33)
CM-A/0.4	.93(.76)	.86(.58)	.85(.54)	.77(.43)
CS-A/2.2	.94(.79)	.91(.75)	.96(.86)	.83(.75)
CS-A/0.6	.93(.82)	.82(.71)	.83(.69)	.65(.55)
AC-H/1.7	2.40(.58)	2.09(.42)	2.22(.60)	1.80(.38)
AC-H/0.5	.87(.24)	.70(.17)	.70(.17)	.57(.15)
MA-C/2.3	.16(.23)	.13(.19)		
MA-C/0.4	.38(.22)	.13(.10)		
AI-E/2.3	2.02(.39)	2.39(.38)	2.26(.32)	1.86(.29)
AI-E/0.5	.77(.23)	.81(.21)	.68(.20)	.55(.15)
AI-I/1.7	2.13(.75)	2.36(.81)	2.25(.88)	1.96(.77)
AI-I/0.6	.77(.33)	.74(.29)	.65(.23)	.59(.20)
AC-I/1.0	1.48(.55)	1.47(.57)	1.27(.52)	.97(.37)
CE-A/1.2	.93(.50)			
CM-A/.99	.88(.37)			
AI-E/.75	1.60(.27)			

DYE	Stability After Given Exposure (kWh/m <sup>2</sup> )			
Host Code/ O. D.	450	600	800	1000

Sulforhodamine-B  
(A<sub>t</sub>)

CE-A/2.9	.40( .45)	.25( .23)		
CE-A/0.5	.57( .30)	.43( .14)		
CE-B/3.6	.13( .26)	( .14)		
CE-B/0.4	.30( .13)	.22( )		
CE-D/3.4	.12( .52)	( .34)	( .10)	
CE-D/0.6	.40( .24)	.26( .12)		
CM-A/1.7	.51( .10)	.31( )		
CM-A/0.4	.55( .10)	.34( )		
CS-A/2.2	.36( .12)	.22( )		
CS-A/0.6	.30( .26)	.17( .13)		
AC-H/1.7	.09( .07)			
AC-H/0.5	.26( .02)	.15( )		
AI-E/2.3	.13( .25)	( .19)		
AI-E/0.5	.29( .03)	.24( )		
AI-I/1.7	.13( .29)	( .22)		
AI-I/0.6	.36( .07)	.31( )		

Sulforhodamine-B  
(S<sub>t</sub>)

CE-A/2.9	.79( .54)	.74( .43)		
CE-A/0.5	.69( .44)	.62( .32)		
CE-B/3.6	1.61(1.03)	( .90)		
CE-B/0.4	.51( .32)	.33( )		
CE-D/3.4	.90( .70)	( .67)	( .56)	
CE-D/0.6	.55( .36)	.46( .24)		
CM-A/1.7	.71( .22)	.59( )		
CM-A/0.4	.68( .26)	.59( )		
CS-A/2.2	.71( .66)	.44( )		
CS-A/0.6	.54( .43)	.40( .29)		
AC-H/1.7	1.44( .42)			
AC-H/0.5	.47( .16)	.38( )		
AI-E/2.3	1.44( .20)	( .18)		
AI-E/0.5	.43( .10)	.35( )		
AI-I/1.7	1.79( .72)	( .65)		
AI-I/0.6	.53( .15)	.48( )		



Dye	Stability After Given Exposure (kWh/m <sup>2</sup> )			
	Host Code/O.D.	50	100	200
Fluorescent Yellow 10-GN (A <sub>t</sub> )				
CE-D/1.0	.36( .76)	.09( .59)	.02( .27)	.01( .07)
Fluorescent Yellow 10-GN (S <sub>t</sub> )				
CE-D/1.0	.64( .89)	.26( .78)	.11( .49)	.10( .18)
Brilliant Orange (A <sub>t</sub> )				
CE-D/ .95	.80( .97)	.72( .95)	.44( .88)	.19( .75)
CE-A/ .64	.74( .90)	.64( .85)	.45( .72)	.20( .55)
Brilliant Orange (S <sub>t</sub> )				
CE-D/ .95	.89( .98)	.94( .96)	.78( .96)	.50( .82)
CE-A/ .64	.83( .94)	.71( .91)	.73( .93)	.60( .83)
Fluorol Yellow -088 (A <sub>t</sub> )				
CE-D/1.10	.79( .66)	.92( .64)	.58( .40)	.50( .39)
Fluorol Yellow -088 (S <sub>t</sub> )				
CE-D/1.10	.20( .34)	.19( .23)	.25( .27)	.25( .27)

Dye	Stability After Given Exposure (kWh/m <sup>2</sup> )			
	Host Code/O.D.	50	100	200
Hostasol Red -GG (A <sub>t</sub> )				
CE-D/ .65	.80( .79)	.69( .69)	.48( .44)	.16( .18)
Hostasol Red -GG (S <sub>t</sub> )				
CE-D/ .65	.95( .84)	.81( .74)	.62( .58)	.36( .37)
Fluorol Green-Gold-084 (A <sub>t</sub> )				
CE-D/ .73	.34( .97)	.15( .95)	.09( .89)	.04( .73)
Fluorol Green-Gold-084 (S <sub>T</sub> )				
CE-D/ .73	.46(1.01)	.27( .89)	.44( .81)	.16( .75)
LD-688 (A <sub>t</sub> )				
CE-D/ .82	.02( .08)	.02( .05)	.01( .04)	
CE-D/ .59	.02( .22)	.03( .07)		
CE-A/ .75	.02( .20)	( .08)		
CM-A/ .69	.03( .20)	( .07)		
AC-H/ .91	.03( .29)	( .09)		
AI-E/ .83	.00( .12)			
AI-E/ .90	.00( .20)			
AI-E/1.00 (2) *	.04( .29)			
AI-E/ .78 (3)	.06( .23)			

Dye	Stability After Given Exposure (kWh/m <sup>2</sup> )			
	Host Code/O.D.	50	100	200
LD-688 (S <sub>t</sub> )				
CE-D/ .82	.05( .19)	.04( .08)	.04( .06)	.05( .05)
CE-D/ .59	.07( .34)	.07( .08)		
CE-A/ .75	.04( .19)	(.05)		
CM-A/ .69	.06( .18)	(.06)		
AC-H/ .91	.06( .23)	(.08)		
AI-E/ .83	.04( .13)			
AI-E/ .90	.04( .19)			
AI-E/1.00 (2) *	.06( .38)			
AI-E/ .78 (3)	.14( .22)			
LD-700 (A <sub>t</sub> )				
CE-D/1.24	.39( .90)	.17( .84)	.06( .66)	.02( .50)
CE-D/1.40	.53( .94)	.28( .68)	.15( .57)	.04( .40)
CE-A/1.10	.44( .95)	.17( .85)	.05( .73)	.02( .55)
CM-A/ .75	.20( .70)	.09( .10)		
AC-H/ .66	.26( .85)	.09( .61)		
AI-E/1.03	.52( .84)	.21( .74)	(.46)	(.34)
AI-E/ .93 (2)	.41( .76)	.15( .63)	(.29)	(.19)
AI-E/ .99 (3)	.38( .73)	.13( .55)	(.21)	(.15)
CE-E/1.1	.06( .50)			
LD-700 (S <sub>t</sub> )				
CE-D/1.24	.86(1.02)	.62( .95)	.35( .93)	.21( .91)
CE-D/1.40	.91(1.00)	.73( .86)	.53( .75)	.35( .73)
CE-A/1.10	1.01(1.03)	.68( .97)	.20( .93)	.29( .96)
CM-A/ .75	.68( .93)	.41( .33)		
AC-H/ .66	.80( .92)	.36( .86)		
AI-E/1.03	.83( .94)	.63( .84)	(.72)	(.67)
AI-E/ .93 (2)	.73( .84)	.52( .81)	(.62)	(.53)
AI-E/ .99 (3)	.70( .88)	.45( .81)	(.59)	(.48)
CE-E/1.1	.80(1.29)			

Dye	Stability After Given Exposure (kWh/m <sup>2</sup> )			
	Host Code/O.D.	50	100	200
LDS-730 (A <sub>t</sub> )				
CE-D/ .74	.11( .73)	.02( .57)	( .35)	( .21)
CE-D/ .90	.09( .90)	.03( .68)	( .55)	( .39)
CE-A/1.05	.09( .81)	( .53)	( .38)	( .19)
CM-A/ .97	.13( .60)	( .17)		
AC-H/1.24	.00( .50)			
AC-H/ .79 (2)*	.00( .40)			
AC-H/1.11 (3)	.01( .41)			
AI-E/1.19	.04( .59)			
AI-E/1.05 (2)	.04( .57)			
AI-E/ .84 (3)	.05( .42)			
LDS-730 (S <sub>t</sub> )				
CE-D/ .74	.42( .88)	.16( .76)	( .61)	( .50)
CE-D/ .90	.40( .82)	.18( .85)	( .76)	( .73)
CE-A/1.05	.55( .96)	.28(1.00)	( .91)	( .82)
CM-A/ .75	.90( .90)	.46( .84)		
AC-H/1.24	.26( .91)			
AC-H/ .79 (2)	.17( .74)			
AC-H/1.07 (3)	.22( .77)			
AI-E/1.19	.27( .73)			
AI-E/1.05 (2)	.34( .74)			
AI-E/ .84 (3)	.25( .64)			
LDS-750 (A <sub>t</sub> )				
CE-D/ .86	.01( .41)	.00( .25)	( .08)	( .07)
CE-D/ .73	.01( .64)	( .29)	( .17)	
CE-A/1.05	.01( .58)	( .22)	( .11)	
CM-A/1.00	.01( .35)	( .04)		
AC-H/1.13	.00( .15)			
AC-H/ .96 (2)	.00( .09)			
AC-H/ .82 (3)	.01( .06)			
AI-E/ .94	.01( .32)			
AI-E/ .86 (2)	.02( .36)			
AI-E/ .94 (3)	.01( .37)			

Dye	Stability After Given Exposure (kWh/m <sup>2</sup> )			
Host Code/O.D.	50	100	200	300
LDS-750 (S <sub>t</sub> )				
CE-D/ .86	.12( .75)	.09( .62)	( .29)	( .19)
CE-D/ .73	.15( .13)	( .08)	( .07)	
CE-A/1.05	.21(1.06)	( .65)	( .46)	
CM-A/1.00	.53( .98)	( .88)		
AC-H/1.13	.59( .98)			
AC-H/ .96 (2) *	.14( .45)			
AC-H/ .83 (3)	.12( .31)			
AI-E/ .94	.13( .63)			
AI-E/ .86 (2)	.09( .55)			
AI-E/1.01 (3)	.11( .62)			
LDS-751 (A <sub>t</sub> )				
CE-D/ .82	.02( .64)	.02( .43)	( .13)	( .07)
LDS-751 (S <sub>t</sub> )				
CE-D/ .82	.14( .76)	.11( .56)	( .30)	( .21)
LDS-798 (A <sub>t</sub> )				
CE-D/ .79	.00( .43)	( .25)		
CE-D/ .75	.01( .69)	( .34)	( .17)	( .06)
CE-A/ .72	.02( .63)	( .26)	( .19)	
CM-A/ .86	.02( .32)	( .09)		
AC-H/ .80	.01( .11)			
AC-H/ .75 (2) *	.01( .18)			
AC-H/ .91 (3)	.01( .17)			
AI-E/ .96	.01( .28)			
AI-E/1.01 (2)	.01( .31)			
AI-E/ .99 (3)	.02( .12)			

Dye	Stability After Given Exposure (kWh/m <sup>2</sup> )			
	Host Code/O.D.	50	100	200
LDS-798 (S <sub>t</sub> )				
CE-D/ .79	.11( .75)	.10( .51)	( .21)	( .08)
CE-D/ .75	.11( .63)	( .50)	( .32)	
CE-A/ .72	.13( .88)	( .53)	( .31)	
CM-A/ .86	.25( .63)	( .27)		
AC-H/ .80	.10( .38)	( .23)		
AC-H/ .75 (2)	.08( .46)	( .28)		
AC-H/ .91 (3)	.06( .45)	( .29)		
AI-E/ .96	.13( .62)	( .50)		
AI-E/1.01 (2)	.12( .61)	( .49)		
AI-E/ .99 (3)	.09( .47)	( .36)		
Hostasol- Yellow 3-G (A <sub>t</sub> )				
CE-D/ .63	.85( .93)	.62( .88)	.38( .74)	.18( .63)
Hostasol- Yellow 3-G (S <sub>t</sub> )				
CE-D/ .63	.95(1.09)	1.04( .94)	.94( .86)	.60( .77)
Hostasol- Yellow 8-G (A <sub>t</sub> )				
CE-D/1.25	.91( .83)	.80( .70)	.75( .53)	.54( .40)
AC-I/ .68	.45( .86)	.27( .81)	.16( .75)	.05( .56)
CE-D/1.00	.67( .70)	.64( .67)	.56( .56)	.46( .53)
CE-A/1.30	.90( .76)	.86( .71)	.79( .58)	.57( .44)
AC-H/ .90	.53( .83)	.37( .79)	.15( .66)	.06( .53)
CM-A/1.07	.91( .61)	.87( .54)	.81( .42)	.71( .31)
AI-E/1.11	.44( .87)	.27( .86)	.12( .54)	( .33)
Hostasol- Yellow 8-G (S <sub>t</sub> )				
CE-D/1.25	.89( .70)	.83( .52)	.79( .54)	.69( .44)
AC-H/ .68	.69( .61)	.58( .60)	.49( .53)	.30( .38)
CE-D/1.00	.84( .82)	.83( .77)	.79( .66)	.72( .75)
CE-A/1.30	.88( .66)	.88( .61)	.82( .60)	.75( .53)
AC-H/ .90	.60( .57)	.52( .52)	.34( .50)	.23( .46)
CM-A/1.07	.86( .67)	.91( .67)	.90( .66)	.92( .63)
AI-E/1.11	.57( .69)	.49( .66)	.31( .58)	( .56)

DYE	Stability After Given Exposure (kWh/m <sup>2</sup> )			
Host Code/ O. D.	450	600	800	1000
Hostasol Yellow-3G (A <sub>t</sub> )				
CE-D/.63	.12( .61)			
Hostasol Yellow-3G (S <sub>t</sub> )				
CE-D/.63	.37( .48)			
Hostasol Yellow-8G (A <sub>t</sub> )				
CE-D/1.3	.46( .36)			
AC-I/.68	( .45)			
CE-D/1.0				
CE-A/1.3				
AC-H/.90				
CM-A/1.1				
AI-E/1.1				
Hostasol Yellow-8G (S <sub>t</sub> )				
CE-D/1.3	.57( .37)			
AC-I/.68	( .35)			
CE-D/1.0				
CE-A/1.3				
AC-H/.90				
CM-A/1.1				
AI-E/1.1				

Dye	Stability After Given Exposure (kWh/m <sup>2</sup> )				
	Host Code/O.D.	50	100	200	300
Eastman DTTC (A <sub>t</sub> )					
CE-D/ .02		.10( .12)			
CE-A/ .30		.02( .06)			
AC-H/ .13		.01( .02)			
CM-A/ .03		.15( .03)			
AI-E/ .09		.01( .05)			
Eastman DTTC (S <sub>t</sub> )					
CE-D/ .02		.64( .69)			
CE-A/ .30		1.47(1.00)			
AC-H/ .13		1.50(1.22)			
CM-A/ .03		.69( .79)			
AI-E/ .09		.43( .40)			
Eastman DTDC (A <sub>t</sub> )					
CE-D/ .05		.09( .02)			
CE-A/ .01		.00( .13)			
AC-H/ .04		.16( .03)			
CM-A/ .03		.18( .03)			
AI-E/ .65		.03( .02)			
Eastman DTDC (S <sub>t</sub> )					
CE-D/ .05		.60( .37)			
CE-A/ .01		.46( .50)			
AC-H/ .04		.64( .61)			
CM-A/ .03		.48( .48)			
AI-E/ .65		.13( .13)			



Dye	Stability After Given Exposure (kWh/m <sup>2</sup> )				
	Host Code/O.D.	50	100	200	300
Exciton DODC (A <sub>t</sub> )					
CE-D/	.19	.01	(.00)		
CE-A/	.01	.25	(.50)		
AC-H/	.35	.00	(.04)		
CM-A/	.23	.03	(.02)		
AI-E/	.60	.18	(.03)		
Exciton DODC (S <sub>t</sub> )					
CE-D/	.19	.21	(.23)		
CE-A/	.01	.39	(.50)		
AC-H/	.35	.34	(.34)		
CM-A/	.23	.24	(.30)		
AI-E/	.60	.08	(.38)		
Exciton DOTC (A <sub>t</sub> )					
CE-D/	.13	.02	(.01)		
CE-A/	.12	.04	(.06)		
AC-H/	.36	.02	(.00)		
CM-A/	.33	.00	(.00)		
AI-E/	.34	.03	(.17)		
Exciton DOTC (S <sub>t</sub> )					
CE-D/	.13	.26	(.30)		
CE-A/	.12	.34	(.36)		
AC-H/	.36	.18	(.18)		
CM-H/	.33	.15	(.18)		
AI-E/	.34	.26	(.29)		

Dye	Stability After Given Exposure (kWh/m <sup>2</sup> )				
	Host Code/O.D.	50	100	200	300
Acridine Red (A <sub>t</sub> )					
CE-D/1.12		.24( .15)			
CE-A/ .74		.21( .11)			
CM-A/ .88		.11( .05)			
AI-E/ .96		.26( .06)			
Acridine Red (S <sub>t</sub> )					
CE-D/1.12		.59( .31)			
CE-A/ .74		.47( .23)			
CM-A/ .88		.36( .12)			
AI-E/ .96		.52( .13)			
BASF-241 (A <sub>t</sub> )					
AI-E/ .83		.29( .35)	.09( .20)	.03( .03)	
AC-H/1.20		.82( .96)	.79(1.00)		
CE-A/ .80		.80( .90)	.88( .98)		
CM-A/ .71		.08( .25)			
CE-D/ .93		.86( .97)	.93( .92)		
BASF-241 (S <sub>t</sub> )					
AI-E/ .83		.30( .19)	.22( .12)	.18( .21)	
AC-H/1.20		.82( .70)	.79( .80)		
CE-A/ .85		.89( .87)	.75( .87)		
CM-A/ .71		.20( .22)			
CE-D/ .93		.76( .92)	.83( .90)		

Dye		Stability After Given Exposure (kWh/m <sup>2</sup> )			
Host Code/O.D.		50	100	200	300
Rhodamine 101 (A <sub>t</sub> )					
AI-E/1.32		.34( .55)	.09( .42)	( .16)	
AI-E/1.22	(2) *	.48( .56)	.16( .43)	( .07)	
AI-E/	.92 (4)	.30( .14)	.06		
AC-H/	.95	.02( .15)			
AC-H/	.99 (2)	.02( .03)			
AC-H/	.90 (4)	.05( .05)			
CE-A/	.92	.02( .39)	( .28)	( .09)	
CE-A/1.04	(2)	.07( .43)	( .01)		
CE-A/1.02	(4)	.11( .40)	( .26)	( .10)	
CM-A/	.91	.04( .10)			
CM-A/1.00	(2)	.12( .05)			
CM-A/	.92 (4)	.14( .04)			
CE-D/	.95	.01( .43)	( .27)	( .07)	
CE-D/1.10	(2)	.07( .24)			
CE-D/	.94 (4)	.09( .23)			
Rhodamine 101 (S <sub>t</sub> )					
AI-E/1.32		.58( .48)	.30( .43)	( .28)	
AI-E/1.22	(2)	.65( .49)	.44( .43)	( .26)	
AI-E/	.92 (4)	.53( .21)	.24		
AC-H/	.95	.17( .15)			
AC-H/	.99 (2)	.13( .08)			
AC-H/	.90 (4)	.22( .08)			
CE-A/	.92	.17( .60)			
CE-A/1.04	(2)	.25( .58)	( .47)		
CE-A/1.02	(4)	.32( .54)	( .47)	( .21)	
CM-A/	.91	.21( .26)			
CM-A/1.00	(2)	.33( .14)			
CM-A/	.92 (4)	.36( .14)			
CE-D/	.95	.15( .60)	( .45)	( .21)	
CE-D/1.10	(2)	.26( .41)			
CE-D/	.91 (4)	.27( .41)			

Dye	Stability After Given Exposure (kWh/m <sup>2</sup> )			
Host Code/O.D.	50	100	200	300
Rhodamine 6-G (A <sub>t</sub> )				
CE-D/ .96	.60( .38)	.35( .23)	.05( .07)	
AI-E/ .88	.68( .03)	.33	.01	
Rhodamine 6-G (S <sub>t</sub> )				
CE-D/ .96	.79( .49)	.54( .35)	.25( .23)	
AI-E/ .88	.68( .09)	.42	.16	
Rhodamine 19 (A <sub>t</sub> )				
CE-D/1.12	.29( .30)	.20( .22)	.01( .01)	
AI-E/ .43	.62( .09)	.43	.19	
Rhodamine 19 (S <sub>t</sub> )				
CE-D/1.12	.77( .48)	.68( .36)	.24( .17)	
AI-E/ .43	.66( .16)	.38	.27	
Rhodamine-B (A <sub>t</sub> )				
CE-D/1.07	.36( .24)	.14( .09)		
AI-E/ .80	.76( .28)	.34	.09	
Rhodamine-B (S <sub>t</sub> )				
CE-D/1.07	.73( .43)	.47( .28)		
AI-E/ .80	.69( .20)	.49	.34	

Dye	Stability After Given Exposure (kWh/m <sup>2</sup> )				
	Host Code/O.D.	50	100	200	300
Rhodamine-110 (A <sub>t</sub> )					
CE-D/ .73		.17( .14)	.06		
AC-I/ .47		.05( .48)	( .27)		
Rhodamine-110 (S <sub>t</sub> )					
CE-D/ .73		.52( .47)	.32		
AC-I/ .47		1.30( .86)	( .95)		
Coumarin-440 (A <sub>t</sub> )					
CE-D/1.35		.05			
CM-A/ .89		.04			
AI-E/1.05		.05			
Coumarin-440 (S <sub>t</sub> )					
CE-D/1.35		.41			
CM-A/ .89		.56			
AI-E/1.05		.64			
Coumarin-445 (A <sub>t</sub> )					
CE-D/1.02		.02			
CM-A/ .94		.02			
Coumarin-445 (S <sub>t</sub> )					
CE-D/1.02		.47			
CM-A/ 94		.29			

Dye	Stability After Given Exposure (kWh/m <sup>2</sup> )				
	Host Code/O.D.	50	100	200	300
Coumarin-450 (A <sub>t</sub> )					
CE-D/	.90	.02			
CM-A/	.98	.01			
Coumarin-450 (S <sub>t</sub> )					
CE-D/	.90	.38			
CM-A/	.98	.14			
Coumarin-460 (A <sub>t</sub> )					
CE-D/	1.27	.01			
CM-A/	.98	.03			
AI-E/	1.14	.04			
Coumarin-460 (S <sub>t</sub> )					
CE-D/	1.27	.14			
CM-A/	.98	.28			
AI-E/	1.14	.39			
Stilbene-420 (A <sub>t</sub> )					
CE-D/	.96	.01			
AI-E/	.86	.20			
Stilbene-420 (S <sub>t</sub> )					
CE-D/	.96	.14			
AI-E/	.86	.71			

Dye	Stability After Given Exposure (kWh/m <sup>2</sup> )				
	Host Code/O.D.	50	100	200	300
LD-423 (A <sub>t</sub> )					
CE-D/1.06		.00			
AI-E/ .98		.04			
LD-423 (S <sub>t</sub> )					
CE-D/1.06		.34			
AI-E/ .98		.44			
LD-425 (A <sub>t</sub> )					
CE-D/ .90		.00			
AI-E/ .87		.06			
LD-425 (S <sub>t</sub> )					
CE-D/ .90		.40			
AI-E/ .87		.36			
LD-466 (A <sub>t</sub> )					
CE-D/ .87		.01			
AI-E/ .81		.04			
LD-466 (S <sub>t</sub> )					
CE-D/ .87		.18			
AI-E/ .81		.22			
Fluorol-555 (A <sub>t</sub> )					
AC-I/ .90		.09( .61)	( .35)	( .18)	
CE-D/ .94		.03( .64)	.02( .09)		
Fluorol-555 (S <sub>t</sub> )					
AC-I/ .90		.24( .66)	( .49)	( .30)	
CE-D/ .94		.15( .74)	.10( .52)		

Dye	Stability After Given Exposure (kWh/m <sup>2</sup> )				
	Host Code/O.D.	50	100	200	300
Rad-Glo #14 (A <sub>t</sub> )					
AC-H/ .82	.26( .63)	.18( .39)	( .17)		
CE-D/ .83	.20( .66)	( .40)	( .20)		
CM-A/ .81	.20( .50)	( .29)	( .09)		
CE-A/ .68	.17( .53)	( .27)	( .05)		
AI-E/ .67	.63( .87)	.50( .66)	.22( .39)		(.19)
Rad-Glo #14 (S <sub>t</sub> )					
AC-H/ .82	.42( .26)	.43( .31)	( .26)		
CE-D/ .83	.48( .35)	( .34)	( .22)		
CM-A/ .81	.26( .20)	( .18)	( .10)		
CE-A/ .68	.30( .25)	( .24)	( .22)		
AI-E/ .67	.47( .21)	.39( .21)	.22( .20)		(.15)
Rad-Glo #9 Clear (A <sub>t</sub> )					
AC-H/ .45	.06				
CE-D/ .47	.02				
CM-A/ .65	.04				
CE-A/ .64	.05				
AI-E/ .67	.02				
Rad-Glo #9 Clear (S <sub>t</sub> )					
AC-H/ .45	.45				
CE-D/ .47	.49				
CM-A/ .65	.41				
CE-A/ .64	.34				
AI-E/ .67	.42				



Dye	Stability After Given Exposure (kWh/m <sup>2</sup> )			
	Host Code/O.D.	50	100	200
Lisa Mobay (A <sub>t</sub> )				
Green 52-G				
PC /3.28	.96	.96	.96	.96
PMMA/3.27	.94	.94	.94	.94
Amber 59-YR				
PC /2.26	.95	.95	.95	.95
PMMA/3.24	.93	.93	.93	.93
Orange 61-R				
PC /3.39	.89	.89	.89	.89
PMMA/3.40	.92	.92	.92	.92
Orange				
PC /2.40	.93	.93	.93	.93
Yellow				
PC /1.21	.85	.85	.85	.85
Lisa Mobay Plates (S <sub>t</sub> )				
Green 52-G				
PC /3.28	.88	.88	.88	.88
PMMA/3.27	.96	.96	.96	.96
Amber 59-YR				
PC /2.26	1.13	1.13	1.13	1.13
PMMA/3.24	.60	.60	.60	.60
Orange 61-R				
PC /3.39	.94	.94	.94	.94
PMMA/3.40	.82	.82	.82	.82
Orange				
PC /2.40	.93	.93	.93	.93
Yellow				
PC /1.21	1.02	1.02	1.02	1.02



## APPENDIX II

### RELATIVE EDGE LUMINESCENCE VALUES FOR LSC TEST PLATES

The definition of the relative edge luminescence is given in Section IV. The actual data tables listing these values appear in this Appendix. Interpretation of the data and footnotes, however, requires some explanation.

The data tables are based on three different size plates: 27 cm<sup>2</sup> (4.4 x 6.2 cm), 49 cm<sup>2</sup> (7.0 x 7.0 cm), and 196 cm<sup>2</sup> (14.0 x 14.0 cm). All plates were fabricated out of 1/8 - inch Plexiglas, which measures approximately 3.5mm thick. Unless otherwise specified, only one edge of each plate has been optically polished, and this is the edge from which all measurements have been made. The other three edges had a "rough ground glass" finish. For plates with a large number of thin film dye coats, half the coats are on each side of the plate so as to avoid excessive warping. For the far red absorbing dyes, measurements have been made with and without a 59 D type cover plate<sup>3</sup> to test the efficiency of the "stacked plate" concept.<sup>48</sup> In order to get an indication of the radiative transport efficiency<sup>3</sup> (see Section V) and hence the scalability, a number of 196 cm<sup>2</sup> plates were masked with a 49 cm<sup>2</sup> aperture. Finally, for strongly fluorescent plates with an optical density greater than two (2), errors due to escaping fluorescence from the plate surface reaching the detector become progressively more serious as the absorbance peak gets larger. Thus, for plates with high optical density, the peak absorbance was calculated from the ratio of the shoulder-to-peak absorption from a shoulder having an optical density of 1.5 to 2.0.

RELATIVE EDGE LUMINESCENCE ( $L_r$ )

Plate #	Area (cm <sup>2</sup> )	Dye	# Coats	Host	Abs. <sup>2</sup>	$L_r$
GG17	58	Uranium Standard			1.48	
1753	49	Brilliant Yellow	1	CAP. 504-0.2	3.09	1.34
1754	49	Brilliant Yellow	1	CAP. 504-0.2	3.15	1.38
1757	49	Brilliant Yellow	1	CAP. 504-0.2	0.46	1.85
1758	49	Brilliant Yellow	1	CAP. 504-0.2	0.47	1.76
1765	49	SRB	1	CAP. 504-0.2	3.35	2.11
1766	49	SRB	1	CAP. 504-0.2	3.27	1.97
1769	49	SRB	1	CAP. 504-0.2	0.56	2.23
1770	49	SRB	1	CAP. 504-0.2	0.54	2.18
1777	49	R-101	1	CAP. 504-0.2	2.56	3.18
1778	49	R-101	1	CAP. 504-0.2	2.65	3.07
1781	49	R-101	1	CAP. 504-0.2	0.41	2.29
1782	49	R-101	1	CAP. 504-0.2	0.42	2.27
1789	49	Coumarin-6	1	CAP. 504-0.2	2.62	3.72
1790	49	Coumarin-6	1	CAP. 504-0.2	2.65	3.29
1793	49	Coumarin-6	1	CAP. 504-0.2	0.49	2.96
1794	49	Coumarin-6	1	CAP. 504-0.2	0.49	2.76
1801	49	Nile Blue	1	CAP. 504-0.2	2.94	0.42
1802	49	Nile Blue	1	CAP. 504-0.2	2.89	0.42
1805	49	Nile Blue	1	CAP. 504-0.2	0.67	1.12
1806	49	Nile Blue	1	CAP. 504-0.2	0.66	1.13
1813	49	Oxazine-725	1	CAP. 504-0.2	3.19	0.68

- 1) Area is cm<sup>2</sup>; dimensions (in cm) of various size plates are: 4.4 x 6.2 (27 cm<sup>2</sup>), 7.0 x 7.0 (49 cm<sup>2</sup>), 14.0 x 14.0 (196 cm<sup>2</sup>)
- 2) Peak absorbance
- 3) 59-D plate placed over sample
- 4) Metal mask placed over sample; 49 cm<sup>2</sup> surface left open

RELATIVE EDGE LUMINESCENCE ( $L_r$ )

Plate #	Area (cm <sup>2</sup> )	Dye	# Coats	Host	Abs. <sup>2</sup>	$L_r$
1814	49	Oxazine-725	1	CAP. 504-0.2	3.24	0.66
1817	49	Oxazine-725	1	CAP. 504-0.2	0.43	1.08
1818	49	Oxazine-725	1	CAP. 504-0.2	0.44	1.05
1825	49	Brilliant Yellow	1	CAB. 553-0.4	2.79	1.47
1826	49	Brilliant Yellow	1	CAB. 553-0.4	2.84	1.39
1829	49	Brilliant Yellow	1	CAB. 553-0.4	0.59	2.72
1830	49	Brilliant Yellow	1	CAB. 553-0.4	0.60	2.39
1837	49	SRB	1	CAB. 553-0.4	2.94	3.27
1838	49	SRB	1	CAB. 553-0.4	2.96	3.23
1841	49	SRB	1	CAB. 553-0.4	0.51	2.18
1842	49	SRB	1	CAB. 553-0.4	0.51	2.13
1849	49	R-101	1	CAB. 553-0.4	3.04	3.74
1850	49	R-101	1	CAB. 553-0.4	3.09	3.63
1853	49	R-101	1	CAB. 553-0.4	0.39	2.46
1854	49	R-101	1	CAB. 553-0.4	0.41	2.09
1861	49	Coumarin-6	1	CAB. 553-0.4	3.37	4.07
1862	49	Coumarin-6	1	CAB. 553-0.4	3.36	4.03
1865	49	Coumarin-6	1	CAB. 553-0.4	0.47	2.89
1866	49	Coumarin-6	1	CAB. 553-0.4	0.46	2.81
1873	49	Nile Blue	1	CAB. 553-0.4	2.07	0.14
1874	49	Nile Blue	1	CAB. 553-0.4	2.09	0.13
1877	49	Nile Blue	1	CAB. 553-0.4	0.59	1.20

- 1) Area is cm<sup>2</sup>; dimensions (in cm) of various size plates are: 4.4 x 6.2 (27 cm<sup>2</sup>), 7.0 x 7.0 (49 cm<sup>2</sup>), 14.0 x 14.0 (196 cm<sup>2</sup>)
- 2) Peak absorbance
- 3) 59-D plate placed over sample
- 4) Metal mask placed over sample; 49 cm<sup>2</sup> surface left open

RELATIVE EDGE LUMINESCENCE ( $L_T$ )

Plate #	Area (cm <sup>2</sup> ) <sup>1</sup>	Dye	# Coats	Host	Abs. <sup>2</sup>	$L_T$
1878	49	Nile Blue	1	CAB. 553-0.4	0.59	1.37
1885	49	Oxazine-725	1	CAB. 553-0.4	3.17	1.11
1886	49	Oxazine-725	1	CAB. 553-0.4	3.21	1.07
1889	49	Oxazine-725	1	CAB. 553-0.4	0.48	1.12
1890	49	Oxazine-725	1	CAB. 553-0.4	0.50	1.19
1897	49	Brilliant Yellow	1	CAP. 482-0-20	2.96	0.91
1898	49	Brilliant Yellow	1	CAP. 482-0-20	2.94	0.85
1901	49	Brilliant Yellow	1	CAP. 482-0-20	0.42	2.36
1902	49	Brilliant Yellow	1	CAP. 482-0-20	0.42	2.36
1909	49	SRB	1	CAP. 482-0-20	3.55	1.19
1910	49	SRB	1	CAP. 482-0-20	3.54	1.09
1913	49	SRB	1	CAP. 482-0-20	0.43	1.94
1914	49	SRB	1	CAP. 482-0-20	0.43	1.66
1921	49	Nile Blue	1	CAP. 482-0-20	3.22	0.35
1922	49	Nile Blue	1	CAP. 482-0-20	3.26	0.33
1925	49	Nile Blue	1	CAP. 482-0-20	0.48	0.65
1926	49	Nile Blue	1	CAP. 482-0-20	0.49	0.73
1933	49	Coumarin-6	1	CAP. 482-0-20	2.03	0.38
1934	49	Coumarin-6	1	CAP. 482-0-20	2.02	0.37
1937	49	Coumarin-6	1	CAP. 482-0-20	0.47	2.79
1938	49	Coumarin-6	1	CAP. 482-0-20	0.48	2.70
1945	49	R-101	1	CAP. 482-0-20	1.34	3.24

- 1) Area is cm<sup>2</sup>; dimensions (in cm) of various size plates are: 4.4 x 6.2 (27 cm<sup>2</sup>), 7.0 x 7.0 (49 cm<sup>2</sup>), 14.0 x 14.0 (196 cm<sup>2</sup>)
- 2) Peak absorbance
- 3) 59-D plate placed over sample
- 4) Metal mask placed over sample; 49 cm<sup>2</sup> surface left open

RELATIVE EDGE LUMINESCENCE ( $L_T$ )

Plate #	Area (cm <sup>2</sup> ) <sup>1</sup>	Dye	# Coats	Host	Abs. <sup>2</sup>	$L_T$
1949	49	R-101	1	CAP. 482-0-20	1.36	3.19
1949	49	R-101	1	CAP. 482-0-20	0.46	2.28
1950	49	R-101	1	CAP. 482-0-20	0.45	2.21
1957	49	Oxazine-725	1	CAP. 482-0-20	2.07	0.77
1958	49	Oxazine-725	1	CAP. 482-0-20	2.08	0.74
1961	49	Oxazine-725	1	CAP. 482-0-20	0.54	1.12
1962	49	Oxazine-725	1	CAP. 482-0-20	0.50	1.19
1969	49	Brilliant Yellow	1	Elvacite 2010	1.54	1.24
1970	49	Brilliant Yellow	1	Elvacite 2010	1.56	1.22
1973	49	Brilliant Yellow	1	Elvacite 2010	0.49	2.09
1974	49	Brilliant Yellow	1	Elvacite 2010	0.48	1.98
1981	49	SRB	1	Elvacite 2010	1.65	0.70
1982	49	SRB	1	Elvacite 2010	1.53	0.63
1985	49	SRB	1	Elvacite 2010	0.45	1.98
1986	49	SRB	1	Elvacite 2010	0.48	2.11
1993	49	Coumarin-6	1	Elvacite 2010	1.70	3.75
1994	49	Coumarin-6	1	Elvacite 2010	1.76	3.82
1997	49	Coumarin-6	1	Elvacite 2010	0.51	2.98
1998	49	Coumarin-6	1	Elvacite 2010	0.53	3.02
2005	49	R-101	1	Elvacite 2010	1.82	3.39
2006	49	R-101	1	Elvacite 2010	1.85	3.66
2009	49	R-101	1	Elvacite 2010	0.53	2.72

- 1) Area is cm<sup>2</sup>; dimensions (in cm) of various size plates are: 4.4 x 6.2 (27 cm<sup>2</sup>), 7.0 x 7.0 (49 cm<sup>2</sup>), 14.0 x 14.0 (196 cm<sup>2</sup>)
- 2) Peak absorbance
- 3) 59-D plate placed over sample
- 4) Metal mask placed over sample; 49 cm<sup>2</sup> surface left open

RELATIVE EDGE LUMINESCENCE ( $L_r$ )

Plate #	Area <sub>g</sub> (cm <sup>2</sup> ) <sub>1</sub>	Dye	# Coats	Host	Abs. <sup>2</sup>	$L_r$
2010	49	R-101	1	Elvacite 2010	0.52	2.58
2017	49	Nile Blue	1	Elvacite 2010	2.14	0.28
2018	49	Nile Blue	1	Elvacite 2010	2.18	0.28
2021	49	Nile Blue	1	Elvacite 2010	0.56	0.82
2022	49	Nile Blue	1	Elvacite 2010	0.56	0.82
2029	49	Oxazine-725	1	Elvacite 2010	2.83	1.60
2030	49	Oxazine-725	1	Elvacite 2010	2.79	1.47
2033	49	Oxazine-725	1	Elvacite 2010	0.41	1.46
2034	49	Oxazine-725	1	Elvacite 2010	0.41	1.47
2041	49	Brilliant Yellow	1	Polytex 910/Cymel 303	1.74	1.73
2042	49	Brilliant Yellow	1	Polytex 910/Cymel 303	1.74	1.70
2045	49	Brilliant Yellow	1	Polytex 910/Cymel 303	0.50	2.16
2046	49	Brilliant Yellow	1	Polytex 910/Cymel 303	0.51	2.28
2053	49	SRB	1	Polytex 910/Cymel 303	2.27	1.65
2054	49	SRB	1	Polytex 910/Cymel 303	2.23	1.57
2057	49	SRB	1	Polytex 910/Cymel 303	0.38	1.83
2058	49	SRB	1	Polytex 910/Cymel 303	0.36	1.78
2065	49	R-101	1	Polytex 910/Cymel 303	1.78	3.84
2066	49	R-101	1	Polytex 910/Cymel 303	1.78	3.81
2069	49	R-101	1	Polytex 910/Cymel 303	0.53	1.80
2070	49	R-101	1	Polytex 910/Cymel 303	0.55	1.95
2077	49	Coumarin-6	1	Polytex 910/Cymel 303	1.52	3.44

- 1) Area is cm<sup>2</sup>; dimensions (in cm) of various size plates are: 4.4 x 6.2 (27 cm<sup>2</sup>), 7.0 x 7.0 (49 cm<sup>2</sup>), 14.0 x 14.0 (196 cm<sup>2</sup>)
- 2) Peak absorbance
- 3) 59-D plate placed over sample
- 4) Metal mask placed over sample; 49 cm<sup>2</sup> surface left open

RELATIVE EDGE LUMINESCENCE ( $L_r$ )

Plate #	Area <sub>g</sub> (cm <sup>2</sup> ) <sub>1</sub>	Dye	# Coats	Host	Abs. <sup>2</sup>	$L_r$
2078	49	Coumarin-6	1	Polytex 910/Cymel 303	1.55	3.82
2081	49	Coumarin-6	1	Polytex 910/Cymel 303	0.46	2.61
2082	49	Coumarin-6	1	Polytex 910/Cymel 303	0.46	2.61
2089	49	Nile Blue	1	Polytex 910/Cymel 303	1.69	0.33
2090	49	Nile Blue	1	Polytex 910/Cymel 303	1.72	0.31
2093	49	Nile Blue	1	Polytex 910/Cymel 303	0.39	0.97
2094	49	Nile Blue	1	Polytex 910/Cymel 303	0.40	0.98
2101	49	Oxazine-725	1	Polytex 910/Cymel 303	1.78	1.12
2102	49	Oxazine-725	1	Polytex 910/Cymel 303	0.33	1.12
2105	49	Oxazine-725	1	Polytex 910/Cymel 303	0.33	1.13
2106	49	Oxazine-725	1	Polytex 910/Cymel 303	2.15	1.15
2113	49	Brilliant Yellow	1	CAP. 504-0.2/hy. EOS	2.15	0.93
2114	49	Brilliant Yellow	1	CAP. 504-0.2/hy. EOS	1.90	0.91
2117	49	Brilliant Yellow	1	CAP. 504-0.2/hy. EOS	0.72	1.74
2118	49	Brilliant Yellow	1	CAP. 504-0.2/hy. EOS	0.71	1.75
2126	49	SRB	1	CAP. 504-0.2/hy. EOS	2.18	2.25
2127	49	SRB	1	CAP. 504-0.2/hy. EOS	2.20	2.25
2129	49	SRB	1	CAP. 504-0.2/hy. EOS	0.59	2.09
2130	49	SRB	1	CAP. 504-0.2/hy. EOS	0.60	2.01
2137	49	R-101	1	CAP. 504-0.2/hy. EOS	1.71	3.25
2138	49	R-101	1	CAP. 504-0.2/hy. EOS	1.74	3.29
2141	49	R-101	1	CAP. 504-0.2/hy. EOS	0.59	2.29

- 1) Area is cm<sup>2</sup>; dimensions (in cm) of various size plates are: 4.4 x 6.2 (27 cm<sup>2</sup>), 7.0 x 7.0 (49 cm<sup>2</sup>), 14.0 x 14.0 (196 cm<sup>2</sup>)
- 2) Peak absorbance
- 3) 59-D plate placed over sample
- 4) Metal mask placed over sample; 49 cm<sup>2</sup> surface left open

RELATIVE EDGE LUMINESCENCE ( $L_r$ )

Plate #	Area (cm <sup>2</sup> )	Dye	# Coats	Host	Abs. <sup>2</sup>	$L_r$
2142	49	R-101	1	CAP. 504-0.2/hy. EOS	0.59	2.58
2149	49	Coumarin-6	1	CAP. 504-0.2/hy. EOS	1.90	3.14
2150	49	Coumarin-6	1	CAP. 504-0.2/hy. EOS	1.92	3.08
2153	49	Coumarin-6	1	CAP. 504-0.2/hy. EOS	0.78	3.28
2154	49	Coumarin-6	1	CAP. 504-0.2/hy. EOS	0.78	3.45
2161	49	Nile Blue	1	CAP. 504-0.2/hy. EOS	2.12	0.16
2162	49	Nile Blue	1	CAP. 504-0.2/hy. EOS	2.09	0.14
2165	49	Nile Blue	1	CAP. 504-0.2/hy. EOS	0.63	0.73
2166	49	Nile Blue	1	CAP. 504-0.2/hy. EOS	0.62	0.73
2173	49	Oxazine-725	1	CAP. 504-0.2/hy. EOS	2.20	0.40
2174	49	Oxazine-725	1	CAP. 504-0.2/hy. EOS	2.25	0.40
2177	49	Oxazine-725	1	CAP. 504-0.2/hy. EOS	0.66	1.11
2178	49	Oxazine-725	1	CAP. 504-0.2/hy. EOS	0.69	1.16
2185	49	Brilliant Yellow	1	CAP. 504-0.2/Cymel 303	2.24	1.63
2186	49	Brilliant Yellow	1	CAP. 504-0.2/Cymel 303	2.37	1.58
2189	49	Brilliant Yellow	1	CAP. 504-0.2/Cymel 303	0.41	2.06
2190	49	Brilliant Yellow	1	CAP. 504-0.2/Cymel 303	0.42	2.44
2197	49	SRB	1	CAP. 504-0.2/Cymel 303	1.74	3.65
2198	49	SRB	1	CAP. 504-0.2/Cymel 303	1.84	3.68
2201	49	SRB	1	CAP. 504-0.2/Cymel 303	0.42	2.00
2202	49	SRB	1	CAP. 504-0.2/Cymel 303	0.43	1.91
2208	49	R-101	1	CAP. 504-0.2/Cymel 303	1.36	3.66

- 1) Area is cm<sup>2</sup>; dimensions (in cm) of various size plates are: 4.4 x 6.2 (27 cm<sup>2</sup>), 7.0 x 7.0 (49 cm<sup>2</sup>), 14.0 x 14.0 (196 cm<sup>2</sup>)
- 2) Peak absorbance
- 3) 59-D plate placed over sample
- 4) Metal mask placed over sample; 49 cm<sup>2</sup> surface left open

RELATIVE EDGE LUMINESCENCE ( $L_r$ )

Plate #	Area (cm <sup>2</sup> )	Dye	# Coats	Host	Abs. <sup>2</sup>	$L_r$
2209	49	R-101	1	CAP. 504-0.2/Cymel 303	1.38	3.83
2213	49	R-101	1	CAP. 504-0.2/Cymel 303	0.44	2.22
2214	49	R-101	1	CAP. 504-0.2/Cymel 303	0.40	2.35
2221	49	Coumarin-6	1	CAP. 504-0.2/Cymel 303	2.38	4.05
2222	49	Coumarin-6	1	CAP. 504-0.2/Cymel 303	2.49	4.20
2225	49	Coumarin-6	1	CAP. 504-0.2/Cymel 303	0.48	2.83
2226	49	Coumarin-6	1	CAP. 504-0.2/Cymel 303	0.49	2.77
2233	49	Nile Blue	1	CAP. 504-0.2/Cymel 303	1.72	0.39
2234	49	Nile Blue	1	CAP. 504-0.2/Cymel 303	1.62	0.40
2237	49	Nile Blue	1	CAP. 504-0.2/Cymel 303	0.31	1.38
2238	49	Nile Blue	1	CAP. 504-0.2/Cymel 303	0.29	1.30
2245	49	Oxazine-725	1	CAP. 504-0.2/Cymel 303	1.88	1.23
2246	49	Oxazine-725	1	CAP. 504-0.2/Cymel 303	1.89	1.26
2249	49	Oxazine-725	1	CAP. 504-0.2/Cymel 303	0.49	1.26
2250	49	Oxazine-725	1	CAP. 504-0.2/Cymel 303	0.49	1.26
2257	49	Brilliant Yellow	1	Polytex 975/KL-5-2444	1.81	1.74
2258	49	Brilliant Yellow	1	Polytex 975/KL-5-2444	1.79	1.62
2261	49	Brilliant Yellow	1	Polytex 975/KL-5-2444	0.52	2.83
2262	49	Brilliant Yellow	1	Polytex 975/KL-5-2444	0.54	2.84
2269	49	SRB	1	Polytex 975/KL-5-2444	2.26	0.94
2270	49	SRB	1	Polytex 975/KL-5-2444	2.21	0.87
2273	49	SRB	1	Polytex 975/KL-5-2444	0.50	1.99

- 1) Area is cm<sup>2</sup>; dimensions (in cm) of various size plates are: 4.4 x 6.2 (27 cm<sup>2</sup>), 7.0 x 7.0 (49 cm<sup>2</sup>), 14.0 x 14.0 (196 cm<sup>2</sup>)
- 2) Peak absorbance
- 3) 59-D plate placed over sample
- 4) Metal mask placed over sample; 49 cm<sup>2</sup> surface left open

RELATIVE EDGE LUMINESCENCE ( $L_r$ )

Plate #	Area (cm <sup>2</sup> )	Dye	# Coats	Host	Abs. <sup>2</sup>	$L_r$
2274	49	SRB	1	Polytex 975/KL-5-2444	0.49	1.94
2281	49	R-101	1	Polytex 975/KL-5-2444	1.59	3.89
2282	49	R-101	1	Polytex 975/KL-5-2444	1.61	3.89
2285	49	R-101	1	Polytex 975/KL-5-2444	0.41	2.44
2286	49	R-101	1	Polytex 975/KL-5-2444	0.40	2.32
2293	49	Coumarin-6	1	Polytex 975/KL-5-2444	2.39	4.01
2294	49	Coumarin-6	1	Polytex 975/KL-5-2444	2.26	4.20
2297	49	Coumarin-6	1	Polytex 975/KL-5-2444	0.51	2.97
2298	49	Coumarin-6	1	Polytex 975/KL-5-2444	0.50	2.86
2305	49	Oxazine-725	1	Polytex 975/KL-5-2444	1.72	1.74
2306	49	Oxazine-725	1	Polytex 975/KL-5-2444	1.76	1.76
2309	49	Oxazine-725	1	Polytex 975/KL-5-2444	0.65	1.64
2310	49	Oxazine-725	1	Polytex 975/KL-5-2444	0.63	1.60
2317	49	Brilliant Yellow	1	At-400/Z-4370	2.05	1.50
2318	49	Brilliant Yellow	1	At-400/Z-4370	2.08	1.47
2321	49	Brilliant Yellow	1	At-400/Z-4370	0.43	2.14
2322	49	Brilliant Yellow	1	At-400/Z-4370	0.43	2.13
2339	49	SRB	1	At-400/Z-4370	1.73	0.69
2340	49	SRB	1	At-400/Z-4370	1.77	0.67
2343	49	SRB	1	At-400/Z-4370	0.47	1.93
2344	49	SRB	1	At-400/Z-4370	0.47	1.96
2351	49	R-101	1	At-400/Z-4370	1.67	3.85

- 1) Area is cm<sup>2</sup>; dimensions (in cm) of various size plates are: 4.4 x 6.2 (27 cm<sup>2</sup>), 7.0 x 7.0 (49 cm<sup>2</sup>), 14.0 x 14.0 (196 cm<sup>2</sup>)
- 2) Peak absorbance
- 3) 59-D plate placed over sample
- 4) Metal mask placed over sample; 49 cm<sup>2</sup> surface left open

RELATIVE EDGE LUMINESCENCE ( $L_r$ )

Plate #	Area (cm <sup>2</sup> )	Dye	# Coats	Host	Abs. <sup>2</sup>	$L_r$
2352	49	R-101	1	At-400/Z-4370	1.66	3.84
2355	49	R-101	1	At-400/Z-4370	0.52	2.51
2356	49	R-101	1	At-400/Z-4370	0.51	2.53
2363	49	Coumarin-6	1	At-400/Z-4370	1.77	3.70
2364	49	Coumarin-6	1	At-400/Z-4370	1.77	3.74
2367	49	Coumarin-6	1	At-400/Z-4370	0.46	2.78
2368	49	Coumarin-6	1	At-400/Z-4370	0.46	2.67
2375	49	Oxazine-725	1	At-400/Z-4370	1.96	1.46
2376	49	Oxazine-725	1	At-400/Z-4370	1.94	1.44
2379	49	Oxazine-725	1	At-400/Z-4370	0.42	1.24
2380	49	Oxazine-725	1	At-400/Z-4370	0.41	1.22
2387	49	Fluorescent Yellow 10GN	1	CAP. 504-0.2	1.03	2.89
2388	49	Fluorescent Yellow 10GN	1	CAP. 504-0.2	1.04	2.77
2395	49	Brilliant Orange	1	CAP. 504-0.2	1.00	2.46
2396	49	Brilliant Orange	1	CAP. 504-0.2	0.96	2.50
2403	49	Fluorol Green Gold 084	1	CAP. 504-0.2	0.72	2.05
2404	49	Fluorol Green Gold 084	1	CAP. 504-0.2	0.73	2.04
2411	49	Fluorol Yellow 088	1	CAP. 504-0.2	0.04	1.04
2412	49	Fluorol Yellow 088	1	CAP. 504-0.2	0.07	0.91
2419	49	Hostasol Red GG Hoeschr 13-3399	1	CAP. 504-0.2	0.66	2.01
2420	49	Hostasol Red GG Hoeschr 13-3399	1	CAP. 504-0.2	0.65	2.12
2427	49	ID-688	1	CAP. 504-0.2	0.81	4.16

- 1) Area is cm<sup>2</sup>; dimensions (in cm) of various size plates are: 4.4 x 6.2 (27 cm<sup>2</sup>), 7.0 x 7.0 (49 cm<sup>2</sup>), 14.0 x 14.0 (196 cm<sup>2</sup>)
- 2) Peak absorbance
- 3) 59-D plate placed over sample
- 4) Metal mask placed over sample; 49 cm<sup>2</sup> surface left open



RELATIVE EDGE LUMINESCENCE ( $L_T$ )

Plate #	Area (cm <sup>2</sup> )	Dye	# Coats	Host	Abs. <sup>2</sup>	$L_T$
2428	49	LD-688	1	CAP. 504-0.2	0.81	4.23
2435	49	Fluorol 555	1	CAP. 504-0.2	0.91	2.83
2436	49	Fluorol 555	1	CAP. 504-0.2	0.92	2.53
2443	49	Hoescht 11-5200 Hostasol Yellow 8-G	1	CAP. 504-0.2	1.27	3.00
2444	49	Hoescht 11-5200 Hostasol Yellow 8-G	1	CAP. 504-0.2	1.25	3.06
2451	49	Hoescht 11-5100 Hostasol Yellow 3-G	1	CAP. 504-0.2	0.62	1.25
2452	49	Hoescht 11-5100 Hostasol Yellow 3-G	1	CAP. 504-0.2	0.69	1.28
2459	49	LD-700	1	CAP. 504-0.2	1.07	1.67
2460	49	LD-700	1	CAP. 504-0.2	1.11	1.75
2467	49	LDS-730	1	CAP. 504-0.2	0.75	1.68
2468	49	LDS-730	1	CAP. 504-0.2	0.74	1.74
2475	49	LDS-750	1	CAP. 504-0.2	0.65	1.95
2476	49	LDS-750	1	CAP. 504-0.2	0.65	1.94
2483	49	LDS-751	1	CAP. 504-0.2	0.68	1.86
2484	49	LDS-751	1	CAP. 504-0.2	0.65	1.79
2491	49	LDS-798	1	CAP. 504-0.2	0.76	2.42
2492	49	LDS-798	1	CAP. 504-0.2	0.72	2.21
2499	49	LDS-820	1	CAP. 504-0.2	0.47	1.38
2500	49	LDS-820	1	CAP. 504-0.2	0.47	1.64
2646	49	Brilliant Yellow	1	Elvacite 2041	1.01	0.29
2647	49	Brilliant Yellow	1	Elvacite 2041	1.01	0.31
2654	49	Coumarin-6	1	Elvacite 2041	0.85	2.89

- 1) Area is cm<sup>2</sup>; dimensions (in cm) of various size plates are: 4.4 x 6.2 (27 cm<sup>2</sup>), 7.0 x 7.0 (49 cm<sup>2</sup>), 14.0 x 14.0 (196 cm<sup>2</sup>)
- 2) Peak absorbance
- 3) 59-D plate placed over sample
- 4) Metal mask placed over sample; 49 cm<sup>2</sup> surface left open

RELATIVE EDGE LUMINESCENCE ( $L_T$ )

Plate #	Area (cm <sup>2</sup> )	Dye	# Coats	Host	Abs. <sup>2</sup>	$L_T$
2655	49	Coumarin-6	1	Elvacite 2041	0.75	2.84
2662	49	Fluorol 555	1	Elvacite 2041	0.93	1.80
2663	49	Fluorol 555	1	Elvacite 2041	0.87	2.07
2670	49	Hostasol Yellow 8-G	1	Elvacite 2041	0.67	1.59
2671	49	Hostasol Yellow 8-G	1	Elvacite 2041	0.68	1.37
2678	49	R-101	1	Elvacite 2041	0.62	2.36
2679	49	R-101	1	Elvacite 2041	0.64	2.01
2686	49	SRB	1	Elvacite 2041	0.90	0.54
2687	49	SRB	1	Elvacite 2041	0.77	0.96
		Commercial		LISA		Sample Plates
	49	Mobay Red	(U)	Polycarbonate	2.36	4.62
	49	Mobay Yellow	(U)	Polycarbonate	1.23	3.42
	49	Mobay Green	(U)	Polycarbonate	2.03	1.86
2698A	49	LD-688	1	CAP. 504-0.2	0.56	3.13
2698B	49	LD-688	1	CAP. 504-0.2	0.56	3.20
2698C	49	LD-688	1	CAP. 504-0.2	0.59	2.83
2698D	49	LD-688	1	CAP. 504-0.2	0.58	2.74
2702A	49	LD-700	1	CAP. 504-0.2	1.34	1.95
2702B	49	LD-700	1	CAP. 504-0.2	1.43	1.91
2702C	49	LD-700	1	CAP. 504-0.2	1.37	1.83

- 1) Area is cm<sup>2</sup>; dimensions (in cm) of various size plates are: 4.4 x 6.2 (27 cm<sup>2</sup>), 7.0 x 7.0 (49 cm<sup>2</sup>), 14.0 x 14.0 (196 cm<sup>2</sup>)
- 2) Peak absorbance
- 3) 59-D plate placed over sample
- 4) Metal mask placed over sample; 49 cm<sup>2</sup> surface left open
- 5) (U)-Dye uniformly distributed throughout (2mm) thickness of plate

RELATIVE EDGE LUMINESCENCE ( $L_T$ )

Plate #	Area (cm <sup>2</sup> )	Dye	# Coats	Host	Abs. <sup>2</sup>	$L_T$
2702D	49	LD-700	1	CAP. 504-0.2	1.40	1.83
2706A	49	LDS-730	1	CAP. 504-0.2	0.91	1.66
2706B	49	LDS-730	1	CAP. 504-0.2	0.89	1.72
2706C	49	LDS-730	1	CAP. 504-0.2	0.90	1.47
2706D	49	LDS-730	1	CAP. 504-0.2	0.86	1.60
2710A	49	LDS-750	1	CAP. 504-0.2	0.74	1.50
2710B	49	LDS-750	1	CAP. 504-0.2	0.72	1.53
2710C	49	LDS-750	1	CAP. 504-0.2	0.69	1.47
2710D	49	LDS-750	1	CAP. 504-0.2	0.73	1.39
2714A	49	LDS-798	1	CAP. 504-0.2	0.74	1.95
2714B	49	LDS-798	1	CAP. 504-0.2	0.76	1.91
2714C	49	LDS-798	1	CAP. 504-0.2	0.75	1.77
2714D	49	LDS-798	1	CAP. 504-0.2	0.73	1.78
2718A	49	LD-688	1	CAB. 553-0.4	0.71	3.98
2718B	49	LD-688	1	CAB. 553-0.4	0.70	4.15
2718C	49	LD-688	1	CAB. 553-0.4	0.74	3.89
2718D	49	LD-688	1	CAB. 553-0.4	0.75	4.04
2722A	49	LD-700	1	CAB. 553-0.4	1.16	1.59
2722B	49	LD-700	1	CAB. 553-0.4	1.11	1.64
2722C	49	LD-700	1	CAB. 553-0.4	1.14	1.57
2722D	49	LD-700	1	CAB. 553-0.4	1.09	1.59
2726A	49	LDS-730	1	CAB. 553-0.4	1.06	1.30

- 1) Area is cm<sup>2</sup>; dimensions (in cm) of various size plates are: 4.4 x 6.2 (27 cm<sup>2</sup>), 7.0 x 7.0 (49 cm<sup>2</sup>), 14.0 x 14.0 (196 cm<sup>2</sup>)
- 2) Peak absorbance
- 3) 59-D plate placed over sample
- 4) Metal mask placed over sample; 49 cm<sup>2</sup> surface left open

RELATIVE EDGE LUMINESCENCE ( $L_T$ )

Plate #	Area (cm <sup>2</sup> )	Dye	# Coats	Host	Abs. <sup>2</sup>	$L_T$
2726B	49	LDS-730	1	CAB. 553-0.4	1.05	1.30
2726C	49	LDS-730	1	CAB. 553-0.4	1.05	1.30
2726D	49	LDS-730	1	CAB. 553-0.4	1.06	1.15
2730A	49	LDS-750	1	CAB. 553-0.4	0.74	1.43
2730B	49	LDS-750	1	CAB. 553-0.4	0.73	1.57
2730C	49	LDS-750	1	CAB. 553-0.4	0.73	1.47
2730D	49	LDS-750	1	CAB. 553-0.4	0.72	1.31
2734A	49	LDS-798	1	CAB. 553-0.4	0.71	2.22
2734B	49	LDS-798	1	CAB. 553-0.4	0.72	2.28
2734C	49	LDS-798	1	CAB. 553-0.4	0.72	2.13
2734D	49	LDS-798	1	CAB. 553-0.4	0.70	2.08
2738A	49	LD-688	1	CAP. 504-0.2/Cymel 303	0.67	3.74
2738B	49	LD-688	1	CAP. 504-0.2/Cymel 303	0.67	3.92
2738C	49	LD-688	1	CAP. 504-0.2/Cymel 303	0.68	3.54
2738D	49	LD-688	1	CAP. 504-0.2/Cymel 303	0.67	3.63
2742A	49	LD-700	1	CAP. 504-0.2/Cymel 303	0.74	1.47
2742B	49	LD-700	1	CAP. 504-0.2/Cymel 303	0.75	1.52
2742C	49	LD-700	1	CAP. 504-0.2/Cymel 303	0.74	1.46
2742D	49	LD-700	1	CAP. 504-0.2/Cymel 303	0.75	1.50
2746A	49	LDS-730	1	CAP. 504-0.2/Cymel 303	0.97	1.11
2746B	49	LDS-730	1	CAP. 504-0.2/Cymel 303	0.97	1.09
2746C	49	LDS-730	1	CAP. 504-0.2/Cymel 303	0.97	0.98

- 1) Area is cm<sup>2</sup>; dimensions (in cm) of various size plates are: 4.4 x 6.2 (27 cm<sup>2</sup>), 7.0 x 7.0 (49 cm<sup>2</sup>), 14.0 x 14.0 (196 cm<sup>2</sup>)
- 2) Peak absorbance
- 3) 59-D plate placed over sample
- 4) Metal mask placed over sample; 49 cm<sup>2</sup> surface left open

RELATIVE EDGE LUMINESCENCE ( $L_T$ )

Plate #	Area <sub>1</sub> (cm <sup>2</sup> )	Dye	# Coats	Host	Abs. <sup>2</sup>	$L_T$
2746D	49	LDS-730	1	CAP. 504-0.2/Cymel 303	0.97	1.01
2750A	49	LDS-750	1	CAP. 504-0.2/Cymel 303	0.97	0.52
2750B	49	LDS-750	1	CAP. 504-0.2/Cymel 303	0.99	0.53
2750C	49	LDS-750	1	CAP. 504-0.2/Cymel 303	1.02	0.54
2750D	49	LDS-750	1	CAP. 504-0.2/Cymel 303	0.99	0.55
2754A	49	LDS-798	1	CAP. 504-0.2/Cymel 303	0.85	2.19
2754B	49	LDS-798	1	CAP. 504-0.2/Cymel 303	0.88	2.24
2754C	49	LDS-798	1	CAP. 504-0.2/Cymel 303	0.85	2.32
2754D	49	LDS-798	1	CAP. 504-0.2/Cymel 303	0.85	2.20
2698	196	LD-688	1	CAP. 504-0.2	0.95	4.78
2698	196 <sup>3</sup>	LD-688	1	CAP. 504-0.2	0.95	0.75
2698	49 <sup>4</sup>	LD-688	1	CAP. 504-0.2	0.95	2.15
2699	196	LD-688	2	CAP. 504-0.2	1.30	7.09
2699	196 <sup>3</sup>	LD-688	2	CAP. 504-0.2	1.30	1.06
2699	49 <sup>4</sup>	LD-688	2	CAP. 504-0.2	1.30	3.04
2700	196	LD-688	4	CAP. 504-0.2	1.10	6.86
2700	196 <sup>3</sup>	LD-688	4	CAP. 504-0.2	1.10	1.10
2700	49 <sup>4</sup>	LD-688	4	CAP. 504-0.2	1.10	3.07
2702	196	LD-700	1	CAP. 504-0.2	1.10	2.74
2702	196 <sup>3</sup>	LD-700	1	CAP. 504-0.2	1.10	1.59
2702	49 <sup>4</sup>	LD-700	1	CAP. 504-0.2	1.10	1.24
2703	196	LD-700	2	CAP. 504-0.2	0.85	2.39

- 1) Area is cm<sup>2</sup>; dimensions (in cm) of various size plates are: 4.4 x 6.2 (27 cm<sup>2</sup>), 7.0 x 7.0 (49 cm<sup>2</sup>), 14.0 x 14.0 (196 cm<sup>2</sup>)
- 2) Peak absorbance
- 3) 59-D plate placed over sample
- 4) Metal mask placed over sample; 49 cm<sup>2</sup> surface left open

RELATIVE EDGE LUMINESCENCE ( $L_T$ )

Plate #	Area <sub>1</sub> (cm <sup>2</sup> )	Dye	# Coats	Host	Abs. <sup>2</sup>	$L_T$
2703	196 <sup>3</sup>	LD-700	2	CAP. 504-0.2	0.85	1.47
2703	49 <sup>4</sup>	LD-700	2	CAP. 504-0.2	0.85	1.09
2704	196	LD-700	4	CAP. 504-0.2	1.05	2.54
2704	196 <sup>3</sup>	LD-700	4	CAP. 504-0.2	1.05	1.50
2704	49 <sup>4</sup>	LD-700	4	CAP. 504-0.2	1.05	1.17
2706	196	LDS-730	1	CAP. 504-0.2	0.93	2.10
2706	196 <sup>3</sup>	LDS-730	1	CAP. 504-0.2	0.93	2.36
2706	49 <sup>4</sup>	LDS-730	1	CAP. 504-0.2	0.93	1.17
2707	196	LDS-730	2	CAP. 504-0.2	0.80	2.72
2707	196 <sup>3</sup>	LDS-730	2	CAP. 504-0.2	0.80	1.58
2707	49 <sup>4</sup>	LDS-730	2	CAP. 504-0.2	0.80	1.34
2708	196	LDS-730	4	CAP. 504-0.2	0.99	2.83
2708	196 <sup>3</sup>	LDS-730	4	CAP. 504-0.2	0.99	1.62
2708	49 <sup>4</sup>	LDS-730	4	CAP. 504-0.2	0.99	1.41
2710	196	LDS-750	1	CAP. 504-0.2	0.83	1.98
2710	196 <sup>3</sup>	LDS-750	1	CAP. 504-0.2	0.83	1.00
2710	49 <sup>4</sup>	LDS-750	1	CAP. 504-0.2	0.83	0.99
2711	196	LDS-750	2	CAP. 504-0.2	0.80	3.29
2711	196 <sup>3</sup>	LDS-750	2	CAP. 504-0.2	0.80	1.64
2711	49 <sup>4</sup>	LDS-750	2	CAP. 504-0.2	0.80	1.59
2712	196	LDS-750	4	CAP. 504-0.2	0.91	3.62
2712	196 <sup>3</sup>	LDS-750	4	CAP. 504-0.2	0.91	1.86

- 1) Area is cm<sup>2</sup>; dimensions (in cm) of various size plates are: 4.4 x 6.2 (27 cm<sup>2</sup>), 7.0 x 7.0 (49 cm<sup>2</sup>), 14.0 x 14.0 (196 cm<sup>2</sup>)
- 2) Peak absorbance
- 3) 59-D plate placed over sample
- 4) Metal mask placed over sample; 49 cm<sup>2</sup> surface left open

RELATIVE EDGE LUMINESCENCE ( $L_r$ )

Plate #	Area (cm <sup>2</sup> ) <sup>1</sup>	Dye	# Coats	Host	Abs. <sup>2</sup>	$L_r$
2712	49 <sup>4</sup>	LDS-750	4	CAP. 504-0.2	0.91	1.83
2714	196	LDS-798	1	CAP. 504-0.2	0.83	2.48
2714	196 <sup>3</sup>	LDS-798	1	CAP. 504-0.2	0.83	1.16
2714	49 <sup>4</sup>	LDS-798	1	CAP. 504-0.2	0.83	1.24
2715	196	LDS-798	2	CAP. 504-0.2	1.21	3.39
2715	196 <sup>3</sup>	LDS-798	2	CAP. 504-0.2	1.21	1.47
2715	49 <sup>4</sup>	LDS-798	2	CAP. 504-0.2	1.21	1.67
2716	196	LDS-798	4	CAP. 504-0.2	0.83	3.60
2716	196 <sup>3</sup>	LDS-798	4	CAP. 504-0.2	0.83	1.71
2716	49 <sup>4</sup>	LDS-798	4	CAP. 504-0.2	0.83	1.79
2718	196	LD-688	1	CAB. 553-0.4	0.86	6.31
2718	196 <sup>3</sup>	LD-688	1	CAB. 553-0.4	0.86	0.96
2718	49 <sup>4</sup>	LD-688	1	CAB. 553-0.4	0.86	2.67
2719	196	LD-688	2	CAB. 553-0.4	1.02	6.84
2719	196 <sup>3</sup>	LD-688	2	CAB. 553-0.4	1.02	0.89
2719	49 <sup>4</sup>	LD-688	2	CAB. 553-0.4	1.02	2.93
2720	196	LD-688	4	CAB. 553-0.4	1.06	6.41
2720	196 <sup>3</sup>	LD-688	4	CAB. 553-0.4	1.06	0.97
2720	49 <sup>4</sup>	LD-688	4	CAB. 553-0.4	1.06	1.00
2722	196	LD-700	1	CAB. 553-0.4	1.24	2.18
2722	196 <sup>3</sup>	LD-700	1	CAB. 553-0.4	1.24	1.36
2722	49 <sup>4</sup>	LD-700	1	CAB. 553-0.4	1.24	1.19

- 1) Area is cm<sup>2</sup>; dimensions (in cm) of various size plates are: 4.4 x 6.2 (27 cm<sup>2</sup>), 7.0 x 7.0 (49 cm<sup>2</sup>), 14.0 x 14.0 (196 cm<sup>2</sup>)
- 2) Peak absorbance
- 3) 59-D plate placed over sample
- 4) Metal mask placed over sample; 49 cm<sup>2</sup> surface left open

RELATIVE EDGE LUMINESCENCE ( $L_r$ )

Plate #	Area (cm <sup>2</sup> ) <sup>1</sup>	Dye	# Coats	Host	Abs. <sup>2</sup>	$L_r$
2723	196	LD-700	2	CAB. 553-0.4	1.10	2.72
2723	196 <sup>3</sup>	LD-700	2	CAB. 553-0.4	1.10	1.63
2723	49 <sup>4</sup>	LD-700	2	CAB. 553-0.4	1.10	1.25
2724	196	LD-700	4	CAB. 553-0.4	0.94	2.84
2724	196 <sup>3</sup>	LD-700	4	CAB. 553-0.4	0.94	1.69
2724	49 <sup>4</sup>	LD-700	4	CAB. 553-0.4	0.94	1.26
2726	196	LDS-730	1	CAB. 533-0.4	1.12	1.78
2726	196 <sup>3</sup>	LDS-730	1	CAB. 553-0.4	1.12	0.98
2726	49 <sup>4</sup>	LDS-730	1	CAB. 553-0.4	1.12	0.89
2727	196	LDS-730	2	CAB. 553-0.4	1.22	2.39
2727	196 <sup>3</sup>	LDS-730	2	CAB. 553-0.4	1.22	1.36
2727	49 <sup>4</sup>	LDS-730	2	CAB. 553-0.4	1.22	1.22
2728	196	LDS-730	4	CAB. 553-0.4	1.17	2.78
2728	196 <sup>3</sup>	LDS-730	4	CAB. 553-0.4	1.17	1.62
2728	49 <sup>4</sup>	LDS-730	4	CAB. 553-0.4	1.17	1.43
2730	196	LDS-750	1	CAB. 553-0.4	0.80	1.97
2730	196	LDS-750	1	CAB. 553-0.4	0.80	1.01
2730	49 <sup>4</sup>	LDS-750	1	CAB. 553-0.4	0.80	0.98
2731	196	LDS-750	2	CAB. 553-0.4	1.14	3.44
2731	196 <sup>3</sup>	LDS-750	2	CAB. 553-0.4	1.14	1.75
2731	49 <sup>4</sup>	LDS-750	2	CAB. 553-0.4	1.14	1.69
2732	169	LDS-750	4	CAB. 553-0.4	1.03	4.19

- 1) Area is cm<sup>2</sup>; dimensions (in cm) of various size plates are: 4.4 x 6.2 (27 cm<sup>2</sup>), 7.0 x 7.0 (49 cm<sup>2</sup>), 14.0 x 14.0 (196 cm<sup>2</sup>)
- 2) Peak absorbance
- 3) 59-D plate placed over sample
- 4) Metal mask placed over sample; 49 cm<sup>2</sup> surface left open

RELATIVE EDGE LUMINESCENCE ( $L_r$ )

Plate #	Area (cm <sup>2</sup> ) <sup>1</sup>	Dye	# Coats	Host	Abs. <sup>2</sup>	$L_r$
2732	196 <sup>3</sup>	LDS-750	4	CAB. 553-0.4	1.03	2.18
2732	49 <sup>4</sup>	LDS-750	4	CAB. 553-0.4	1.03	1.98
2734	196	LDS-798	1	CAB. 553-0.4	0.85	3.05
2734	196 <sup>3</sup>	LDS-798	1	CAB. 553-0.4	0.85	1.36
2734	49 <sup>4</sup>	LDS-798	1	CAB. 553-0.4	0.85	1.48
2735	196	LDS-798	2	CAB. 553-0.4	0.83	3.72
2735	196 <sup>3</sup>	LDS-798	2	CAB. 553-0.4	0.83	1.75
2735	49 <sup>4</sup>	LDS-798	2	CAB. 553-0.4	0.83	1.78
2736	196	LDS-798	4	CAB. 553-0.4	0.91	3.84
2736	196 <sup>3</sup>	LDS-798	4	CAB. 553-0.4	0.91	1.82
2736	49 <sup>4</sup>	LDS-798	4	CAB. 553-0.4	0.91	1.90
2738	196	LD-688	1	CAP. 504-0.2/Cymel 303	0.85	5.81
2738	196 <sup>3</sup>	LD-688	1	CAP. 504-0.2/Cymel 303	0.85	0.87
2738	49 <sup>4</sup>	LD-688	1	CAP. 504-0.2/Cymel 303	0.85	2.42
2739	196	LD-688	2	CAP. 504-0.2/Cymel 303	1.23	7.08
2739	196 <sup>3</sup>	LD-688	2	CAP. 504-0.2/Cymel 303	1.23	1.07
2739	49 <sup>4</sup>	LD-688	2	CAP. 504-0.2/Cymel 303	1.23	3.14
2740	196	LD-688	4	CAP. 504-0.2/Cymel 303	1.21	7.49
2740	196 <sup>3</sup>	LD-688	4	CAP. 504-0.2/Cymel 303	1.21	1.15
2740	49 <sup>4</sup>	LD-688	4	CAP. 504-0.2/Cymel 303	1.21	3.31
2742	196	LD-700	1	CAP. 504-0.2/Cymel 303	0.97	2.17
2742	196 <sup>3</sup>	LD-700	1	CAP. 504-0.2/Cymel 303	0.97	1.39

- 1) Area is cm<sup>2</sup>; dimensions (in cm) of various size plates are: 4.4 x 6.2 (27 cm<sup>2</sup>), 7.0 x 7.0 (49 cm<sup>2</sup>), 14.0 x 14.0 (196 cm<sup>2</sup>)
- 2) Peak absorbance
- 3) 59-D plate placed over sample
- 4) Metal mask placed over sample; 49 cm<sup>2</sup> surface left open

RELATIVE EDGE LUMINESCENCE ( $L_r$ )

Plate #	Area (cm <sup>2</sup> ) <sup>1</sup>	Dye	# Coats	Host	Abs. <sup>2</sup>	$L_r$
2742	49 <sup>4</sup>	LD-700	1	CAP. 504-0.2/Cymel 303	0.97	0.97
2743	196	LD-700	2	CAP. 504-0.2/Cymel 303	0.82	2.34
2743	196 <sup>3</sup>	LD-700	2	CAP. 504-0.2/Cymel 303	0.82	1.53
2743	49 <sup>4</sup>	LD-700	2	CAP. 504-0.2/Cymel 303	0.82	1.05
2744	196	LD-700	4	CAP. 504-0.2/Cymel 303	0.80	2.32
2744	196 <sup>3</sup>	LD-700	4	CAP. 504-0.2/Cymel 303	0.80	1.62
2744	49 <sup>4</sup>	LD-700	4	CAP. 504-0.2/Cymel 303	0.80	1.04
2746	196	LDS-730	1	CAP. 504-0.2/Cymel 303	1.04	1.14
2746	196 <sup>3</sup>	LDS-730	1	CAP. 504-0.2/Cymel 303	1.04	0.77
2746	49 <sup>4</sup>	LDS-730	1	CAP. 504-0.2/Cymel 303	1.04	0.69
2747	196	LDS-730	2	CAP. 504-0.2/Cymel 303	1.43	2.64
2747	196 <sup>3</sup>	LDS-730	2	CAP. 504-0.2/Cymel 303	1.43	1.46
2747	49 <sup>4</sup>	LDS-730	2	CAP. 504-0.2/Cymel 303	1.43	1.29
2748	196	LDS-730	4	CAP. 504-0.2/Cymel 303	1.17	3.01
2748	196 <sup>3</sup>	LDS-730	4	CAP. 504-0.2/Cymel 303	1.17	1.66
2748	49 <sup>4</sup>	LDS-730	4	CAP. 504-0.2/Cymel 303	1.17	1.47
2750	196	LDS-750	1	CAP. 504-0.2/Cymel 303	1.20	0.63
2750	196 <sup>3</sup>	LDS-750	1	CAP. 504-0.2/Cymel 303	1.20	0.35
2750	49 <sup>4</sup>	LDS-750	1	CAP. 504-0.2/Cymel 303	1.20	0.34
2751	196	LDS-750	2	CAP. 504-0.2/Cymel 303	1.13	1.77
2751	196 <sup>3</sup>	LDS-750	2	CAP. 504-0.2/Cymel 303	1.13	0.95
2751	49 <sup>4</sup>	LDS-750	2	CAP. 504-0.2/Cymel 303	1.13	0.89

- 1) Area is cm<sup>2</sup>; dimensions (in cm) of various size plates are: 4.4 x 6.2 (27 cm<sup>2</sup>), 7.0 x 7.0 (49 cm<sup>2</sup>), 14.0 x 14.0 (196 cm<sup>2</sup>)
- 2) Peak absorbance
- 3) 59-D plate placed over sample
- 4) Metal mask placed over sample; 49 cm<sup>2</sup> surface left open

RELATIVE EDGE LUMINESCENCE ( $L_r$ )

Plate #	Area (cm <sup>2</sup> )	Dye	# Coats	Host	Abs. <sup>2</sup>	$L_r$
2752	196	LDS-750	4	CAP. 504-0.2/Cymel 303	1.24	3.07
2752	196 <sup>3</sup>	LDS-750	4	CAP. 504-0.2/Cymel 303	1.24	1.57
2752	49 <sup>4</sup>	LDS-750	4	CAP. 504-0.2/Cymel 303	1.24	1.54
2754	196	LDS-798	1	CAP. 504-0.2/Cymel 303	0.93	3.05
2754	196 <sup>3</sup>	LDS-798	1	CAP. 504-0.2/Cymel 303	0.93	1.38
2754	49 <sup>4</sup>	LDS-798	1	CAP. 504-0.2/Cymel 303	0.93	1.42
2755	196	LDS-798	2	CAP. 504-0.2/Cymel 303	1.24	3.07
2755	196 <sup>3</sup>	LDS-798	2	CAP. 504-0.2/Cymel 303	1.24	1.42
2755	49 <sup>4</sup>	LDS-798	2	CAP. 504-0.2/Cymel 303	1.24	1.48
2756	196	LDS-798	4	CAP. 504-0.2/Cymel 303	0.85	3.83
2756	196 <sup>3</sup>	LDS-798	4	CAP. 504-0.2/Cymel 303	0.85	1.80
2756	49 <sup>4</sup>	LDS-798	4	CAP. 504-0.2/Cymel 303	0.85	1.80
2758	196	LD-688	1	Elvacite 2010	1.10	6.02
2758	196 <sup>3</sup>	LD-688	1	Elvacite 2010	1.10	0.93
2758	49 <sup>4</sup>	LD-688	1	Elvacite 2010	1.10	2.64
2759	196	LD-688	2	Elvacite 2010	0.95	5.36
2759	196 <sup>3</sup>	LD-688	2	Elvacite 2010	0.95	0.80
2759	49 <sup>4</sup>	LD-688	2	Elvacite 2010	0.95	2.47
2760	196	LD-688	4	Elvacite 2010	1.23	3.74
2760	196 <sup>3</sup>	LD-688	4	Elvacite 2010	1.23	1.03
2760	49 <sup>4</sup>	LD-688	4	Elvacite 2010	1.23	2.07

- 1) Area is cm<sup>2</sup>; dimensions (in cm) of various size plates are: 4.4 x 6.2 (27 cm<sup>2</sup>), 7.0 x 7.0 (49 cm<sup>2</sup>), 14.0 x 14.0 (196 cm<sup>2</sup>)
- 2) Peak absorbance
- 3) 59-D plate placed over sample
- 4) Metal mask placed over sample; 49 cm<sup>2</sup> surface left open

RELATIVE EDGE LUMINESCENCE ( $L_r$ )

Plate #	Area (cm <sup>2</sup> )	Dye	# Coats	Host	Abs. <sup>2</sup>	$L_r$
2762	196	LD-700	1	Elvacite 2010	0.80	1.94
2762	196 <sup>3</sup>	LD-700	1	Elvacite 2010	0.80	1.24
2762	49 <sup>4</sup>	LD-700	1	Elvacite 2010	0.80	0.77
2763	196	LD-700	2	Elvacite 2010	1.21	1.97
2763	196 <sup>3</sup>	LD-700	2	Elvacite 2010	1.21	1.18
2763	49 <sup>4</sup>	LD-700	2	Elvacite 2010	1.21	0.81
2764	196	LD-700	4	Elvacite 2010	1.10	2.60
2764	196 <sup>3</sup>	LD-700	4	Elvacite 2010	1.10	1.63
2764	49 <sup>4</sup>	LD-700	4	Elvacite 2010	1.10	1.14
2766	196	LDS-730	1	Elvacite 2010	1.30	1.59
2766	196 <sup>3</sup>	LDS-730	1	Elvacite 2010	1.30	0.89
2766	49 <sup>4</sup>	LDS-730	1	Elvacite 2010	1.30	0.77
2767	196	LDS-730	2	Elvacite 2010	0.87	2.50
2767	196 <sup>3</sup>	LDS-730	2	Elvacite 2010	0.87	1.49
2767	49 <sup>4</sup>	LDS-730	2	Elvacite 2010	0.87	1.24
2768	196	LDS-730	4	Elvacite 2010	1.18	2.93
2768	196 <sup>3</sup>	LDS-730	4	Elvacite 2010	1.18	1.69
2768	49 <sup>4</sup>	LDS-730	4	Elvacite 2010	1.18	1.38
2770	196	LDS-750	1	Elvacite 2010	1.28	0.29
2770	196 <sup>3</sup>	LDS-750	1	Elvacite 2010	1.28	0.16
2770	49 <sup>4</sup>	LD -750	1	Elvacite 2010	1.28	0.15

- 1) Area is cm<sup>2</sup>; dimensions (in cm) of various size plates are: 4.4 x 6.2 (27 cm<sup>2</sup>), 7.0 x 7.0 (49 cm<sup>2</sup>), 14.0 x 14.0 (196 cm<sup>2</sup>)
- 2) Peak absorbance
- 3) 59-D plate placed over sample
- 4) Metal mask placed over sample; 49 cm<sup>2</sup> surface left open

RELATIVE EDGE LUMINESCENCE ( $L_r$ )

Plate #	Area (cm <sup>2</sup> )	Dye	# Coats	Host	Abs. <sup>2</sup>	$L_r$
2766	49	LDS-730	1	Elvacite 2010	1.24	1.29
2766N	49	LDS-730	1	Elvacite 2010	1.23	1.31
2767	49	LDS-730	2	Elvacite 2010	0.78	1.85
2767N	49	LDS-730	2	Elvacite 2010	0.80	1.76
2768	49	LDS-730	4	Elvacite 2010	1.10	1.90
2768N	49	LDS-730	4	Elvacite 2010	1.12	1.91
2770	49	LDS-750	1	Elvacite 2010	1.13	0.24
2770N	49	LDS-750	1	Elvacite 2010	1.14	0.27
2771	49	LDS-750	2	Elvacite 2010	0.96	1.13
2771N	49	LDS-750	2	Elvacite 2010	0.92	1.05
2772	49	LDS-750	4	Elvacite 2010	0.85	1.39
2772N	49	LDS-750	4	Elvacite 2010	0.82	1.50
2774	49	LDS-798	1	Elvacite 2010	0.79	1.56
2774N	49	LDS-798	1	Elvacite 2010	0.79	1.81
2775	49	LDS-798	2	Elvacite 2010	0.75	2.10
2775N	49	LDS-798	2	Elvacite 2010	0.73	2.12
2776	49	LDS-798	4	Elvacite 2010	0.90	2.68
2776N	49	LDS-798	4	Elvacite 2010	0.91	2.60
2778	49	LD-688	1	Polytex 975/KL-5-2444	0.83	4.01
2778N	49	LD-688	1	Polytex 975/KL-5-2444	0.82	3.84
2779	49	LD-688	2	Polytex 975/KL-5-2444	0.90	3.87
2779N	49	LD-688	2	Polytex 975/KL-5-2444	0.87	3.68

- 1) Area is cm<sup>2</sup>; dimensions (in cm) of various size plates are: 4.4 x 6.2 (27 cm<sup>2</sup>), 7.0 x 7.0 (49 cm<sup>2</sup>), 14.0 x 14.0 (196 cm<sup>2</sup>)
- 2) Peak absorbance
- 3) 59-D plate placed over sample
- 4) Metal mask placed over sample; 49 cm<sup>2</sup> surface left open

RELATIVE EDGE LUMINESCENCE ( $L_r$ )

Plate #	Area (cm <sup>2</sup> )	Dye	# Coats	Host	Abs. <sup>2</sup>	$L_r$
2780	49	LD-688	4	Polytex 975/KL-5-2444	0.88	3.37
2780N	49	LD-688	4	Polytex 975/KL-5-2444	0.88	3.38
2782	49	LD-700	1	Polytex 975/KL-5-2444	1.00	1.75
2782N	49	LD-700	1	Polytex 975/KL-5-2444	1.03	1.58
2783	49	LD-700	2	Polytex 975/KL-5-2444	0.93	1.71
2783N	49	LD-700	2	Polytex 975/KL-5-2444	0.92	1.64
2784	49	LD-700	4	Polytex 975/KL-5-2444	0.98	1.83
2784N	49	LD-700	4	Polytex 975/KL-5-2444	0.99	1.72
2786	49	LDS-730	1	Polytex 975/KL-5-2444	1.19	2.00
2786N	49	LDS-730	1	Polytex 975/KL-5-2444	1.18	2.18
2787	49	LDS-730	2	Polytex 975/KL-5-2444	1.04	1.80
2787N	49	LDS-730	2	Polytex 975/KL-5-2444	1.04	2.08
2788	49	LDS-730	4	Polytex 975/KL-5-2444	0.83	1.72
2788N	49	LDS-730	4	Polytex 975/KL-5-2444	0.82	1.33
2790	49	LDS-750	1	Polytex 975/KL-5-2444	0.92	1.28
2790N	49	LDS-750	1	Polytex 975/KL-5-2444	0.94	1.38
2791	49	LDS-750	2	Polytex 975/KL-5-2444	0.87	2.02
2791N	49	LDS-750	2	Polytex 975/KL-5-2444	0.84	2.05
2792	49	LDS-750	4	Polytex 975/KL-5-2444	1.06	2.31
2792N	49	LDS-750	4	Polytex 975/KL-5-2444	1.07	2.41
2794	49	LDS-798	1	Polytex 975/KL-5-2444	0.97	2.06
2794N	49	LDS-798	1	Polytex 975/KL-5-2444	0.93	2.14

- 1) Area is cm<sup>2</sup>; dimensions (in cm) of various size plates are: 4.4 x 6.2 (27 cm<sup>2</sup>), 7.0 x 7.0 (49 cm<sup>2</sup>), 14.0 x 14.0 (196 cm<sup>2</sup>)
- 2) Peak absorbance
- 3) 59-D plate placed over sample
- 4) Metal mask placed over sample; 49 cm<sup>2</sup> surface left open

RELATIVE EDGE LUMINESCENCE ( $L_r$ )

Plate #	Area (cm <sup>2</sup> )	Dye	# Coats	Host	Abs. <sup>2</sup>	$L_r$
2771	196	LDS-750	2	Elvacite 2010	1.09	1.49
2771	196 <sup>3</sup>	LDS-750	2	Elvacite 2010	1.09	0.77
2771	49 <sup>4</sup>	LDS-750	2	Elvacite 2010	1.09	0.76
2772	196	LDS-750	4	Elvacite 2010	0.94	2.03
2772	196 <sup>3</sup>	LDS-750	4	Elvacite 2010	0.94	1.07
2772	49 <sup>4</sup>	LDS-750	4	Elvacite 2010	0.94	1.22
2774	196	LDS-798	1	Elvacite 2010	0.86	2.67
2774	196 <sup>3</sup>	LDS-798	1	Elvacite 2010	0.86	1.22
2774	49 <sup>4</sup>	LDS-798	1	Elvacite 2010	0.86	1.22
2775	196	LDS-798	2	Elvacite 2010	0.79	3.15
2775	196 <sup>3</sup>	LDS-798	2	Elvacite 2010	0.79	1.41
2775	49 <sup>4</sup>	LDS-798	2	Elvacite 2010	0.79	1.49
2776	196	LDS-798	4	Elvacite 2010	0.99	3.77
2776	196 <sup>3</sup>	LDS-798	4	Elvacite 2010	0.99	1.71
2776	49 <sup>4</sup>	LDS-798	4	Elvacite 2010	0.99	1.49
2778	196	LD-688	1	Polytex 975/KL-5-2444	0.91	5.85
2778	196 <sup>3</sup>	LD-688	1	Polytex 975/KL-5-2444	0.91	0.93
2778	49 <sup>4</sup>	LD-688	1	Polytex 975/KL-5-2444	0.91	2.62
2779	196	LD-688	2	Polytex 975/KL-5-2444	0.96	5.77
2779	196 <sup>3</sup>	LD-688	2	Polytex 975/KL-5-2444	0.96	0.93
2779	49 <sup>4</sup>	LD-688	2	Polytex 975/KL-5-2444	0.96	2.60
2780	196	LD-688	4	Polytex 975/KL-5-2444	0.92	6.40

- 1) Area is cm<sup>2</sup>; dimensions (in cm) of various size plates are: 4.4 x 6.2 (27 cm<sup>2</sup>), 7.0 x 7.0 (49 cm<sup>2</sup>), 14.0 x 14.0 (196 cm<sup>2</sup>)
- 2) Peak absorbance
- 3) 59-D plate placed over sample
- 4) Metal mask placed over sample; 49 cm<sup>2</sup> surface left open

RELATIVE EDGE LUMINESCENCE ( $L_r$ )

Plate #	Area (cm <sup>2</sup> )	Dye	# Coats	Host	Abs. <sup>2</sup>	$L_r$
2780	196 <sup>3</sup>	LD-688	4	Polytex 975/KL-5-2444	0.92	1.04
2780	49 <sup>4</sup>	LD-688	4	Polytex 975/KL-5-2444	0.92	2.62
2782	196	LD-700	1	Polytex 975/KL-5-2444	1.04	2.56
2782	196 <sup>3</sup>	LD-700	1	Polytex 975/KL-5-2444	1.04	1.57
2782	49 <sup>4</sup>	LD-700	1	Polytex 975/KL-5-2444	1.04	1.23
2783	196	LD-700	2	Polytex 975/KL-5-2444	1.02	2.78
2783	196 <sup>3</sup>	LD-700	2	Polytex 975/KL-5-2444	1.02	1.69
2783	49 <sup>4</sup>	LD-700	2	Polytex 975/KL-5-2444	1.02	1.23
2784	196	LD-700	4	Polytex 975/KL-5-2444	1.04	2.80
2784	196 <sup>3</sup>	LD-700	4	Polytex 975/KL-5-2444	1.04	1.70
2784	49 <sup>4</sup>	LD-700	4	Polytex 975/KL-5-2444	1.04	1.26
2786	196	LDS-730	1	Polytex 975/KL-5-2444	1.24	2.95
2786	196 <sup>3</sup>	LDS-730	1	Polytex 975/KL-5-2444	1.24	1.71
2786	49 <sup>4</sup>	LDS-730	1	Polytex 975/KL-5-2444	1.24	1.39
2787	196	LDS-730	2	Polytex 975/KL-5-2444	1.09	3.22
2787	196 <sup>3</sup>	LDS-730	2	Polytex 975/KL-5-2444	1.09	1.89
2787	49 <sup>4</sup>	LDS-730	2	Polytex 975/KL-5-2444	1.09	1.49
2788	196	LDS-730	4	Polytex 975/KL-5-2444	0.84	3.07
2788	196 <sup>3</sup>	LDS-730	4	Polytex 975/KL-5-2444	0.84	1.92
2788	49 <sup>4</sup>	LDS-730	4	Polytex 975/KL-5-2444	0.84	1.44
2790	196	LDS-750	1	Polytex 975/KL-5-2444	0.95	1.77

- 1) Area is cm<sup>2</sup>; dimensions (in cm) of various size plates are: 4.4 x 6.2 (27 cm<sup>2</sup>), 7.0 x 7.0 (49 cm<sup>2</sup>), 14.0 x 14.0 (196 cm<sup>2</sup>)
- 2) Peak absorbance
- 3) 59-D plate placed over sample
- 4) Metal mask placed over sample; 49 cm<sup>2</sup> surface left open



RELATIVE EDGE LUMINESCENCE ( $L_T$ )

Plate #	Area (cm <sup>2</sup> )	Dye	# Coats	Host	Abs. <sup>2</sup>	$L_T$
2795	49	LDS-798	2	Polytex 975/KL-5-2444	1.06	2.17
2795N	49	LDS-798	2	Polytex 975/KL-5-2444	1.01	2.12
2796	49	LDS-798	4	Polytex 975/KL-5-2444	0.99	2.14
2796N	49	LDS-798	4	Polytex 975/KL-5-2444	0.99	2.13
2798	49	Eastman DTTC	1	CAP. 504-0.2	0.02	0.21
2798N	49	Eastman DTTC	1	CAP. 504-0.2	0.02	0.21
2800	49	Eastman DTDC	1	CAP. 504-0.2	0.04	0.31
2800N	49	Eastman DTDC	1	CAP. 504-0.2	0.05	0.37
2802	49	Eastman DODC	1	CAP. 504-0.2	0.19	0.62
2802N	49	Eastman DODC	1	CAP. 504-0.2	0.26	0.84
2804	49	Exciton DOTC	1	CAP. 504-0.2	0.12	0.59
2804N	49	Exciton DOTC	1	CAP. 504-0.2	0.08	0.52
2806	49	Hostasol Yellow 8-G	1	CAP. 504-0.2	0.10	2.79
2806N	49	Hostasol Yellow 8-G	1	CAP. 504-0.2	0.09	2.34
2808	49	Acridine Red	1	CAP. 504-0.2	1.11	2.57
2808N	49	Acridine Red	1	CAP. 504-0.2	1.12	2.47
2812	49	Eastman DTTC	1	CAB. 553-0.4	0.27	0.10
2812N	49	Eastman DTTC	1	CAB. 553-0.4	0.28	0.09
2814	49	Eastman DTTC	1	CAB. 553-0.4	0.08	0.30
2814N	49	Eastman DTDC	1	CAB. 553-0.4	0.07	0.29
2816	49	Exciton DODC	1	CAB. 553-0.4	0.00	0.44
2816N	49	Exciton DODC	1	CAB. 553-0.4	0.01	0.35

- 1) Area is cm<sup>2</sup>; dimensions (in cm) of various size plates are: 4.4 x 6.2 (27 cm<sup>2</sup>), 7.0 x 7.0 (49 cm<sup>2</sup>), 14.0 x 14.0 (196 cm<sup>2</sup>)
- 2) Peak absorbance
- 3) 59-D plate placed over sample
- 4) Metal mask placed over sample; 49 cm<sup>2</sup> surface left open

RELATIVE EDGE LUMINESCENCE ( $L_T$ )

Plate #	Area (cm <sup>2</sup> )	Dye	# Coats	Host	Abs. <sup>2</sup>	$L_T$
2818	49	Exciton DOTC	1	CAB. 553-0.4	0.11	0.47
2818N	49	Exciton DOTC	1	CAB. 553-0.4	0.12	0.49
2820	49	Hostasol Yellow 8-G	1	CAB. 553-0.4	1.30	2.69
2820N	49	Hostasol Yellow 8-G	1	CAB. 553-0.4	1.30	2.75
2822	49	Acridine Red	1	CAB. 553-0.4	0.75	2.30
2822N	49	Acridine Red	1	CAB. 553-0.4	0.72	2.26
2824	49	SRB	1	CAB. 553-0.4	1.24	2.44
2824N	49	SRB	1	CAB. 553-0.4	1.10	2.25
2827	49	Brilliant Orange	1	CAB. 553-0.4	0.61	1.82
2827N	49	Brilliant Orange	1	CAB. 553-0.4	0.67	1.80
2829	49	Eastman DTTC	1	Elvacite 2010	0.12	0.11
2829N	49	Eastman DTTC	1	Elvacite 2010	0.11	0.11
2831	49	Eastman DTDC	1	Elvacite 2010	0.04	0.28
2831N	49	Eastman DTDC	1	Elvacite 2010	0.03	0.24
2833	49	Exciton DODC	1	Elvacite 2010	0.36	0.59
2833N	49	Exciton DODC	1	Elvacite 2010	0.34	0.59
2835	49	Exciton DOTC	1	Elvacite 2010	0.38	0.94
2835N	49	Exciton DOTC	1	Elvacite 2010	0.34	0.87
2837	49	Hostasol Yellow 8-G	1	Elvacite 2010	0.90	2.22
2837N	49	Hostasol Yellow 8-G	1	Elvacite 2010	0.89	2.61
2839	49	Acridine Red	1	Elvacite 2010	0.94	2.39
2839N	49	Acridine Red	1	Elvacite 2010	0.96	2.21

- 1) Area is cm<sup>2</sup>; dimensions (in cm) of various size plates are: 4.4 x 6.2 (27 cm<sup>2</sup>), 7.0 x 7.0 (49 cm<sup>2</sup>), 14.0 x 14.0 (196 cm<sup>2</sup>)
- 2) Peak absorbance
- 3) 59-D plate placed over sample
- 4) Metal mask placed over sample; 49 cm<sup>2</sup> surface left open

RELATIVE EDGE LUMINESCENCE ( $L_r$ )

Plate #	Area (cm <sup>2</sup> )	Dye	# Coats	Host	Abs. <sup>2</sup>	$L_r$
2790	196 <sup>3</sup>	LDS-750	1	Polytex 975/KL-5-2444	0.95	1.04
2790	49 <sup>4</sup>	LDS-750	1	Polytex 975/KL-5-2444	0.95	0.87
2791	196	LDS-750	2	Polytex 975/KL-5-2444	0.92	2.88
2791	196 <sup>3</sup>	LDS-750	2	Polytex 975/KL-5-2444	0.92	1.61
2791	49 <sup>4</sup>	LDS-750	2	Polytex 975/KL-5-2444	0.92	1.38
2792	196	LDS-750	4	Polytex 975/KL-5-2444	1.14	3.52
2792	196 <sup>3</sup>	LDS-750	4	Polytex 975/KL-5-2444	1.14	1.98
2792	49 <sup>4</sup>	LDS-750	4	Polytex 975/KL-5-2444	1.14	1.73
2794	196	LDS-798	1	Polytex 975/KL-5-2444	1.07	3.35
2794	196 <sup>3</sup>	LDS-798	1	Polytex 975/KL-5-2444	1.07	1.73
2794	49 <sup>4</sup>	LDS-798	1	Polytex 975/KL-5-2444	1.07	1.62
2795	196	LDS-798	2	Polytex 975/KL-5-2444	1.06	3.32
2795	196 <sup>3</sup>	LDS-798	2	Polytex 975/KL-5-2444	1.06	1.75
2795	49 <sup>4</sup>	LDS-798	2	Polytex 975/KL-5-2444	1.06	1.67
2796	196	LDS-798	4	Polytex 975/KL-5-2444	1.04	3.39
2796	196 <sup>3</sup>	LDS-798	4	Polytex 975/KL-5-2444	1.04	1.78
2796	49 <sup>4</sup>	LDS-798	4	Polytex 975/KL-5-2444	1.04	1.69
2798	196	Eastman DTTC	1	CAP. 504-0.2	0.16	0.47
2798	196 <sup>3</sup>	Eastman DTTC	1	CAP. 504-0.2	0.16	0.40
2798	49 <sup>4</sup>	Eastman DTTC	1	CAP. 504-0.2	0.16	0.22
2800	196	Eastman DTDC	1	CAP. 504-0.2	0.20	1.26

- 1) Area is cm<sup>2</sup>; dimensions (in cm) of various size plates are: 4.4 x 6.2 (27 cm<sup>2</sup>), 7.0 x 7.0 (49 cm<sup>2</sup>), 14.0 x 14.0 (196 cm<sup>2</sup>)
- 2) Peak absorbance
- 3) 59-D plate placed over sample
- 4) Metal mask placed over sample; 49 cm<sup>2</sup> surface left open

RELATIVE EDGE LUMINESCENCE ( $L_r$ )

Plate #	Area (cm <sup>2</sup> )	Dye	# Coats	Host	Abs. <sup>2</sup>	$L_r$
2800	196 <sup>3</sup>	Eastman DTDC	1	CAP. 504-0.2	0.20	1.06
2800	49 <sup>4</sup>	Eastman DTDC	1	CAP. 504-0.2	0.20	0.53
2802	196	Eastman DODC	1	CAP. 504-0.2	0.51	1.55
2802	196 <sup>3</sup>	Eastman DODC	1	CAP. 504-0.2	0.51	0.42
2802	49 <sup>4</sup>	Eastman DODC	1	CAP. 504-0.2	0.51	0.74
2804	196	Exciton DOTC	1	CAP. 504-0.2	0.50	1.40
2804	196 <sup>3</sup>	Exciton DOTC	1	CAP. 504-0.2	0.50	1.22
2804	49 <sup>4</sup>	Exciton DPTC	1	CAP. 504-0.2	0.50	0.67
2806	196	Hostasol Yellow 8-G	1	CAP. 504-0.2	0.81	4.53
2806	196 <sup>3</sup>	Hostasol Yellow 8-G	1	CAP. 504-0.2	0.81	0.35
2806	49 <sup>4</sup>	Hostasol Yellow 8-G	1	CAP. 504-0.2	0.81	1.82
2808	196	Eastman Acridine Red	1	CAP. 504-0.2	1.18	3.84
2808	196 <sup>3</sup>	Eastman Acridine Red	1	CAP. 504-0.2	1.18	0.65
2808	49 <sup>4</sup>	Eastman Acridine Red	1	CAP. 504-0.2	1.18	1.64
2812	196	Eastman DTTC	1	CAB. 553-0.4	0.61	0.09
2812	196 <sup>3</sup>	Eastman DTTC	1	CAB. 553-0.4	0.61	0.06
2812	49 <sup>4</sup>	Eastman DTTC	1	CAB. 553-0.4	0.61	0.05
2814	196	Eastman DTDC	1	CAB. 553-0.4	0.40	0.71
2814	196 <sup>3</sup>	Eastman DTDC	1	CAB. 553-0.4	0.40	0.61
2814	49 <sup>4</sup>	Eastman DTDC	1	CAB. 553-0.4	0.40	0.31
2816	196	Exciton DODC	1	CAB. 553-0.4	0.50	0.94

- 1) Area is cm<sup>2</sup>; dimensions (in cm) of various size plates are: 4.4 x 6.2 (27 cm<sup>2</sup>), 7.0 x 7.0 (49 cm<sup>2</sup>), 14.0 x 14.0 (196 cm<sup>2</sup>)
- 2) Peak absorbance
- 3) 59-D plate placed over sample
- 4) Metal mask placed over sample; 49 cm<sup>2</sup> surface left open

RELATIVE EDGE LUMINESCENCE ( $L_T$ )

Plate #	Area (cm <sup>2</sup> ) <sup>1</sup>	Dye	# Coats	Host	Abs. <sup>2</sup>	$L_T$
2816	196 <sup>3</sup>	Exciton DODC	1	CAB. 553-0.4	0.50	0.29
2816	49 <sup>4</sup>	Exciton DODC	1	CAB. 553-0.4	0.50	0.41
2818	196	Exciton DOTC	1	CAB. 553-0.4	0.51	1.09
2818	196 <sup>3</sup>	Exciton DOTC	1	CAB. 553-0.4	0.51	0.92
2818	49 <sup>4</sup>	Exciton DOTC	1	CAB. 553-0.4	0.51	0.58
2820	196	Hostasol Yellow 8-G	1	CAB. 553-0.4	1.30	4.04
2820	196 <sup>3</sup>	Hostasol Yellow 8-G	1	CAB. 553-0.4	1.30	0.39
2820	49 <sup>4</sup>	Hostasol Yellow 8-G	1	CAB. 553-0.4	1.30	1.74
2822	196	Eastman Acridine Red	1	CAB. 553-0.4	0.77	3.66
2822	196 <sup>3</sup>	Eastman Acridine Red	1	CAB. 553-0.4	0.77	0.64
2822	49 <sup>4</sup>	Eastman Acridine	1	CAB. 553-0.4	0.77	1.50
2824	196	SRB	1	CAB. 553-0.4	1.20	3.52
2824	196 <sup>3</sup>	SRB	1	CAB. 553-0.4	1.20	0.58
2824	49 <sup>4</sup>	SRB	1	CAB. 553-0.4	1.20	1.52
2827	196	Brilliant Orange	1	CAB. 553-0.4	0.71	2.63
2827	196 <sup>3</sup>	Brilliant Orange	1	CAB. 553-0.4	0.71	0.44
2827	49 <sup>4</sup>	Brilliant Orange	1	CAB. 553-0.4	0.71	1.13
2829	196	Eastman DTTC	1	Elvacite 2010	0.52	0.11
2829	196 <sup>3</sup>	Eastman DTTC	1	Elvacite 2010	0.52	0.08
2829	49 <sup>4</sup>	Eastman DTTC	1	Elvacite 2010	0.52	0.06
2831	196	Eastman DTDC	1	Elvacite 2010	0.24	1.00

- 1) Area is cm<sup>2</sup>; dimensions (in cm) of various size plates are: 4.4 x 6.2 (27 cm<sup>2</sup>), 7.0 x 7.0 (49 cm<sup>2</sup>), 14.0 x 14.0 (196 cm<sup>2</sup>)
- 2) Peak absorbance
- 3) 59-D plate placed over sample
- 4) Metal mask placed over sample; 49 cm<sup>2</sup> surface left open

RELATIVE EDGE LUMINESCENCE ( $L_T$ )

Plate #	Area (cm <sup>2</sup> ) <sup>1</sup>	Dye	# Coats	Host	Abs. <sup>2</sup>	$L_T$
2831	196 <sup>3</sup>	Eastman DTDC	1	Elvacite 2010	0.24	0.77
2831	49 <sup>4</sup>	Eastman DTDC	1	Elvacite 2010	0.24	0.49
2833	196	Exciton DODC	1	Elvacite 2010	0.82	1.45
2833	196 <sup>3</sup>	Exciton DODC	1	Elvacite 2010	0.82	0.47
2833	49 <sup>4</sup>	Exciton DODC	1	Elvacite 2010	0.82	0.65
2835	196	Exciton DOTC	1	Elvacite 2010	0.99	1.56
2835	196 <sup>3</sup>	Exciton DOTC	1	Elvacite 2010	0.99	1.26
2835	49 <sup>4</sup>	Exciton DOTC	1	Elvacite 2010	0.99	0.77
2837	196	Hostasol Yellow 8-G	1	Elvacite 2010	0.94	2.74
2837	196 <sup>3</sup>	Hostasol Yellow 8-G	1	Elvacite 2010	0.94	0.39
2837	49 <sup>4</sup>	Hostasol Yellow 8-G	1	Elvacite 2010	0.94	1.30
2839	196	Eastman Acridine Red	1	Elvacite 2010	0.96	3.48
2839	196 <sup>3</sup>	Eastman Acridine Red	1	Elvacite 2010	0.96	0.59
2839	49 <sup>4</sup>	Eastman Acridine Red	1	Elvacite 2010	0.96	1.48
2843	196	Eastman DTTC	1	CAP. 504-0.2/Cymel 303	0.34	0.42
2843	196 <sup>3</sup>	Eastman DTTC	1	CAP. 504-0.2/Cymel 303	0.34	0.37
2843	49 <sup>4</sup>	Eastman DTTC	1	CAP. 504-0.2/Cymel 303	0.34	0.22
2845	196	Eastman DTDC	1	CAP. 504-0.2/Cymel 303	0.23	1.22
2845	196 <sup>3</sup>	Eastman DTDC	1	CAP. 504-0.2/Cymel 303	0.23	1.05
2845	49 <sup>4</sup>	Eastman DTDC	1	CAP. 504-0.2/Cymel 303	0.23	0.48
2847	196	Eastman DTDC	1	CAP. 504-0.2/Cymel 303	0.75	1.56
2847	196 <sup>3</sup>	Eastman DODC	1	CAP. 504-0.2/Cymel 303	0.75	0.49

- 1) Area is cm<sup>2</sup>; dimensions (in cm) of various size plates are: 4.4 x 6.2 (27 cm<sup>2</sup>), 7.0 x 7.0 (49 cm<sup>2</sup>), 14.0 x 14.0 (196 cm<sup>2</sup>)
- 2) Peak absorbance
- 3) 59-D plate placed over sample
- 4) Metal mask placed over sample; 49 cm<sup>2</sup> surface left open

RELATIVE EDGE LUMINESCENCE ( $L_r$ )

Plate #	Area (cm <sup>2</sup> )	Dye	# Coats	Host	Abs. <sup>2</sup>	$L_r$
2843	49	Eastman DTTC	1	CAP. 504-0.2/Cymel 303	0.02	0.21
2843N	49	Eastman DTTC	1	CAP. 504-0.2/Cymel 303	0.03	0.19
2845	49	Eastman DTDC	1	CAP. 504-0.2/Cymel 303	0.02	0.32
2845N	49	Eastman DTDC	1	CAP. 504-0.2/Cymel 303	0.01	0.28
2847	49	Eastman DODC	1	CAP. 504-0.2/Cymel 303	0.23	0.69
2847N	49	Eastman DODC	1	CAP. 504-0.2/Cymel 303	0.21	0.66
2849	49	Eastman DOTC	1	CAP. 504-0.2/Cymel 303	0.35	0.95
2849N	49	Eastman DOTC	1	CAP. 504-0.2/Cymel 303	0.28	0.94
2851	49	Hostasol Yellow 8-G	1	CAP. 504-0.2/Cymel 303	1.06	2.50
2851N	49	Hostasol Yellow 8-G	1	CAP. 504-0.2/Cymel 303	1.08	2.33
2853	49	Acridine Red	1	CAP. 504-0.2/Cymel 303	0.88	1.97
2853N	49	Acridine Red	1	CAP. 504-0.2/Cymel 303	0.88	1.93
2855	49	SRB	1	CAP. 504-0.2/Cymel 303	0.99	2.24
2855N	49	SRB	1	CAP. 504-0.2/Cymel 303	0.99	2.20
2857	49	LD-688	1	CAP. 504-0.2/Cymel 303	0.79	2.41
2857N	49	LD-688	1	CAP. 504-0.2/Cymel 303	0.77	2.45
2861	49	Eastman DTTC	1	Polytex 975/KL-5-2444	0.08	0.34
2861N	49	Eastman DTTC	1	Polytex 975/KL-5-2444	0.08	0.30
2863	49	Eastman DTDC	1	Polytex 975/KL-5-2444	0.64	1.29
2863N	49	Eastman DTDC	1	Polytex 975/KL-5-244	0.64	1.22
2865	49	Eastman DODC	1	Polytex 975/KL-5-244	0.66	1.47
2865N	49	Eastman DODC	1	Polytex 975/KL-5-244	0.60	1.33

- 1) Area is cm<sup>2</sup>; dimensions (in cm) of various size plates are: 4.4 x 6.2 (27 cm<sup>2</sup>), 7.0 x 7.0 (49 cm<sup>2</sup>), 14.0 x 14.0 (196 cm<sup>2</sup>)
- 2) Peak absorbance
- 3) 59-D plate placed over sample
- 4) Metal mask placed over sample; 49 cm<sup>2</sup> surface left open

RELATIVE EDGE LUMINESCENCE ( $L_r$ )

Plate #	Area (cm <sup>2</sup> )	Dye	# Coats	Host	Abs. <sup>2</sup>	$L_r$
2867	49	Eastman DOTC	1	Polytex 975/KL-5-2444	0.33	0.65
2867N	49	Eastman DOTC	1	Polytex 975/KL-5-2444	0.33	0.68
2869	49	Hostasol Yellow 8-G	1	Polytex 975/KL-5-2444	1.11	2.49
2869N	49	Hostasol Yellow 8-G	1	Polytex 975/KL-5-2444	1.13	2.38
2871	49	Acridine Red	1	Polytex 975/KL-5-2444	0.97	1.71
2871N	49	Acridine Red	1	Polytex 975/KL-5-2444	0.93	1.84
2873	49	SRB	1	Polytex 975/KL-5-2444	0.76	0.53
2873N	49	SRB	1	Polytex 975/KL-5-2444	0.74	0.55
2875	49	BASF - 241	1	Polytex 975/KL-5-2444	0.85	2.27
2875N	49	BASF - 241	1	Polytex 975/KL-5-2444	0.82	2.18
2878	196	R-101	1	Polytex 975/KL-5-2444	1.31	4.16
2878	196 <sup>3</sup>	R-101	1	Polytex 975/KL-5-2444	1.31	0.89
2878	49 <sup>4</sup>	R-101	1	Polytex 975/KL-5-2444	1.31	1.90
2879	196	R-101	2	Polytex 975/KL-5-2444	1.18	4.33
2879	196 <sup>4</sup>	R-101	2	Polytex 975/KL-5-2444	1.18	0.91
2879	49 <sup>4</sup>	R-101	2	Polytex 975/KL-5-2444	1.18	1.96
2880	196	R-101	4	Polytex 975/KL-5-2444	0.91	4.09
2880	196 <sup>3</sup>	R-101	4	Polytex 975/KL-5-2444	0.91	0.80
2880	49 <sup>4</sup>	R-101	4	Polytex 975/KL-5-2444	0.91	1.84
2882	196	R-101	1	Elvacite 2010	0.97	3.83
2882	196 <sup>3</sup>	R-101	1	Elvacite 2010	0.97	0.74
2882	49 <sup>4</sup>	R-101	1	Elvacite 2010	0.97	1.71

- 1) Area is cm<sup>2</sup>; dimensions (in cm) of various size plates are: 4.4 x 6.2 (27 cm<sup>2</sup>), 7.0 x 7.0 (49 cm<sup>2</sup>), 14.0 x 14.0 (196 cm<sup>2</sup>)
- 2) Peak absorbance
- 3) 59-D plate placed over sample
- 4) Metal mask placed over sample; 49 cm<sup>2</sup> surface left open

RELATIVE EDGE LUMINESCENCE ( $L_r$ )

Plate #	Area (cm <sup>2</sup> )	Dye	# Coats	Host	Abs. <sup>2</sup>	$L_r$
2847	49 <sup>4</sup>	Eastman DODC	1	CAP. 504-0.2/Cymel 303	0.75	0.70
2849	196	Eastman DOTC	1	CAP. 504-0.2/Cymel 303	0.97	1.91
2849	196 <sup>3</sup>	Eastman DOTC	1	CAP. 504-0.2/Cymel 303	0.97	1.63
2849	49 <sup>4</sup>	Eastman DOTC	1	CAP. 504-0.2/Cymel 303	0.97	0.90
2851	196	Hostasol Yellow 8-G	1	CAP. 504-0.2/Cymel 303	1.15	3.70
2851	196 <sup>3</sup>	Hostasol Yellow 8-G	1	CAP. 504-0.2/Cymel 303	1.15	0.32
2851	49 <sup>4</sup>	Hostasol Yellow 8-G	1	CAP. 504-0.2/Cymel 303	1.15	1.59
2853	196	Eastman Acridine Red	1	CAP. 504-0.2/Cymel 303	0.97	3.22
2853	196 <sup>3</sup>	Eastman Acridine Red	1	CAP. 504-0.2/Cymel 303	0.97	0.49
2853	49 <sup>4</sup>	Eastman Acridine Red	1	CAP. 504-0.2/Cymel 303	0.97	1.43
2855	196	SRB	1	CAP. 504-0.2/Cymel 303	1.02	3.64
2855	196 <sup>3</sup>	SRB	1	CAP. 504-0.2/Cymel 303	1.02	0.55
2855	49 <sup>4</sup>	SRB	1	CAP. 504-0.2/Cymel 303	1.02	1.55
2857	196	LD-688	1	CAP. 504-0.2/Cymel 303	0.90	3.39
2857	196 <sup>3</sup>	LD-688	1	CAP. 504-0.2/Cymel 303	0.90	1.00
2857	49 <sup>4</sup>	LD-688	1	CAP. 504-0.2/Cymel 303	0.90	1.93
2861	196	Eastman DTTC	1	Polytex 975/KL-5-2444	0.24	0.47
2861	196 <sup>3</sup>	Eastman DTTC	1	Polytex 975/KL-5-2444	0.24	0.40
2861	49 <sup>4</sup>	Eastman DTTC	1	Polytex 975/KL-5-2444	0.24	0.25
2863	196	Eastman DTDC	1	Polytex 975/KL-5-2444	0.90	2.06
2863	196 <sup>3</sup>	Eastman DTDC	1	Polytex 975/KL-5-2444	0.90	1.74

- 1) Area is cm<sup>2</sup>; dimensions (in cm) of various size plates are: 4.4 x 6.2 (27 cm<sup>2</sup>), 7.0 x 7.0 (49 cm<sup>2</sup>), 14.0 x 14.0 (196 cm<sup>2</sup>)
- 2) Peak absorbance
- 3) 59-D plate placed over sample
- 4) Metal mask placed over sample; 49 cm<sup>2</sup> surface left open

RELATIVE EDGE LUMINESCENCE ( $L_r$ )

Plate #	Area (cm <sup>2</sup> )	Dye	# Coats	Host	Abs. <sup>2</sup>	$L_r$
2863	49 <sup>4</sup>	Eastman DTDC	1	Polytex 975/KL-5-2444	0.90	0.94
2865	196	Eastman DODC	1	Polytex 975/KL-5-2444	0.76	2.06
2865	196 <sup>3</sup>	Eastman DODC	1	Polytex 975/KL-5-2444	0.76	0.68
2865	49 <sup>4</sup>	Eastman DODC	1	Polytex 975/KL-5-2444	0.76	0.98
2867	196	Eastman DOTC	1	Polytex 975/KL-5-2444	0.40	1.62
2867	196 <sup>3</sup>	Eastman DOTC	1	Polytex 975/KL-5-2444	0.40	1.41
2867	49 <sup>4</sup>	Eastman DOTC	1	Polytex 975/KL-5-2444	0.40	0.73
2869	196	Hostasol Yellow 8-G	1	Polytex 975/KL-5-2444	1.10	4.00
2869	196 <sup>3</sup>	Hostasol Yellow 8-G	1	Polytex 975/KL-5-2444	1.10	0.33
2869	49 <sup>4</sup>	Hostasol Yellow 8-G	1	Polytex 975/KL-5-2444	1.10	1.77
2871	196	Eastman Acridine Red	1	Polytex 975/KL-5-2444	1.00	3.62
2871	196 <sup>3</sup>	Eastman Acridine Red	1	Polytex 975/KL-5-2444	1.00	0.59
2871	49 <sup>4</sup>	Eastman Acridine Red	1	Polytex 975/KL-5-2444	1.00	1.67
2873	196	SRB	1	Polytex 975/KL-5-2444	0.80	0.94
2873	196 <sup>3</sup>	SRB	1	Polytex 975/KL-5-2444	0.80	0.21
2873	49 <sup>4</sup>	SRB	1	Polytex 975/KL-5-2444	0.80	0.41
2875	196	BASF -241	1	Polytex 975/KL-5-2444	0.94	4.00
2875	196 <sup>3</sup>	BASF -241	1	Polytex 975/KL-5-2444	0.94	0.75
2875	49 <sup>4</sup>	BASF -241	1	Polytex 975/KL-5-2444	0.94	1.66

- 1) Area is cm<sup>2</sup>; dimensions (in cm) of various size plates are: 4.4 x 6.2 (27 cm<sup>2</sup>), 7.0 x 7.0 (49 cm<sup>2</sup>), 14.0 x 14.0 (196 cm<sup>2</sup>)
- 2) Peak absorbance
- 3) 59-D plate placed over sample
- 4) Metal mask placed over sample; 49 cm<sup>2</sup> surface left open

RELATIVE EDGE LUMINESCENCE ( $L_r$ )

Plate #	Area (cm <sup>2</sup> )	Dye	# Coats	Host	Abs. <sup>2</sup>	$L_r$
2883	196	R-101	2	Elvacite 2010	1.01	4.52
2883	196 <sup>3</sup>	R-101	2	Elvacite 2010	1.01	0.88
2883	49 <sup>4</sup>	R-101	2	Elvacite 2010	1.01	1.99
2884	196	R-101	4	Elvacite 2010	0.88	3.90
2884	196 <sup>3</sup>	R-101	4	Elvacite 2010	0.88	0.74
2884	49 <sup>4</sup>	R-101	4	Elvacite 2010	0.88	1.73
2886	196	R-101	1	CAB. 553-0.4	0.94	4.43
2886	196 <sup>3</sup>	R-101	1	CAB. 553-0.4	0.94	0.90
2886	49 <sup>4</sup>	R-101	1	CAB. 553-0.4	0.94	1.89
2887	196	R-101	2	CAB. 553-0.4	1.03	4.15
2887	196 <sup>3</sup>	R-101	2	CAB. 553-0.4	1.03	0.81
2887	49 <sup>4</sup>	R-101	2	CAB. 553-0.4	1.03	1.84
2888	196	R-101	4	CAB. 553-0.4	1.02	4.59
2888	196 <sup>3</sup>	R-101	4	CAB. 553-0.4	1.02	0.92
2888	49 <sup>4</sup>	R-101	4	CAB. 553-0.4	1.02	1.97
2890	196	R-101	1	CAP. 504-0.2/Cymel 303	0.88	4.03
2890	196 <sup>3</sup>	R-101	1	CAP. 504-0.2/Cymel 303	0.88	0.77
2890	49 <sup>4</sup>	R-101	1	CAP. 504-0.2/Cymel 303	0.88	1.76
2891	196	R-101	2	CAP. 504-0.2/Cymel 303	1.01	4.31
2891	196 <sup>3</sup>	R-101	2	CAP. 504-0.2/Cymel 303	1.01	0.80
2891	49 <sup>4</sup>	R-101	2	CAP. 504-0.2/Cymel 303	1.01	1.85

- 1) Area is cm<sup>2</sup>; dimensions (in cm) of various size plates are: 4.4 x 6.2 (27 cm<sup>2</sup>), 7.0 x 7.0 (49 cm<sup>2</sup>), 14.0 x 14.0 (196 cm<sup>2</sup>)
- 2) Peak absorbance
- 3) 59-D plate placed over sample
- 4) Metal mask placed over sample; 49 cm<sup>2</sup> surface left open

RELATIVE EDGE LUMINESCENCE ( $L_r$ )

Plate #	Area (cm <sup>2</sup> )	Dye	# Coats	Host	Abs. <sup>2</sup>	$L_r$
2892	196	R-101	4	CAP. 504-0.2/Cymel 303	0.92	4.40
2892	196 <sup>3</sup>	R-101	4	CAP. 504-0.2/Cymel 303	0.92	0.81
2892	49 <sup>4</sup>	R-101	4	CAP. 504-0.2/Cymel 303	0.92	1.87
2894	196	R-101	1	CAP. 504-0.2	0.98	3.85
2894	196 <sup>3</sup>	R-101	1	CAP. 504-0.2	0.98	0.75
2894	49 <sup>4</sup>	R-101	1	CAP. 504-0.2	0.98	1.66
2895	196	R-101	2	CAP. 504-0.2	1.07	4.31
2895	196 <sup>3</sup>	R-101	2	CAP. 504-0.2	1.07	0.82
2895	49 <sup>4</sup>	R-101	2	CAP. 504-0.2	1.07	1.88
2896	196	R-101	4	CAP. 504-0.2	0.90	4.01
2896	196 <sup>3</sup>	R-101	4	CAP. 504-0.2	0.90	0.73
2896	49 <sup>4</sup>	R-101	4	CAP. 504-0.2	0.90	1.77
2898	196	RH-6G	1	CAP. 504-0.2	0.96	3.54
2898	196 <sup>3</sup>	RH-6G	1	CAP. 504-0.2	0.96	0.72
2898	49 <sup>4</sup>	RH-6G	1	CAP. 504-0.2	0.96	1.53
2900	196	RH-19	1	CAP. 504-0.2	1.16	2.90
2900	196 <sup>3</sup>	RH-19	1	CAP. 504-0.2	1.16	0.59
2900	49 <sup>4</sup>	RH-19	1	CAP. 504-0.2	1.16	1.30
2902	196	RH-B	1	CAP. 504-0.2	1.07	3.32
2902	196 <sup>3</sup>	RH-B	1	CAP. 504-0.2	1.07	0.55
2902	49 <sup>4</sup>	RH-B	1	CAP. 504-0.2	1.07	1.45

- 1) Area is cm<sup>2</sup>; dimensions (in cm) of various size plates are: 4.4 x 6.2 (27 cm<sup>2</sup>), 7.0 x 7.0 (49 cm<sup>2</sup>), 14.0 x 14.0 (196 cm<sup>2</sup>)
- 2) Peak absorbance
- 3) 59-D plate placed over sample
- 4) Metal mask placed over sample; 49 cm<sup>2</sup> surface left open

RELATIVE EDGE LUMINESCENCE ( $L_T$ )

Plate #	Area (cm <sup>2</sup> )	Dye	# Coats	Host	Abs. <sup>2</sup>	$L_T$
2904	196	RH-110	1	CAP. 504-0.2	0.73	1.98
2904	196 <sup>3</sup>	RH-110	1	CAP. 504-0.2	0.73	0.41
2904	49 <sup>4</sup>	RH-110	1	CAP. 504-0.2	0.73	0.89
2906	196	RH-6G	1	Polytex 975/KL-5-2444	0.86	2.94
2906	196 <sup>3</sup>	RH-6G	1	Polytex 975/KL-5-2444	0.86	0.59
2906	49 <sup>4</sup>	RH-6G	1	Polytex 975/KL-5-2444	0.86	1.32
2908	196	RH-19	1	Polytex 975/KL-5-2444	0.39	2.32
2908	196 <sup>3</sup>	RH-19	1	Polytex 975/KL-5-2444	0.39	0.50
2908	49 <sup>4</sup>	RH-19	1	Polytex 975/KL-5-2444	0.39	1.02
2910	196	RH-B	1	Polytex 975/KL-5-2444	0.81	3.56
2910	196 <sup>3</sup>	RH-B	1	Polytex 975/KL-5-2444	0.81	0.59
2910	49 <sup>4</sup>	RH-B	1	Polytex 975/KL-5-2444	0.81	1.53
2912	196	RH-110	1	Elvacite 2010	0.48	0.12
2912	196 <sup>3</sup>	RH-110	1	Elvacite 2010	0.48	0.12
2912	49 <sup>4</sup>	RH-110	1	Elvacite 2010	0.48	0.04
2878	49	R-101	1	Polytex 975/KL-5-2444	1.32	2.62
2878N	49	R-101	1	Polytex 975/KL-5-2444	1.31	2.74
2879	49	R-101	2	Polytex 975/KL-5-2444	1.21	2.47
2879N	49	R-101	2	Polytex 975/KL-5-2444	1.21	2.66
2880	49	R-101	4	Polytex 975/KL-5-2444	0.92	2.32
2880N	49	R-101	4	Polytex 975/KL-5-2444	0.90	2.88

- 1) Area is cm<sup>2</sup>; dimensions (in cm) of various size plates are: 4.4 x 6.2 (27 cm<sup>2</sup>), 7.0 x 7.0 (49 cm<sup>2</sup>), 14.0 x 14.0 (196 cm<sup>2</sup>)
- 2) Peak absorbance
- 3) 59-D plate placed over sample
- 4) Metal mask placed over sample; 49 cm<sup>2</sup> surface left open

RELATIVE EDGE LUMINESCENCE ( $L_T$ )

Plate #	Area (cm <sup>2</sup> )	Dye	# Coats	Host	Abs. <sup>2</sup>	$L_T$
2882	49	R-101	1	Elvacite 2010	0.96	2.35
2882N	49	R-101	1	Elvacite 2010	0.93	2.43
2883	49	R-101	2	Elvacite 2010	0.99	2.68
2883N	49	R-101	2	Elvacite 2010	0.98	2.82
2884	49	R-101	4	Elvacite 2010	0.90	2.31
2884N	49	R-101	4	Elvacite 2010	0.89	2.50
2886	49	R-101	1	CAB. 553-0.4	0.94	2.59
2886N	49	R-101	1	CAB. 553-0.4	0.90	2.97
2887	49	R-101	2	CAB. 553-0.4	1.05	1.76
2887N	49	R-101	2	CAB. 553-0.4	1.03	1.85
2888	49	R-101	4	CAB. 553-0.4	1.01	2.75
2888N	49	R-101	4	CAB. 553-0.4	1.02	2.91
2890	49	R-101	1	CAP. 504-0.2/Cymel 303	0.89	2.36
2890N	49	R-101	1	CAP. 504-0.2/Cymel 303	0.92	2.71
2891	49	R-101	2	CAP. 504-0.2/Cymel 303	1.01	2.49
2891N	49	R-101	2	CAP. 504-0.2/Cymel 303	0.99	2.61
2892	49	R-101	4	CAP. 504-0.2/Cymel 303	0.91	2.71
2892N	49	R-101	4	CAP. 504-0.2/Cymel 303	0.92	2.67
2894	49	R-101	1	CAP. 504-0.2	0.96	2.48
2894N	49	R-101	1	CAP. 504-0.2	0.94	2.84
2895	49	R-101	2	CAP. 504-0.2	1.07	2.80

- 1) Area is cm<sup>2</sup>; dimensions (in cm) of various size plates are: 4.4 x 6.2 (27 cm<sup>2</sup>), 7.0 x 7.0 (49 cm<sup>2</sup>), 14.0 x 14.0 (196 cm<sup>2</sup>)
- 2) Peak absorbance
- 3) 59-D plate placed over sample
- 4) Metal mask placed over sample; 49 cm<sup>2</sup> surface left open

RELATIVE EDGE LUMINESCENCE ( $L_r$ )

Plate #	Area (cm <sup>2</sup> )	Dye	# Coats	Host	Abs. <sup>2</sup>	$L_r$
2895N	49	R-101	2	CAP. 504-0.2	1.11	3.10
2896	49	R-101	4	CAP. 504-0.2	0.93	2.65
2896N	49	R-101	4	CAP. 504-0.2	0.88	2.46
2898	49	RH-6G	1	CAP. 504-0.2	0.95	2.32
2898N	49	RH-6G	1	CAP. 504-0.2	0.96	2.37
2900	49	RH-19	1	CAP. 504-0.2	1.11	1.91
2900N	49	RH-19	1	CAP. 504-0.2	1.12	2.15
2902	49	RH-B	1	CAP. 504-0.2	1.07	2.16
2902N	49	RH-B	1	CAP. 504-0.2	1.07	2.37
2904	49	RH-110	1	CAP. 504-0.2	0.74	1.33
2904N	49	RH-110	1	CAP. 504-0.2	0.72	1.46
2906	49	RH-6G	1	Polytex 975/KL-5-2444	0.88	1.88
2906N	49	RH-6G	1	Polytex 975/KL-5-2444	0.87	2.00
2908	49	RH-19	1	Polytex 975/KL-5-2444	0.42	1.49
2908N	49	RH-19	1	Polytex 975/KL-5-2444	0.43	1.50
2910	49	RH-B	1	Polytex 975/KL-5-2444	0.80	2.15
2910N	49	RH-B	1	Polytex 975/KL-5-2444	0.79	2.19
2912	49	RH-110	1	Elvacite 2010	0.46	0.14
2912N	49	RH-110	1	Elvacite 2010	0.46	0.12
2919	49	Coumarin - 440	1	CAP. 504-0.2	1.34	0.62
2920	49	Coumarin - 445	1	CAP. 504-0.2	1.02	0.98

- 1) Area is cm<sup>2</sup>; dimensions (in cm) of various size plates are: 4.4 x 6.2 (27 cm<sup>2</sup>), 7.0 x 7.0 (49 cm<sup>2</sup>), 14.0 x 14.0 (196 cm<sup>2</sup>)
- 2) Peak absorbance
- 3) 59-D plate placed over sample
- 4) Metal mask placed over sample; 49 cm<sup>2</sup> surface left open

RELATIVE EDGE LUMINESCENCE ( $L_r$ )

Plate #	Area (cm <sup>2</sup> )	Dye	# Coats	Host	Abs. <sup>2</sup>	$L_r$
2921	49	Coumarin - 450	1	CAP. 504-0.2	0.90	0.74
2922	49	Coumarin - 450	1	CAP. 504-0.2	1.26	1.02
2923	49	Stilbene - 420	1	CAP. 504-0.2	0.95	0.91
2924	49	LD-423	1	CAP. 504-0.2	1.05	0.69
2925	49	LD-425	1	CAP. 504-0.2	0.89	0.98
2926	49	LD-466	1	CAP. 504-0.2	0.87	1.20
2927	49	Coumarin - 440	1	CAP. 504-0.2/Cymel 303	0.89	0.77
2928	49	Coumarin - 445	1	CAP. 504-0.2/Cymel 303	0.93	0.71
2929	49	Coumarin - 450	1	CAP. 504-0.2/Cymel 303	0.97	1.15
2930	49	Coumarin - 460	1	CAP. 504-0.2/Cymel 303	0.97	1.04
2931	49	Coumarin - 440	1	Polytex 975/KL-5-2444	1.04	0.37
2932	49	Coumarin - 460	1	Polytex 975/KL-5-2444	1.13	1.04
2933	49	Stilbene - 420	1	Polytex 975/KL-5-2444	0.86	0.55
2934	49	LD-423	1	Polytex 975/KL-5-2444	0.97	0.55
2935	49	LD-425	1	Polytex 975/KL-5-2444	0.86	0.54
2936	49	LD-466	1	Polytex 975/KL-5-2444	0.80	0.82
2937	196	Coumarin-6	2	CAP. 504-0.2	2.10	4.36
2938	196	Coumarin-6	3	CAP. 504-0.2	4.16	5.21
2939	196	Coumarin-6	5	CAP. 504-0.2	6.40	5.41
2940	196	Hostasol Yellow 8-G	3	CAP. 504-0.2	2.38	4.11
2941	196	Hostasol Yellow 8-G	5	CAP. 504-0.2	4.35	4.60

- 1) Area is cm<sup>2</sup>; dimensions (in cm) of various size plates are: 4.4 x 6.2 (27 cm<sup>2</sup>), 7.0 x 7.0 (49 cm<sup>2</sup>), 14.0 x 14.0 (196 cm<sup>2</sup>)
- 2) Peak absorbance
- 3) 59-D plate placed over sample
- 4) Metal mask placed over sample; 49 cm<sup>2</sup> surface left open



RELATIVE EDGE LUMINESCENCE ( $L_r$ )

Plate #	Area (cm <sup>2</sup> )	Dye	# Coats	Host	Abs. <sup>2</sup>	$L_r$
2942	196	Hostasol Yellow 8-G	9	CAP. 504-0.2	6.91	4.56
2943	196	BASF - 241	1	Elvacite 2010	1.17	4.42
2944	196	BASF - 241	1	CAP. 504-0.2/Cymel 303	0.68	4.26
2945	196	BASF - 241	1	CAB. 531-0.1	0.81	3.65
2946	196	BASF - 241	1	CAB. 531-0.1	0.90	4.35
2947	196	Brilliant Yellow	1	CAB. 531-0.1	0.75	2.74
2948	196	Brilliant Yellow	1	CAB. 531-0.1	0.08	1.99
2949	196	Hostasol Yellow 8-G	1	CAB. 531-0.1	1.01	3.65
2950	196	Hostasol Yellow 8-G	1	CAB. 531-0.1	0.15	2.14
2951	196	SRB	1	CAB. 531-0.1	0.88	1.61
2952	196	SRB	1	CAB. 531-0.1	0.08	1.33
2953	196	R-101	1	CAB. 531-0.1	0.58	3.30
2954	196	R-101	1	CAB. 531-0.1	0.04	1.13
2955	196	LD-688	1	CAB. 531-0.1	0.58	2.24
2956	196	LD-688	1	CAB. 531-0.1	0.00	1.15
2957	196	LD-700	1	CAB. 531-0.1	1.16	1.10
2958	196	LD-700	1	CAB. 531-0.1	0.16	1.27
2959	196	LDS-750	1	CAB. 531-0.1	0.70	1.41
2960	196	LDS-750	1	CAB. 531-0.1	0.07	1.61
2961	196	Oxazine-725	1	CAB. 531-0.1	1.23	1.41
2962	196	Oxazine-725	1	CAB. 531-0.1	0.22	1.05

- 1) Area is cm<sup>2</sup>; dimensions (in cm) of various size plates are: 4.4 x 6.2 (27 cm<sup>2</sup>), 7.0 x 7.0 (49 cm<sup>2</sup>), 14.0 x 14.0 (196 cm<sup>2</sup>)
- 2) Peak absorbance
- 3) 59-D plate placed over sample
- 4) Metal mask placed over sample; 49 cm<sup>2</sup> surface left open

RELATIVE EDGE LUMINESCENCE ( $L_r$ )

Plate #	Area (cm <sup>2</sup> )	Dye	# Coats	Host	Abs. <sup>2</sup>	$L_r$
2963	196	Coumarin-6	1	CAB. 531-0.1	1.07	3.61
2964	196	Coumarin-6	1	CAB. 531-0.1	0.11	2.26
2965	196	Radglo - #14 Orange - Red	1	Elvacite 2010	0.78	5.90
2966	196	Radglo - #14 Orange - Red	1	Elvacite 2010	0.07	2.81
2967	196	Radglo - #14 Orange - Red	1	CAP. 504-0.2	0.77	5.69
2968	196	Radglo - #14 Orange - Red	1	CAP. 504-0.2	0.11	3.16
2969	196	Radglo - #14 Orange - Red	1	CAP. 504-0.2/Cymel 303	0.75	6.49
2970	196	Radglo - #14 Orange - Red	1	CAP. 504-0.2/Cymel 303	0.11	3.16
2971	196	Radglo - #14 Orange - Red	1	CAB. 553-0.4	0.64	6.43
2972	196	Radglo - #14 Orange - Red	1	CAB. 553-0.4	0.15	3.54
2973	196	Radglo - #14 Orange - Red	1	Polytex - 975/KL-5-2444	0.49	6.72
2974	196	Radglo - #14 Orange - Red	1	Polytex - 975/KL-5-2444	0.02	2.66
2943	49	BASF - 241	1	Elvacite 2010	1.20	3.28
2943N	49	BASF - 241	1	Elvacite 2010	1.20	3.18
2944	49	BASF - 241	1	CAP. 504-0.2/Cymel 303	0.71	2.63
2944N	49	BASF - 241	1	CAP. 504-0.2/Cymel 303	0.70	2.67
2945	49	BASF - 241	1	CAB. 553-0.4	0.84	2.42
2945N	49	BASF - 241	1	CAB. 553-0.4	0.84	2.30
2946	49	BASF - 241	1	CAP. 504-0.2	0.93	2.87
2946N	49	BASF - 241	1	CAP. 504-0.2	0.93	2.60

- 1) Area is cm<sup>2</sup>; dimensions (in cm) of various size plates are: 4.4 x 6.2 (27 cm<sup>2</sup>), 7.0 x 7.0 (49 cm<sup>2</sup>), 14.0 x 14.0 (196 cm<sup>2</sup>)
- 2) Peak absorbance
- 3) 59-D plate placed over sample
- 4) Metal mask placed over sample; 49 cm<sup>2</sup> surface left open

RELATIVE EDGE LUMINESCENCE ( $L_r$ )

Plate #	Area (cm <sup>2</sup> )	Dye	# Coats	Host	Abs. <sup>2</sup>	$L_r$
2947	49	Brilliant Yellow	1	CAB. 531-0.1	0.90	1.78
2947N	49	Brilliant Yellow	1	CAB. 531-0.1	0.75	1.90
2949	49	Hostasol Yellow 8-G	1	CAB. 531-0.1	1.01	2.51
2949N	49	Hostasol Yellow 8-G	1	CAB. 531-0.1	1.00	2.76
2951	49	SRB	1	CAB. 531-0.1	0.95	1.13
2951N	49	SRB	1	CAB. 531-0.1	0.90	1.40
2953	49	R-101	1	CAB. 531-0.1	0.57	1.96
2953N	49	R-101	1	CAB. 531-0.1	0.56	2.22
2955	49	LD-688	1	CAB. 531-0.1	0.38	1.95
2955N	49	LD-688	1	CAB. 531-0.1	0.32	1.56
2957	49	LD-700	1	CAB. 531-0.1	1.17	0.60
2957N	49	LD-700	1	CAB. 531-0.1	1.15	0.82
2959	49	LDS-750	1	CAB. 531-0.1	0.73	1.03
2959N	49	LDS-750	1	CAB. 531-0.1	0.74	1.00
2961	49	Oxazine-725	1	CAB. 531-0.1	1.27	0.96
2961N	49	Oxazine-725	1	CAB. 531-0.1	1.33	0.97
2963	49	Coumarin-6	1	CAB. 531-0.1	1.09	2.53
2963N	49	Coumarin-6	1	CAB. 531-0.1	1.09	2.42
2965	49	Radglo - #14 Orange - Red	1	Elvacite 2010	0.82	3.63
2965N	49	Radglo - #14 Orange - Red	1	Elvacite 2010	0.82	4.16
2967	49	Radglo - #14 Orange - Red	1	CAP. 504-0.2	0.82	3.75

- 1) Area is cm<sup>2</sup>; dimensions (in cm) of various size plates are: 4.4 x 6.2 (27 cm<sup>2</sup>), 7.0 x 7.0 (49 cm<sup>2</sup>), 14.0 x 14.0 (196 cm<sup>2</sup>)
- 2) Peak absorbance
- 3) 59-D plate placed over sample
- 4) Metal mask placed over sample; 49 cm<sup>2</sup> surface left open

RELATIVE EDGE LUMINESCENCE ( $L_r$ )

Plate #	Area (cm <sup>2</sup> )	Dye	# Coats	Host	Abs. <sup>2</sup>	$L_r$
2967N	49	Radglo - #14 Orange - Red	1	CAP. 504-0.2	0.84	3.70
2969	49	Radglo - #14 Orange - Red	1	CAP. 504-0.2/Cymel 303	0.81	4.07
2969N	49	Radglo - #14 Orange - Red	1	CAP. 504-0.2/Cymel 303	0.81	3.94
2971	49	Radglo - #14 Orange - Red	1	CAB. 553-0.4	0.68	4.13
2971N	49	Radglo - #14 Orange - Red	1	CAB. 553-0.4	0.68	4.03
2973	49	Radglo - #14 Orange - Red	1	Polytex 975/KL-5-2444	0.67	4.17
2973N	49	Radglo - #14 Orange - Red	1	Polytex 975/KL-5-2444	0.67	4.24
2975	49	Radglo - #09 Clear	1	Elvacite 2010	0.45	1.15
2976	49	Radglo - #09 Clear	1	CAP. 504-0.2	0.47	0.97
2977	49	Radglo - #09 Clear	1	CAP. 504-0.2	0.65	1.01
2978	49	Radglo - #09 Clear	1	CAB. 553-0.4	0.64	0.94
2979	49	Radglo - #09 Clear	1	Polytex 975/KL-5-2444	0.42	0.93
2980	49	Lisa Mobay Green - 52G	(U)	Polycarbonate	3.28	1.90
2981	49	Lisa Mobay Amber 59YR	(U)	Polycarbonate	2.26	2.63
2981A	49	Lisa Mobay Amber 59YR	(U)	PMMA	3.24	3.04
2982	49	Lisa Mobay Orange 61R	(U)	Polycarbonate	3.39	3.85
2982A	49	Lisa Mobay Orange 61R	(U)	PMMA	3.40	4.61
2982B	49	Lisa Mobay Orange	(U)	Polycarbonate	2.40	4.25
2983	49	Lisa Mobay Green 51GB	(U)	PMMA	3.28	1.87
2984	49	Lisa Mobay Yellow	(U)	Polycarbonate	1.21	2.26

- 1) Area is cm<sup>2</sup>; dimensions (in cm) of various size plates are: 4.4 x 6.2 (27 cm<sup>2</sup>), 7.0 x 7.0 (49 cm<sup>2</sup>), 14.0 x 14.0 (196 cm<sup>2</sup>)
- 2) Peak absorbance
- 3) 59-D plate placed over sample
- 4) Metal mask placed over sample; 49 cm<sup>2</sup> surface left open
- 5) (U)-Dye uniformly distributed throughout (2mm) thickness of plate

RELATIVE EDGE LUMINESCENCE ( $L_r$ )

Plate #	Area (cm <sup>2</sup> )	Dye	# Coats	Host	Abs. <sup>2</sup>	$L_r$
	27	Brilliant Yellow #1	1	CAP. 482-0-20	1.39	0.80
	27	Brilliant Yellow #2	1	CAP. 482-0-20	1.25	1.04
	27	Brilliant Yellow #3	1	CAP. 482-0-20	1.23	0.94
	27	Hostasol Yellow 8-G #1	1	CAP. 482-0-20	1.23	1.61
	27	Hostasol Yellow 8-G #2	1	CAP. 482-0-20	1.30	1.95
	27	Hostasol Yellow 8-G #3	1	CAP. 482-0-20	1.25	1.63
	27	R-101 - #1	1	CAP. 482-0-20	0.93	1.91
	27	R-101 - #1	1	CAP. 482-0-20	1.06	1.68
	27	R-101 - #1	1	CAP. 482-0-20	0.92	1.81
	27	Oxazine - 725 #1	1	CAP. 482-0-20	0.79	0.63
	27	Oxazine - 725 #2	1	CAP. 482-0-20	0.82	0.59
	27	Oxazine - 725 #3	1	CAP. 482-0-20	0.81	0.65
	27	LD-688 - #1	1	CAP. 482-0-20	0.72	2.36
	27	LD-688 - #2	1	CAP. 482-0-20	0.79	2.30
	27	LD-688 - #3	1	CAP. 482-0-20	0.86	2.45
	27	SRB - #4	1	CAP. 482-0-20	1.29	1.62
	27	SRB - #5	1	CAP. 482-0-20	1.29	1.29
	27	SRB - #6	1	CAP. 482-0-20	1.09	1.31
2985	196	Kodak - 15071	1	CAP. 504-0.2	0.05	0.42
2986	196	Kodak - 15071	1	CAP. 504-0.2	0.02	0.21
2987	196	Kodak - 15072	1	CAP. 504-0.2	0.80	0.67

- 1) Area is cm<sup>2</sup>; dimensions (in cm) of various size plates are: 4.4 x 6.2 (27 cm<sup>2</sup>), 7.0 x 7.0 (49 cm<sup>2</sup>), 14.0 x 14.0 (196 cm<sup>2</sup>)
- 2) Peak absorbance
- 3) 59-D plate placed over sample
- 4) Metal mask placed over sample; 49 cm<sup>2</sup> surface left open

RELATIVE EDGE LUMINESCENCE ( $L_r$ )

Plate #	Area (cm <sup>2</sup> )	Dye	# Coats	Host	Abs. <sup>2</sup>	$L_r$
2997	49	LDS-765	1	Elvacite 2010	0.80	0.14
2997N	49	LDS-765	1	Elvacite 2010	0.82	0.18
2999	49	LDS-821	1	Elvacite 2010	1.26	1.42
2999N	49	LDS-821	1	Elvacite 2010	1.25	1.17
3001	49	LDS-860	1	Elvacite 2010	0.89	0.91
3001N	49	LDS-860	1	Elvacite 2010	0.88	1.01
3003	49	LDS-867	1	Elvacite 2010	1.05	0.09
3003N	49	LDS-867	1	Elvacite 2010	1.05	0.08
3005	49	LDS-698	1	CAP. 504-0.2	0.99	2.11
3005N	49	LDS-698	1	CAP. 504-0.2	0.99	2.01
3007	49	LDS-722	1	CAP. 504-0.2	0.88	2.72
3007N	49	LDS-722	1	CAP. 504-0.2	0.86	2.68
3009	49	LDS-765	1	CAP. 504-0.2	0.59	0.33
3009N	49	LDS-765	1	CAP. 504-0.2	0.59	0.32
3011	49	LDS-821	1	CAP. 504-0.2	1.01	1.22
3011N	49	LDS-821	1	CAP. 504-0.2	1.02	1.25
3013	49	LDS-860	1	CAP. 504-0.2	0.60	1.31
3013N	49	LDS-860	1	CAP. 504-0.2	0.60	1.27
3015	49	LDS-867	1	CAP. 504-0.2	0.60	0.12
3015N	49	LDS-867	1	CAP. 504-0.2	0.60	0.16

- 1) Area is cm<sup>2</sup>; dimensions (in cm) of various size plates are: 4.4 x 6.2 (27 cm<sup>2</sup>), 7.0 x 7.0 (49 cm<sup>2</sup>), 14.0 x 14.0 (196 cm<sup>2</sup>)
- 2) Peak absorbance
- 3) 59-D plate placed over sample
- 4) Metal mask placed over sample; 49 cm<sup>2</sup> surface left open

RELATIVE EDGE LUMINESCENCE ( $L_T$ )

Plate #	Area (cm <sup>2</sup> )	Dye	# Coats	Host	Abs. <sup>2</sup>	$L_T$
2988	196	Kodak 15072	1	CAP. 504-0.2	0.09	0.40
2989	196	Kodak 15071	1	Elvacite 2010	0.89	0.34
2990	196	Kodak 15071	1	Elvacite 2010	0.14	0.48
2991	196	Kodak 15072	1	Elvacite 2010	1.02	0.75
2992	196	Kodak 15072	1	Elvacite 2010	0.16	0.65
2993	196	LDS-698	1	Elvacite 2010	1.99	3.13
2994	196	LDS-698	1	Elvacite 2010	0.29	2.30
2995	196	LDS-722	1	Elvacite 2010	1.32	5.12
2996	196	LDS-722	1	Elvacite 2010	0.22	3.30
2997	196	LDS-765	1	Elvacite 2010	0.83	0.14
2998	196	LDS-765	1	Elvacite 2010	0.19	0.36
2999	196	LDS-821	1	Elvacite 2010	1.27	1.79
3000	196	LDS-821	1	Elvacite 2010	0.10	1.23
3001	196	LDS-860	1	Elvacite 2010	0.91	1.25
3002	196	LDS-860	1	Elvacite 2010	0.11	0.86
3003	196	LDS-867	1	Elvacite 2010	1.03	0.15
3004	196	LDS-867	1	Elvacite 2010	0.13	0.27
3005	196	LDS-698	1	CAP. 504-0.2	1.01	3.04
3006	196	LDS-698	1	CAP. 504-0.2	0.17	1.61
3007	196	LDS-722	1	CAP. 504-0.2	0.88	3.66
3008	196	LDS-722	1	CAP. 504-0.2	0.23	3.36

- 1) Area is cm<sup>2</sup>; dimensions (in cm) of various size plates are: 4.4 x 6.2 (27 cm<sup>2</sup>), 7.0 x 7.0 (49 cm<sup>2</sup>), 14.0 x 14.0 (196 cm<sup>2</sup>)
- 2) Peak absorbance
- 3) 59-D plate placed over sample
- 4) Metal mask placed over sample; 49 cm<sup>2</sup> surface left open

RELATIVE EDGE LUMINESCENCE ( $L_T$ )

Plate #	Area (cm <sup>2</sup> )	Dye	# Coats	Host	Abs. <sup>2</sup>	$L_T$
3009	196	LDS-765	1	CAP. 504-0.2	0.62	0.40
3010	196	LDS-765	1	CAP. 504-0.2	0.14	1.45
3011	196	LDS-821	1	CAP. 504-0.2	1.03	1.61
3012	196	LDS-821	1	CAP. 504-0.2	0.24	1.95
3013	196	LDS-860	1	CAP. 504-0.2	0.62	1.18
3014	196	LDS-860	1	CAP. 504-0.2	0.08	0.80
3015	196	LDS-867	1	CAP. 504-0.2	0.80	0.13
3016	196	LDS-867	1	CAP. 504-0.2	0.31	0.56
2985	49	Kodak 15071	1	CAP. 504-0.2	0.05	0.59
2985N	49	Kodak 15071	1	CAP. 504-0.2	0.05	0.47
2987	49	Kodak 15072	1	CAP. 504-0.2	0.80	0.59
2987N	49	Kodak 15072	1	CAP. 504-0.2	0.80	0.48
2989	49	Kodak 15071	1	Elvacite 2010	0.89	0.35
2989N	49	Kodak 15071	1	Elvacite 2010	0.87	0.34
2991	49	Kodak 15072	1	Elvacite 2010	1.02	0.64
2991N	49	Kodak 15072	1	Elvacite 2010	1.00	0.63
2993	49	LDS-698	1	Elvacite 2010	1.08	2.06
2993N	49	LDS-698	1	Elvacite 2010	1.09	1.94
2995	49	LDS-722	1	Elvacite 2010	1.32	3.27
2995N	49	LDS-722	1	Elvacite 2010	1.31	2.93

- 1) Area is cm<sup>2</sup>; dimensions (in cm) of various size plates are: 4.4 x 6.2 (27 cm<sup>2</sup>), 7.0 x 7.0 (49 cm<sup>2</sup>), 14.0 x 14.0 (196 cm<sup>2</sup>)
- 2) Peak absorbance
- 3) 59-D plate placed over sample
- 4) Metal mask placed over sample; 49 cm<sup>2</sup> surface left open

RELATIVE EDGE LUMINESCENCE ( $L_T$ )

Plate #	Area (cm <sup>2</sup> )	Dye	# Coats	Host	Abs. <sup>2</sup>	$L_T$
GG 17	196	Uranium Standard			1.48	
3017-1	196	Radglo - #14 Orange - Red	1	At-400/Z-4370	0.87	3.21
3017-2	196	Radglo - #14 Orange - Red	1	At-400/Z-4370	0.87	3.21
3017-3	196	Radglo - #14 Orange - Red	1	At-400/Z-4370	0.87	3.26
3017-4	196	Radglo - #14 Orange - Red	1	At-400/Z-4370	0.87	3.28
3018-1	196	Radglo - #14 Orange - Red	1	At-400/Z-4370	1.81	3.42
3018-2	196	Radglo - #14 Orange - Red	1	At-400/Z-4370	1.81	3.39
3018-3	196	Radglo - #14 Orange - Red	1	At-400/Z-4370	1.81	3.43
3018-4	196	Radglo - #14 Orange - Red	1	At-400/Z-4370	1.81	3.41
3019-1	196	Radglo - #14 Orange - Red	2	At-400/Z-4370	2.03	3.01
3019-2	196	Radglo - #14 Orange - Red	2	At-400/Z-4370	2.03	2.79
3019-3	196	Radglo - #14 Orange - Red	2	At-400/Z-4370	2.03	3.03
3019-4	196	Radglo - #14 Orange - Red	2	At-400/Z-4370	2.03	3.02
3020-1	196	Radglo - #14 Orange - Red	4	At-400/Z-4370	1.86	6.11
3020-2	196	Radglo - #14 Orange - Red	4	At-400/Z-4370	1.86	6.32
3020-3	196	Radglo - #14 Orange - Red	4	At-400/Z-4370	1.86	7.46
3020-4	196	Radglo - #14 Orange - Red	4	At-400/Z-4370	1.86	6.64
3021-1	196	Radglo - #14 Orange - Red	8	At-400/Z-4370	2.14	7.09
3021-2	196	Radglo - #14 Orange - Red	8	At-400/Z-4370	2.14	7.13
3021-3	196	Radglo - #14 Orange - Red	8	At-400/Z-4370	2.14	7.24
3021-4	196	Radglo - #14 Orange - Red	8	At-400/Z-4370	2.14	6.90
3022-1	196	Radglo - #14 Orange - Red	8*	At-400/Z-4370	2.15	7.13

- 1) Area is cm<sup>2</sup>; dimensions (in cm) of various size plates are:  
4.4 x 6.2 (27 cm<sup>2</sup>), 7.0 x 7.0 (49 cm<sup>2</sup>), 14.0 x 14.0 (196 cm<sup>2</sup>)
- 2) Peak absorbance
- 3) 59-D plate placed over sample
- 4) Metal mask placed over sample; 49 cm<sup>2</sup> surface left open
- 5) \* One half the number of coats are on each side

RELATIVE EDGE LUMINESCENCE ( $L_T$ )

Plate #	Area (cm <sup>2</sup> )	Dye	# Coats	Host	Abs. <sup>2</sup>	$L_T$
3022-2	196	Radglo - #14 Orange - Red	8*	At-400/Z-4370	2.15	7.30
3022-3	196	Radglo - #14 Orange - Red	8*	At-400/Z-4370	2.15	7.47
3022-4	196	Radglo - #14 Orange - Red	8*	At-400/Z-4370	2.15	7.02
3025-1	196	Radglo - #14 Orange - Red	1	Polytex 975/KL-5-2444	1.27	5.91
3025-2	196	Radglo - #14 Orange - Red	1	Polytex 975/KL-5-2444	1.27	6.01
3025-3	196	Radglo - #14 Orange - Red	1	Polytex 975/KL-5-2444	1.27	6.37
3025-4	196	Radglo - #14 Orange - Red	1	Polytex 975/KL-5-2444	1.27	6.35
3026-1	196	Radglo - #14 Orange - Red	1	Polytex 975/KL-5-2444	1.61	6.04
3026-2	196	Radglo - #14 Orange - Red	1	Polytex 975/KL-5-2444	1.61	6.13
3026-3	196	Radglo - #14 Orange - Red	1	Polytex 975/KL-5-2444	1.61	5.47
3026-4	196	Radglo - #14 Orange - Red	1	Polytex 975/KL-5-2444	1.61	5.71
3027-1	196	Radglo - #14 Orange - Red	2	Polytex 975/KL-5-2444	2.04	5.68
3027-2	196	Radglo - #14 Orange - Red	2	Polytex 975/KL-5-2444	2.04	6.54
3027-3	196	Radglo - #14 Orange - Red	2	Polytex 975/KL-5-2444	2.04	6.39
3027-4	196	Radglo - #14 Orange - Red	2	Polytex 975/KL-5-2444	2.04	6.03
3028-1	196	Radglo - #14 Orange - Red	4	Polytex 975/KL-5-2444	1.71	5.99
3028-2	196	Radglo - #14 Orange - Red	4	Polytex 975/KL-5-2444	1.71	6.53
3028-3	196	Radglo - #14 Orange - Red	4	Polytex 975/KL-5-2444	1.71	6.36
3028-4	196	Radglo - #14 Orange - Red	4	Polytex 975/KL-5-2444	1.71	5.85
3029-1	196	Radglo - #14 Orange - Red	8	Polytex 975/KL-5-2444	1.36	6.16
3029-2	196	Radglo - #14 Orange - Red	8	Polytex 975/KL-5-2444	1.36	6.22
3029-3	196	Radglo - #14 Orange - Red	8	Polytex 975/KL-5-2444	1.36	6.81

- 1) Area is cm<sup>2</sup>; dimensions (in cm) of various size plates are:  
4.4 x 6.2 (27 cm<sup>2</sup>), 7.0 x 7.0 (49 cm<sup>2</sup>), 14.0 x 14.0 (196 cm<sup>2</sup>)
- 2) Peak absorbance
- 3) 59-D plate placed over sample
- 4) Metal mask placed over sample; 49 cm<sup>2</sup> surface left open
- 5) \* One half the number of coats are on each side

RELATIVE EDGE LUMINESCENCE ( $L_r$ )

Plate #	Area (cm <sup>2</sup> ) <sup>1</sup>	Dye	# Coats	Host	Abs. <sup>2</sup>	$L_r$	
3017-1	196	Radglo - #14 Orange - Red	1	At-400/Z-4370	0.87	3.04	*
3017-2	196	Radglo - #14 Orange - Red	1	At-400/Z-4370	0.87	3.13	*
3071-3	196	Radglo - #14 Orange - Red	1	At-400/Z-4370	0.87	3.02	*
3017-4	196	Radglo - #14 Orange - Red	1	At-400/Z-4370	0.87	2.95	*
3021-1	196	Radglo - #14 Orange - Red	8	At-400/Z-4370	2.14	7.23	*
3021-2	196	Radglo - #14 Orange - Red	8	At-400/Z-4370	2.14	7.23	*
3021-3	196	Radglo - #14 Orange - Red	8	At-400/Z-4370	2.14	6.77	*
3021-4	196	Radglo - #14 Orange - Red	8	At-400/Z-3470	2.14	6.80	*
3025-1	196	Radglo - #14 Orange - Red	1	Polytex 975/KL-5-2444	1.25	5.04	*
3025-2	196	Radglo - #14 Orange - Red	1	Polytex 975/KL-5-2444	1.25	5.24	*
3025-3	196	Radglo - #14 Orange - Red	1	Polytex 975/KL-5-2444	1.25	5.88	*
3025-4	196	Radglo - #14 Orange - Red	1	Polytex 975/KL-5-2444	1.25	5.29	*
3029-1	196	Radglo - #14 Orange - Red	8	Polytex 975/KL-5-2444	1.36	6.76	*
3029-2	196	Radglo - #14 Orange - Red	8	Polytex 975/KL-5-2444	1.36	6.30	*
3029-3	196	Radglo - #14 Orange - Red	8	Polytex 975/KL-5-2444	1.36	6.37	*
3029-4	196	Radglo - #14 Orange - Red	8	Polytex 975/KL-5-2444	1.36	6.98	*
3033-1	196	Hostasol Yellow 8-G	1	CAP. 482-0-20	0.88	3.86	*
3033-2	196	Hostasol Yellow 8-G	1	CAP. 482-0-20	0.88	3.89	*
3033-3	196	Hostasol Yellow 8-G	1	CAP. 482-0-20	0.88	3.58	*
3033-4	196	Hostasol Yellow 8-G	1	CAP. 482-0-20	0.88	3.63	*
3034-1	196	Hostasol Yellow 8-G	1	CAP. 482-0-20	0.26	2.13	*
3034-2	196	Hostasol Yellow 8-G	1	CAP. 482-0-20	0.26	2.37	*

- 1) Area is cm<sup>2</sup>; dimensions (in cm) of various size plates are: 4.4 x 6.2 (27 cm<sup>2</sup>), 7.0 x 7.0 (49 cm<sup>2</sup>), 14.0 x 14.0 (196 cm<sup>2</sup>)
- 2) Peak absorbance
- 3) 59-D plate placed over sample
- 4) Metal mask placed over sample; 49 cm<sup>2</sup> surface left open
- 5) \* - All plate edges have been polished

RELATIVE EDGE LUMINESCENCE ( $L_r$ )

Plate #	Area (cm <sup>2</sup> ) <sup>1</sup>	Dye	# Coats	Host	Abs. <sup>2</sup>	$L_r$	
3034-3	196	Hostasol Yellow 8-G	1	CAP. 482-0-20	0.26	2.24	*
3034-4	196	Hostasol Yellow 8-G	1	CAP. 482-0-20	0.26	1.98	*
3035-1	196	SRB	1	CAP. 482-0-20	0.81	1.66	*
3035-2	196	SRB	1	CAP. 482-0-20	0.81	1.78	*
3035-3	196	SRB	1	CAP. 482-0-20	0.81	1.86	*
3035-4	196	SRB	1	CAP. 482-0-20	0.81	1.57	*
3036-1	196	SRB	1	CAP. 482-0-20	0.21	1.41	*
3036-2	196	SRB	1	CAP. 482-0-20	0.21	1.41	*
3036-3	196	SRB	1	CAP. 482-0-20	0.21	1.59	*
3036-4	196	SRB	1	CAP. 482-0-20	0.21	1.62	*
3037-1	196	R-101	1	CAP. 482-0-20	0.73	3.08	*
3037-2	196	R-101	1	CAP. 482-0-20	0.73	3.68	*
3037-3	196	R-101	1	CAP. 482-0-20	0.73	3.72	*
3037-4	196	R-101	1	CAP. 482-0-20	0.73	2.90	*
3038-1	196	R-101	1	CAP. 482-0-20	0.24	2.17	*
3038-2	196	R-101	1	CAP. 482-0-20	0.24	2.25	*
3038-3	196	R-101	1	CAP. 482-0-20	0.24	2.35	*
3038-4	196	R-101	1	CAP. 482-0-20	0.24	2.32	*
3039-1	196	LD-700	1	CAP. 482-0-20	0.72	2.38	*
3039-2	196	LD-700	1	CAP. 482-0-20	0.72	2.51	*
3039-3	196	LD-700	1	CAP. 482-0-20	0.72	2.67	*
3039-4	196	LD-700	1	CAP. 482-0-20	0.72	2.58	*

- 1) Area is cm<sup>2</sup>; dimensions (in cm) of various size plates are: 4.4 x 6.2 (27 cm<sup>2</sup>), 7.0 x 7.0 (49 cm<sup>2</sup>), 14.0 x 14.0 (196 cm<sup>2</sup>)
- 2) Peak absorbance
- 3) 59-D plate placed over sample
- 4) Metal mask placed over sample; 49 cm<sup>2</sup> surface left open
- 5) \* - All plate edges have been polished

RELATIVE EDGE LUMINESCENCE ( $L_r$ )

Plate #	Area (cm <sup>2</sup> )	Dye	# Coats	Host	Abs. <sup>2</sup>	$L_r$
3029-4	196	Radglo - #14 Orange - Red	8	Polytex 975/KL-5-2444	1.36	6.87
3030-1	196	Radglo - #14 Orange - Red	8*	Polytex 975/KL-5-2444	1.42	7.20
3030-2	196	Radglo - #14 Orange - Red	8*	Polytex 975/KL-5-2444	1.42	6.48
3030-3	196	Radglo - #14 Orange - Red	8*	Polytex 975/KL-5-2444	1.42	7.09
3030-4	916	Radglo - #14 Orange - Red	8*	Polytex 975/KL-5-2444	1.42	7.36
3033-1	196	Hostasol Yellow 8-G	1	CAP. 482-0-20	0.87	3.87
3033-2	196	Hostasol Yellow 8-G	1	CAP. 482-0-20	0.87	4.05
3033-3	196	Hostasol Yellow 8-G	1	CAP. 482-0-20	0.87	3.87
3033-4	196	Hostasol Yellow 8-G	1	CAP. 482-0-20	0.87	3.86
3034-1	196	Hostasol Yellow 8-G	1	CAP. 482-0-20	0.25	2.08
3034-2	196	Hostasol Yellow 8-G	1	CAP. 482-0-20	0.25	2.32
3034-3	196	Hostasol Yellow 8-G	1	CAP. 482-0-20	0.25	2.40
3034-4	196	Hostasol Yellow 8-G	1	CAP. 482-0-20	0.25	1.75
3035-1	196	SRB	1	CAP. 482-0-20	0.86	1.68
3035-2	196	SRB	1	CAP. 482-0-20	0.86	2.02
3035-3	196	SRB	1	CAP. 482-0-20	0.86	1.95
3035-4	196	SRB	1	CAP. 482-0-20	0.86	1.73
3036-1	196	SRB	1	CAP. 482-0-20	0.21	1.50
3036-2	196	SRB	1	CAP. 482-0-20	0.21	1.48
3036-3	196	SRB	1	CAP. 482-0-20	0.21	1.71
3036-4	196	SRB	1	CAP. 482-0-20	0.21	1.71
3037-1	196	R-101	1	CAP. 482-0-20	0.73	3.23

- 1) Area is cm<sup>2</sup>; dimensions (in cm) of various size plates are: 4.4 x 6.2 (27 cm<sup>2</sup>), 7.0 x 7.0 (49 cm<sup>2</sup>), 14.0 x 14.0 (196 cm<sup>2</sup>)
- 2) Peak absorbance
- 3) 59-D plate placed over sample
- 4) Metal mask placed over sample; 49 cm<sup>2</sup> surface left open
- 5) \* One half the number of coats are on each side

RELATIVE EDGE LUMINESCENCE ( $L_r$ )

Plate #	Area (cm <sup>2</sup> )	Dye	# Coats	Host	Abs. <sup>2</sup>	$L_r$
3037-2	196	R-101	1	CAP. 482-0-20	0.73	3.79
3037-3	196	R-101	1	CAP. 482-0-20	0.73	3.85
3037-4	196	R-101	1	CAP. 482-0-20	0.73	3.99
3038-1	196	R-101	1	CAP. 482-0-20	0.24	2.22
3038-2	196	R-101	1	CAP. 482-0-20	0.24	2.31
3038-3	196	R-101	1	CAP. 482-0-20	0.24	2.48
3038-4	196	R-101	1	CAP. 482-0-20	0.24	2.35
3039-1	196	LD-700	1	CAP. 482-0-20	0.77	2.58
3039-2	196	LD-700	1	CAP. 482-0-20	0.77	2.63
3039-3	196	LD-700	1	CAP. 482-0-20	0.77	2.67
3039-4	196	LD-700	1	CAP. 482-0-20	0.77	2.65
3040-1	196	LD-700	1	CAP. 482-0-20	0.23	1.70
3040-2	196	LD-700	1	CAP. 482-0-20	0.23	1.90
3040-3	196	LD-700	1	CAP. 482-0-20	0.23	2.01
3040-4	196	LD-700	1	CAP. 482-0-20	0.23	1.90
3041-1	196	R-101	2	Polytex 975/KL-5-2444	1.81	4.35
3041-2	196	R-101	2	Polytex 975/KL-5-2444	1.81	4.80
3041-3	196	R-101	2	Polytex 975/KL-5-2444	1.81	5.05
3041-4	196	R-101	2	Polytex 975/KL-5-2444	1.81	4.82
3042-1	196	R-101	1	Polytex 975/KL-5-2444	1.32	4.52
3042-2	196	R-101	1	Polytex 975/KL-5-2444	1.32	4.33
3042-3	196	R-101	1	Polytex 975/KL-5-2444	1.32	4.59

- 1) Area is cm<sup>2</sup>; dimensions (in cm) of various size plates are: 4.4 x 6.2 (27 cm<sup>2</sup>), 7.0 x 7.0 (49 cm<sup>2</sup>), 14.0 x 14.0 (196 cm<sup>2</sup>)
- 2) Peak absorbance
- 3) 59-D plate placed over sample
- 4) Metal mask placed over sample; 49 cm<sup>2</sup> surface left open

RELATIVE EDGE LUMINESCENCE ( $L_r$ )

Plate #	Area (cm <sup>2</sup> )	Dye	# Coats	Host	Abs. <sup>2</sup>	$L_r$
3042-4	196	R-101	1	Polytex 975/KL-5-2444	1.32	4.37
3043-1	196	R-101	1	Polytex 975/KL-5-2444	0.35	2.59
3043-2	196	R-101	1	Polytex 975/KL-5-2444	0.35	2.55
3043-3	196	R-101	1	Polytex 975/KL-5-2444	0.35	2.53
3043-4	196	R-101	1	Polytex 975/KL-5-2444	0.35	2.65
3044-1	196	R-101	2	At-400/Z-4370	1.92	5.11
3044-2	196	R-101	2	At-400/Z-4370	1.92	5.15
3044-3	196	R-101	2	At-400/Z-4370	1.92	4.71
3044-4	196	R-101	2	At-400/Z-4370	1.92	5.06
3045-1	196	R-101	1	At-400/Z-4370	0.81	3.92
3045-2	196	R-101	1	At-400/Z-4370	0.81	3.92
3045-3	196	R-101	1	At-400/Z-4370	0.81	3.94
3045-4	916	R-101	1	At-400/Z-4370	0.81	3.98
3046-1	196	R-101	1	At-400/Z-4370	0.17	1.79
3046-2	196	R-101	1	At-400/Z-4370	0.17	1.95
3046-3	196	R-101	1	At-400/Z-4370	0.17	1.72
3046-4	196	R-101	1	At-400/Z-4370	0.17	1.82

- 1) Area is cm<sup>2</sup>; dimensions (in cm) of various size plates are: 4.4 x 6.2 (27 cm<sup>2</sup>), 7.0 x 7.0 (49 cm<sup>2</sup>), 14.0 x 14.0 (196 cm<sup>2</sup>)
- 2) Peak absorbance
- 3) 59-D plate placed over sample
- 4) Metal mask placed over sample; 49 cm<sup>2</sup> surface left open

RELATIVE EDGE LUMINESCENCE ( $L_r$ )

Plate #	Area (cm <sup>2</sup> )	Dye	# Coats	Host	Abs. <sup>2</sup>	$L_r$
3047	196	Radglo - #14 Orange - Red /R-101	8*	At-400/Z-4370	2.84	7.71
3048	196	Radglo - #14 Orange - Red /R-101	8*	At-400/Z-4370	3.04	7.92
3049	196	Radglo - #14 Orange - Red /R-101	16*	At-400/Z-4370	5.4	8.60
3050	196	Radglo - #14 Orange - Red /R-101	16*	At-400/Z-4370	5.5	8.51
3051	196	Radglo - #14 Orange - Red /R-101	4*	At-400/KL-5-2444	4.2	6.78
3052	196	Radglo - #14 Orange - Red /R-101	4*	At-400/KL-5-2444	4.4	6.77
3053	196	Radglo - #14 Orange - Red /R-101	8*	At-400/KL-5-2444	10	7.33
3054	196	Radglo - #14 Orange - Red /R-101	8*	At-400/KL-5-2444	8.5	7.46
3055	196	Radglo - #14 Orange - Red /R-101	16*	At-400/KL-5-2444	18	6.74
3056	196	Radglo - #14 Orange - Red /R-101	16*	At-400/KL-5-2444	17	6.97
3057	196	Radglo - #14 Orange - Red	2	At-400/Z-4370	0.65	4.85
3058	196	Radglo - #14 Orange - Red	2	At-400/Z-4370	0.85	4.87
3059	196	Radglo - #14 Orange - Red	2	At-400/Z-4370	2.02	3.39
3060	196	Radglo - #14 Orange - Red	2	At-400/Z-4370	2.40	3.09
3061	196	Radglo - #14 Orange - Red	2	At-400/Z-4370	2.89	3.59
3062	196	Radglo - #14 Orange - Red	2	At-400/Z-4370	3.23	2.45
3063	196	Radglo - #14 Orange - Red	2	At-400/Z-4370	----	2.17
3064	196	Radglo - #14 Orange - Red	1	At-400/Z-4370	2.50	2.63
3065	196	Radglo - #14 Orange - Red	2	At-400/Z-4370	2.13	3.64
3066	196	Radglo - #14 Orange - Red	3	At-400/Z-4370	1.96	4.22
3067	196	Radglo - #14 Orange - Red	4	At-400/Z-4370	2.03	5.37

- 1) Area is cm<sup>2</sup>; dimensions (in cm) of various size plates are: 4.4 x 6.2 (27 cm<sup>2</sup>), 7.0 x 7.0 (49 cm<sup>2</sup>), 14.0 x 14.0 (196 cm<sup>2</sup>)
- 2) Peak absorbance
- 3) 59-D plate placed over sample
- 4) Metal mask placed over sample; 49 cm<sup>2</sup> surface left open
- 5) \* One half the number of coats are on each side









<b>Document Control Page</b>	1. SERI Report No. SERI/STR-211-3149	2. NTIS Accession No.	3. Recipient's Accession No.
4. Title and Subtitle Luminescent Solar Concentrator Development, Final Subcontract Report, 1 June 1982 - 31 December 1984		5. Publication Date April 1987	
7. Author(s) P. S. Friedman, C. R. Parent		8. Performing Organization Rept. No.	
9. Performing Organization Name and Address Owens/Illinois, Inc. Toledo, Ohio		10. Project/Task/Work Unit No. 3475.10	
		11. Contract (C) or Grant (G) No. (C) XE-2-02145-01 (G)	
12. Sponsoring Organization Name and Address Solar Energy Research Institute A Division of Midwest Research Institute 1617 Cole Boulevard Golden, Colorado 80401-3393		13. Type of Report & Period Covered Technical Report	
15. Supplementary Notes Technical Monitor: John Benner		14.	
16. Abstract (Limit: 200 words) An investigation of luminescent solar concentrators (LSCs) was begun by the U.S. Department of Energy (DOE) at Owens-Illinois, Inc., in 1978. Experimental and theoretical results of that investigation are summarized in this report. An assessment of the LSC technology was compiled to provide a concise description to guide future research in this field. Since 1978, tremendous progress was made in the development of this device as a practical nonimaging concentrator for achieving solar concentration ratios on the order of 10X. The two most important technical achievements appear to be first, the understanding that dye self-absorption of radiated energy is not as serious a problem as originally thought; and second, the demonstration that organic dyes in polymeric hosts are capable of surviving outdoors in bright sunlight for years without serious degradation. System efficiencies approaching 4% have been achieved for photovoltaic conversion and theoretical efficiencies on the order of 9% appear feasible for large-area devices.			
17. Document Analysis			
a. Descriptors Photovoltaic conversion ; solar concentrators ; organic compounds ; dyes			
b. Identifiers/Open-Ended Terms			
c. UC Categories			
63			
18. Availability Statement National Technical Information Service U.S. Department of Commerce 5285 Port Royal Road Springfield, Virginia 22161		19. No. of Pages 204	
		20. Price A10	